Treatment of the Cyanotoxins Cylindrospermopsin, Microcystin-LR, and Anatoxin-a by Activated Carbon in Drinking Water

by

Yanting Liu

A thesis
presented to the University of Waterloo
in fulfillment of the
thesis requirement for the degree of
Master of Applied Science
in
Civil Engineering (Water)

Waterloo, Ontario, Canada, 2017

Author's Declaration

I hereby declare that I am the sole author of this thesis. This is a true copy of the thesis, including any required final revisions, as accepted by my examiners.

I understand that my thesis may be made electronically available to the public.

Abstract

Cyanotoxins are known to cause human and animal illness, in some cases resulting in death, and their presence in drinking water is a potential risk to public health. Cylindrospermopsin (CYL), microcystin-LR (MC-LR), and anatoxin-a (ANTA) are among the most detected and studied cyanotoxins in North American surface water. While microcystin is regulated in drinking water in most North American jurisdictions, lower maximum contaminant limits may be coming as well as the potential addition of CYL and ANTA as regulated contaminants. Powdered and granular activated carbon (PAC and GAC) may be cost-effective barriers for extracellular cyanotoxins in conventional drinking water treatment plants but not all carbons and toxins have been studied. Even less information is available at PAC contact times that are relevant to practice. The primary objective of this research was to investigate the adsorption behavior (rate and capacity) of CYL, MC-LR, and ANTA during treatment with PAC and GAC.

Adsorption of CYL, MC-LR, and ANTA was investigated using three commercially available PACs: coal-based COL-PL60-800 (Carbon Activated Corporation), wood-based BG-HHM (Calgon Carbon), and coconut-based WPC® (Calgon Carbon). Initially adsorption was studied in ultrapure water to establish baseline performance and for inter-lab comparisons now and in the future. The BG-HHM (wood) and the WPC (coconut) adsorbed CYL the fastest, the BG-HHM (wood) adsorbed MC-LR the fastest, while the BG-HHM (wood) and WPC (coconut) adsorbed ANTA the fastest. Adsorption capacity was evaluated under both equilibrium and non-equilibrium conditions (0.5 h and 1 h contact times). At equilibrium, the BG-HHM (wood) had the highest CYL capacity, the COL-PL60-800 (coal) had the highest MC-LR capacity, and the WPC (coconut) had the highest capacity for ANTA adsorption. Interestingly, PAC had substantially different capacities under non-equilibrium conditions which serve to more accurately simulate PAC contact times typically available in full-scale water treatment plants. Under non-equilibrium conditions, the wood-based BG-HHM outperformed the other two PACs with the highest capacity for the all three cyanotoxins investigated in this study.

The adsorption of CYL, MC-LR, and ANTA was then investigated using Lake Erie water (adjusted to pH 7) collected from the Elgin Area Water Treatment Plant (Southern Ontario, Canada), again using the same PAC products as studied in the ultrapure water investigations. The BG-HHM (wood) adsorbed CYL and MC-LR the fastest, whereas the WPC (coconut) adsorbed ANTA the fastest. At

equilibrium, the COL-PL60-800 (coal) had the greatest CYL capacity, the BG-HHM (wood) had the highest MC-LR capacity, and the WPC (coconut) and BG-HHM (wood) retained the greatest and similar capacity for ANTA. Under non-equilibrium conditions, the BG-HHM (wood) had the highest capacity for CYL and MC-LR, while the WPC (coconut) performed best for ANTA removal. Compared to the ultrapure water results, a substantial reduction in adsorptive capacity and a slight decrease in the rate of adsorption were observed in Lake Erie water. To describe the competitive adsorption of cyanotoxins and dissolved natural organic matter (NOM) in Lake Erie water, a competitive adsorption model, the simplified equivalent background compound model (SEBCM), was successfully utilized in this study to predict PAC dose to achieve target removals of each of CYL, MC-LR and ANTA under non-equilibrium conditions (0.5 h contact time). Based on the SEBCM results, an economic analysis was conducted and it was found that the BG-HHM (wood) was the most cost-effective alternative for CYL and MC-LR removal, while none of the selected PACs in this study was an effective barrier for ANTA.

CYL adsorption was then investigated in ultrapure water using three virgin GACs, including coal-based F-300® (Calgon Carbon), wood-based C Gran (Norit), and coconut-based Aqua Carb (Siemens), and a preloaded coal-based F-300, previously prepared by Vlad (2015). Among all virgin GACs, the C Gran (wood) adsorbed CYL the fastest, while the F-300 (coal) was slowest. The F-300 (coal) retained the highest equilibrium capacity, while the C Gran (wood) had the lowest. Comparing the performance of virgin and preloaded F-300 (coal), both the rate of adsorption and capacity deteriorated as a result of preloading.

Overall, PAC adsorption for CYL and MC-LR is a promising treatment option. Further investigations are required to explain differences observed for ANTA removal by PAC in this study vs. that reported by Vlad (2015). In the case of CYL adsorption by GAC, bench-scale testing has demonstrated that larger scale investigations are justified (at pilot- or full-scale in the event of a bloom). At present, the price and availability of the cyanotoxins is such that larger scale experiments may be cost prohibitive. Additional bench-scale PAC and GAC studies in other water sources are warranted.

Acknowledgements

First and foremost, I would like to express my sincerest gratitude to my supervisors Drs. Sigrid Peldszus and William B. Anderson for their expert guidance throughout this tough but exciting research project. During the challenging times, they were always capable of providing insights and guidance, and giving encouragement and hope. I am truly grateful for their valuable counsel, constant support, and professional expertise. I also wish to extend my thanks to the readers of my thesis, Drs. Wayne J. Parker and G. Wayne Brodland.

I gratefully acknowledge the exceptional support from the NSERC Industrial Research Chair in Water Treatment. I am grateful to Silvia Vlad for her guidance on the initial set-up of my research and sharing her freeze-dried preloaded GAC samples with me. Profound thanks go to Guy Milton for his help with LC-MS/MS maintenance and trouble-shooting and to Chuan Liu for sharing his experience with LC-MS/MS trouble-shooting. Thanks to Jangchuk Tashi for the TOC/DOC training and to Victoria Chennette for demonstrating the experimental procedure for determining pH_{PZC}. I would like to thank student intern Andrea Steuer for conducting the pH_{PZC} tests for the three PAC samples. Great thanks go to Dr. Fei (Alex) Chen for his kind suggestions and help at every stage of my degree. Thanks to my fellow graduate students and friends, Sabrina Bedjera, Zhanyang (Andy) Gong, Lin Shen, Saloni Singh; it has been a pleasure to work with you all.

My sincere thanks go to Dr. Monica Tudorancea for her generous help in lab. Special thanks go to Dana Herriman for her kind assistance.

I would also like to thank Andrew Kacheff from the Department of Chemical Engineering at the University of Waterloo for conducting the pore distribution tests for the three PACs which were used in this study.

I am grateful to the tremendous support from Mark Merlau and Mark Sobon, who were always willing to help with trouble-shooting in the lab. Thanks to Leslie Bragg from the Department of

Biology at the University of Waterloo for her valuable suggestions for LC-MS/MS column maintenance. Thanks to Jane Russwurm from the Writing Centre at the University of Waterloo for her help in refining this thesis.

This project was conducted in partnership with the Walkerton Clean Water Centre and the Lake Huron and Elgin Area Water Supply Systems. I would like to acknowledge Dr. Souleymane Ndiongue, Dr. Xiaohui Jin, and Tory Hewlett of the Walkerton Clean Water Centre (WCWC) for their valuable feedback and Carolyn de Groot of the City of London for providing carbon samples and Elgin Water Treatment Plant data as well as Simon Flanagan and Greg Henderson for their assistance with sampling at that plant.

Finally, I would like to thank my family and friends for their constant support and encouragement. I could not have made this far without them. Heartfelt thanks to my parents, parents-in-laws, grandparents, and my husband for their love, patience, and encouragement.

Funding for this project was provided by the Natural Sciences and Engineering Research Council of Canada (NSERC) in the form of an Industrial Research Chair in Water Treatment at the University of Waterloo. The current Chair partners include: Associated Engineering Group Ltd., the cities of Barrie, Brantford, Guelph, Hamilton, and Ottawa, EPCOR Water Services, GE Water & Process Technologies Canada, GHD Waterloo, Lake Huron and Elgin Area Water Supply Systems, the Ontario Clean Water Agency (OCWA), the Regions of Durham, Halton, Niagara, and Waterloo, Toronto Water, and the Walkerton Clean Water Centre.

Table of Contents

List of Figures

List of Tables

List of Acronyms

ANTA – anatoxin-a

AOP – advanced oxidation process

BET – Brunauer, Emmett and Teller

c(RADfV) – Cyclo-(Arg-Ala-Asp-D-Phe-Val)

CCL – candidate contaminant list

CUR – carbon usage rate

CYL – cylindrospermopsin

DFT – density functional theory

DOC – dissolved organic carbon

EBC – equivalent background compound

EBCT – empty bed contact time

ECM – equilibrium column model

GAC – granular activated carbon

HSDM – homogeneous surface diffusion model

IAST – ideal adsorbed solution theory

JCR – joint confidence region

LC-MS – liquid chromatography mass spectrometry

LC-MS/MS – liquid chromatography tandem mass spectrometry

MAC – maximum acceptable concentration

MCL – maximum contaminant level

MC-LR – microcystin-LR

MC-RR – microcystin-RR

MCs - microcystins

MDL – method detection limit

MIB – 2-methylisoborneol

MRM – multiple reaction monitoring

MTZ – mass transfer zone

NOM – natural organic material

PAC – powdered activated carbon

pH_{PZC} – pH at the point of net zero surface charge

pKa – acid dissociation constant

SEBCM – simplified equivalent background compound model

SUVA – specific ultraviolet absorbance

TOC – total organic carbon

USEPA – United States Environmental Protection Agency

UV_{254} – Ultraviolet 254 nm

VFDF – very fast death factor

Chapter 1
Introduction

1.1 Problem Statement

Cyanobacteria are a large and diverse phylum of bacteria that obtain energy through photosynthesis and produce oxygen as by-product. Cyanobacteria initially attracted the attention of scientists in 1878, after livestock were found dead subsequent to ingesting water during a cyanobacterial bloom in Australia (Francis, 1878). Over the past few decades, the incidence of cyanobacterial blooms in freshwater is on the rise due to increasing levels of nutrients caused by intensive fertilizer application, detergent usage, and sewage discharges (Merel et al., 2013). Climate change also stimulates cyanobacterial growth. Harmful cyanobacteria have now been identified in 27 countries on all continents including Antarctica. Yet, their worldwide occurrence can vary significantly. Blooms may be detected year-round in tropical areas whereas they only develop in warm seasons in temperate climates, including North America.

Approximately 50% of cyanobacteria are known to produce toxic metabolites (or cyanotoxins) (Codd, 1995). Cyanotoxins present a hazard to drinking water safety, threating human and animal health mainly by ingestion of contaminated water. Diverse in chemical structure and toxicity, cyanotoxins can cause various health issues including abdominal pain, vomiting, diarrhea, skin irritation, hypoxia, paralysis, respiratory or cardiac arrest, and even death (Merel et al., 2013).

In North America, cyanobacterial blooms have been reported in many surface waters. Lake Erie, an important water source for over 11 million people from Canada and USA, is now experiencing annual algal blooms (Watson et al., 2016). The most intensive cyanobacterial bloom in Lake Erie formed in 2015 (NOAA, 2015). Previously, a 2011 cyanobacteria bloom occupied over 5,000 km^2, nearly one-fifth of the lake's surface (Michalak et al., 2013). Such harmful cyanobacterial blooms have the potential to greatly impact drinking water quality for Ontario, Ohio and Michigan residents

who depend on Lake Erie water. Indeed, a 3-day "do not drink or boil" advisory was issued in 2014 in Toledo, Ohio in response to the detection of the cyanotoxin, microcystin-LR (MC-LR), in treated water, which affected nearly 500,000 residents (USEPA, 2015).

Among various cyanotoxins, cylindrospermopsin (CYL), MC-LR, and anatoxin-a (ANTA) are the most regulated and commonly detected cyanotoxins in North America. CYL has been reported in concentrations up to 202 µg/L in the states of Florida, Louisiana (Yilmaz & Philips, 2011), and New York, as well as in the Lower Great Lakes (Boyer, 2008). MC-LR has been widely reported in North America, including New York, Nebraska, New Hampshire and Florida, and detections of microcystins (MCs) in ambient waters have ranged from no detection to 31,470 µg/L (Fristachi et al., 2008). In Canada, MC-LR has been detected in the raw intake water in plants in Alberta, Manitoba, Ontario, and Quebec (Health Canada, 2002; Carrière et al., 2010). In Ontario, MC-LR was the most frequently detected cyanotoxin with a maximum concentration of 3.4 µg/L, measured in samples collected from 17 municipal WTPs that draw water from 12 different water bodies (Kingston, 2015). It was detected in treated tap water at a maximum concentration of 0.55 µg/L following the identification of a cyanobacterial bloom in Shoal Lake (Ontario, Canada) (Health Canada, 2002). Generally, the concentration of ANTA in surface water used for drinking water production, when found, is low (< 5 µg/L) (Fristachi et al., 2008). In Canada, the maximum reported ANTA concentrations were as 0.17 µg/L in Ontario and 2.3 µg/L in Quebec (Carrière et al., 2010; Kingston, 2015). However, some reports of ANTA concentrations as high as 156 µg/L in natural water have been documented and a concentration of approximately 10 µg/L has been reported in a treated drinking water in Florida (Burns, 2005).

In response to reports of cyanotoxins being detected in surface water, in 2015 the USEPA issued health advisories for the cyanotoxins, CYL and total MCs (USEPA, 2015). For total MCs, a health advisory of 0.3 µg/L was set for children under six, while an advisory concentration of 1.6 µg/L was issued for all others. As for CYL, health advisories of 0.7 µg/L and 3.7 µg/L were issued for

those under age 6 and all others, respectively. CYL, MC-LR, and anatoxin-a (ANTA) are listed in the Contaminant Candidate List 4 (CCL4), requiring that they be studied to determine if maximum contaminant levels (MCLs) are necessary (USEPA, 2016). Although no national MCLs exist in the US at present, several states, including Minnesota, Ohio, Oregon, and Vermont, have implemented cyanotoxin standards or guidelines. In Canada, only one cyanotoxin, MC-LR, is federally-regulated in the form of a guideline with a maximum acceptable concentration (MAC) of 1.5 µg/L (Health Canada, 2017). This guideline was recently reviewed and it is being proposed that the MAC apply to total microcystins (MCs) vs. MC-LR). The province of Ontario has adopted an MC-LR MAC of 1.5 µg/L (O. Reg. 169/03). In Quebec, a 3.7 µg/L provincial guideline has been proposed for ANTA (Institut National de Santé Publique, 2005). Therefore, investigations on effective treatment barriers are required to remove or inactivate those cyanotoxins in drinking water.

Activated carbon has been considered an effective treatment barrier for extracellular cyanotoxins in conventional drinking water treatment plants. Activated carbon is commonly implemented for the control of taste and odor compounds such as geosmin and 2-methylisoborneol (MIB), and other micropollutants (Westrick et al., 2010)). However, CYL adsorption by granular activated carbon (GAC) is not yet adequately described. Adsorptive performance of powdered activated carbon (PAC) and GAC is restricted by the competitive adsorption of dissolved natural organic matter (NOM) in natural water. A number of studies have investigated PAC adsorption for extracellular cyanotoxin removal especially for MC-LR but to a lesser degree for CYL and ANTA. Almost all studies examined PAC performance under equilibrium conditions, which provide sufficient contact time for PACs to reach their maximum adsorptive capacities. However, there is little known about PAC adsorption with respect to the short contact times which are typical in drinking water treatment.

1.2 Research Objectives

The primary objective of this research was to examine the removal of three cyanotoxins (CYL, MC-LR, and ANTA) by PAC and GAC for seasonal application under conditions representative of typical water treatment practice. Specifically, the main objectives were to:

1) Select a representative group of commercially available PAC and GAC products (each with different base materials) and investigate the effects of their physico-chemical properties on the removal of each cyanotoxin in ultrapure and/or Lake Erie water;
2) Evaluate and compare adsorption rates and capacities (as equilibrium adsorption isotherms) of CYL, MC-LR, and ANTA onto the selected PACs in both ultrapure and Lake Erie waters, and compare their adsorption capacities with those of other cyanobacteria metabolites, such as the cyanobacterial taste and odor compounds, geosmin and MIB;
3) Determine and compare short-term (0.5 h and 1 h) adsorption rates and carbon loading for CYL, MC-LR, and ANTA in both ultrapure and Lake Erie waters since these short-term PAC applications are reflective of water treatment practice;
4) Investigate the effects of NOM competition on cyanotoxin adsorption by comparing results from ultrapure water and surface water investigations;
5) Estimate PAC dosages needed to treat cyanotoxins by applying the simplified equivalent background compound model (SEBCM), to equilibrium isotherms and non-equilibrium loading data obtained for the adsorption of CYL, MC-LR, and ANTA onto each selected PAC product in Lake Erie water;
6) Conduct an economic analysis of cyanotoxin treatment by PAC based on SEBCM results
7) Study and compare both the capacities and adsorption rates of CYL onto selected commercially available GACs in ultrapure water, and compare those results with the adsorption capacities of other cyanobacterial metabolites such as MC-LR;
8) Investigate the impact of GAC preloading by NOM on CYL adsorption in ultrapure water.

1.3 Research Approach and Thesis Structure

This thesis consists of six chapters, with Chapters 3 to 5 structured in journal article format (Figure 1.1). Chapter 2 is a literature review, providing an overview of current knowledge and research into CYL, MC-LR, and ANTA, including cyanotoxin properties, toxicity, occurrence, and common drinking water treatment options. Chapter 3 describes the development of the liquid chromatography-tandem mass spectrometry (LC-MS/MS) analytical method for quantifying aqueous CYL, MC-LR, and ANTA concentrations. It also describes the results of characterization tests for each selected PAC product (coal-, wood-, and coconut-based), and investigates the adsorption of each cyanotoxin onto each PAC product in ultrapure water. Chapter 4 considers the adsorptive performance of the three cyanotoxins in Lake Erie surface water using selected commercially available PAC products, and uses a competitive adsorption model, the SEBCM, to obtain PAC dosages required to treat cyanotoxins at short contact times i.e. under non-equilibrium conditions. Chapter 5 describes CYL adsorption onto three virgin GAC products (manufactured from coal-, wood-, and coconut-based material) in ultrapure water and quantifies the impact of carbon preloading by NOM on CYL adsorption using preloaded GAC prepared by Vlad et al. (2015). Chapter 6 provides a summary of the findings of this work, as well as proposing recommendations for future research pertaining to drinking water treatment practices to remove CYL, MC-LR, and ANTA. A comprehensive list of references from all chapters is provided at the end of this thesis. Supplementary material can be found in a series of appendices.

Chapter 1	Provides research motivations, objectives, and thesis structure
Chapter 2	Presents a literature review of current knowledge on treatment of CYL, MC-LR, and ANTA in drinking water
Chapter 3	Describes the results of the adsorption of CYL, MC-LR, and ANTA onto PACs in ultrapure water
Chapter 4	Investigates the adsorption of CYL, MC-LR, and ANTA onto PAC in Lake Erie water and provides PAC dose and cost estimates of such treatment
Chapter 5	Examines CYL adsorption by virgin and preloaded GAC in ultrapure water
Chapter 6	Presents an overall discussion of conclusions and recommendations for future studies
Appendix A	Provides supporting information for Chapter 3
Appendix B	Provides supplementary material for Chapter 4
Appendix C	Provides additonal information for Chapter 5

Figure 1.1 Thesis structure and relevant information

Chapter 2
Literature Review

2.1 Introduction

Cyanobacteria are a diverse group of prokaryotes amongst the earliest organisms on Earth providing an oxygen-rich atmosphere (Merel et al., 2013). As they were initially classified phenotypically they were grouped with eukaryotic algae, and as such cyanobacteria have been mistakenly described as "blue-green algae" (O'Neil et al., 2012). To-date, approximately 40 species of cyanobacteria have been identified worldwide, existing in very diverse environments, such as in Antarctic coastal water and volcanic hot springs, where other organisms are challenged to survive (Svrcek & Smith, 2004; Westrick et al., 2010). In the last 20 years, most of cyanobacteria-related literature has focused on the ubiquitous cyanobacterial blooms and the harmful cyanobacterial metabolites, associated with eutrophic waters (Merel et al., 2013).

Cyanobacteria are responsible for the production of a wide group of metabolites, including the taste and odor compounds geosmin and 2-methylisoborneol (2-MIB), and harmful cyanotoxins. Cyanotoxins are secondary metabolites of cyanobacteria, which can be formed at various stages of cyanobacterial growth. Generally, cyanotoxins are present in the cell (termed intracellular toxin) until cell lysis due to aging or stress, releasing them into the surrounding water (termed extracellular toxin) (Sivonen & Jones, 1999). Typically, the majority of cyanotoxins are present intercellularly in the late logarithmic growth phase, with toxin content positively correlated with cyanobacteria biomass (Carmichael, 2001). During the period of decline of blooms with breakdown of cyanobacteria biomass, cyanotoxins transit from the intracellular to extracellular phase. However, some cyanotoxins, such as cylindrospermopsin (CYL), are detected at high extracellular concentrations in all stages of the life cycle (Carmichael, 2001). This being said, the presence of cyanobacteria does not necessarily infer the presence of a cyanotoxin (Westrick et al., 2010). On

the other hand, some cyanobacteria can produce multiple types of cyanotoxin (Svrcek & Smith, 2004).

Cyanotoxins are generally classified into 3 groups based on their chemical structure: cyclic peptides, alkaloids, and lipopolysaccharides (Sivonen & Jones, 1999). Cyclic peptide toxins are generally hepatotoxic and are the most commonly found in cyanobacterial blooms in both fresh and brackish waters, including the most ubiquitous cyanotoxins, the microcystins (MCs) (Sivonen & Jones, 1999). Cyanotoxins in this group are typically large metabolites with molecular weights ranging from 800 to 1100 (Svrcek & Smith, 2004). The alkaloid toxins are a relatively diverse group of cyanotoxins and can be further classified 3 sub-categories based on their mammalian toxicity: neurotoxic alkaloids, cytotoxic alkaloids, and dermatoxic alkaloids. ANTA (previously known as very fast death factor, or VFDF) and saxitoxin (also called paralytic shellfish poison, or PSPs) are both alkaloid neurotoxins. The sulfonated alkaloid CYL is typically hepatotoxic, but it can also be cytotoxic and genotoxic. Lipopolysaccharide toxins (also known as endotoxins) are rarely described in association with cyanotoxins but they are often responsible for health effects associated with exposure to cyanobacterial blooms (Anderson et al., 2002). Among the various cyanotoxins, MC-LR and CYL are the most commonly found and regulated cyanotoxins in North America, and these are the focus of this review.

2.2 Cyanotoxins: Property, Toxicity, and Regulations

2.2.1 Cylindrospermopsin

CYL was named based on its production and identification in *Cylindrospermopsis raciborskii* but other cyanobacteria including *Aphanizomenon flos-aquae, Aphanizomenon gracile, Aphanizomenon ovalisporum, Umezakia natans, Anabaena bergii, Anabaena lapponica, Anabaena planctonica, Lyngbya wollei, Rhaphidiopsis curvata,* and *Rhaphidiopsis mediterranea* can also generate this toxin (Table 2.3). As shown in Figure 2.1, CYL is a 415 Da tricyclic alkaloid enclosing

a guanidine entity with a uracil moiety which potentially is responsible for the toxicity (Banker et al., 2001). In the pH range of importance for drinking water treatment (6.0 to 8.5), CYL is zwitterionic (Table 2.2), as this toxin includes a negatively charged sulfate group and a positively charged guanidinium portion, leaving a net charge of zero (de la Cruz et al., 2013).

Table 2.1 Toxicity of various cyanotoxins (Valentine et al., 1991, Svrcek & Smith, 2004, van Apeldoorn et al., 2007, USEPA, 2015)

Cyanotoxin	**Main Effect**	**LD_{50} (µg/kg, mouse bioassay)**	**Producer**
CYL	Hepatotoxin: liver and kidney failure	2100	*Cylindrospermopsis raciborskii (C. raciborskii), Aphanizomenon flos-aquae, Aphanizomenon gracile, Aphanizomenon ovalisporum, Umezakia natans, Anabaena bergii, Anabaena lapponica, Anabaena planctonica, Lyngbya wollei, Rhaphidiopsis curvata, Rhaphidiopsis mediterranea*
MC-LR	Hepatotoxin: liver failure and hepatic hemorrhage	50	*Anabaena, Anabaenopsis, Aphanocapsa, Hapalosiphon, Microcystis, Nostoc, Oscilatoria, Nodularia, Fishcherella, Planktothrix, Gloeotrichia*
ANTA	Neurotoxin: muscular paralysis	380	*Anabaena, Aphanizomenon, Oscillatoria*

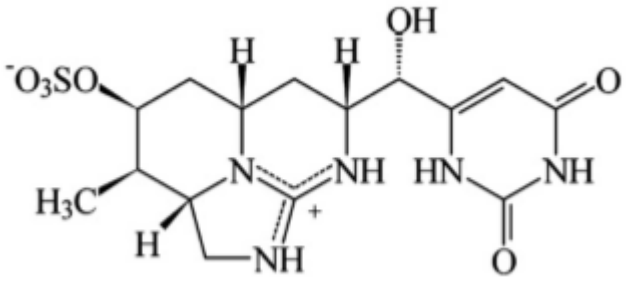

Figure 2.1 Molecular structure of CYL (Ho et al., 2011)

Table 2.2 Characteristics of cyanotoxins used in this study (Ho et al., 2011, Vlad et al., 2015)

Cyanotoxin	Molecular Weight (g/mol)	Dominant Species	Net Charge at pH 6.0-8.5
CYL	415	$(SO_4^-)(NH^+)$	0
MC-LR	995	$(COO^-)_2(NH_2^+)$	-
ANTA	165	(NH_2^+)	+

CYL is highly water-soluble and its half-life is more than 10 days in ultrapure water (Chiswell et al., 1999). However, CYL decomposes rapidly (half-life of 1.5 h) with exposure to sunlight in algal extract solutions (Chiswell et al., 1999). pH in the range of 6.0 to 8.5 does not appear to influence CYL degradation (Chiswell et al., 1999).

CYL is hepatotoxic, as this toxin impacts liver tissues via the irreversible inhibition of protein synthesis, resulting in death (Table 2.1). The LD_{50} is 2100 µg/kg in mice at 24 h following injection (van Apeldoorn et al., 2007). CYL exposure is also associated with tumor initiation, micronucleus induction and chromosome loss (Merel et al., 2013).

CYL was initially considered to be a tropical toxin, as it was primarily detected in tropical areas such as Australia and New Zealand, it has since been found in temperate areas, including Germany about a decade ago (Merel et al., 2013). In North America, CYL has been reported at concentrations of up to 202 µg/L in the states of Florida and Louisiana (Yilmaz & Philips, 2011), and has also been reported in the state of New York and in the Lower Great Lakes basins (Boyer, 2008).

Some authorities have issued maximum acceptable concentrations (MACs) or maximum contaminant levels (MCLs) for CYL in drinking water, based on the current state of knowledge of CYL toxicity and potential health effects, as shown in Table 2.1. Humpage and Falconer (2003) suggested a CYL drinking water guideline of 1 µg/L. In 2015, the USEPA issued a 10-day health advisory for CYL as 0.7 µg/L for those under 6 years of age and 3.0 µg/L for all others (USEPA, 2015), leading to the release of a CYL guideline in several states, including Minnesota and Ohio

(Table 2.3). However, CYL guideline concentrations vary from 1 µg/L in New Zealand to 15 µg/L in Brazil, indicating that further study on CYL is required to set appropriate guidelines.

Table 2.3 Regulations and guidelines for cyanotoxin concentrations in drinking water

Cyanotoxin	Location	MAC	Source
CYL	US	No national guidelines available, but EPA issued 10-day health advisory of 0.7 µg/L for children < 6-years old; 3.0 µg/L for all others	USEPA, 2015
	Ohio, US	0.7 µg/L for children < 6; 3.0 µg/L for all others	USEPA, 2017
	Oregon, US	0.7 µg/L for children < 5-years old; 3.0 µg/L for all others	USEPA, 2017
	Vermont, US	0.5 µg/L	USEPA, 2017
	Brazil	15.0 µg/L	Chorus I., 2005
	New Zealand	1.0 µg/L	New Zealand Ministry of Health, 2016
		Suggested guideline of 1.0 µg/L based on suspected genotoxicity	Humpage & Falconer, 2003
MCs	WHO	1.0 µg/L for MC-LR	WHO, 2004
	Canada	1.5 µg/L for MC-LR	Health Canada, 2017
	Ontario, Canada	1.5 µg/L for MC-LR	O. Reg. 169/03
	US	No national guidelines available, but EPA issued 10-day health advisory as 0.3 µg/L for children < 6-years old; 1.6 µg/L for all others	USEPA, 2015b
	Minnesota, US	0.1 µg/L for MC-LR	USEPA, 2017
	Ohio, US	0.3 µg/L for children < 6-years old; 1.6 µg/L for all others	USEPA, 2017
	Oregon, US	0.3 µg/L for children < 5-years old; 1.6 µg/L for all others	USEPA, 2017
	Vermont, US	0.16 µg/L for MC-LR	USEPA, 2017
	Australia	1.3 µg/L as MC-LR toxicity equivalent	NHMRC/NRMMC, 2004
	Brazil	1.0 µg/L	Chorus, 2005
	China	1.0 µg/L for MC-LR adopted from WHO	Ministry of Health of China, 2006
	Czech Republic	1.0 µg/L for MC-LR adopted from WHO	Chorus, 2005
	France	1.0 µg/L for MC-LR adopted from WHO	Chorus, 2005
	Italy	1.0 µg/L for MC-LR adopted from WHO	Chorus, 2005
	Japan	1.0 µg/L for MC-LR adopted from WHO	Chorus, 2005
	Korea	1.0 µg/L for MC-LR adopted from WHO	Chorus, 2005

	New Zealand	1.0 µg/L as MC-LR toxicity equivalent	New Zealand Ministry of Health, 2016
	Norway	1.0 µg/L for MC-LR adopted from WHO	Chorus, 2005
	Poland	1.0 µg/L for MC-LR	Poland Ministry of Health regulation, 2002
	South Africa	0-0.8 µg/L for MC-LR	DWAF, 1999
	Spain	1.0 µg/L for MC-LR adopted from WHO	Chorus, 2005
ANTA	Quebec, Canada	3.7 µg/L	Institut National de Santé Publique, 2005 du Québec, 2005
	Minnesota, US	0.1 µg/L	USEPA, 2017
	Ohio, US	20 µg/L	USEPA, 2017
	Oregon, US	0.7 µg/L for children < 5-years old; 3.0 µg/L for all others	USEPA, 2017
	Vermont, US	0.5 µg/L	USEPA, 2017
	New Zealand	6.0 µg/L	New Zealand Ministry of Health, 2016
		Suggested guideline of 1.0 µg/L	Fawell et al., 1999

2.2.2 Microcystin-LR

The cyclic polypeptides, microcystins (MCs), are the most diverse and prevalent class of cyanotoxins, named based on *Microcystis*, the first genera of cyanobacteria capable of producing oxygen (Merel et al., 2013). MCs are toxins produced by a number of cyanobacterial species, including members of *Microcystis, Anabaena, Nodularia, Nostoc, Oscillatoria, Fischerella, Planktothrix, and Gloeotrichia* (Table 2.1). Typically, MCs are characterized as cyclic peptides, containing a seven amino acid ring (He et al., 2016). To-date, over 100 microcystin congeners have been detected in water, varying based on amino acid composition, as well as through methylation or demethylation at selected sites within the cyclic peptide (Duy et al., 2000). MC-LR is the most frequently studied and the most widespread congener, recognized by its amino acids, leucine (L) and arginine (A) (Figure 2.2), with a molecular weight of approximately 995 (USEPA, 2015). MC-LR also contains three ionisable groups, including two carbosyl and one amino acid, indicating varying net charge at various pHs (de Maagd et al., 1999). The pKa of these groups are reported as 2.09, 2.19, and 12.48, respectively (de Maagd et al., 1999). Therefore, MC-LR contains one negatively charged group in the typical natural water pH range (6.0-8.5), as shown in Table 2.2.

MC-LR is a water-soluble molecule, which is resistant to chemical hydrolysis or oxidation at near neutral pH (Chorus & Bartram, 1999). MC-LR may persist for months in natural water, with no light exposure (Chorus & Bartram, 1999), depending on concentration and water chemistry. However, hydrolysis can be effective for the destruction of MC-LR with exposure to sunlight at high temperature (40°C) and/or extreme pH levels (Chorus & Bartram, 1999; Tsuji et al., 1994). In full sunlight, MC-LR undergoes slow photochemical destruction and isomerisation, which can be enhanced by the presence of water-soluble cell pigments, presumably phycobiliproteins, leading to in excess of 90% removal in about two weeks, depending on the pigment concentration (Tsuji et al., 1994).

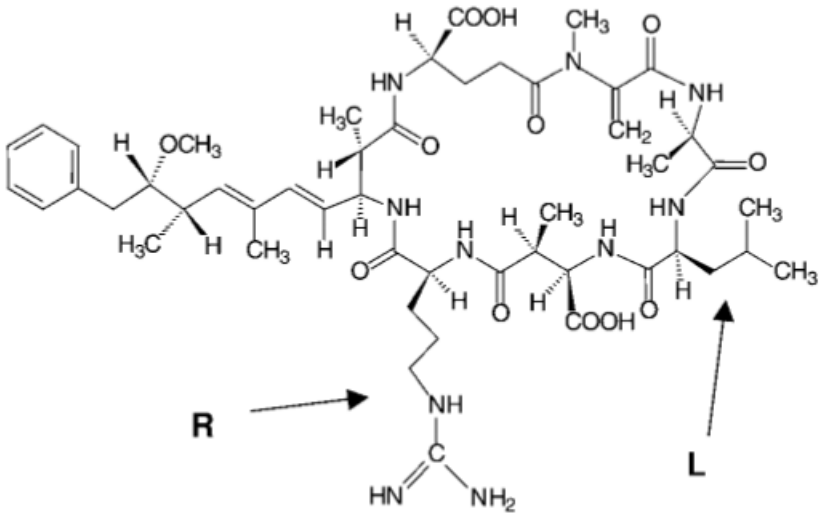

Figure 2.2 Molecular structure of MC-LR with two amino acids indicated as leucine (L) and arginine (R) (Newcombe & Nicholson, 2004)

The toxicity of MC-LR was detected as 50 µg/kg in mouse bioassay shown in Table 2.2 (Valentine et al., 1991). The primary source of MC-LR exposure is drinking water, while other routes are also identified including food, recreational waters, and nutritional supplements. The distribution of MC-LR in tissues is mainly facilitated by the membrane receptors in the organic acid transporter polypeptide family, limiting the ability of MC-LR to penetrate across cell membrane (He et al., 2016). These polypeptides located mainly in liver, brain, testes, lungs, kidney, and other tissues, making them more vulnerable to MC-LR (Cheng et al., 2005). Once inside the cell, MC-LR quickly

binds to the enzymes, protein phosphatase (PP1 and PP2A), resulting in successively to the accumulation of phosphorylated proteins in the tissue, cell necrosis, and even death (Merel et al., 2013; He et al., 2016). MC-LR is also considered as a potential tumor promoter (Falconer 1991).

In temperate regions, including the Great Lakes in North America, cyanobacterial blooms tend to occur in the summer and fall, when temperature and nutrient conditions are ideal (Merel et al., 2013). MC-LR has been widely reported in North America, including in the states of New York, Nebraska, New Hampshire and Florida, and detections of microcystins in ambient waters have been observed to range from no detection to 31,470 µg/L (Fristachi et al., 2008). In a study of 180 New York lakes and rivers, more than half of the collected samples contained detectable levels of microcystins with concentrations ranging from 0 to over 1000 µg/L (Boyer et al., 2004). Lake Erie, the shallowest of the Great Lakes, has frequently experienced large cyanobacterial blooms. In 2014, concentrations of total MC were found to be up to 2.5 µg/L in the finished drinking water in Toledo whose plant is located on the shore of Lake Erie. This led to a 3-day "do not drink or boil advisory" (USEPA, 2015).

A guideline maximum concentration of 1 µg/L for MC-LR was issued by WHO more than a decade ago, and this guideline has now been adopted in many jurisdictions, including China (Table 2.3). Recently, Health Canada issued a MAC value of 1.5 µg/L for MC-LR (Table 2.3). Although no national guideline exists in the US, the USEPA released a 10-day health advisory for total MCs, at 0.3 µg/L for those under 6 years of age and 1.6 µg/L for all others, based on body weight (Table 2.3).

2.2.3 Anatoxin-a

ANTA (along with its analogue homoanatoxin-a) was the first cyanotoxin that was functionally and chemically defined (Syrcek & Smith, 2004). ANTA is an alkaloid neurotoxin with a relatively low molecular weight (MW = 165) and a pK_a of 9.36, which is mainly produced by three genera of cyanobacteria (*Anabaena*, *Aphanizomenon* and *Planktothrix*) (van Apeldoom et al., 2007; Vlad et

al., 2014; Merel et al., 2013). This toxin exists predominantly in cationic form, a more stable protonated form, shown in Figure 2.3, in drinking water in the pH range of 6-9 (Devlin et al., 1976; van Apeldoom et al., 2007; Vlad et al., 2014). While ANTA is completely protonated (< 1% deprotonated) at pH 6, approximately 24% of ANTX-a is deprotonated at pH 9 (Figure 2.3 b as per Vlad et al., 2014). ANTX-a is unstable, particularly in its protonated form, and is fully or partially photodegraded, the rate of which is highly dependent on pH, sunlight intensity, temperature and oxygen availability (Stevens & Krieger, 1991). This toxin tends to be inactivated at elevated temperatures and under alkaline conditions (Vlad et al., 2014; Carmichael et al., 1997). In the pH range of 8-9 and in the presence of sunlight, ANTX-a's half-life is reported to be 1 to 2 h (Stevens & Krieger, 1991). However, ANTA can persist for weeks or even months in dark conditions, as is the case in typical drinking water treatment plants and distribution systems (Stevens & Krieger, 1991).

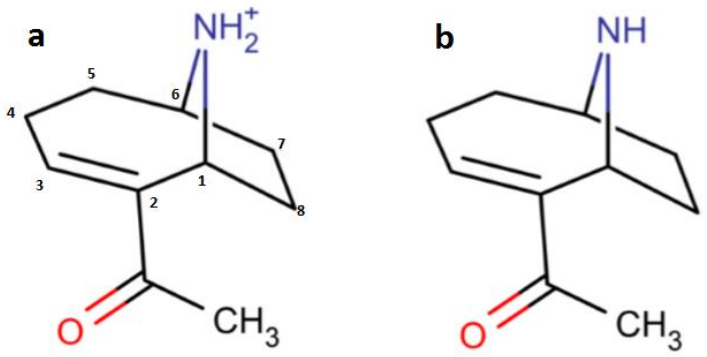

Figure 2.3 Molecular structures of ANTA: a) protonated ANTA stereoisomer, b) deprotonated ANTA (Vlad et al., 2014)

ANTA is an acutely neurotoxic alkaloid and was formerly known as very fast death factor, VFDF, with an LD_{50} of 380 µg/kg (i.p. mouse) (Table 2.2), resulting in considerable numbers of animal deaths globally (Valentine et al., 1991; Faassen et al., 2012). High-level exposure of ANTA causes muscular paralysis and even death from respiratory arrest; however, the chronic effects associated

with low-level exposure remain to be clearly investigated, particularly with respect to human and animal reproduction (Osswald et al., 2007).

Generally, ANTA is detected at low environmental concentrations (below 10 µg/L) (Fristachi et al., 2008; Szlag et al., 2015). Based on a Midwest U.S. survey, 30% of the lake samples contained ANTA with concentrations ranging from 0.05 - 9.5 µg/L (Graham et al., 2010). However, ANTA has been detected at concentrations up to 156 µg/L in raw water, while it has been reported that up to 10 µg/L has been measured in treated drinking water in Florida (Burns, 2005). Some regulators have issued maximum ANTA target concentrations for the purpose of drinking water protection, based on current knowledge of ANTA toxicity, potential health effects, as well as the frequency and concentrations of ANTA detections, as shown in Table 2.3 (Vlad et al., 2014). In addition, Fawell et al. (1999) recommended a drinking water guideline value for this toxin to be 1 µg/L, aiming to provide a safety margin of three orders of magnitude of protection against the adverse effects (based on LD_{50}). At present, no national regulations or guidelines exist in the United States or Canada, but ANTA along with MC-LR and CYL is included in the USEPA CCL4 (USEPA, 2016), which reaffirms the need for further study on ANTA and the potential for forthcoming regulations.

2.3 Drinking Water Treatment of Extracellular Cyanotoxins

2.3.1 Activated Carbon Adsorption

Typically, two forms of activated carbon are employed in drinking water treatment, including powdered activated carbon (PAC) applied at the front end of a plant on an as-needed basis, and granulated activated carbon (GAC) which is contained in a filter or contactor. PAC and GAC are typically made from three base materials, including coal, wood, and coconut, and are produced via various activation methods, such as steam activation, to create a large volume of pores with a large number of potential adsorption sites. While activated carbons have no impact on intercellular

cyanotoxins, they can effectively remove extracellular MC-LR, CYL, and ANTA (Merel et al., 2013).

2.3.1.1 Powdered Activated Carbon

As cyanobacterial blooms are seasonal in many countries, PAC is currently a more popular adsorptive treatment option for cyanobacterial metabolites, such as geosmin, providing greater flexibility and being less impacted by pre-loading effects than is GAC (Vlad et al., 2014). However, most cyanotoxins are present intercellularly during the bloom growth phase. As it is typically applied at the front end of plant, the effectiveness of PAC can therefore be limited, given PAC is only effective for the removal of extracellular toxins (Vlad et al., 2014). The intercellular toxin which is unaffected by PAC, might be released by cell lysis in subsequent treatment processes, such as oxidation, resulting in the release of extracellular toxin.

Donati et al. (1994) investigated the adsorption of MC-LR on 8 PACs and found that PACs with the greatest volume of mesopores (pore diameter in the range of 2-50 nm) were the most efficient adsorbent in surface water. Ho et al. (2011) reported that CYL, whose molecular dimensions are smaller than those of MC-LR, was more quickly adsorbed than MC-LR using two coal-based PACs. PAC removal studies for ANTA are extremely limited, but Hart et al. (1998) showed that PAC was effective for ANTA removal, but that the doses required to achieve high degrees of toxin removal were much higher than those normally used in water treatment. This suggested that, from a practical perspective, PAC might not be able to remove ANTA in isolation. Vlad et al. (2014) investigated ANTA adsorption using 6 GACs and 1 PAC, and as expected, found that PAC vastly outpaced the GACs with much greater capacity in both ultrapure and natural water, in batch tests. However, PAC performance is highly affected by competition from background natural organic carbon (NOM), which is discussed in Section 2.4.

2.3.1.2 Granular Activated Carbon

GAC can be integrated into a filter media (typically replacing anthracite) or as a contactor which contains only GAC (Westrick et al., 2010). GAC filters are used to remove particulates, adsorb chemicals, and biodegrade organic contaminants, and as is the case with contactors may need to be replaced after a few months or years in service. Replacement of GAC is usually dictated by regulatory exceedances in cases where biological activity is insufficient to reduce the contaminant levels to specified target concentrations (such as in the case of perfluoroalkyl substances).

Newcombe (2002) found MCs in the effluent of a pilot-scale GAC column with 80% TOC breakthrough within 2 months of service, which was a much shorter service life than expected, making the technology, as utilized, ineffective for MC removal. But, GAC adsorbers with appropriate replacement or regeneration might be able to remove MCs effectively. Newcombe et al. (2003) revealed that the net charge of MC-LR potentially affects GAC adsorption by electrostatic interactions and that biodegradation might occur on pre-loaded GAC, resulting in enhanced MC-LR removal. Chennette (2017) investigated various seasonal storage methods for pre-loaded GAC to maintain its capacity for MC-LR treatment. This work found that storage under low moisture content conditions provided the most benefit.

Very few studies have focused on GAC adsorption of ANTA. Hart et al. (1998) examined a rapid small-scale column filled with coal-based GAC with an EBCT of 6 minutes and obtained over 90% initial removal of ANTA but 80% breakthrough occurred after 35,000 bed volumes (equivalent to 18-weeks of operation) with an influent concentration of 8.2 µg/L. Another study pointed out that the two removal mechanisms of ANTA, adsorption and biodegradation, were hard to distinguish (UKWIR, 1996). Vlad (2014) compared the ANTA adsorption performance of 6 GACs made from three base materials (coal, wood, and coconut) in both ultrapure and natural water, using the bottle-point method. The author found that the coal-based GACs had the highest capacity but slowest adsorption rate.

No studies of CYL adsorption on GAC could be found in the refereed literature, indicating the need for further investigation.

2.3.2 Membrane Filtration

Typically, membranes separate cyanotoxins by size and charge associated with their physio-chemical properties. The separation processes discussed here are categorized into three groups, including reverse osmosis, nanofiltration, and ultrafiltration (Westrick et al., 2010). Gijsbertsen-Abrahamse et al. (2006) reported over 96% removal of MC-LR and ANTA using reverse osmosis, with only ANTA being detected in the permeate. In this study, the authors predicted a rejection of 90% at full-scale for the two tested cyanotoxins. Teixeira & Rosa (2006) investigated the removal of MCs and ANTA using negatively charged nanofiltration membrane, and found that ANTA rejection involved electrostatic interactions and steric hindrance, while MC rejection was only associated with steric hindrance. No studies on CYL removal by nanofiltration and reverse osmosis filtration could be found. Further investigation of the mechanisms of cyanotoxin membrane rejection is necessary, as this treatment barrier may be pH- or variant-dependent, if the rejection is involved with intermolecular interactions (Westrick et al., 2010).

2.3.3 Biofiltration

Biofiltration has been reported to be a potentially effective technology for removal of cyanotoxins, while its performance is highly dependent on environmental variables, including temperature, pH, and NOM composition (Newcombe, 2002). Grutzmacher et al. (2002) conducted two full-scale experiments using biologically activated slow sand filtration and reported over 95% removal of MCs in the summer, but less than 65% removal in fall. The remarkable reduction of removal efficiency was most likely related to a decrease in temperature. Ho et al. (2006) confirmed biodegradation through rapid sand biofiltration for MC-LR at batch-scale at room temperature (20 ± 2°C), with a lag period of 3 days prior to the commencement of degradation. The lag period suggests that the bacteria responsible for MC-LR degradation might require some time to establish

a critical biomass to initiate MC-LR degradation. In this study, no MC-LR was detected in the effluent after 4 days, even under typical rapid sand conditions with short contact times. A similar experiment was conducted using the wood-based Picazine® GAC and the lag period was found to be 8 days prior to the commencement of degradation (Ho & Newcombe, 2007). Ho et al. (2005) further examined biofiltration of CYL in parallel pilot-scale roughing and sand filters and following an acclimation period of 12 months found almost complete removal of soluble CYL after 20 days of biofiltration, given an initial concentration of 23 µg/L in surface water. Rapala et al. (1994) conducted a batch-scale sediment experiment on the biodegradation of ANTA in natural water, and found a 4 days lag period before commencement of degradation.

2.3.4 UV Disinfection

Typically, UV is implemented to inactivate pathogens in drinking water by breaking molecular bonds without chemical addition (Westrick et al., 2010). CYL, MC-LR, and ANTA can undergo photolytic destruction at UV doses ranging from 1,530 and 20,000 mJ/cm^2, which are much higher than the dose normally used for disinfection (10 to 40 mJ/cm^2) (Tsuji et al., 1994; Chorus & Bartram, 1999; Senogles et al., 2000). Given the high dose required, UV treatment in isolation might not be a viable treatment barrier for cyanotoxins (Westrick et al., 2010).

2.3.5 Oxidation and Advanced Oxidation Processes

Typically, the oxidants used in drinking water include one or more of the following: chlorine, chloramine, chlorine dioxide, ozone, hydroxyl radical, and potassium permanganate. Table 2.4 summarizes the inactivation potential of cyanotoxins by these oxidants.

As the primary oxidant used in drinking water disinfection over the last 100 years, chlorine has been investigated for its ability to remove organic contaminants, such as cyanotoxins. Inactivation of cyanotoxins by chlorine is generally pH-dependent due to the pK_a of hypochlorous acid (7.6) (Westrick et al., 2010). Ho et al. (2006) reported that chlorine was effective for MC-LR inactivation, achieving 90% MC-LR removal in two natural waters with a chlorine dose of 1.5 mg/L and 0.5 h

contact time at DOC levels lower than 5 mg/L. Acero et al. (2005) found increasing MC-LR half-life with enhancing pH levels, indicating chlorine was more effective in the lower pH range (pH < 8) within typical contact times in drinking water treatment plants. Chlorine is also able to inactivate CYL between pH 6 and 9 (Nicholson et al., 1994; Senogles et al., 2000); however, two hepatoxic by-products, chlorouracil, 5-chloro-cylindrospermopsin (Senogles et al., 2000) and a carboxylic acid derivative (Banker et al., 2001), were identified. Unlike MC-LR, CYL was determined to be more susceptible to chlorination at higher pH levels (Senogles et al., 2000). In contrast, Rodríguez et al. (2007) found that the maximum chlorination destruction rate of CYL was at pH 7. The inactivation of ANTA by chlorine is too slow a process to be considered as an effective treatment barrier (Hrudey et al., 1999; Rodríguez et al., 2007).

Chloramine and chlorine dioxide are not effective treatment barriers for CYL, MC-LR, and ANTA in natural water due to the oxidant demand exerted by background NOM (Westrick et al., 2010).

Potassium permanganate has been found to be an effective oxidant for the inactivation of MC-LR and ANTA (Rodríguez et al., 2007), by reacting with double bonds to create diols but very little information on its reactivity with amines is available (Westrick et al., 2010). The reactivity of this oxidant is not pH-dependant for MC-LR inactivation (Westrick et al., 2010). Unlike MC-LR, the inactivation of ANTA by potassium permanganate is highly pH-dependent, and the apparent rate constant doubles between pH 8 and 10 (Rodríguez et al., 2007). CYL cannot be inactivated by potassium permanganate at dosages commonly employed (Banker et al., 2001; Rodríguez et al., 2007).

Oxidation and hydroxyl radicals are the two typical ozonation mechanisms (Westrick et al., 2010), as ozone targets alkene, activated aromatic, and neutral amine functional groups, whereas hydroxyl radicals randomly react specifically with the carbon-hydrogen bonds in cyanotoxins (Von Gunten & Hoigné, 1994). Onstad et al. (2007) found molecular ozone targeted the conjugated double bond and single double bond in the Adda and the Mdha group, respectively, of MC-LR and that this

reaction is not pH-dependent. However, ozone oxidation of CYL and ANTA is pH-dependent between pH 7 and 10, and pH 4 and 10, respectively, in agreement with the pK_a values of the CYL uracil moiety and ANTA amine (Onstad et al., 2007). The reaction rates of cyanotoxins by ozone oxidation are ordered as follows: MC-LR > CYL > ANTA at pH 8 (Onstad et al., 2007).

Advanced oxidation processes are those associated with generating and using relatively non-selective hydroxyl radicals by either photochemical (UV) or non-photochemical approaches (ozone) (Westrick et al., 2010). Hydroxyl radicals have been reported to effectively inactivate cyanotoxins in the same order as does molecular ozone: MC-LR > CYL > ANTA (Song et al., 2006; Onstad et al., 2007).

Table 2.4 Summary of cyanotoxin inactivation potential by oxidants (Westrick et al., 2010)

	CYL	MC-LR	ANTA
Chlorine	Yes	Yes	No
Ozone	Yes	Yes	Yes
Chloramine	No	No	No
Chlorine dioxide	No	No	No
Hydroxyl radical	Yes	Yes	Yes
Potassium permanganate	No	Yes	Yes

2.4 Competitive Effect of Micropollutant Adsorption in Natural Water

In general, the adsorption process can be summarized in four consecutive steps: 1) bulk liquid phase transport, in which an adsorbate transports from the bulk liquid phase to the hydrodynamic boundary layer surrounding the adsorbent particle, 2) film diffusion or external diffusion, in which an adsorbate transports through the boundary layer to the exterior of the adsorbent, 3) intraparticle diffusion or internal diffusion, in which an adsorbate is transported into the interior of the adsorbent particle by pore diffusion (diffusion in the pore liquid) and/or by surface diffusion (diffusion in the adsorbed state along the internal surface), and 4) final adsorption, in which the adsorbate develops an energetic interaction at the final adsorption sites (Worch, 2012).

During the adsorption process, micropollutants such as cyanotoxins compete for adsorption sites with NOM in all natural waters, resulting in a substantial reduction in the adsorption capacity for micropollutant (Sontheimer et al., 1988). As the concentration of NOM is much higher than that of micropollutants in natural waters, competitive adsorption negatively impacts micropollutant removal (Worch, 2010). The mechanism of this competitive effect is generally summarized as: 1) direct competition, as small NOM molecules directly compete with micropollutant for access to the adsorption sites; 2) pore blockage by NOM, as large NOM molecules accumulate and block the small pores or access to the pores, preventing a micropollutant from accessing adsorption sites (Yu, 2007). Given the short contact time in the application of PAC, the competitive effect is mainly attributed to direct competition rather than pore blockage (Matsui et al., 2003). In contrast, the pore blockage mechanism is predominant for activated carbons preloaded with NOM, which is likely the case for GAC contactors with long service lives (Knappe et al., 1999).

Research has focused on the competitive effect of NOM on micropollutants in natural waters and unknown mixtures since the mid 1980's (e.g. Andrews, 1990). Najm et al. (1991) developed the concept of the single equivalent background compound (EBC), representing a portion of NOM that could directly compete for the adsorption sites in natural water, based on the ideal adsorbed solution theory (IAST) and Freundlich isotherm model. Since then, this IAST-EBC or EBC concept has been widely applied to describe competitive adsorption on PAC in natural water, which is dominated by direct competition. Knappe (1996) and Gillogly (1998) successfully predicted the adsorption of atrazine and MIB in natural water using the EBC concept, and reported that the percent removal of the target compound was essentially independent on its initial concentrations. Graham et al. (2000) found that the interactions between different micropollutants are negligible in the presence of the strong competitive effect of NOM. Further studies indicated that the NOM competition varied for different micropollutants. For example, a low molecular weight NOM fraction was found to the most likely to directly compete with MIB for adsorption sites (Newcombe

et al., 2002; Hepplewhite et al., 2004). Matsui et al. (2003) found NOM had negligible effect on pore diffusion, suggesting direct competition instead of pore diffusion as the main mechanism for the reduction of PAC capacity for a target micropollutant. However, Ebie et al. (2001) reported that both direct competition and pore blockage contributed to the reduction of PAC capacity for four agricultural chemicals, including dichiorvos, fenobucarb, fenitrothion, and thiobencarb. Qi et al. (2007) derived a simplified version of the EBC model, the SEBCM, based on the assumption that the EBC had similar adsorptive potential to the adsorption sites and was present at a much higher concentration than the target micropollutant. The SEBCM was applied to describe the competitive adsorption of geosmin and 2-MIB in natural water under both equilibrium and non-equilibrium conditions (Zoschke et al., 2011). This study confirmed the applicability of the SEBCM and demonstrated that the SEBCM which was developed for equilibrium conditions can also be used to describe competitive adsorption under non-equilibrium conditions. This finding made the simplified model even more acceptable and practical for engineering, as the PAC contact time in drinking water treatment plant is typically shorter than the time required to reach adsorption equilibrium.

2.5 Conclusions and Research Gaps

Cyanobacteria have long been known to produce toxins which may be of concern to the health of animals and humans. With the advent of new detection methods and regulatory limits being set or considered, drinking water providers now need to assess the potential for their existing technologies to remove these toxins, and if necessary, upgrade their treatment processes. Activated carbon can be an effective barrier for extracellular cyanotoxins in conventional drinking water treatment plants. However, activated carbon performance is highly affected by competitive adsorption of NOM which is present in virtually all natural waters. The majority of PAC studies published to-date have focused on its performance as a treatment strategy for extracellular cyanotoxins under equilibrium

conditions, but there has been very little quantification of PAC adsorption with respect to the short contact time typical in water treatment. Furthermore, GAC performance for CYL removal remains uncertain, as no previously published research articles could be located at this time.

Chapter 3
Cyanotoxin Adsorption by Powdered Activated Carbon in Ultrapure Water

3.1 Summary

The adsorption of CYL, MC-LR, and ANTA by three commercially available PACs (with different base materials: coal, wood, and coconut) was examined using the bottle point technique in ultrapure water buffered to pH 7. The wood-based BG-HHM removed all three cyanotoxins the fastest, while the coal-based COL-PL60-800 was the slowest. The mesoporous BG-HHM (wood) favors the adsorption of larger molecules, such as MC-LR and CYL. Toxin type influences adsorption rate, as ANTA was much more slowly adsorbed than the other two cyanotoxins, regardless of the PAC used in this study. At equilibrium, the capacity of the three cyanotoxins was quite different with the BG-HHM (wood) having the greatest capacity for CYL, the COL-PL60-800 (coal) retained the greatest capacity for MC-LR, and the WPC (coconut) had the greatest capacity for ANTA. However, PAC contact times in full-scale WTPs are typically shorter than the time it takes to reach equilibrium. To address this, experiments were conducted under non-equilibrium conditions using contact times of 0.5 and 1 h which are more typical of treatment practice (and compared to equilibrium data). Under these conditions the wood-based PAC outperformed the other two carbons, as it had the highest carbon loading for all 3 toxins.

3.2 Introduction

Cylindrospermopsin (CYL), anatoxin-a (ANTA), and microcystin-LR (MC-LR) are included in the fourth iteration of the USEPA Contaminant Candidate List (CCL 4) (USEPA, 2016). The USEPA also issued health advisories for CYL and microcystins in 2015; 0.7 µg/L CYL and 0.3 µg/L MC-LR for children younger than 6-years old, and 3 µg/L CYL and 1.6 µg/L MC-LR for the remaining population (USEPA, 2015). The Canadian Drinking Water Guidelines stipulate a maximum

acceptable concentration (MAC) for MC-LR in drinking water of 1.5 µg/L (Health Canada, 2017). This guideline was recently reviewed and it has been proposed to extend the MAC of 1.5µg/L to total microcystins. While no current US or Canadian regulations exist for ANTA in drinking water, the Province of Quebec has a provisional guideline of 3.7 µg/L (Institute National de Santé Publique du Québec, 2005).

So far, toxic cyanobacteria have been discovered in 27 countries worldwide. CYL, ANTA, and MC-LR are the three most detected and studied cyanotoxins in North American surface water (Merel et al., 2013). In North America, CYL has been reported in concentrations of up to 202 µg/L in the states of Florida and Louisiana (Yilmaz & Philips, 2011), and CYL was also reported in the state of New York and the Lower Great Lakes (Boyer, 2008). ANTA has been widely detected in North American surface water, including western Lake Erie, Lake Ontario, Lake Champlain (New York State), and the lower Great Lakes watershed (Yang, 2005). ANTA concentration of up to 5.6 µg/L have been detected in Canada with numerous reports of animal poisoning and death (Manitoba Water Stewardship, 2011). MC-LR is widely reported in North America, including New York, Nebraska, New Hampshire and Florida, and detections of microcystins in ambient waters have been observed with concentrations of up to 31,470 µg/L (Fristachi et al., 2008). In a study of 180 New York lakes and rivers, more than half of the collected samples had detectable levels of microcystins, some with concentrations of over 1000 µg/L (Boyer et al., 2004).

Based on a review of cyanotoxin drinking water treatment technologies, powdered activated carbon could potentially be a promising treatment barrier for all three studied cyanotoxins, however, systematic studies on the adsorption of ANTA and CYL remain to be conducted (Westrick et al., 2010; He et al., 2016). PAC has been widely used at the front end of water treatment plants for taste and odor control primarily treating the cyanobacterial metabolites, geosmin and MIB. It would be practical and cost-effective to use the PAC that is already applied for taste and odor control to remove cyanotoxins as well. It should be noted that PAC is only effective for extracellular

cyanotoxins i.e. dissolved cyanotoxins. Intracellular cyanotoxins cannot be removed by the PAC since they are contained within the cyanobacterial cells (Merel et al., 2013). Some oxidants, such as ozone, can increase the risk of cell lysis in the WTP, which may lead to toxin release after PAC contact.

The adsorptive capacity of PAC for a specific adsorbate depends on a variety of factors including carbon properties, water matrix, temperature, as well as the properties and concentrations of the adsorbate (Crittenden et al., 2012). Bailey et al. (1999) reported high CYL removal efficiency by a wood-based PAC at doses below 30 mg/L in natural water, with 30 minutes of contact time. Aldridge et al. (2001) reported 50% CYL removal using only 2.7 mg/L of PAC for an initial CYL concentration of 2.5 µg/L. However, no details were provided regarding the contact time or type of activated carbon. Limited data are available on the adsorption of ANTA by PAC. Hart & Stott (1993) reported very different adsorption performance of a chemically activated wood-based PAC for removal of ANTA and MC-LR in natural water, suggesting that the most suitable carbon could be different for the two compounds. Keijola et al. (1988) also obtained reasonable removal of ANTA, while no details on the type of PAC or water quality were provided. Vlad (2015) reported about 70% of ANTA removal within 0.5 h of contact with a coal-based PAC (AC Watercarb 800) in ultrapure water, at an initial concentration of 100 µg/L. Several studies have reported that chemically activated wood-based PACs are superior for MC-LR adsorption (Hart & Stott, 1993; Donati et al., 1994). Donati et al. (1994) attributed the high removal efficiency to the volume of large pores (2 - 50 nm) in the wood-based carbons, being appropriately sized for MC-LR molecule. Based on the available literature, different cyanotoxins can be adsorbed differently on a single PAC product, and the most suitable PAC is potentially different for each cyanotoxin. Examining cyanotoxin adsorption in ultrapure water provides a baseline of adsorption behavior of each cyanotoxin, which makes is easier to compare PAC treatment performance for the various cyanotoxins. Ultrapure water results for a single cyanotoxin can also be compared among various

PAC products to identify promising candidates for the removal of a particular carbon. However, very few PAC studies in ultrapure water PAC could be found in the literature.

The primary objective of this study was to investigate the removal of CYL, MC-LR, and ANTA by PAC adsorption in ultrapure water to provide baseline performance data to compare with other studies. Ultrapure water experiments provide a baseline a baseline of adsorption behavior with which other studies can compare with when done. The detailed objectives of this research were to 1) evaluate the rate of adsorption for each of the target cyanotoxins for each of the selected PACs, and 2) compare the PAC adsorption capacities for each target cyanotoxin under both equilibrium and non-equilibrium conditions. In a departure from some previous studies carbon capacities were also determined under non-equilibrium conditions, using PAC contact times of 0.5 and 1 h, more typical of full-scale water treatment practice.

3.3 Materials and Methods

3.3.1 Materials

BG-HHM (wood) and WPC® (coconut) PACs were donated by Brenntag Canada (Ontario, Canada), the distributor of Calgon Carbon Corporation (PA, USA) at no charge. The COL-PL60-800 coal-based PAC manufactured by Carbon Activated Corporation (NY, USA) was provided by City of London (Canada), where it is used seasonally for taste and odor control.

CYL was obtained from GreenWater Laboratories (FL, USA), microcystin-LR was obtained from EMD Millipore (ON, CA), ± anatoxin-a fumarate was obtained from Cayman Chemical (MI, USA), potassium phosphate monobasic, potassium phosphate dibasic, 1,9-diaminononane and formic acid were obtained from Sigma-Aldrich (WI, USA), while cyclo (ArgAla-Asp-D-Phe-Val) (cyclo) (c(RADfV)) was obtained from Peptides International (KY, USA). Acetonitrile was of liquid chromatography-mass spectrometry (LC-MS) grade. High purity water was produced by a

Millipore Milli-Q® UV PLUS water system (MA, USA). The Luer lock syringe and the 4 mm diameter 0.45 µm nylon syringe filters were provided by VWR International (PA, USA).

Stock solutions for each cyanotoxin were prepared by dissolving 1 mg of solid standard into 10 mL of Milli-Q® water. For each cyanotoxin, a working solution of 1 mg/L was then prepared from its stock solution. A 100 mg/L c(RADfV) stock solution of was prepared with Milli-Q® water, and was diluted to a 1 mg/L working solution. A 1000 mg/L stock solution of 1,9-diamininonane was prepared using Milli-Q® water, and was diluted to a working solution of 10 mg/L. Stock solutions were prepared monthly, whereas working solutions were refreshed weekly. All prepared solutions were stored in amber glassware at -20 °C.

3.3.2 Carbon Analysis

The PAC samples were analyzed by the Waterloo Institute for Nanotechnology (ON, Canada) for porosity and surface area. The Brunauer-Emmett-Teller (BET) adsorption theory was used to determine surface area, and the density functional theory (DFT) was used to measure pore distribution of each PAC product (Graf & Kappl, 2006). The measurements of BET surface area and DFT pore volumes were performed in the Chemical Engineering Department at the University of Waterloo. The point of zero charge (pH_{PZC}), indicating the pH at which PACs carry a net-zero charge density, was determined based on Summers (1986).

3.3.3 Sample Preparation and Handling

The bottle-point method (Droste, 1997) was employed to investigate the adsorption of each of the three cyanotoxins by PACs in Milli-Q® water at bench-scale. As recommended by Worch (2012) and adapted from Sontheimer et al. (1988), the PACs were dried at 110 °C for 24-36 h, and then stored in desiccators prior to measuring the dry weight of each adsorbent.

Milli-Q® water was produced and collected as a batch, stored to equilibrate overnight, and adjusted to pH 7 using potassium phosphate buffer. The adsorption behavior of PAC in ultrapure water was compared to that in surface water in Chapter 4.

This study used single-solute solutions. For each cyanotoxin, one batch experiment was designed for each PAC product. For each batch, 4.5 L of 100 µg/L cyanotoxin solution was prepared in a reservoir using buffered ultrapure water at pH7 which was then distributed to 9 glass bottles with 500 mL of cyanotoxin solution in each bottle. Among the 9 bottles, 8 were used for PAC adsorption test. For each PAC type, a range from 5-50 mg/L of carbon was added into 8 bottles. One of the 9 bottles which did not contain PAC, was used as a positive control to monitor cyanotoxin degradation. A negative control containing 500 mL of Milli-Q® water and 50 mg/L of PAC, and one blank containing only 500 mL of Milli-Q® water were included to exclude any compounds that could possibly be misidentified as the test cyanotoxin.

All samples and controls were placed onto 3 orbital shakers at 150 rpm with an opaque cover to minimize light exposure. The cyanotoxin concentrations in the sample bottles containing the highest PAC dose (50 mg/L) were monitored by analyzing 1 mL aliquot from the bottles at pre-set time intervals. Concentrations of each selected cyanotoxin in each of the sample and control bottles were measured at 0.5 h and 1 h contact time and at equilibrium, and then used to generate Freundlich adsorption loading plots and isotherms. For CYL adsorption, COL-PL60-800 (coal), BG-HHM (wood) and WPC (coconut) reached equilibrium after 6 h, 2 h and 2 h, respectively. In terms of MC-LR adsorption, the equilibrium times for COL-PL60-800 (coal) and WPC (coconut) were 6 h, while BG-HHM (wood) reached equilibrium the fastest after 1 h. With respect to ANTA adsorption, BG-HHM (wood) and WPC (coconut) achieved equilibrium after 72 h and COL-PL60-800 (coal) needed 168 h to reach equilibrium. The positive controls remained relatively stable throughout the study with reduction losses being less than 10%. Equilibrium concentrations below

the method detection limit (listed in Section 3.3.4) of the LC-MS/MS method were not considered for isotherm estimation (less than 5% of all measured data points).

3.3.4 Cyanotoxin Analysis by LC-MS/MS

CYL, MC-LR and ANTA concentrations were measured using a Shimadzu 8030 liquid chromatography tandem mass spectrometer (LC-MS/MS) system, composed of a Shimadzu DGU-20A3R degassing unit and a Shimadzu LC-20 ADXR pump with 100 µL looping system. The system contained a tandem quadrupole mass spectrometer analyzing various analytes via a multiple reaction monitoring (MRM) technique, which monitored a specific precursor ion and corresponding product ion(s) for each analyte. A 50 mm x 2.1 mm Pinnacle DB C18 analytical column with 1.9 µm packing (Restek, PA, USA) was used and heated to 35 ℃ for analysis. Two internal standards, 1,9-diaminononane and c(RADfV), were selected for analysis at concentrations of 10 mg/L and 1 mg/L, respectively, based on Bogialli et al. (2006). The binary eluent employed an aqueous (with 0.1% formic acid) and an acetonitrile (with 0.1% formic acid) mobile phase at a flow rate of 0.3 mL/min, adapted from Oehrle et al. (2010).

Initially, a gradient method was developed to measure CYL, MC-LR, and ANTA simultaneously (Appendix A.1). Ultimately, the adsorption experiments were designed to use single-solute solutions. The gradient LC-MS/MS method was then split into two isocratic methods, an MC-LR method and a combined CYL/ANTA method, based on cyanotoxin characteristics. For the CYL/ANTA method, the eluent was composed of 4% of acidified organic mobile phase (0.1% formic acid in acetonitrile) and 96% of acidified aqueous mobile phase (0.1% formic acid in ultrapure water). In the MC-LR method, the acidified acetonitrile (0.1% formic acid in acetonitrile) was initially run at 20% for one minute and then increased to 80% over one minute and kept at 80% for three minutes, then increased to 100% over one minute and washed at 100% for four minutes, and finally returned to 20% over one minute and stayed at 20% for three minutes prior to the next injection. Injection volumes for both methods were adjusted to 20 µL and flow rates were 0.3

mL/min in both cases. MRM monitored 415.95>194.10 and 415.95>336.25 transitions for CYL, 498.30>135.05 and 995.20>134.95 transitions for MC-LR, 166.05>43.0 and 166.05>149.05 transitions for ANTA, 159.10>142.15 transition for 1,9-dianinononane, and 589.05>120.0 transition for c(RADfV). An eight-point linear calibration was established for each selected cyanotoxin in the range of 0.5-100 µg/L. The MDL for each cyanotoxin was evaluated based on Standard Methods (2012). The ultrapure water MDLs were determined as 0.2 µg/L for CYL, 0.1 µg/L for MC-LR, and 0.3 µg/L for ANTA. The Lake Erie water MDLs were provided in Section 4.3.2. Internal standard quantification was applied in the analysis using 1,9-diaminononane for CYL and ANTA analysis and c(RADfV) for MC-LR analysis. Samples were stored at -20 ℃. All samples were measured within 3 days of sampling. The frozen samples were thawed before measurements. One quality control standard was inserted after every ten samples to assure measurement stability. One set of calibration standards was measured along with one set of samples to correct instrument errors.

3.3.5 Data Analysis

3.3.5.1 Pseudo-First Order Model

The empirical pseudo-first order model is regarded as an effective tool to describe the kinetic behavior of GAC adsorption for a wide range of compounds in batch tests (Ho & McKay, 1999). Adsorption kinetics in a batch process can be modeled as:

$$\frac{dq_t}{dt} = k_1 * (q_e - q_t) \ldots\ldots\ldots\ldots\ldots\ldots\ldots\ldots\ldots\ldots (1)$$

where t represents the number of days elapsed, q_t (µg/mg) represents the amount of toxin adsorbed at time t, q_e is the amount of toxin adsorbed at equilibrium, and k_1 is the pseudo-first order adsorption constant.

By integrating Equation 1 over time (t), cyanotoxin adsorbed (q_t) yields:

$$\log(q_e - q_t) = log q_e - \frac{k_1}{2.303} * t \ldots \ldots (2)$$

3.3.5.2 Pseudo-Second Order Model

The empirical pseudo-second order model has also been widely used in batch tests to describe the kinetic behavior of GAC adsorption of a variety of compounds (Ho & McKay, 1999). The mathematical expression of the pseudo-second order model is demonstrated as follows:

$$\frac{dq_t}{dt} = k_2 * (q_e - q_t)^2 \ldots \ldots (3)$$

where t, q_t, and q_e are defined as per Equation 1, and k_2 represents the pseudo-second order adsorption constant.

By integrating Equation 3 over time (t), cyanotoxin adsorbed (q_t) yields:

$$q_t = \frac{q_e^2 * k_2 * t}{(1 + q_e * k_2 * t)} \ldots \ldots (4)$$

Equation 4 can be linearized as follows:

$$\frac{t}{q_t} = \frac{1}{k_2 * q_e^2} + \frac{1}{q_e} * t \ldots \ldots (5)$$

3.3.5.3 Freundlich Isotherm Model

The empirical Freundlich isotherm model is usually considered as having the best fit for activated carbon adsorption in the environmental treatment field (Reed et al., 1993) and is regularly applied in water treatment studies (Worch, 2012). The mathematical expression of the Freundlich isotherm model is as follows:

$$q_e = K_F * C_e^{1/n} \ldots \ldots (6)$$

Where q_e represents carbon loading (or amount of micropollutant, such as CYL, in µg that is adsorbed on the solid phase, or GAC in this study, in mg at equilibrium), C_e represents CYL

concentration at equilibrium in µg/L, and K_F and n are Freundlich parameters indicating adsorption strength and energetic heterogeneity of the adsorbent surface, respectively (Worch, 2012). If $n < 1$, adsorptive bond energies increase with surface density; if $n > 1$, bond energies decrease with surface density; and when $n = 1$, all adsorptive sites are equivalent (Reed et al., 1993).

In this study, the Freundlich isotherm model was applied to both the equilibrium and non-equilibrium data (contact times of 0.5 h and 1 h) obtained from bottle-point experiments, using non-linear least squares regression, as suggested by Worch (2012). Linear regression was not considered in this study, because the assumptions made for linear regression that errors are normally, identically and independently distributed about zero, will not hold when applying the linearized form of the Freundlich equation (Worch, 2012).

3.4 Results and Discussion

3.4.1 Carbon Properties

Three PACs were selected to round out the portfolio of commercially available products for drinking water treatment, representing a range of source materials, porosities, and particle size (Table 3.1).

Table 3.1 PAC properties

Product Name	Manufacturer	Base Material	Median Diameter[1] (nm)	pH_{PZC}[2]	BET Surface Area[1] (m^2/g)	DFT Method Pore Volume[1] (cm^3/g)	DFT Pore Size Distribution[1]			% of Pore Volume in Micropores[1,3]
							Primary Micropores <0.8nm (cm^3/g)	Secondary Micropores 0.8-2 nm (cm^3/g)	Mesopores 2-24 nm (cm^3/g)	
COL-PL60-800	Carbon Activated Corp.	Coal	45.1	10.8	837	0.44	0.09	0.16	0.18	57
BG-HHM	Calgon Carbon	Wood	31.9	3.5	1295	1.13	0.11	0.29	0.71	35
WPC	Calgon Carbon	Coconut	22.1	10.1	703	0.35	0.09	0.22	0.04	89

[1]experimentally determined by the Nanotechnology Lab at the University of Waterloo (external lab); [2]experimentally determined by the Wet Lab at the University of Waterloo; [3]micropores defined as < 2nm (Rouquerol et al., 1994)

3.4.1.1 Porosity and Surface Area

Based on median diameter (Table 3.1), the coal-based COL-PL60-800 was the largest particle among the three selected carbons, whereas the coconut-based WPC was the smallest. The wood-based BG-HHM had the greatest pore volume in the secondary micropore (0.8 - 2 nm) and mesopore range (2 - 24 nm). It also had the highest BET surface area and pore volume. The pore volume of the COL-PL60-800 (coal) was much closer to the WPC (coconut) carbon, although the WPC (coconut) had very little volume in the mesopore range, but the highest micropore portion as percentage of total pore volume. The molecular dimensions of cyanotoxins were calculated by MarvinSketch chemical editor (ChemAxon, Budapest, Hungary). CYL was 1.572 x 0.901 nm, MC-LR was 2.032 x 1.259 nm, and ANTA was 0.970 x 0.633 nm. With these dimensions, CYL might adsorb in a portion of the 0.8 - 2.0 nm secondary micropores, and along with MC-LR, the two toxins would fit within the 2 - 24 nm mesopores. ANTA would fit within the secondary micropores and the larger mesopores.

3.4.1.2 pH Point of Zero Charge

The surface charge of activated carbon is highly pH dependent, as the oxygen-containing functional groups on their surface can shift between protonated and deprotonated states at different pH levels, displaying either acidic and basic characteristics (Worch, 2010). Therefore, ionic adsorbates, such as cyanotoxins, can further interact with activated carbons by attraction or repulsion.

pH_{PZC} was employed in this study as a preliminary indicator of surface charge of activated carbon at target pH levels. The pH_{PZC} values for the selected PACs are reported in Table 3.1. The chemically-activated wood-based BG-HHM had the lowest pH_{PZC}, possibly due to the use of acid in the production process. The coal-based COL-PL60-800 and the coconut-based WPC had very similar points of zero charge values above 10, indicating that their surfaces would be positively charged below pH 10. In a typical drinking water treatment scenario with pH in the range from 6

to 8, the COL-PL60-800 (coal) and WOC (coconut) are positively charged, whereas the BG-HHM (wood) is negatively charged.

3.4.2 Rate of Adsorption in Ultrapure Water

The percent removal of each cyanotoxin in ultrapure water using the three PACs as a function of time is presented in Figure 3.1. All PACs achieved equilibrium for each toxin within 7 days, albeit at different rates. For CYL adsorption, the wood-based BG-HHM adsorbed the toxin the fastest and had similar performance to the coconut-based WPC throughout the test, achieving equilibrium after 2 h. The coal-based COL-PL60-800 adsorbed CYL at a slower pace, reaching equilibrium after 6 h. With respect to MC-LR adsorption, the BG-HHM (wood) outpaced all others and reached equilibrium after only 1 h. The COL-PL-60-800 (coal) and the WPC (coconut) both needed 6 h to achieve equilibrium for MC-LR adsorption. In terms of ANTA adsorption, BG-HHM (wood) and WPC (coconut) performed similarly reaching equilibrium after 72 h, while COL-PL60-800 (coal) had a much lower rate of adsorption, achieving equilibrium after 168 h. Comparing the adsorption rate among all studied cyanotoxins, ANTA was adsorbed much slower than CYL and MC-LR no matter which PAC was applied. Interestingly, the BG-HHM (wood) all three cyanotoxins the fastest, particularly at the first 1 h of contact. It should be noted that while mixing was maintained at a controlled constant shaker speed of 150 rpm, this batch test cannot be assumed to represent the mixing occurring in a full-scale plant, as it is highly variable and is influenced by reactor dimensions, shape, paddle type, etc.

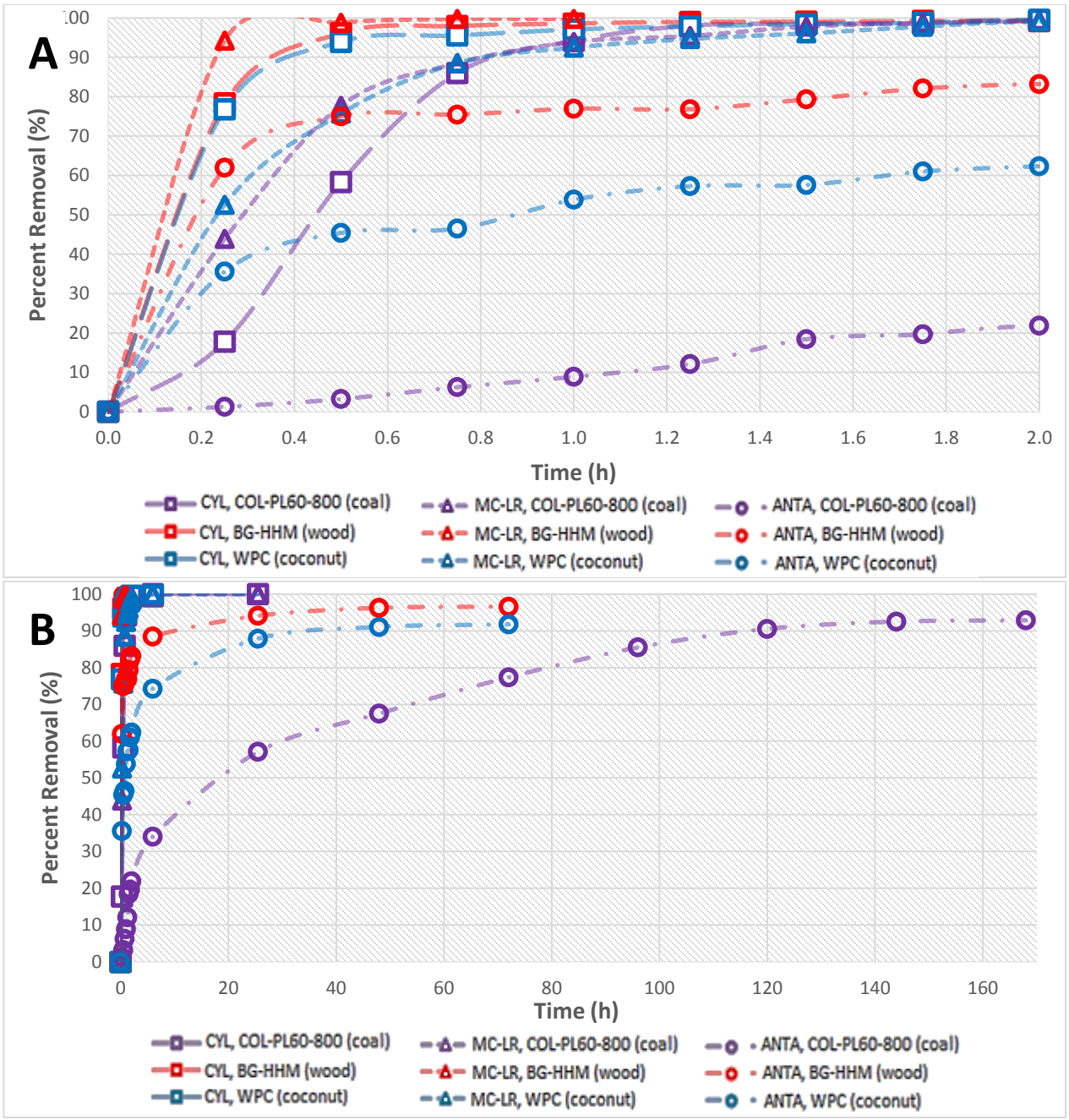

Figure 3.1 Percent removal of CYL, MC-LR and ANTA as a function of time in buffered ultrapure water (pH 7); 100 µg/L initial cyanotoxin concentration, 50 mg/L PAC dose. A) 2 h exposure; B) 170 h exposure.

Both pseudo-first and -second order models were fit to the cyanotoxin percent removal data obtained from the highest PAC dose bottle over time. The two empirical models are curve-fitting relationships describing experimental data and are used to compare adsorption performance among

PACs under the conditions investigated in this study. The R^2 values for the pseudo-first order model (Appendix A.3.) were lower than those of the pseudo-second order model (Table 3.2) and the predicted q_e deviated further from the experimentally determined value for the first order model compared to the second order model. In addition to R^2 calculations, residual plots were prepared to test for systematic errors. Analysis of the plots revealed that in the case of both the first- and second-order models (Appendix A.3). As is evident, there is trend of systematic error was detected in all pseudo-first order fittings and some of the pseudo-second order fittings. Therefore, neither the pseudo-first nor -second order model can accurately describe the cyanotoxin adsorption by PAC in ultrapure water. Pseudo-first order model often provided lower estimates of carbon loading, whereas the other model can provide closer estimates. Further investigation is required to identify a better kinetic model for the cyanotoxin adsorption data, while this is beyond the scope of this work. As such, the pseudo-second order model better described the observed kinetic data, so only this model was used to compare adsorption rates for cyanotoxin adsorption by the selected PACs in this study (Figure 3.2). Pseudo-first order model plots/data are shown in Appendix A.3.

Based on the pseudo-second order adsorption rate (k_2), the BG-HHM (wood) outperformed the COL-PL60-800 (coal) and the WPC (coconut) for adsorption of each studied cyanotoxin, with k_2 values ranging from 1.66 - 69.68 mg/µg/h (Table 3.2). This may be partially attributed to the higher proportion of mesopores in the BG-HHM (wood) carbon (0.71 cm^3/g) as compared to the COL-PL60-800 (coal) and WPC (coconut) (0.04 - 0.18 cm^3/g) (Table 3.1), providing shorter diffusion paths to the adsorption sites. Similarly to Vlad et al. (2015), the lower point of zero charge of the BG-HHM (wood) likely contributes to its faster adsorption of ANTA compared to the other two PACs. At the pH of the ultrapure water (6.4), ANTA (pKa = 9.4) exists predominantly in its protonated, positively-charged state, and the BG-HHM (wood) is negatively charged, resulting in attractive interactions, which may have increased the adsorption rate. Electrostatic interactions seem to play a role in ANTA adsorption, but this does not seem the case for MC-LR. The net charge

of MC-LR is negative in the pH range from 2.19 to 12.48 (de Maagd et al., 1999) and the BG-HHM (wood) is also negatively charged, producing the potential for repulsive forces that may reduce the rate of MC-LR adsorption. CYL exists as a zwitterion with no net charge at typical drinking water pH values i.e. 6.0 - 8.5, and carbon surface charge might not result in additional interactions (attraction or repulsion) between CYL and the adsorbent.

The WPC (coconut) PAC (14.58 mg/µg/h) adsorbed CYL substantially faster than did the COL-PL60-800 (coal) (2.23 mg/µg/h). In the case of MC-LR adsorption, the COL-PL60-800 (coal) and WPC (coconut) performed very similarly (2.07 mg/µg/h for COL-PL60-800 and 2.01 mg/µg/h for WPC). The rate of ANTA adsorption by the WPC (coconut) (0.67 mg/µg/h) was faster than that of the COL-PL60-800 (coal) (0.05 mg/µg/h). The calculated rate constants (Table 3.2) agree with the findings obtained by visual observation from Figure 3.1.

The experimental and modeled equilibrium carbon capacity (q_e) values were quite similar with all values being close to 2 µg/mg, while the modeled q_e value estimates were only very slightly higher than the experimental q_e results in all cases.

Table 3.2 Pseudo-second order kinetic model parameters for PACs in buffered ultrapure water

Toxin	PAC	Equilibrium Carbon Capacity, qe experimental (µg/mg)	Equilibrium Carbon Capacity, qe predicted (µg/mg)	k_2 (mg/µg/h)	R^2
CYL	COL-PL60-800 (Coal)	2.18	2.20	2.23	0.9979
CYL	BG-HHM (Wood)	2.15	2.16	24.56	0.9999
CYL	WPC (Coconut)	2.15	2.17	14.58	0.9999
MC-LR	COL-PL60-800 (Coal)	2.06	2.07	5.73	0.9999
MC-LR	BG-HHM (Wood)	2.11	2.12	69.68	0.9998
MC-LR	WPC (Coconut)	2.01	2.01	5.80	0.9999
ANTA	COL-PL60-800 (Coal)	1.90	1.99	0.05	0.9907
ANTA	BG-HHM (Wood)	2.11	2.11	1.66	0.9999
ANTA	WPC (Coconut)	1.94	1.96	0.67	0.9997

3.4.3 Ultrapure Water Isotherms

3.4.3.1 Freundlich Parameter Joint Confidence Region

Based on the mathematical structure of the Freundlich isotherm equation (Equation 6), the two isotherm parameters (K_F and 1/n) are highly correlated, indicating that the estimates of one parameter is greatly impacted by the estimates of the other parameter. Therefore, the confidence interval of a single parameter cannot provide a thorough profile of the model estimates based on experimental data. However, joint confidence regions (JCRs) take the correlation between parameters into consideration, and JCRs were calculated at the 95% confidence level for k_F and 1/n for the adsorption of each selected cyanotoxin by each studied PAC. Calculation procedures are provided in Appendix A.5. The JCR results are summarized in Figure 3.2, showing a high level of correlation between the two isotherm parameters. For CYL adsorption, the JCRs for the COL-PL60-800 (coal) and the WPC (coconut) almost completely overlap, indicating that statistically no difference exists between the estimates of isotherm parameters for those two carbons at the 95% confidence level, which is consistent with their similar performance. Those two completely overlapping CYL JCRs slightly overlap with the COL-PL60-800 (coal) JCR calculated from MC-LR batch. All other JCRs do not overlap and therefore they are statistically distinguishable from each other and from the 3 overlapping JCRs.

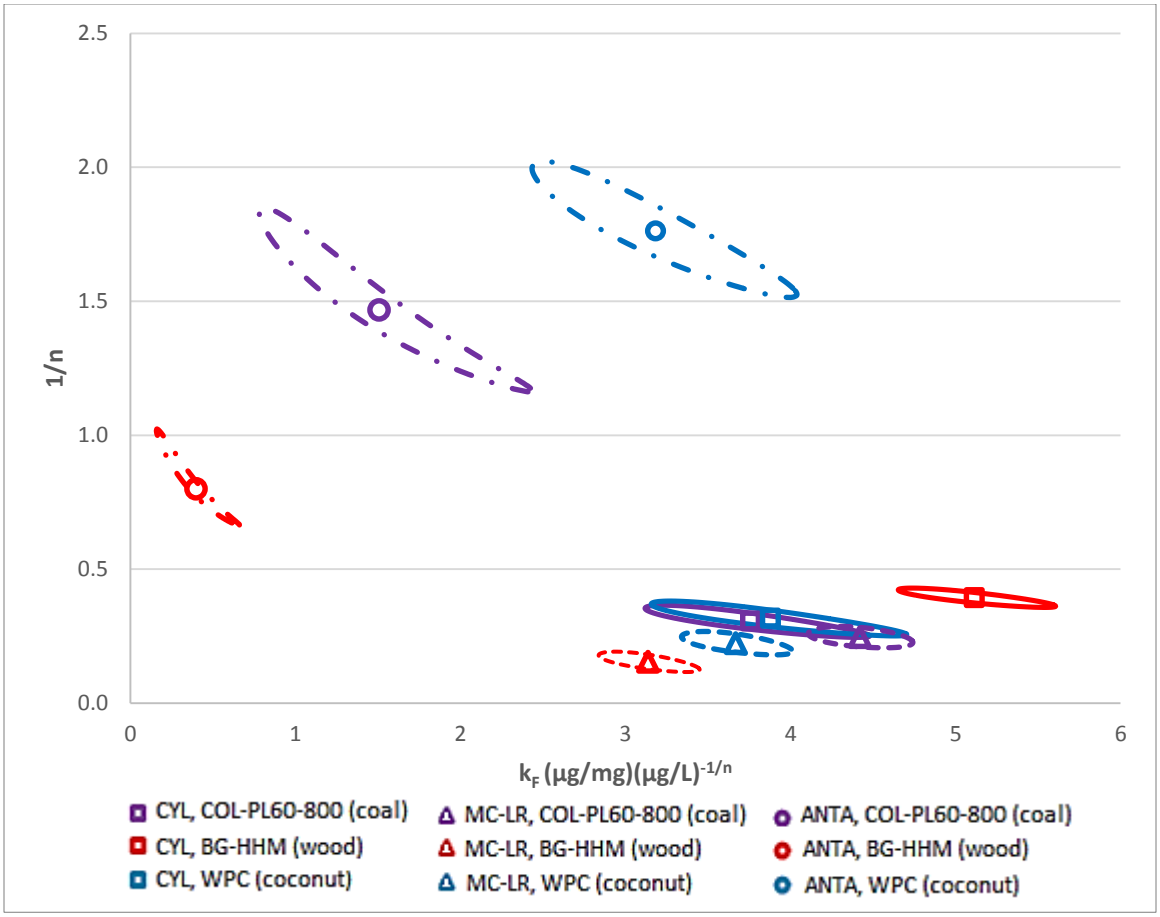

Figure 3.2 95% joint confidence regions and point estimates of the Freundlich isotherm parameters of for the adsorption of CYL, MC-LR and ANTA onto the selected PACs in ultrapure water at equilibrium (Ellipses represent JCRs; symbols positioned in the centre of each ellipse represent the point estimates)

3.4.3.2 Freundlich Parameter Determination

The Freundlich isotherm model (Equation 6) was applied to the equilibrium data obtained from the bottle-point technique for the adsorption of each cyanotoxin onto each PAC in ultrapure water, as shown in Figure 3.3. In this study, 'capacity' is defined as the amount of cyanotoxin adsorbed at time 't' under controlled experimental conditions.

In terms of CYL adsorption, the BG-HHM (wood) had a higher capacity than the other two PACs at equilibrium concentration from about 0.5 to 100 µg/L (Figure 3.3). The COL-PL60-800 (coal) and the WPC (coconut) had similar CYL capacity in the examined equilibrium concentration range, which is consistent with the JCR results. As per Section 3.4.3.1, adsorption performance of the

three PACs was statistically distinct from each other in the case of MC-LR. The COL-PL60-800 (coal) had the greatest MC-LR capacity, followed by the WPC (coconut), while the BG-HHM (wood) had the lowest MC-LR capacity. With respect to ANTA adsorption, the performance of the selected PACs was also statistically distinguishable (Section 3.4.3.1). The WPC (coconut) retained the highest ANTA capacity, followed by the COL-PL60-800 (coal). The BG-HHM (wood) had substantially lower ANTA capacity than the other two PACs. Interestingly, for each cyanotoxin, the Freundlich isotherm fitting curves of all three PACs were diverging with growing equilibrium concentration, indicating increasing difference between each of them (Figure 3.3).

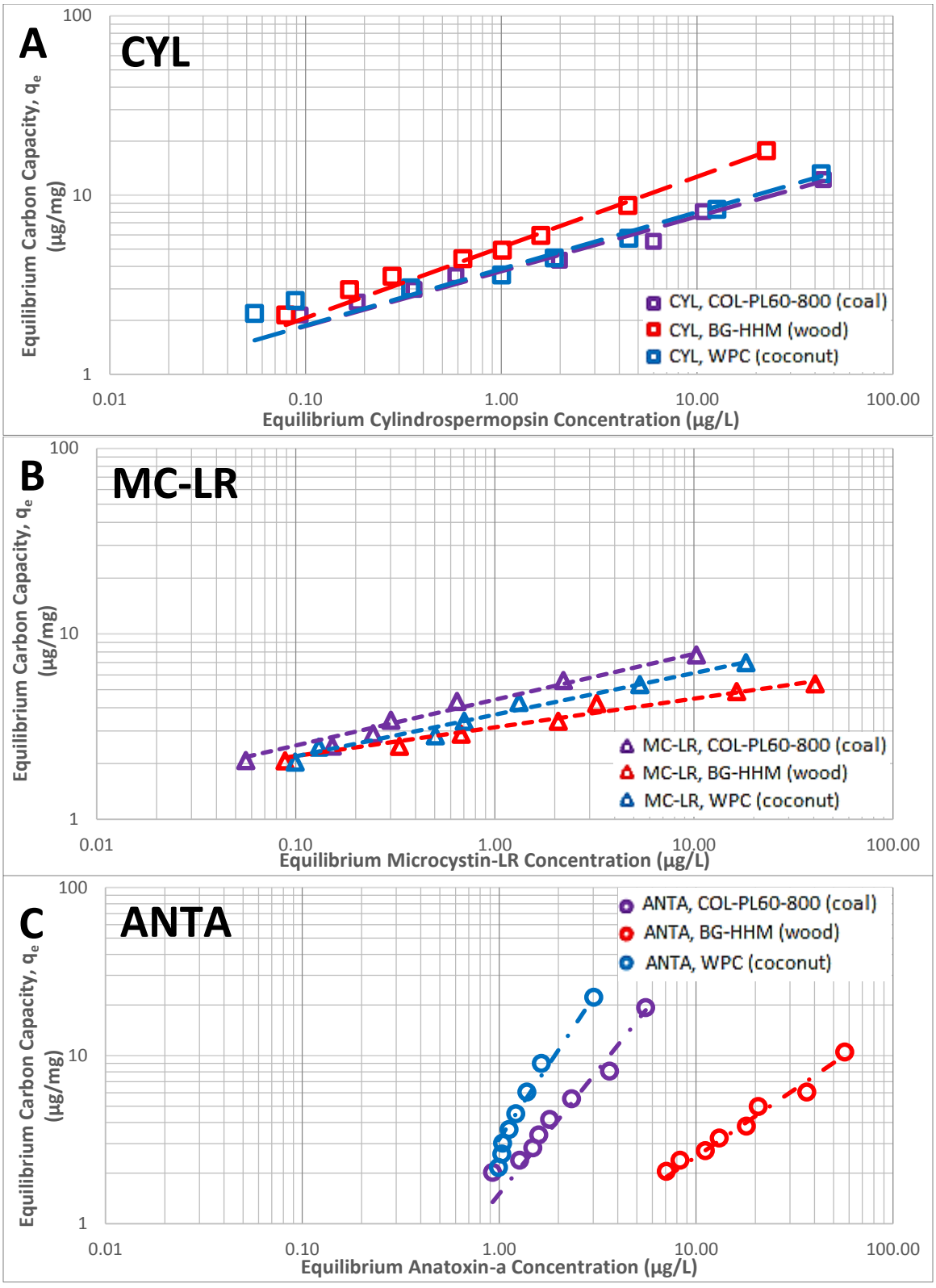

Figure 3.3 Freundlich isotherms for cyanotoxin adsorption by coal-, wood- and coconut-based PACs in ultrapure water. A) CYL, B) MC-LR, C) ANTA. (Straight lines represent Freundlich isotherm model fitting curves and symbols represent experimental data)

The Freundlich isotherm model parameters were determined using non-linear least square regression and are summarized in Table 3.3. The residual plots for the isotherms are provided in Appendix A.4, from which no residual trend was found.

Based on Table 3.3, in terms of CYL adsorption, the BG-HHM (wood) had the highest k_F value (5.11 (µg/mg)(µg/L)$^{-1/n}$), while the COL-PL60-800 (coal) and the WPC (coconut) had lower but similar k_F values (3.76 - 3.88 (µg/mg)(µg/L)$^{-1/n}$) (Table 3.3). The 1/n values were comparable for the COL-PL60-800 (coal) and the WPC (coconut) (0.31 - 0.32), and were slightly higher for the BG-HHM (wood) (0.39). Based on the Freundlich isotherm equation (Equation 6), higher K_F values indicate higher PAC capacities, if 1/n values are the same. Given similar 1/n values for the three PACs (Table 3.3), the BG-HHM (wood) with the highest k_F value for CYL adsorption indicated the highest CYL capacity among all selected PACs, which is consistent with the results from visual inspection of Figure 3.3. The relatively close k_F and 1/n values for COL-PL60-800 (coal) and WPC (coconut) indicated similar performance of those two PACs, agreeing with visual inspection results from Figure 3.3. However, for MC-LR adsorption, the COL-PL60-800 (coal) had the highest k_F value (4.42 (µg/mg)(µg/L)$^{-1/n}$), whereas the BG-HHM (wood) had the lowest k_F value (3.14 (µg/mg)(µg/L)$^{-1/n}$). The 1/n value was slightly lower for the BG-HHM (wood) (0.15), while the 1/n's were comparable for the other PACs (0.22 - 0.25). Neglecting the effect of 1/n values, the COL-PL60-800 (coal) had the greatest MC-LR capacity, followed by the WPC (coconut), and finally the BG-HHM (wood). This capacity order agrees with the one discovered by visual investigation from Figure 3.3. For ANTA adsorption, the k_F value was quite low for the BG-HHM (wood) (0.40 (µg/mg)(µg/L)$^{-1/n}$), while the WPC (coconut) had the highest k_F value (3.18 (µg/mg)(µg/L)$^{-1/n}$). The WPC (coconut) had the highest 1/n value (1.76), while the BG-HHM (wood) had the lowest value (0.80). Again, neglecting the effect of 1/n values, the order of k_F values in Table 3.3 for ANTA adsorption agreed with the order of PAC capacities identified by visual investigation from Figure 3.3.

Table 3.3 Freundlich isotherm parameters for PAC adsorption in ultrapure water

Cyanotoxin	PAC	Number of samples	K_F (μg/mg)(μg/L)$^{-1/n}$	1/n
CYL	COL-PL60-800 (coal)	8	3.76 (3.12,4.48)	0.31 (0.26,0.37)
	BG-HHM (wood)	8	5.11 (4.65,5.61)	0.39 (0.36,0.43)
	WPC (coconut)	8	3.88 (3.16,4.70)	0.32 (0.25,0.38)
MC-LR	COL-PL60-800 (coal)	7	4.42 (4.11,4.74)	0.25 (0.21,0.29)
	BG-HHM (wood)	7	3.14 (2.84,3.45)	0.15 (0.12,0.19)
	WPC (coconut)	7	3.67 (3.34,4.01)	0.22 (0.18,0.27)
ANTA	COL-PL60-800 (coal)	8	1.51 (0.78,2.43)	1.47 (1.16,1.85)
	BG-HHM (wood)	8	0.40 (0.16,0.67)	0.80 (0.66,1.02)
	WPC (coconut)	8	3.18 (2.43,4.04)	1.76 (1.51,2.02)

(95% confidence interval)

Generally, adsorption is a rather complex process and a variety of factors have been identified to govern this process, including transport and access of adsorbate to adsorption sites, and attachment mechanisms between the adsorbate and adsorption sites, such as hydrophobic and electrostatic interactions (Delgado et al., 2012). Typically, complicated interactions among a variety of factors, and not one single factor, are at play, which makes it difficult to elucidate relationships between carbon properties and capacities for the different toxins. As with the adsorptive rate data, no direct relationships could be found between carbon capacity and carbon BET surface area values (Table 3.1).

Different pore size distributions and available surface areas in the pores of the PACs can affect adsorption performance. Based on Table 3.1, on a percentage basis, WPC (coconut) was the most microporous PAC, followed by COL-PL60-800 (coal), and finally BG-HHM (wood). BG-HHM (wood) was more mesoporous than the other 2 PACs. Based on Figure 3.3, CYL was better adsorbed to the more mesoporous PAC, BG-HHM (wood). Given its molecular dimensions (1.572 x 0.901 nm, as per Section 3.4.1.1), CYL can potentially adsorb in a portion of the secondary

micropores (0.8 - 2.0 nm) and it fits well within mesopores (2 - 24 nm) as well as all larger pores. Therefore, CYL adsorption may favor the more mesoporous PAC, which may explain the relevant experimental results. In the ANTA batch, the most microporous PAC, the WPC (coconut), had the highest capacity, whereas the least microporous (or most mesoporous) PAC, the BG-HHM (wood), had the lowest capacity (Figure 3.3). Such PAC order for ANTA capacity indicated that ANTA adsorption may prefer the more microporous PAC. However, according to the molecular dimensions (0.970 x 0.633 nm), ANTA can fit within secondary microporous (0.8 - 2.0 nm) and all larger pores, which cannot full explain the poorer adsorption performance of ANTA. Factors other than access adsorption sites within the pores were important in the adsorption of ANTA. As shown in Figure 3.3, the more microporous PACs, the COL-PL60-800 (coal) and the WPC (coconut), had higher MC-LR capacities than the least microporous (or most mesoporous) PAC, the BG-HHM (wood). However, MC-LR is the largest molecule among the three cyanotoxins in this study (2.032 x 1.259 nm), indicating that MC-LR can only access mesopores (2 - 24 nm) and all larger pores. Therefore, other factors affected MC-LR adsorption capacity.

The surface charges of PAC and cyanotoxins may affect the adsorption process. MC-LR and ANTA carry negative and positive charges, respectively, at the pH of the isotherm experiments (pH 7), while CYL does not have a charge. Based on the point of zero charge results for each PAC (Table 3.1), the BG-HHM (wood) had a negative surface charge at pH 7, whereas the COL-PL60-800 (coal) and WPC (coconut) had positive surface charges. Electrostatic interactions (attraction or repulsion) would be expected to impact (enhance or reduce) binding to adsorption sites. Somewhat unexpectedly, the positively charged COL-PL60-800 (coal) and the WPC (coconut) PACs removed the positively charged ANTA much better than the negatively charged BG-HHM (wood) PAC. MC-LR adsorption occurred as expected in that the positively charged COL-PL60-800 (coal) and WPC (coconut) had higher capacities for the negatively charged MC-LR than the negatively

charged BG-HHM (wood). Overall, no obvious relationships were identified between the adsorption capacity of cyanotoxins and the properties of the investigated PACs.

3.4.3.3 Non-Equilibrium Freundlich Parameter Determination

In practice, PAC contact times are typically shorter than the time required to reach the adsorptin equilibrium, resulting in unsaturated PAC at the end of its service life. It follows that an estimate of the amount of toxin adsorbed onto a PAC at a short contact time would be more useful for comparing PAC adsorption capacity than equilibrium data which are normally used. Therefore, the Freundlich isotherm model was applied to the non-equilibrium experimental data obtained for PAC adsorption of the three cyanotoxins and the corresponding Freundlich parameters are provided in Appendix A.4. The non-equilibrium data were collected at 0.5 and 1 h contact.

Conventionally, the Freundlich isotherm model is used to describe equilibrium adsorption behavior but recently it has been used to fit non-equilibrium adsorption data with the resulting parameters being used as input for the equivalent background compound (EBC) model. For example, Zoschke et al. (2011) generated Freundlich isotherms for geosmin and MIB adsorption by PAC under non-equilibrium conditions at different contact times. The non-equilibrium Freundlich parameters were then used as input parameters to the EBC model to describe competitive adsorption between geosmin or MIB and NOM. Shimabuku et al. (2014) conducted a similar study examining MIB and sulfamethoxazole adsorption by PAC and again, the Freundlich isotherm model was fit to non-equilibrium adsorption data, with the parameters that were generated being used for the EBC model. Zietzschmann et al. (2016) used the EBC model to describe the competitive adsorption between NOM and various micropollutants, including benzotriazole, carbamazepine, and others in drinking water and wastewater. It should be noted that PAC application in a treatment plant is basically a CFSTR whereas this study used batch experiments. Hence, the non-equilibrium results obtained in this study from a batch scale system under controlled conditions cannot be used to predict the performance of a full-scale.

To determine statistically significant differences between K_F and 1/n values for the various PAC/toxin combinations, JCRs were calculated for the adsorption for each toxin by each carbon under non-equilibrium conditions at the 95% confidence level. Details of the calculations are provided in Appendix A.5. The JCRs developed for all PACs under both equilibrium and non-equilibrium conditions are plotted in Figure 3.4. As pointed out in Section 3.4.3.1, at equilibrium, the JCRs for CYL on COL-PL60-800 (coal) and on WPC (coconut) almost completely overlap. All other CYL JCRs do not overlap and therefore they are statistically distinguishable from each other and from the overlapping JCRs, at the 95% confidence level. In terms of MC-LR adsorption, the BG-HHM (wood) reached equilibrium after 1 h. Therefore, the 1 h JCR is also the equilibrium JCR for this wood-based carbon. As shown in Figure 3.4B, the MC-LR JCRs for COL-PL60-800 (coal) and WPC (coconut) almost completely overlap with each other at the 1 h contact time. Those two overlapping JCRs slightly intercept with the JCR for WPC (coconut) at 0.5 h contact. All other MC-LR JCRs do not overlap, indicating that those JCRs are statistically different from each other and from the overlapping JCRs, at the 95% confidence level. The ANTA JCRs for COL-PL60-800 (coal) and WPC (coconut) at both 0.5 h and 1 h contact are positioned together, indicating similar performance (Figure 3.4C). The similar adsorptive behavior of each PAC at 0.5 h and 1 h is symptomatic of the slow adsorption of ANTA by these PACs indicating that there was no appreciable increase in adsorptive capacity from 0.5 h to 1 h contact time. All other ANTA JCRs do not overlap to each other, indicating different performance, at the 95% confidence level.

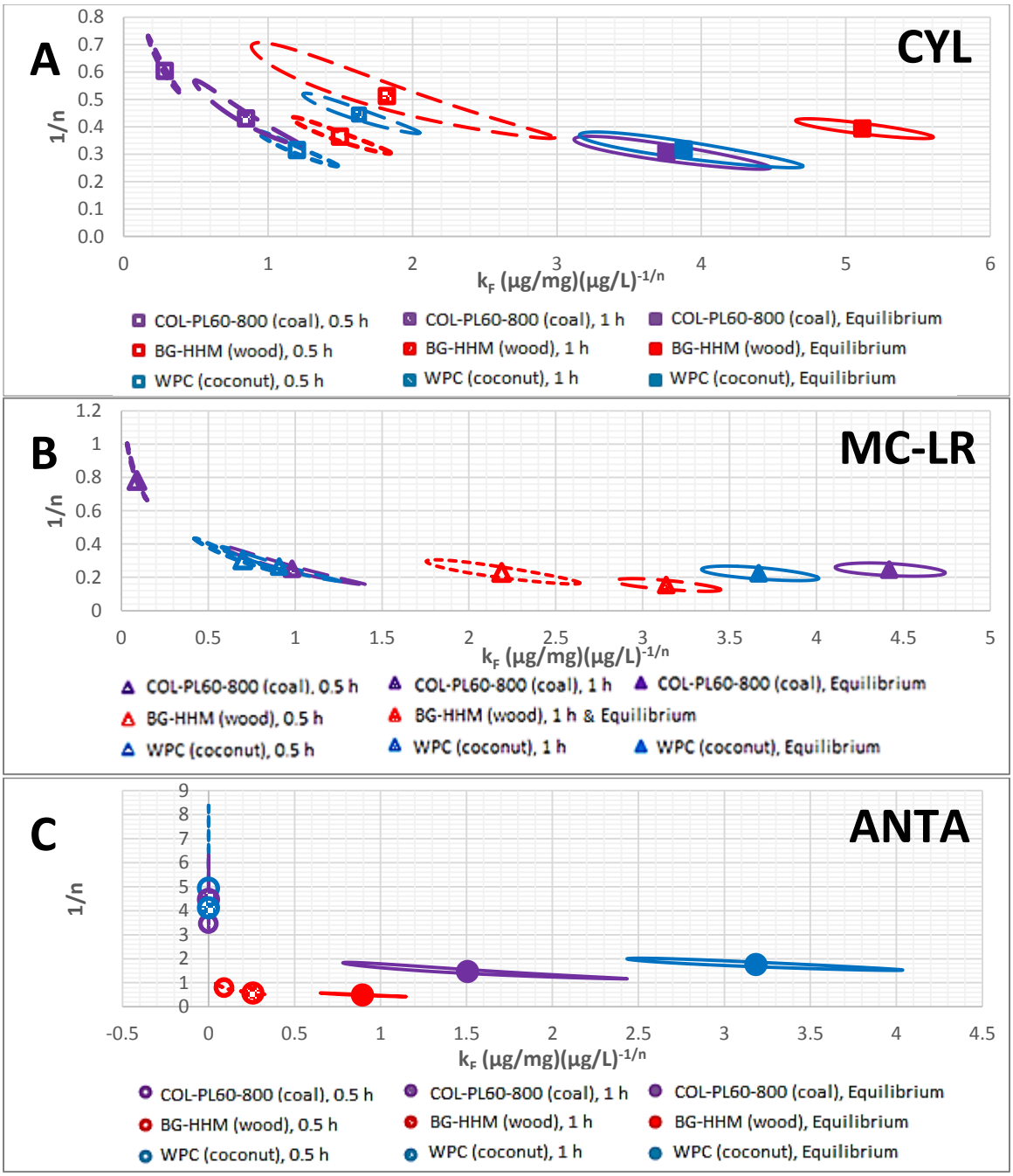

Figure 3.4 95% JCRs and point estimates for the Freundlich parameters of non-equilibrium isotherms generated with the adsorption of CYL, MC-LR, and ANTA using the selected PACs in ultrapure water: A) CYL, B) MC-LR, and C) ANTA (Ellipse curves represent JCRs and symbols in the centre of ellipses represent point estimates) (In terms of MC-LR adsorption, the wood-based BG-HHM reached equilibrium in about 1 h)

The Freundlich isotherm model was fit to both the equilibrium and non-equilibrium data for the adsorption of the three cyanotoxins using all three selected PACs. The MC-LR plots are presented

in Figure 3.5 as an example of the general trends. The same plots for CYL and ANTA are provided in Appendix A.4. As cyanotoxins are adsorbed onto PAC, aqueous cyanotoxin concentrations are decreasing while cyanotoxin loading onto the PAC is increasing, reaching its maximum at equilibrium. As demonstrated in Figure 3.5, for each PAC, the slope of the Freundlich curve decreased whereas the curve intercept increases with increasing contact time. Similar trends were also observed for CYL and ANTA.

As presented in Figure 3.5, the COL-PL60-800 (coal) and the WPC (coconut) had substantially lower MC-LR capacities under non-equilibrium conditions, while the BG-HHM (wood) had similar MC-LR capacities at 0.5 h and 1 h and even reached equilibrium after 1 h. These trends are likely due to the different adsorptive rates among the selected PAC products. As is discussed in Section 3.4.2, the BG-HHM (wood) adsorbed MC-LR the fastest and had significantly greater rates of adsorption for the other two PACs. Although the BG-HHM (wood) had the lowest equilibrium MC-LR capacity, it substantially outperformed the other two PACs under non-equilibrium conditions. Therefore, PAC contact time and its adsorptive rate are also critical when assessing adsorption performance of PACs for practical applications in drinking water treatment facilities.

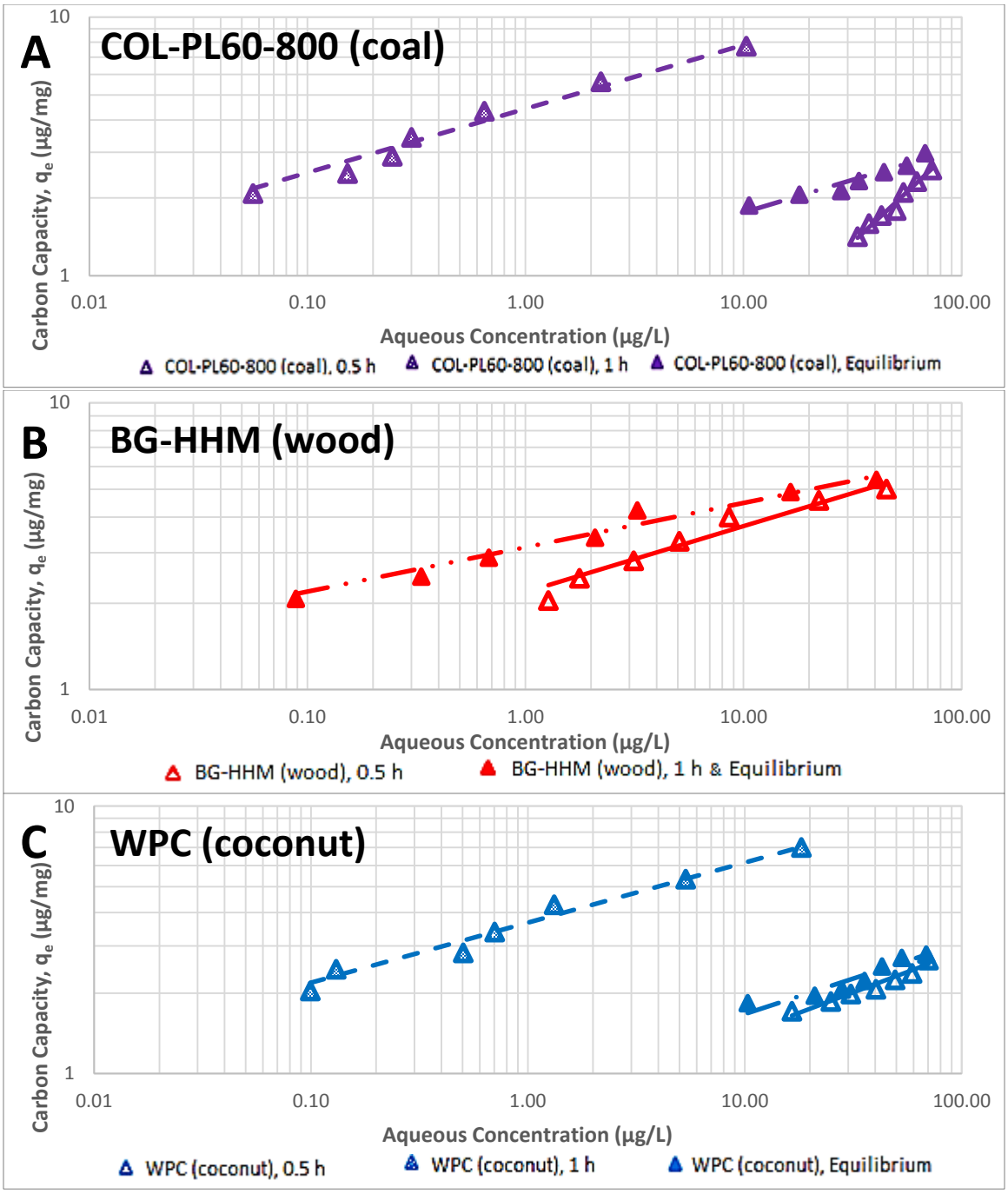

Figure 3.5 Freundlich model plot demonstrating PAC adsorption of MC-LR at contact times of 0.5 h, 1 h and equilibrium. A) coal-based PAC; B) wood-based PAC; C) coconut-based PAC (Straight lines represent Freundlich isotherm model fitting curves and symbols represent experimental data) (In terms of MC-LR adsorption, the wood-based BG-HHM reached equilibrium in about 1 h)

The non-equilibrium Freundlich parameters were calculated for the three cyanotoxins with 95% confidence intervals (Figure 3.6). With respect to CYL adsorption, based on the best-fit Freundlich

adsorption coefficient values (K_F), the more mesoporous BG-HHM (wood) had the highest K_F values at equilibrium conditions, while under non-equilibrium conditions the microporous WPC (coconut) demonstrated similar but a slightly lower adsorption capacity compared to the BG-HHM (wood), which was much greater than those of the coal-based carbon, neglecting 1/n effects. An examination of the 95% confidence intervals for K_F (Figure 3.5A) reveals that the adsorption capacities of the BG-HHM (wood) and WPC (coconut) cannot be concluded to be significantly different after 1 h of contact with CYL. As a result, the BG-HHM (wood) and the WPC (coconut) tested herein are better alternatives for CYL removal than the COL-PL60-800 (coal) under typical water treatment scenarios i.e. contact times of 0.5 and 1 h.

Although the COL-PL60-800 (coal) had the greatest MC-LR capacity and the BG-HHM (wood) had the lowest at equilibrium, in the non-equilibrium scenarios the wood-based carbon had over 60% higher capacity than the COL-PL60-800 (coal) and the WPC (coconut). This is associated with the fastest adsorption kinetics of the wood-based carbon.

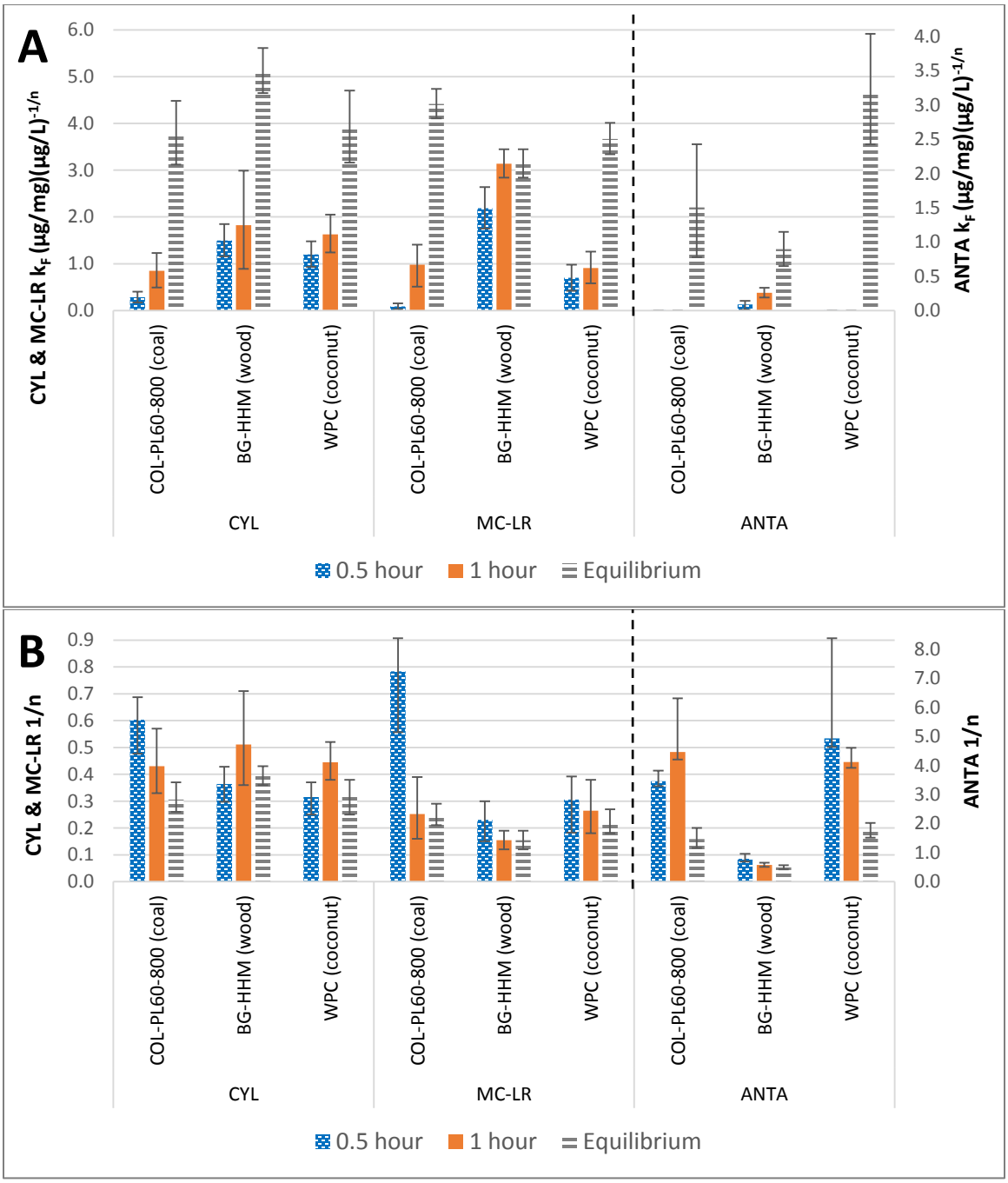

Figure 3.6 Freundlich adsorption parameters (A) K_F and (B) 1/n non-linear fit with 95% confidence intervals (actual values presented in Appendix A.4)

As with MC-LR adsorption, the mesoporous BG-HHM (wood) had the highest adsorption capacity for ANTA under non-equilibrium conditions, whereas its maximum adsorption capacity was the lowest at equilibrium, compared to the microporous COL-PL60-800 (coal) and the WPC (coconut). Adsorption rates played a critical role in ANTA adsorption, as all studied PACs required over 60 h

to reach equilibrium, which are substantially longer contact times than those in real case scenarios, resulting in remarkably low adsorption capacities of all selected PACs at 1 h of contact for ANTA. The BG-HHM (wood) had a much faster rate of adsorption than the other two PACs, resulting in substantially higher non-equilibrium capacities. Despite the slow rate of ANTA adsorption, the BG-HHM (wood) was still able to achieve approximately 75% - 78% ANTA removal under non-equilibrium condition with contact times ranging from 30 to 60 minutes.

The Freundlich exponent 1/n obtained for the adsorption of CYL, MC-LR and ANTA by the three selected PACs under both equilibrium and non-equilibrium conditions is shown in Figure 3.4B. Typically, 1/n values of less than 1 and are considered as "favourable" as they indicate relatively high carbon loading capacity at low concentration range, although 1/n values can be theoretically greater than or equal to 1 (Crittenden et al., 2012). The majority of 1/n values obtained in this study were less than 1, and as such were termed favourable isotherms, except for the values determined from ANTA adsorption experiments with the COL-PL60-800 (coal) and WPC (coconut) PACs. Therefore, the BG-HHM (wood) is the best alternative at contact times between 0.5 to 1 h among the three PACs examined in this study for MC-LR removal, at least in ultrapure water.

3.4.3.4 Comparison with Literature Values

Equilibrium isotherms for CYL, MC-LR, and ANTA adsorption by PACs used in this study were compared to literature values for cyanotoxin equilibrium isotherms established under similar conditions (batch-scale setup in ultrapure water), to provide a measure of relative adsorbability. PAC adsorption is highly dependent on molecular size of the adsorbate with ANTA (MW = 165 Da) being a much smaller molecule than CYL (MW = 415 Da) and MC-LR (MW = 995 Da) (Vlad et al., 2014). Figure 3.6 shows the Freundlich isotherms from this study alongside ANTA isotherms obtained using a coal-based PAC (Vlad, 2015) and isotherms for MC-LR and microcystin-RR (MC-RR) obtained using coal-, wood-, and coconut-based PACs (Zhu et al., 2016). MC-RR is

another commonly found microcystin variant, which has a slightly higher molecular weight (MW = 1038 Da) than MC-LR.

For the coal-based PAC (Figure 3.6A) used in this study, the adsorption capacities for CYL and MC-LR were quite close, which were much lower than that for ANTA removal in equilibrium concentrations higher than about 5 µg/L. While made from the same raw material, PACs provided by different manufacturers can exhibit very different adsorption behavior. The carbon that Zhu et al. (2016) studied had a much higher adsorption capacity for MC-LR than that of the carbon used in this study. The carbon used in this study had a much higher capacity than that of the carbon used by Vlad (2016) in the high equilibrium concentration range, but the capacity was lower in the low concentration range. Zhu et al. (2016) reported that MC-RR is less adsorbed than MC-LR, converging at concentrations higher than 100 µg/L.

In the case of the wood-based PAC (Figure 3.6 B) used in this study, CYL was much better adsorbed than either MC-LR or ANTA. The MC-LR used in this study is less well adsorbed by the carbon than that used by Zhu et al. (2016). MC-RR is much less well adsorbed than MC-LR, based on the results in Zhu et al. (2016).

The coconut-based PAC (Figure 3.6 C) used in this study had a significantly higher ANTA capacity than for MC-LR and CYL. MC-LR and CYL were much less adsorbed in this study than MC-LR and MC-RR in the study of Zhu et al. (2016) who also reported higher capacity for MC-LR adsorption than that of MC-RR adsorption.

Overall, this comparison clearly shows that PAC products made from the same base material might still have different performance.

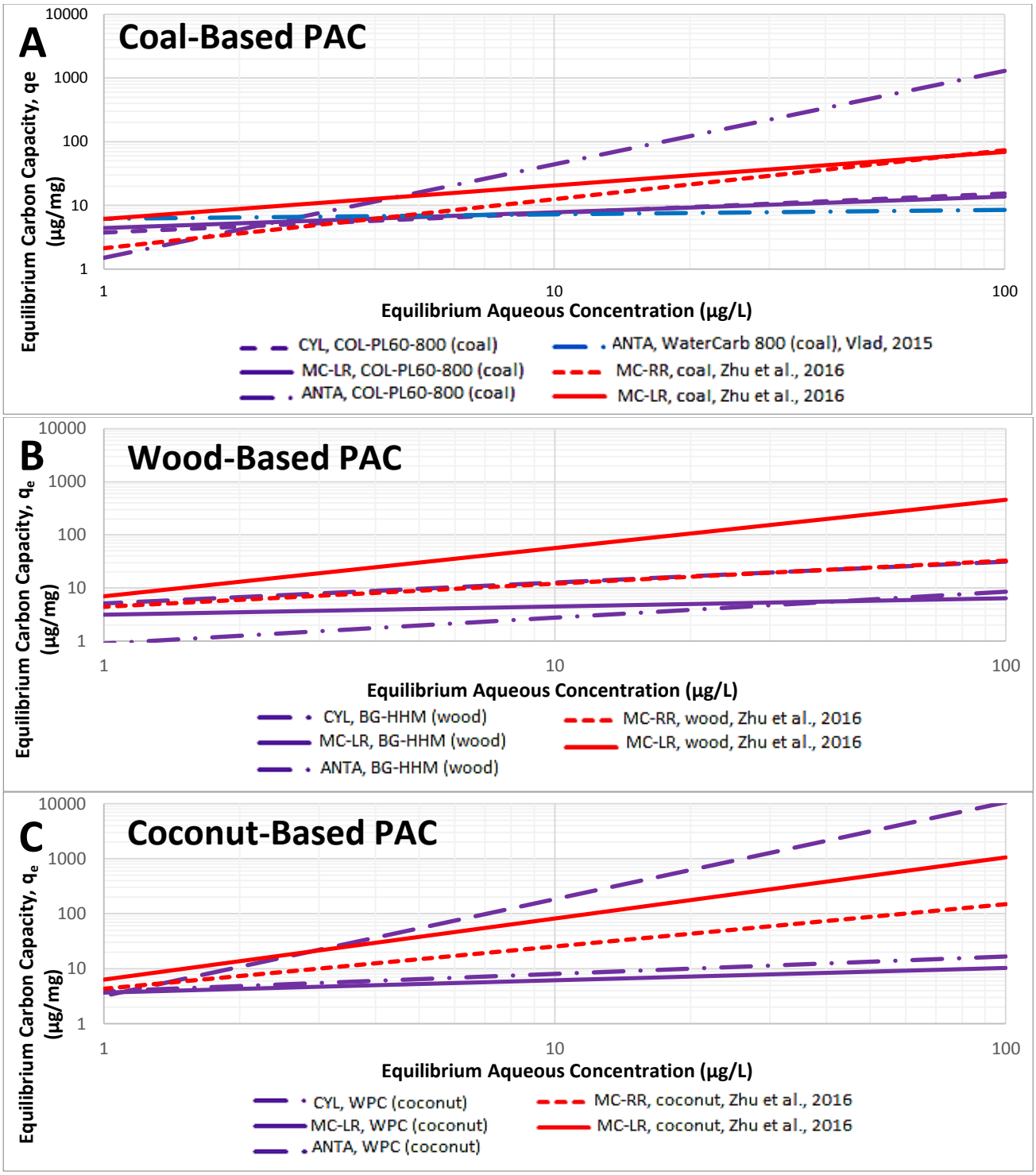

Figure 3.7 Comparison of Freundlich equilibrium isotherms in this study to literature values. CYL, MC-LR, and ANTA isotherms for coal-, wood-, and coconut-based PACs are plotted from the current study. In addition, an ANTA isotherm for a WaterCarb 800 (coal) PAC (Vlad, 2015), and isotherms for MC-LR and MC-RR obtained using coal-, wood-, and coconut-based PACs (Zhu et al., 2016) were plotted based on the Freundlich parameters obtained from the literature using equilibrium concentrations ranging from 1 to 100 µg/L.

3.5 Conclusions

In this study, the adsorption of CYL, MC-LR, and ANTA by three PACs (coal-, wood-, and coconut-based) was examined using the bottle point technique in buffered ultrapure water (to pH 7). The key findings and conclusions drawn from this chapter are summarized below.

- The BG-HHM (wood) removed all three cyanotoxins the fastest, while the COL-PL60-800 (coal) was slowest. The mesoporous BG-HHM (wood) favored the adsorption of the larger MC-LR and CYL molecules. With a pH_{PZC} of 3.5, the BG-HHM (wood) was negatively charged at pH 7, resulting in attractive interactions with the positively charged ANTA.
- Toxin type is critical to adsorption rate, as ANTA was much more slowly adsorbed than the other two cyanotoxins, no matter which type of PAC was used in this study.
- The pseudo-second order rate constant model provided somewhat better fitting to all experimental data than the pseudo-first order model.
- At equilibrium, BG-HHM (wood) had the highest capacity for CYL, while COL-PL60-800 (coal) had the highest MC-LR capacity, and WPC (coconut) had the highest capacity for ANTA.
- Compared to equilibrium conditions, the adsorption capacity of the PACs to remove the three cyanotoxins was very different under non-equilibrium conditions at PAC contact times of 0.5 and 1 h. BG-HHM (wood) outperformed the other two carbons having the highest capacity at the short contact times.

Overall, the findings indicate that adsorption of CYL, MC-LR, and ANTA using PAC is a promising treatment option. However, further investigations are needed to establish whether the adsorption performance of PACs made from the same source material differ between PACs produced by different manufacturers, and it is also necessary to investigate the impact of competing NOM.

Chapter 4
Modelling the Competitive Adsorption of Three Cyanotoxins and NOM onto PACs

4.1 Summary

The adsorption of the cyanotoxins, CYL, MC-LR, and ANTA in Lake Erie water by three commercially available PACs, the coal-based COL-PL60-800, wood-based BG-HHM, and coconut-based WPC, were examined using the bottle-point technique. With respect to adsorption rates, BG-HHM adsorbed CYL and MC-LR the fastest, and along with WPC, the two PACs were the fastest for ANTA adsorption, while ANTA was substantially less quickly adsorbed than other cyanotoxins. PAC capacity was studied under both equilibrium and non-equilibrium conditions, as PAC contact time in a typical WTP is typically not sufficiently long to reach equilibrium. At equilibrium, COL-PL60-800 had the highest capacity for CYL, followed by BG-HHM and WPC with similar performance. Similarly, COL-PL60-800 and BG-HHM demonstrated the highest and similar capacity for MC-LR while WPC had the lowest capacity at equilibrium. ANTA was significantly less well adsorbed than CYL and MC-LR, while WPC and BG-HHM had the highest equilibrium capacity followed by COL-PL60-800 with much less capacity. Capacity of the selected PACs at equilibrium differed significantly from the non-equilibrium capacity. BG-HHM demonstrated the highest non-equilibrium capacity for CYL and MC-LR removal. Again, the capacity of all PACs was substantially less for ANTA under non-equilibrium conditions, while WPC performed the best.

By comparing the DOC and SUVA results collected prior to and after adsorption experiments, it was observed that a fraction of NOM competed with the selected cyanotoxins for adsorption sites, resulting in substantial reduction of capacity and some decrease in adsorption rates in Lake Erie water compared to the ultrapure water results. The Simplified Equilibrium Background Compound Model (SEBCM) was applied in this study to ascertain PAC doses needed to treat cyanotoxins in

Lake Erie water taking into account competitive adsorption by NOM. The model was validated and then used to predict PAC doses to reduce CYL, MC-LR, and ANTA to below a predetermined guideline concentration at 0.5 h and 1 h contact time, which are typical PAC contact times in full-scale WTPs. Based on these modeling results, an economic analysis was also conducted. BG-HHM was the most cost-effective alternative with the lowest dose required for CYL and MC-LR removal at the most environmentally relevant concentrations. However, none of the selected PACs in this study was an effective barrier for ANTA.

4.2 Introduction

Treatment with PAC has been demonstrated to be efficient of the removal the most commonly occurring cyanotoxins in North America, including CYL, MC-LR, and ANTA; however, the efficiency of PAC adsorption in natural water is highly impacted by water quality, due to NOM competition (Newcombe et al., 2002). Typically, NOM is present in drinking water sources with dissolved organic carbon (DOC) concentrations of 2 to 10 mg/L (Zoschke et al., 2011), while the concentration of cyanotoxins is substantially lower, with the difference being about 3 to 4 orders of magnitude. As such, NOM reduces PAC capacity for cyanotoxin adsorption primarily by directly competing with cyanotoxin for adsorption sites (Newcombe et al., 2002).

Typically, PAC contact times in a full-scale WTP (i.e. 0.5 to 1 h) are not long enough to reach the adsorption equilibrium, resulting in the waste of unexhausted PAC, as discussed in Section 3.4.2. This study aimed to investigate the adsorption performance of three commercially available PAC products for the removal of CYL, MC-LR, and ANTA in NOM-containing Lake Erie water, particularly under realistic non-equilibrium conditions. Performance at equilibrium conditions was also assessed.

Several models have been developed to describe the competitive adsorption between micropollutants and NOM, including for example the tracer model, EBC model, and SEBCM

(Worch, 2010). All of these models typically use equilibrium data as input, though their applicability has also been demonstrated for the adsorption of the taste and odor compounds geosmin and MIB under non-equilibrium conditions (Zoschke et al., 2011). These compounds are produced by the same cyanobacteria that produce the cyanotoxins being studied here. In this research, the SEBCM was selected to evaluate the competitive adsorption performance between cyanotoxins and NOM, as Zoschke et al. (2011) suggested that these model results were applicable to practical operations.

The objectives of this research were 1) to investigate the adsorption performance of three selected PACs for the adsorption of CYL, MC-LR, and ANTA in Lake Erie water under both equilibrium and non-equilibrium conditions, 2) to investigate the applicability of SEBCM to non-equilibrium data, and 3) to predict PAC dose and associated cost required to remove the selected cyanotoxins in Lake Erie water under non-equilibrium conditions, based on SEBCM.

4.3 Materials and Methods

4.3.1 Materials

Three commercially available PAC products, HPLC-graded chemicals, and pure CYL, MC-LR and ANTA were obtained as noted in Section 3.3.1. Luer lock syringe and syringe filters of 0.45 μm nylon were from VWR International (PA, USA). The water used in this study was Lake Erie water collected at the Elgin Area Water Treatment Plant located in southern Ontario. The water was collected after raw water pH adjustment (to pH 7) and prior to the flash mixing tank, where PAC is added. Three batches of Lake Erie water were collected from the WTP on Jul. 14, and 28, and on Aug. 18 in 2016 for ANTA, MC-LR, and CYL experiments, respectively. The UV_{254}, pH, TOC, and DOC of Lake Erie water were measured to characterize the water quality. SUVA was calculated by dividing the UV_{254} (m^{-1}) by DOC (mg/L).

The procedures for the preparation of cyanotoxin stock solutions and internal standard solutions were recorded in Section 3.3.1.

4.3.2 Sample Preparation and Handling

The bottle-point method was used to investigate on the adsorption of CYL, MC-LR, and ANTA in Lake Erie water using the coal-based COL-PL60-800, wood-based BG-HHM, and coconut-based WPC PACs, as described in Section 3.3.3. One positive control at a concentration of 100 µg/L was prepared in Lake Erie water for each studied cyanotoxin, and one negative control with the selected PAC in Lake Erie water was included for each selected PAC (i.e. no cyanotoxin). All bottles were placed onto an orbital shaker operating at 150 rpm with shielding to minimize the light exposure to prevent cyanotoxin degradation. In each cyanotoxin experiment, the aqueous toxin concentration of the sample bottle with the highest dose of each PAC, as well as the positive control, were monitored by collecting a 1 mL aliquot which was filtered through 0.45 µm nylon syringe filters (VWR International, PA, USA) and then analyzed by LC-MS/MS. The aqueous concentrations of all sample and control bottles were determined for each studied cyanotoxin, at 0.5 h, 1 h, and at equilibrium. For CYL adsorption, the COL-PL60-800 (coal) and the WPC (coconut) reached equilibrium in 10 h, whereas the BG-HHM (wood) achieved equilibrium in 6 h. In terms of MC-LR adsorption, the BG-HHM (wood), the COL-PL60-800 (coal), and the WPC (coconut) reached equilibrium in 1.5 h, 10 h, and 60 h, respectively. With respect to ANTA adsorption, the WPC (coconut) achieved equilibrium the fastest, in 72 h, while the equilibrium times for the COL-PL60-800 (coal) and BG-HHM (wood) were 221 h and 120 h. Only data points with aqueous concentrations greater than the LC-MS/MS MDL for each cyanotoxin (0.3 µg/L for MC-LR, and 0.1 µg/L for both CYL and ANTA) were included. In general, this excluded less than 5% of the collected data.

4.3.3 Cyanotoxin Analysis by LC-MS/MS

The LC-MS/MS method for determination of concentrations of CYL, MC-LR, and ANTA is described in Section 3.3.4. The cyanotoxin concentrations were then used to calculate adsorption rates and isotherms. JCRs were also plotted for Freundlich isotherm parameters.

4.3.4 Modelling of Competitive Adsorption of NOM and Cyanotoxins

The SEBCM was applied in this study. The SEBCM is described mathematically by a two-parameter equation and the parameters were calculated from the experimentally determined removal curve using the linear regression technique (Equation 4.1, from Worch, 2010).

$$\ln\left(\frac{C_{1,0}}{C_1} - 1\right) = n_1 * \ln\left(\frac{m}{V}\right) - \ln(A) \quad \text{Equation 4.1}$$

Where $C_{1,0}$ represents the initial concentration of the micropollutant, C_1 is the (equilibrium) concentration of the micropollutant, n_1 is the Freundlich exponent for the micropollutant, m is the adsorbent mass, V is the volume of the solution, and A is the model parameter for the micropollutant and the equivalent background compound (EBC).

Parameters including $C_{1,0}$, C_1, m, and V were obtained from the bottle-point experiments. A and n_1 were determined by calculating the fitting parameters for the removal curve, and then the predictions of the adsorbent dose necessary for the target contaminant removal can be determined by Equation 4.2.

$$\frac{m}{V} = A^{1/n_1} * \left(\frac{C_{1,0}}{C_1} - 1\right)^{1/n_1} \quad \text{Equation 4.2}$$

The SEBCM was applied to both equilibrium and non-equilibrium (0.5 and 1 h contact time) isotherm data for all selected cyanotoxins using three PACs.

4.4 Results and Discussion

4.4.1 Lake Erie water Characterization

The properties of Lake Erie water were determined for all three batches of water (Table 4.1). The pre-chlorination of raw water was stopped when samples were taken. Water samples were taken following pH adjustment in the plant, and ranged from 7.1 to 7.2. Turbidity ranged from 5.1 to 18.1 NTU. The sample with highest turbidity results was collected after an intense storm event which disturbed sediment on the lake floor. TOC ranged from 2.4 to 3.3 mg/L while DOC was fairly stable at 2.3 - 2.6 mg/L. SUVA, the ratio of UV_{254} absorbance and DOC concentration, was measured in a range from 1.15 – 1.67 L/(mg-m). The water samples were not filtered before adsorption experiments.

Table 4.1 Lake Erie water properties at the time of collection

	CYL Batch	MC-LR Batch	ANTA Batch
pH	7.2	7.1	7.2
Turbidity (NTU)	5.1	5.9	18.1
TOC (mg/L)	2.4	2.3	3.3
DOC (mg/L)	2.4	2.3	2.6
UV254 (cm-1)	0.027	0.026	0.043
SUVA (L/(m-mg))	1.15	1.12	1.67

4.4.2 Rate of Adsorption in Lake Erie water

Figure 4.1 shows the change of percent removal of each studied cyanotoxin by each of the selected PACs over time. In terms of CYL adsorption, the wood-based BG-HHM adsorbed it most quickly among all of the selected PACs achieving equilibrium after about 6 h contact time, while the coal-based COL-PL60-800 and coconut-based WPC adsorbed CYL less quickly and similarly reaching equilibrium after 10 h. In the case of MC-LR adsorption, the wood-based BG-HHM also adsorbed it the fastest, reaching equilibrium in approximately 1.5 h, followed by the coal-based COL-PL60-800, and finally the coconut-based WPC in 10 h and 60 h, respectively. It is of note that ANTA adsorption was substantially slower than adsorption of CYL and MC-LR. The coconut-based WPC

reached equilibrium in about 72 h, having the fastest rate of adsorption, while the coal-based COL-PL60-800 rate of adsorption was slowest, needing 211 h to reach equilibrium.

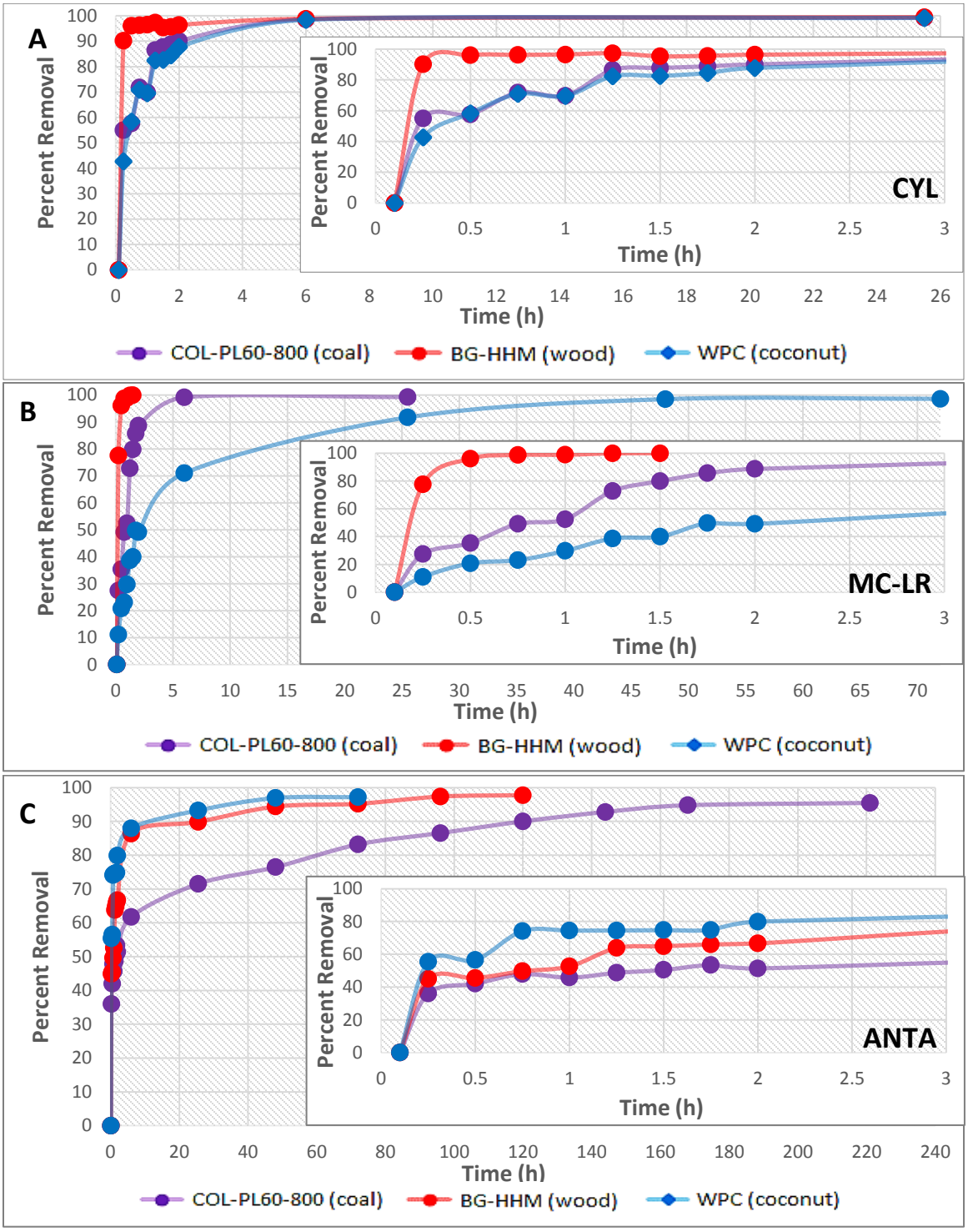

Figure 4.1 Percentage cyanotoxin removal by coal-, wood-, and coconut-based PACs as a function of time: A) CYL removal, B) MC-LR removal, C) ANTA removal.

The pseudo-first and pseudo-second order kinetic models were used to describe the adsorption rate of the PACs for CYL, MC-LR, and ANTA removal. The R^2 values for the pseudo-first order model were lower than those of the pseudo-second order model, with q_e predictions deviating further from the experimental results, and as such the pseudo-second order model better described the observed data. Residual plots do not contradict the assumption of linearity (Appendix B.1). As a result, only the pseudo-second order model adsorption kinetics for cyanotoxin adsorption by the various PACs are discussed in this chapter. Results derived from the pseudo-first order are provided in Appendix C.1.

Based on Table 4.2, the trend of rate constants calculated by the pseudo-second order model agreed with the results shown in Figure 4.1. In the case of CYL adsorption, the wood-based BG-HHM had the fastest rate constant of 11.65 mg/µg/h, while the coal-based COL-PL60-800 and the coconut-based WPC had slower and similar rate constants of 0.86 mg/µg/h and 1.62 mg/µg/h, respectively. In terms of MC-LR, the wood-based BG-HHM had the highest rate constant of 8.27 mg/µg/h, whereas the coal-based COL-PL60-800 and the coconut-based WPC had much lower, though similar rate constants, at 0.63 mg/µg/h and 0.24 mg/µg/h, respectively. Clearly, ANTA was adsorbed much more slowly than CYL and MC-LR, with the highest rate constant of 0.58 mg/µg/h for the coconut-based WPC and the lowest rate constant of 0.09 mg/µg/h for the coal-based COL-PL60-800. The wood-based BG-HHM adsorbed CYL and MC-LR the fastest. This could be partially attributed to the higher proportion of mesopores in this PAC (0.71 cm^3/g) as compared to the coal-based COL-PL60-800 (0.04 cm^3/g) and coconut-based WPC (0.18 cm^3/g) (Table 3.1), providing shorter diffusion paths to the adsorption sites.

Table 4.2 Pseudo-second order kinetic model parameters for CYL, MC-LR, and ANTA adsorption by coal-, wood-, and coconut-based PACs in Lake Erie water

Cyanotoxin	PAC	Equilibrium Carbon Capacity, q_e Experimental (µg/mg)	Equilibrium Carbon Capacity, q_e Predicted (µg/mg)	K_2 (mg/µg/h)	R^2
CYL	COL-PL60-800 (coal)	4.45	4.50	0.86	0.9998
	BG-HHM (wood)	2.03	2.05	11.65	1.0000
	WPC (coconut)	1.91	1.95	1.62	0.9999
MC-LR	COL-PL60-800 (coal)	2.68	2.75	0.63	0.9987
	BG-HHM (wood)	1.79	1.90	8.27	0.9988
	WPC (coconut)	2.05	2.26	0.24	0.9997
ANTA	COL-PL60-800 (coal)	3.31	3.31	0.09	0.9968
	BG-HHM (wood)	3.16	3.25	0.33	0.9998
	WPC (coconut)	3.86	3.87	0.58	0.9999

Overall, based on Figure 4.2, the PACs reached equilibrium more slowly in Lake Erie water than in the ultrapure water, except from the results for ANTA adsorption by the COL-PL60-800 (coal) and the WPC (coconut). The reduction of adsorption rate is likely due in most part from competitive adsorption in the presence of NOM, blocking access to the sites. For ANTA adsorption, the COL-PL60-800 (coal) and the WPC (coconut) had very small and similar rate constants in ultrapure water (0.05 mg/µg/h) and ultrapure water (0.09 mg/µg/h).

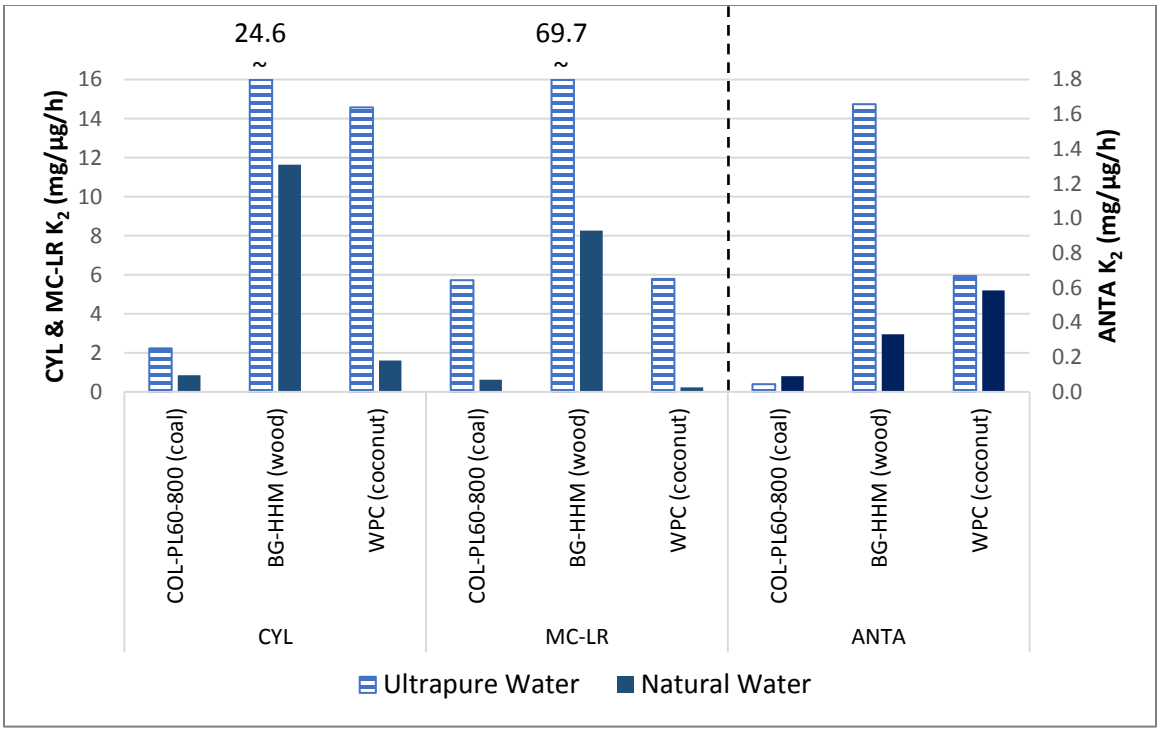

Figure 4.2 Comparison of pseudo-second order rate constants in ultrapure water and Lake Erie water experiments

4.4.3 Isotherms in Lake Erie Water

4.4.3.1 Freundlich Parameters Joint Confidence Regions (Equilibrium Conditions)

The JCRs appear as banana-shaped ellipses, confirming that the two model parameters are highly correlated (Figure 4.3). For CYL adsorption, all JCRs are clearly distinguishable from each other, indicating statistically significant differences among the performances of the three selected PACs. Similar results were observed for MC-LR JCRs, at the 95% confidence interval. In terms of ANTA adsorption, the JCR for the BG-HHM (wood) slightly overlapped with JCR for the WPC (coconut), indicating somewhat similar performance between those two PACs, at the 95% confidence interval. The JCR for the CYL adsorption by the COL-PL60-800 (coal) almost enclosed the JCRs for the MC-LR adsorption by the BG-HHM (wood), the ANTA adsorption by both the BG-HHM (wood) and the WPC (coconut), indicating no statistically significant different performance between this CYL batch and the batches of the enclosed JCRs. The COL-PL60-800 (coal) JCRs for the CYL and ANTA adsorption slightly overlapped to each other, showing somewhat similar performance.

Similar results were obtained for the JCRs of the CYL adsorption by the BG-HHM (wood) and the ANTA adsorption by the WPC (coconut). All other JCRs do not overlap and therefore they are statistically distinguishable from each other and from the overlapping JCRs.

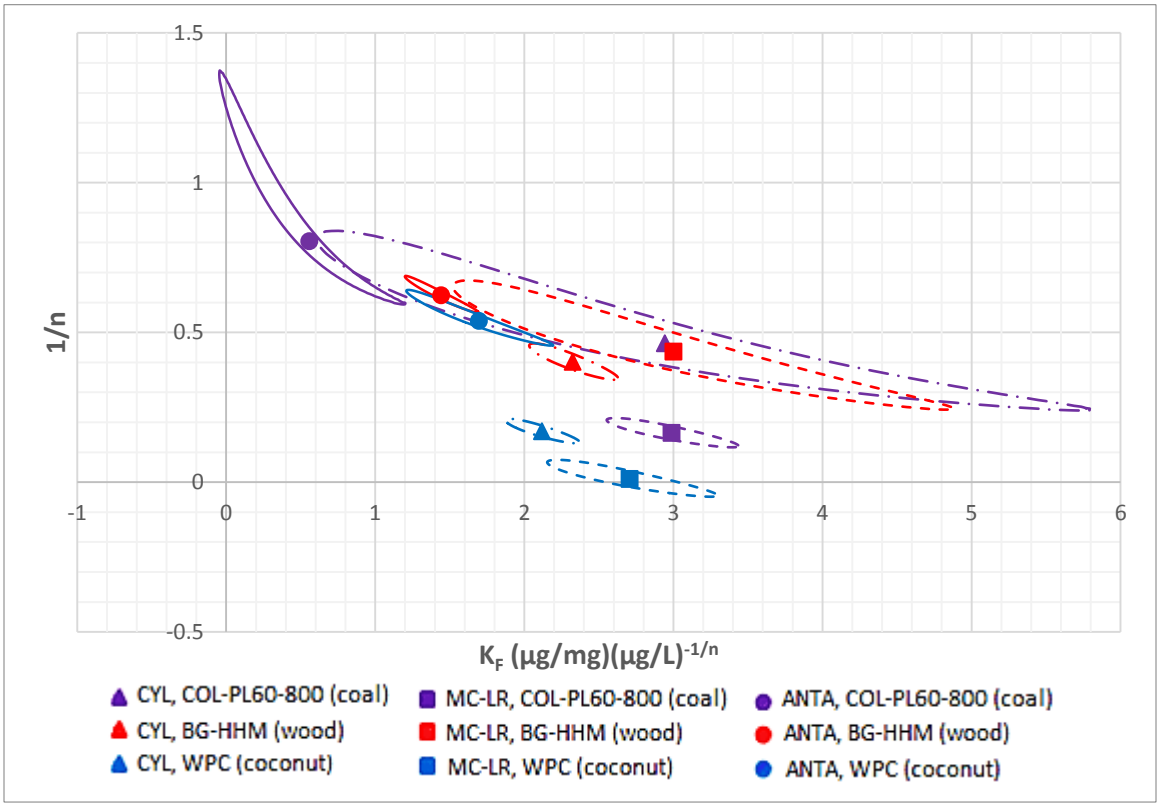

Figure 4.3 95% joint confidence regions and point estimates for CYL, MC-LR, and ANTA adsorption using coal-, wood-, and coconut-based PACs in Lake Erie water at equilibrium (Ellipse curve represents JCR and symbol positioned in the centre of ellipse represents the point estimate)

4.4.3.2 Freundlich Parameter Determination (Equilibrium Conditions)

The Freundlich isotherm model was applied using equilibrium data for the adsorption of CYL, MC-LR, and ANTA by the coal-based COL-PL60-800, wood-based BG-HHM, and coconut-based WPC PACs as shown in Figure 4.4, and the resulting estimates of Freundlich parameters are summarized in Table 4.3. The Freundlich adsorption model was fitted using the non-linear least-squares regression technique, as linear regression was considered invalid in this case due to the violation of the assumption that the residuals are normally distributed following linearization (Worch, 2012).

With respect to CYL adsorption (Figure 4.4), the coal-based COL-PL60-800, at equilibrium, had the greatest capacity in the concentration range from 1 µg/L to 100 µg/L. While the wood-based BG-HHM had greater capacity than the coconut-based WPC throughout most of the experimental range of equilibrium concentrations, the Freundlich fitting curves of those PACs converged at low concentrations, indicating small capacity differences, whereas divergence of model fitting curves at high concentrations demonstrated greater capacity differences. In terms of MC-LR adsorption, the more mesoporous wood-based BG-HHM had the highest capacity, but the more microporous coconut-based WPC demonstrated the lowest capacity. As with the CYL results, the Freundlich fitting curves of all studied PACs converged at low concentrations, resulting in little capacity difference at low equilibrium concentrations, but substantial differences at high concentrations. With respect to ANTA adsorption, the BG-HHM (wood) and WPC (coconut) had similar adsorption capacity, which was higher than the capacity of the COL-PL60-800 (coal). As opposed to the CYL and MC-LR results, the model fitting curves for ANTA adsorption converged at high concentrations.

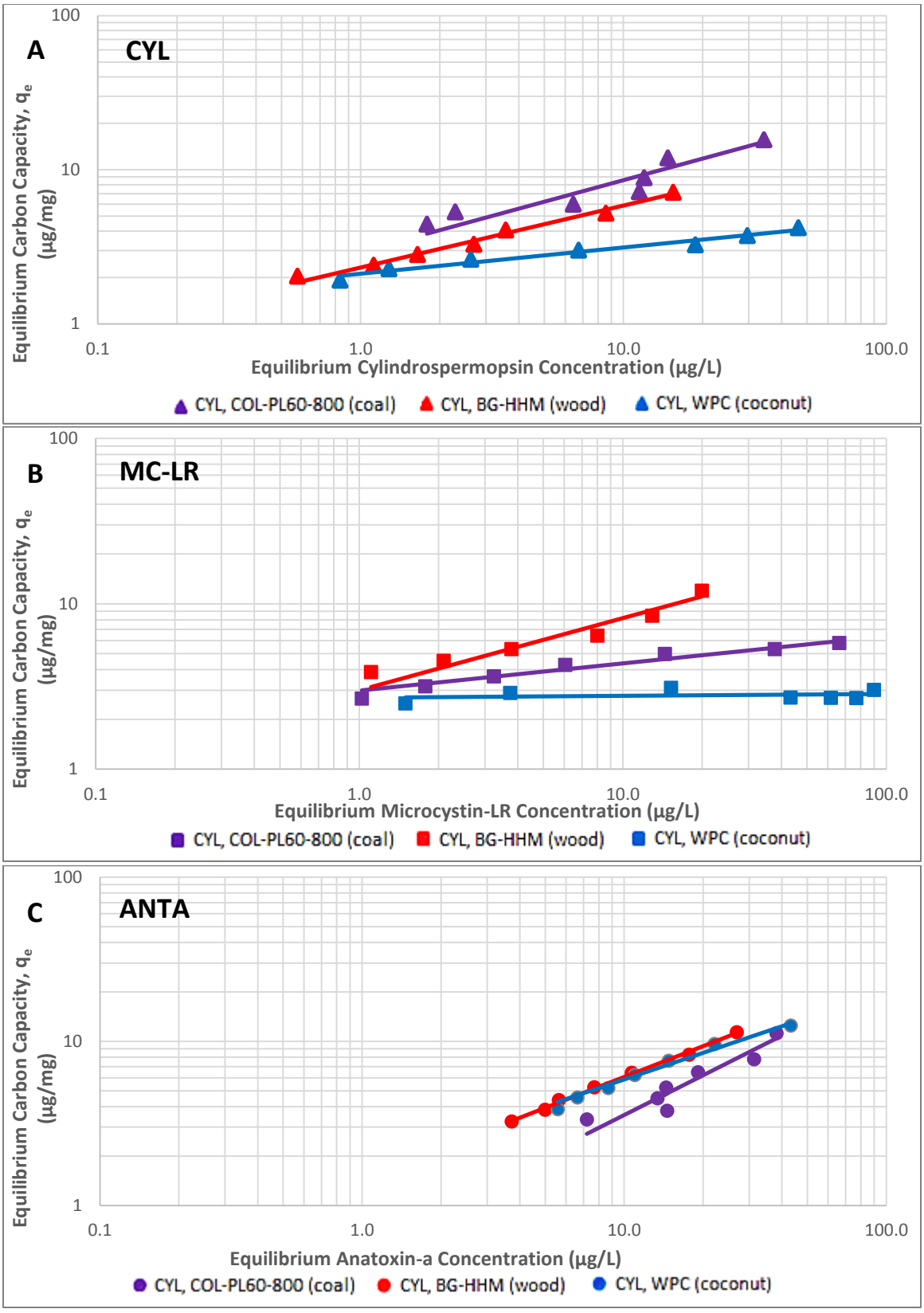

Figure 4.4 Freundlich isotherms for (A) CYL, (B) MC-LR, and (C) ANTA adsorption for coal-, wood-, and coconut-based PACs in Lake Erie water

Freundlich isotherm parameters are summarized in Table 4.3. For CYL adsorption, the COL-PL60-800 (coal) had the highest K_F at 2.94 (µg/mg)(µg/L)$^{-1/n}$, while the WPC (coconut) has the lowest K_F at 2.12 (µg/mg)(µg/L)$^{-1/n}$. The order of K_F values agreed with the order of PAC capacity obtained from Figure 4.4. In terms of MC-LR adsorption, the BG-HHM (wood) and the COL-PL60-800 (coal) had similar K_F values, while the BG-HHM (wood) had higher capacity than the COL-PL60-800 (coal), based on Figure 4.4, indicating that 1/n also affected PAC capacity. The WPC (coconut) had the lowest K_F value for MC-LR adsorption. With respect to ANTA adsorption, the K_F values for the BG-HHM (wood, 1.44 (µg/mg)(µg/L)$^{-1/n}$) and the WPC (coconut, 1.69 (µg/mg)(µg/L)$^{-1/n}$) were similar, which were higher than the COL-PL60-800 (coal, 0.56 (µg/mg)(µg/L)$^{-1/n}$). The order of PAC capacity illustrated in Figure 4.4 was the same as the order of the K_F values. As is shown in Appendix B.4, all PACs reduced DOC concentrations and SUVA in the ANTA batch more than in the other toxin's batch (on a percentage basis), indicating that ANTA was less able to compete with the adsorbable fraction of the NOM; as such, ANTA was substantially less well adsorbed than CYL and MC-LR. Interestingly, both the microporous coconut-based WPC and the mesoporous wood-based BG-HHM had the greatest equilibrium capacities, while the coal-based COL-PL60-800 had a much lower equilibrium capacity. As shown in Appendix B.4, COL-PL60-800 reduced SUVA the most, indicating that certain fractions of the aromatic organic matter were better absorbed than ANTA on this carbon by competing for adsorption sites. In addition, the model fitting curves of COL-PL60-800 and BG-HHM converged at high equilibrium concentrations, but diverged at low concentrations. The residual plots for each of the isotherms confirm that there were no systematic errors (Appendix B.2).

Table 4.3 Freundlich isotherm parameters for CYL, MC-LR, and ANTA adsorption using coal-, wood-, and coconut-based PAC in Lake Erie water with 95% confidence interval in brackets

Toxin	PAC	Number of Samples (n)	K_f (µg/mg)(µg/L)$^{-1/n}$	1/n
CYL	COL-PL60-800 (coal)	7	2.94 (0.61,5.83)	0.46 (0.24,0.84)
	BG-HHM (wood)	7	2.32 (2.03,2.63)	0.40 (0.34,0.46)
	WPC (coconut)	7	2.12 (1.88,2.37)	0.17 (0.13,0.21)
MC-LR	COL-PL60-800 (coal)	7	2.99 (2.55,3.44)	0.16 (0.12,0.21)
	BG-HHM (wood)	6	3.00 (1.52,4.88)	0.44 (0.24,0.67)
	WPC (coconut)	7	2.71 (2.15,3.30)	0.011 (-0.05,0.07)
ANTA	COL-PL60-800 (coal)	7	0.56 (-0.05,1.20)	0.80 (0.59,1.37)
	BG-HHM (wood)	7	1.44 (1.20,1.69)	0.62 (0.57,0.69)
	WPC (coconut)	7	1.69 (1.21,2.19)	0.54 (0.46,0.64)

4.4.3.3 Comparison of Freundlich Parameters under Equilibrium and Non-Equilibrium Conditions

The PAC contact time in a typical WTP is approximately 0.5 h, which is insufficient to reach adsorption equilibrium, resulting in non-equilibrium conditions during drinking water treatment (Zoschke et al., 2011). This is clearly demonstrated in the rate of adsorption experiments (Section 4.4.2). Therefore, investigating PAC capacities under non-equilibrium conditions was an important part of this study.

Figure 4.5 presents the Freundlich model fitting curves prepared for the adsorption of each studied cyanotoxin (CYL, MC-LR, and ANTA) onto the three selected commercially available PAC products (coal-based COL-PL60-800, wood-based BG-HHM, and coconut-based WPC) at 0.5 h, 1.0 h, and at equilibrium. As shown in Section 3.4.3.3, the carbon loading plots for the shorter

contact times were very different than the equilibrium isotherm plots. Similar behavior was observed in the Lake Erie water results.

The corresponding estimated values of the Freundlich parameters are summarized in Figure 4.5 with 95% confidence intervals. The exact Freundlich parameter values are summarized in Appendix B.2. JCR plots for the Freundich parameters demonstrating the 95% confidence intervals for the point estimates are also included in Appendix B.2. Generally, for many of the PAC toxin combinations (Figure 4.5), K_F, as expected, kept increasing while the 1/n kept decreasing with increased adsorption times, indicating an increase in carbon loading until equilibrium is reached.

Under non-equilibrium conditions, the PAC capacity is highly related to it's the rate of adsorption. As discussed in Section 4.4.2, the wood-based BG-HHM adsorbed CYL and MC-LR the quickest and reached equilibrium in less than 2 h for MC-LR and about 6 h for CYL (Figure 4.1). As such, BG-HHM had almost reached its maximum capacity to adsorb CYL and MC-LR at the 0.5 h and 1.0 h contact times. Hence, BG-HHM had greater CYL and MC-LR adsorption capacities than the other two PACs at 0.5 and 1.0 h as is apparent from Figures 4.4 and 4.5. Conversely, ANTA adsorption, as discussed in Section 4.4.2, was adsorbed much more slowly than CYL and MC-LR (Figure 4.1). All studied PACs had very little adsorption capacity for ANTA due to the slow rates of adsorption.

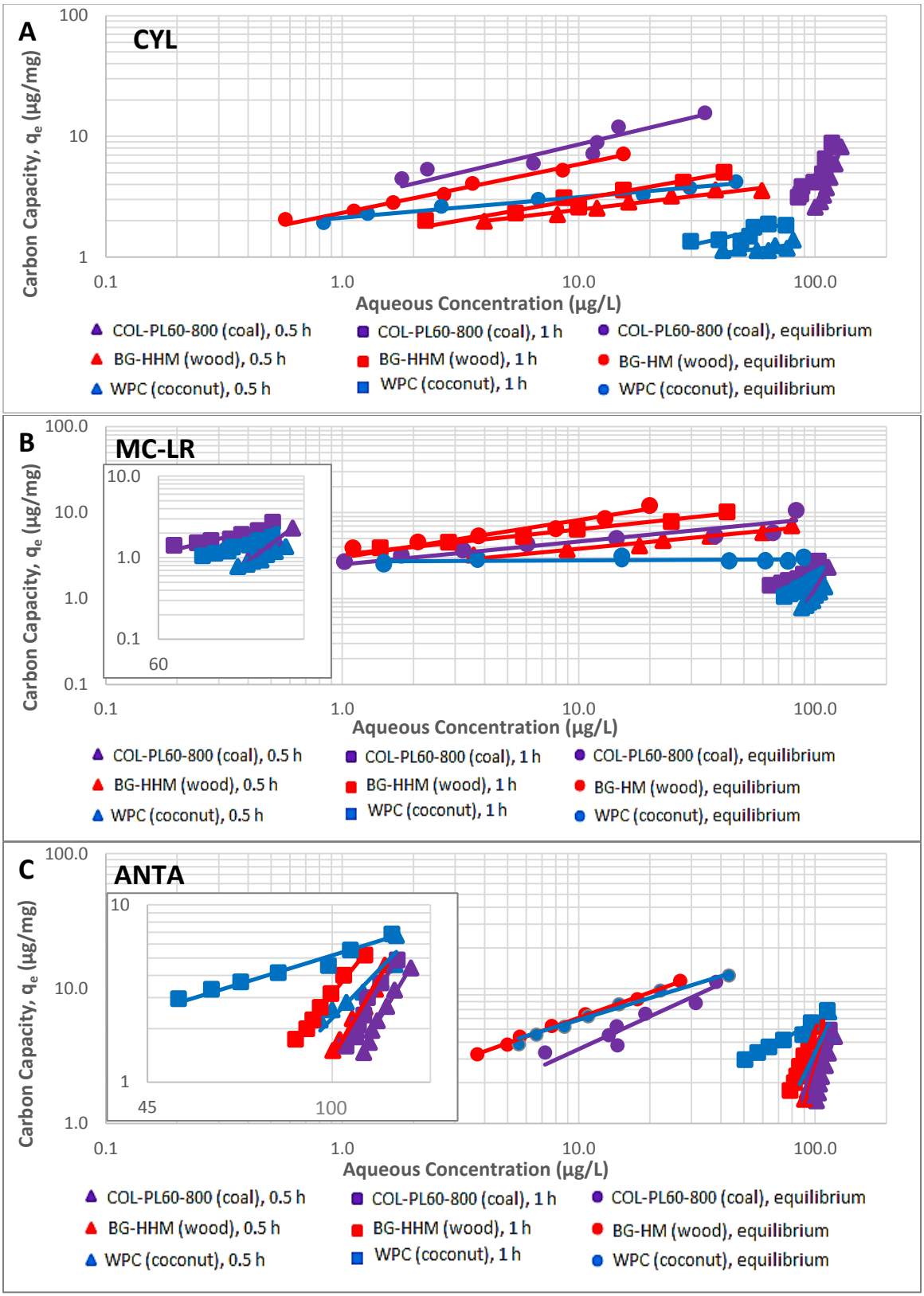

Figure 4.5 Comparison of Freundlich model fitting for three selected PACs at 0.5 h, 1 h, and equilibrium. A) CYL adsorption, B) MC-LR adsorption, and C) ANTA adsorption

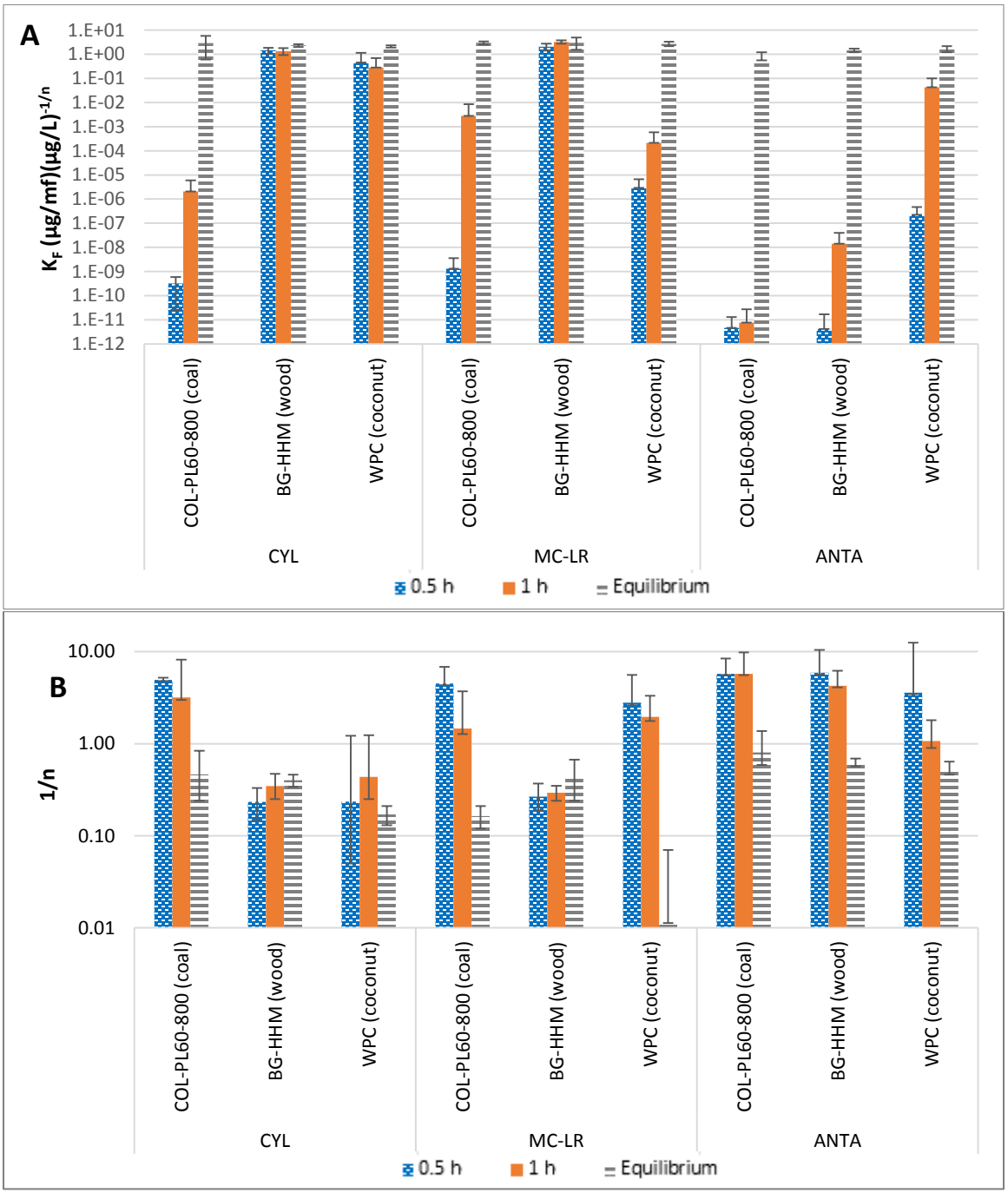

Figure 4.6 Non-linear estimates of Freundlich adsorption parameters with 95% confidence intervals with y-axis in log-scale. A) Freundlich adsorption coefficient (K_F), B) Freundlich model parameter (1/n)

4.4.4 Influence of NOM on the Adsorption of Cyanotoxins

Three batches of Lake Erie water were collected and each batch was used for an adsorption experiment for one cyanotoxin. Therefore, the Lake Erie water properties were somewhat different

among the three batches, and needed to be taken into consideration when comparing the PAC adsorption results. The turbidity was comparable between the CYL and the MC-LR batch but it was substantially higher for the ANTA batch. However, the TOC of the ANTA batch was only somewhat higher than in the other two batches of water, whereas most critically the DOC results were similar for all three Lake Erie water batches (Table 4.1). Based on Table 4.1, the Lake Erie water used for CYL and MC-LR experiments had fairly similar SUVA values (1.15 L/(m-mg) for the CYL batch and 1.12 L/(m-mg) the MC-LR batch), and was slightly higher (1.67 L/(m-mg)) for the ANTA batch. DOC and SUVA were obtained for each batch of Lake Erie water from the bottles with the highest PAC dose at time 0 and after equilibrium was reached. Removal of DOC and reduction in SUVA were calculated and are shown in Appendix B.4. Generally, the coal-based COL-PL60-800 and wood-based BG-HHM had similar DOC removals (43% - 53%) while DOC removals by the coconut-based WPC were somewhat less (24% - 38%). This suggests that the NOM molecules in Lake Erie water were occupying adsorption sites on the more mesoporous BG-HHM and COL-PL60-800 making these sites unavailable for cyanotoxins. DOC was better adsorbed in the surface water batch used for ANTA experiments with around 15% to 21% more DOC removal by COL-PL60-800 and BG-HHM and about 34% to 57% more DOC removal by WPC compared to the other two batches of surface water. The coal-based COL-PL60-800 reduced SUVA (58% - 64%) more than did the other two PACs (33% - 44% in CYL and MC-LR batches, vs. 53% - 57% in ANTA batches). SUVA is an indicator of aromaticity which was well reduced by the selected PACs in this study, indicating reduction of the aromatic portion of the NOM. The SUVA results confirm that aromatic organic matter was in the portion of the NOM competing with cyanotoxins.

Figure 4.7 compares the loading plots of CYL, MC-LR, and ANTA in ultrapure water and Lake Erie water at a contact time of 0.5 h. In almost all cases, the adsorption capacities (or q_e values) of the selected PACs for CYL, MC-LR, and ANTA were substantially decreased in NOM-containing

Lake Erie water vs. ultrapure water with the 0.5 h contact time toxin concentrations ranging from 1 to 100 µg/L. The only exception was the adsorption of MC-LR onto BG-HHM which had very similar capacities in both ultrapure water and surface water at the 0.5 h contact time. As expected, in most cases, the Lake Erie water fitting curve had a steeper slope than the ultrapure water curve, and Lake Erie water q_e values exceeded the ultrapure water q_e values when 0.5 h toxin concentrations exceeded 100 µg/L. The reduction of adsorption capacity in surface water is predominantly associated with the direct competition between NOM and the target cyanotoxins for adsorption sites and pore blocking by large NOM molecules (Zoschke et al., 2011). Some similarly sized NOM molecules to the target cyanotoxins are able to enter the micro- and mesopores, resulting in direct competition with the cyanotoxins for adsorption sites. Kilduff et al. (1998) indicated that the effects resulting from pore blocking and direct site competition are difficult to distinguish due to the similar sizes of the portion of the NOM competing for adsorption sites and the adsorbate (cyanotoxin). Similar results were observed at the 1.0 h contact time and at equilibrium, as shown in Appendix B.2.

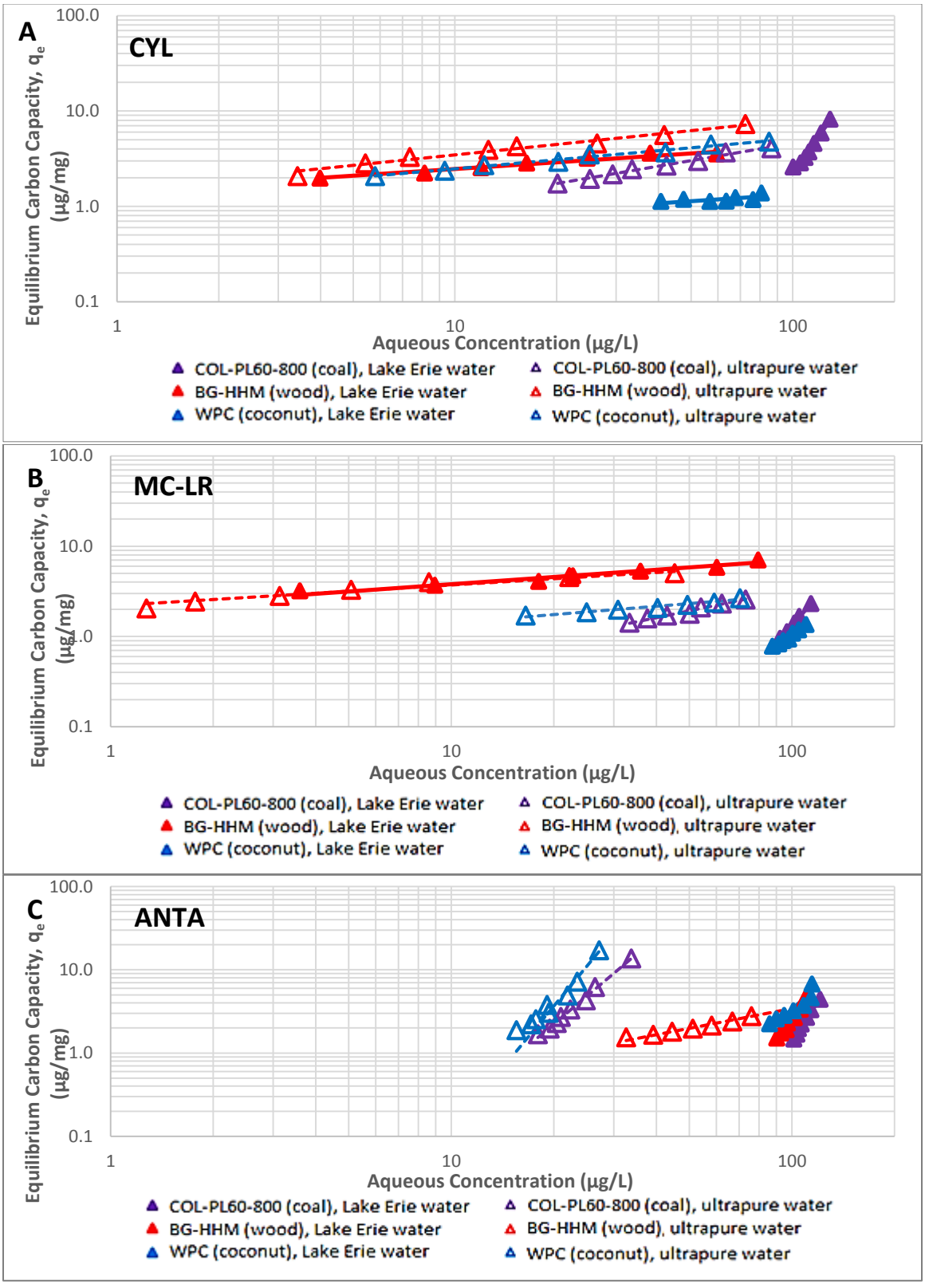

Figure 4.7 Comparison of Freundlich adsorption model fitting for adsorption of three selected PACs for cyanotoxins at 0.5 h contact in both Lake Erie water and ultrapure water. A) CYL adsorption, B) MC-LR adsorption, and C) ANTA adsorption

4.4.5 Simplified Equivalent Background Compound Model (SEBCM)

The SEBCM was used to estimate PAC doses required to treat cyanotoxins while taking the competitive adsorption of cyanotoxins and NOM in Lake Erie water into account. The loading plots/removal curves under non-equilibrium conditions at 0.5 h of contact time were used for modeling. The SEBCM fits two parameters (lnA and 1/n) to the experimentally determined removal curve based on Equation 4.1. The SEBCM fitting curves and model parameters are provided in Appendix B.3 with all having high R^2 values ranging from 0.951 to 0.995 which indicates a high goodness of fit. No systematic trends were revealed from the residual plots of the SEBCM fitting (Appendix B.3). The resulting SEBCM parameters are summarized in Appendix B.3. Plots of the residuals for each of the 0.5 h SEBCM fittings are provided in Appendix B.3, showing no trend in residuals.

As demonstrated in Figure 4.8, SEBCM capacity estimations fit the experimental data very well for adsorption of CYL, MC-LR, and ANTA by all selected PACs, indicating the model can effectively describe the adsorption of cyanotoxins in NOM-containing water under non-equilibrium conditions. This model was also applied to the removal curves obtained at 1 h contact time and equilibrium for the adsorption of each studied cyanotoxin by each selected PACs, and the model fits were good for these data with high R^2 values (Appendix B.3). It should be noted that the underlying premise in this model is that removal of a contaminant is independent from the initial concentration which has been shown by Qi et al (2007) for equilibrium data. Zoschke et al. (2011) confirmed experimentally that this assumption also applies to short contact times (i.e. non-equilibrium conditions). As well, the SEBCM model is only applicable to batch studies and it also assumes a much higher concentration of the competing EBC than the contaminant (Qi et al., 2007). While this condition is fulfilled in most practical cases, it cannot be proven exactly, because typically only the concentrations of cyanotoxins (100 µg/L in this study) and NOM (measured as DOC of 2.3 - 2.6 mg/L in this study) are available, whereas the EBC concentrations are unknown

(Worch, 2012). Furthermore, the fitted SEBCM model parameters are only valid for the specific contact time, cyanotoxin type, and surface water characteristics. Zoschke et al. (2011) also noted that the SEBCM "developed for batch processes can also be applied for completely mixed flow-through reactors, if the adsorbent mass and the solvent (water) volume are substituted with the respective fluxes mass per time and volume per time." However, Zoschke et al. (2011) have not confirmed this experimentally and further investigations are needed in support of this statement. These were beyond the scope of this thesis.

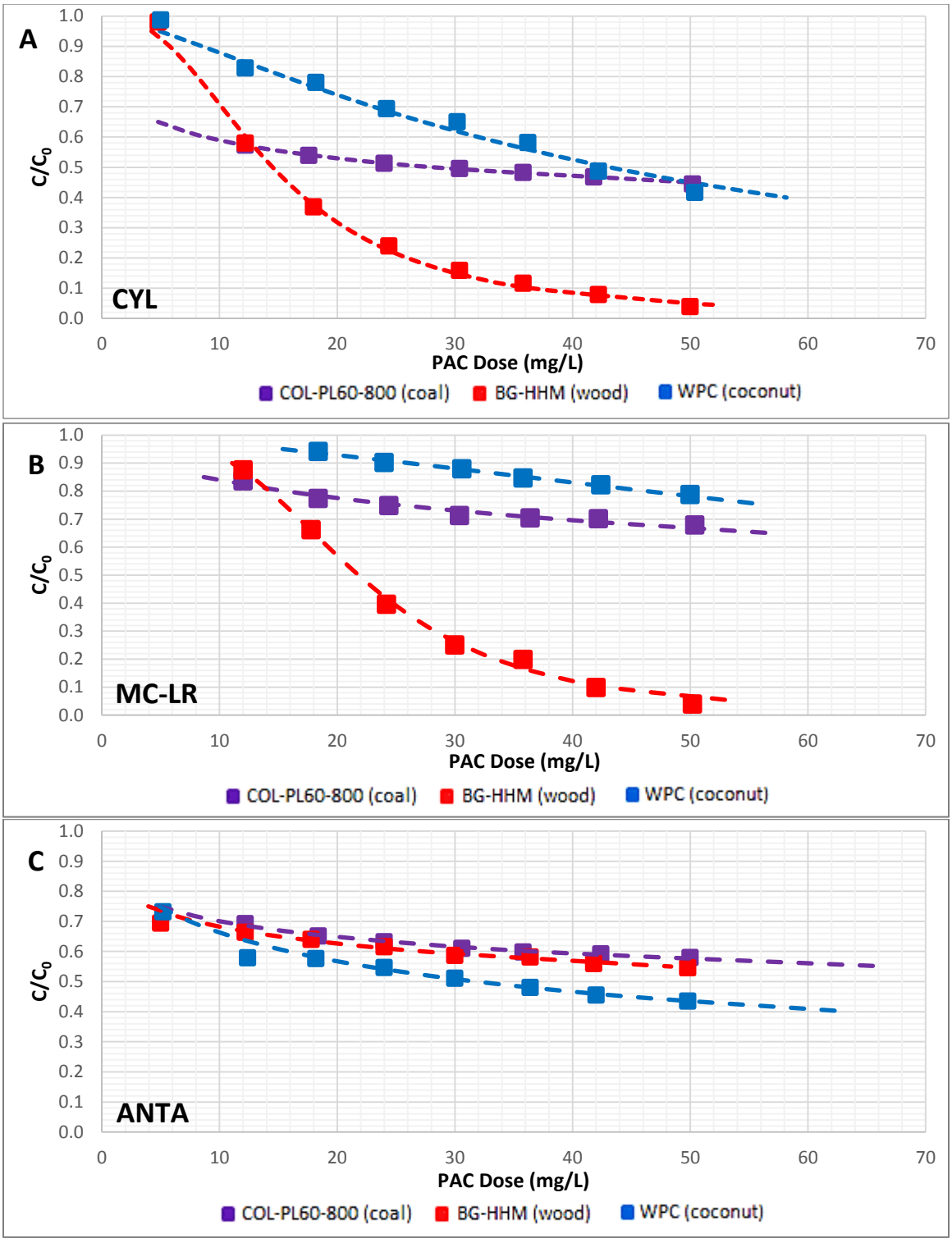

Figure 4.8 Cyanotoxin adsorption in the presence of NOM in Lake Erie water using coal-, wood-, and coconut-based PACs, based on the 0.5 h non-equilibrium data. A) CYL adsorption, B) MC-LR adsorption, C) ANTA adsorption

Once the SEBCM parameters are determined (Appendix B.3), they can then be used to estimate the relative removal (C/C_0) for a given dose of each PAC used for the adsorption of a selected cyanotoxin, according to Equation 4.2. Given a specific concentration value as the target effluent concentration (or C in Equation 4.2), the required dose of each selected PAC can be determined for removal of each cyanotoxin present at certain initial concentrations. As an example, an effluent concentration of 1.5 µg/L was selected in this study, which is the current maximum acceptable concentration (MAC) for MC-LR in drinking water based on the current Canadian Drinking Water Guideline (Health Canada, 2017). This effluent concentration was used for all studied cyanotoxins for the purposes of comparison. As demonstrated in Figure 4.9, the wood-based BG-HHM clearly outperformed all others for the removal of CYL and MC-LR and the coconut-based WPC was the most effective alternative for ANTA removal at the 0.5 h non-equilibrium condition. Nevertheless, with respect to ANTA adsorption, a very large amount of PAC was required even when using the most effective alternative, WPC (coconut), indicating that none of the selected PACs in this study would be an effective barrier for ANTA removal at 0.5 h of contact time. But, when the three studied cyanotoxins occur at fairly low initial concentrations (less than 2 µg/L), which is a common environmental scenario, no significant difference could be determined on the dose for the three selected PACs.

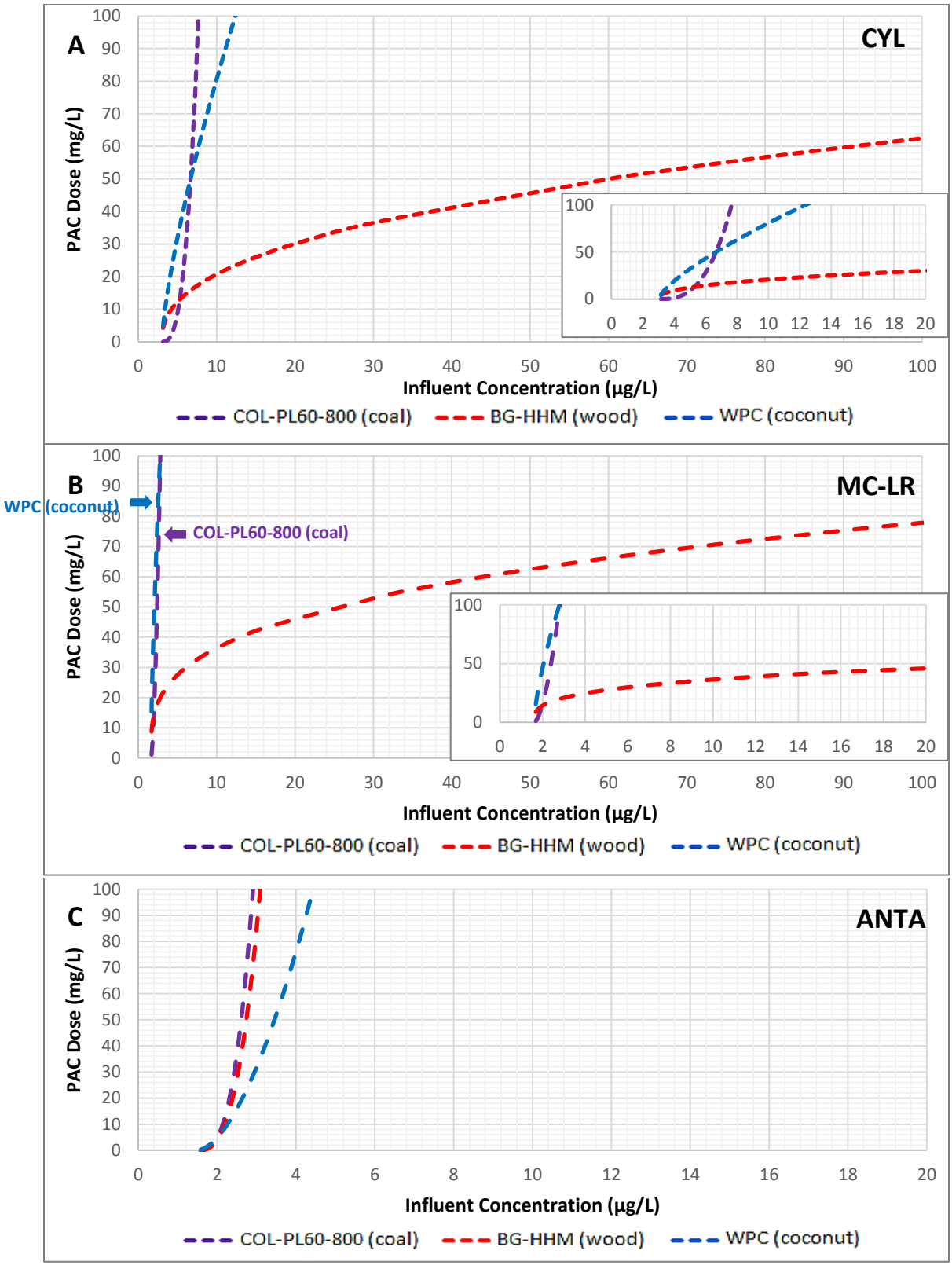

Figure 4.9 Dose estimates for coal-, wood-, and coconut-based PACs for adsorption of A) CYL, B) MC-LR, and C) ANTA in Lake Erie water, based on SEBCM under 0.5 h non-equilibrium condition, given target final concentration of 1.5 µg/L

PAC costs can then be determined for each selected PAC to adsorb each studied cyanotoxin at various influent concentrations, based on the predicted PAC dose and knowing the cost per unit mass of PAC. The PAC unit prices of the coal-based COL-PL60-800, wood-based BG-HHM, and coconut-based WPC were $3.00/kg (provided by the City of London, who made the purchase), $6.37/kg, and $4.67/kg (provided by Brenntag Canada, Calgon Carbon distributor), respectively. The prices are in Canadian dollars. As presented in Figure 4.8, BG-HHM outperformed all others for removal of CYL and MC-LR, whereas none of selected PACs could effectively remove ANTA with only 0.5 h of contact time. Again, no significant difference could be identified among the costs for the selected PACs when the target cyanotoxin is present at very low initial (influent) concentrations (< 3 µg/L).

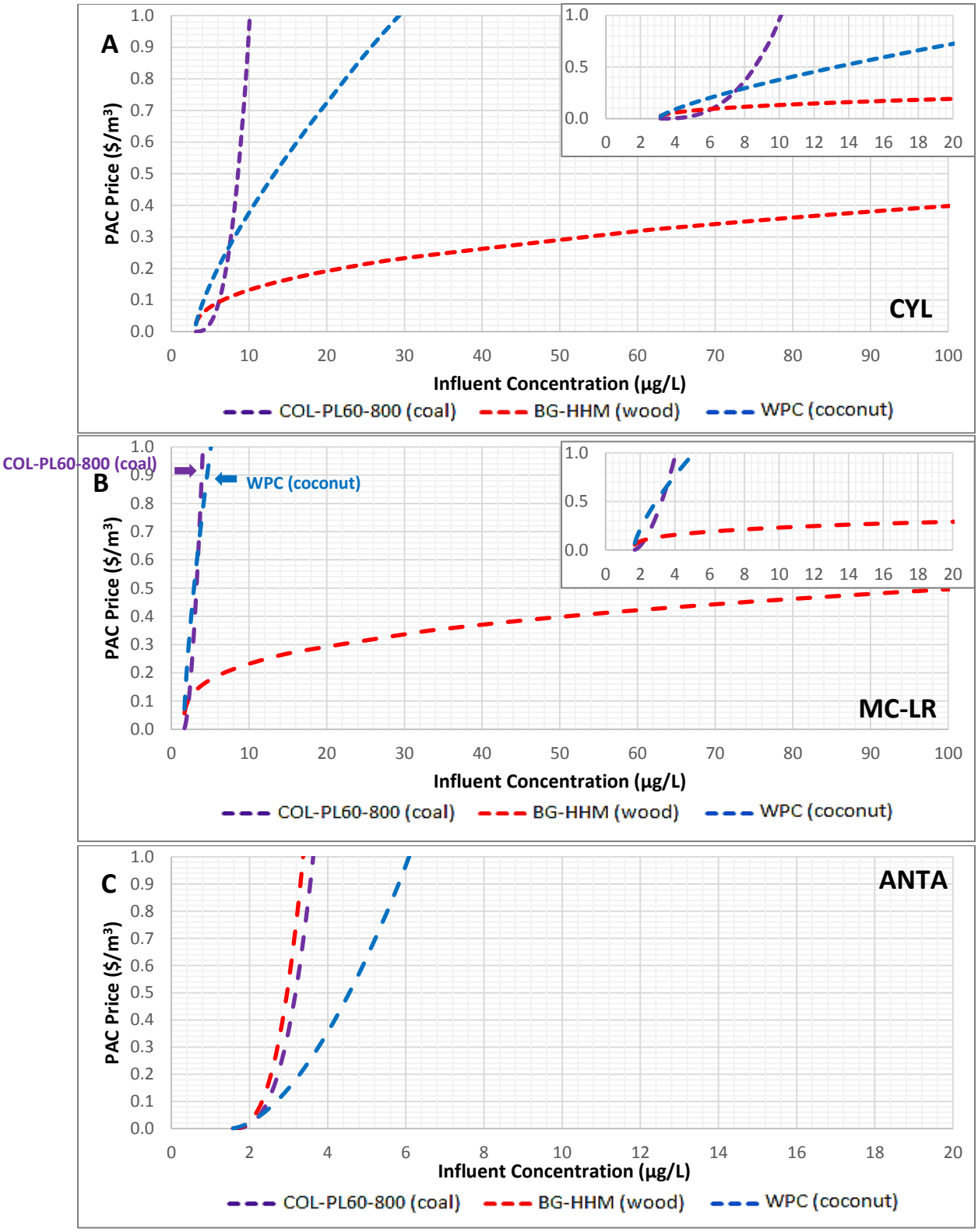

Figure 4.10 Estimate of PAC costs for adsorption of cyanotoxins at given range of influent concentrations in Lake Erie water, based on SEBCM under 0.5 h non-equilibrium conditions, given a target cyanotoxin concentration of 1.5 µg/L. A) CYL, B) MC-LR, C) ANTA

In 2015, the USEPA issued drinking water health advisories for CYL and total microcystins recommending health advisory levels at or below 0.7 µg/L for CYL and 0.3 µg/L for total microcystins in drinking water for those younger than 6, whereas for all others the recommended health advisory levels were at or below 3 µg/L for CYL and 1.6 µg/L for total microcystins (USEPA, 2015). Therefore, at certain initial concentrations of CYL or total microcystins, the required relative removals (C/C_0) are substantially distinct for young children and adults, based on the USEPA health advisories. In order to meet the health advisories for the whole community, U.S. WTPs will in most cases need to adopt the lower health advisory levels as the maximum effluent concentrations for their treatment systems, potentially introducing substantial treatment challenges. To better understand the difference between the additional investments required for WTPs from reducing effluent concentrations from high to low health advisory levels, Figure 4.11 compares the prediction of PAC dose for the adsorption of CYL and MC-LR by the wood-based BG-HHM, the most effective PAC in this study, at 0.5 h, 1 h, and equilibrium and effluent concentrations based on the USEPA health advisories. In this case, the health advisory concentrations for total microsytins were adopted for MC-LR assuming only MC-LR was present as a conservative estimate. With respect to both CYL and MC-LR adsorption, significantly higher PAC doses were required to reduce effluent concentrations from the high to low health advisory concentrations, at given contact times, particularly with high initial concentrations, representing severe blooms events. An alternative to increasing PAC dose a utility could, if possible, increase PAC contact time, by reducing hydraulic loading in the WTP. Of MC-LR adsorption, the BG-HHM (wood) reached equilibrium after 1.5 h; therefore, the 1 h and equilibrium SEBCM results are very similar to each other, as shown in Figure 4.11 B. PAC dose is usually under estimated if only equilibrium data are used in SEBCM without considering the actual PAC contact time in water treatment facilities.

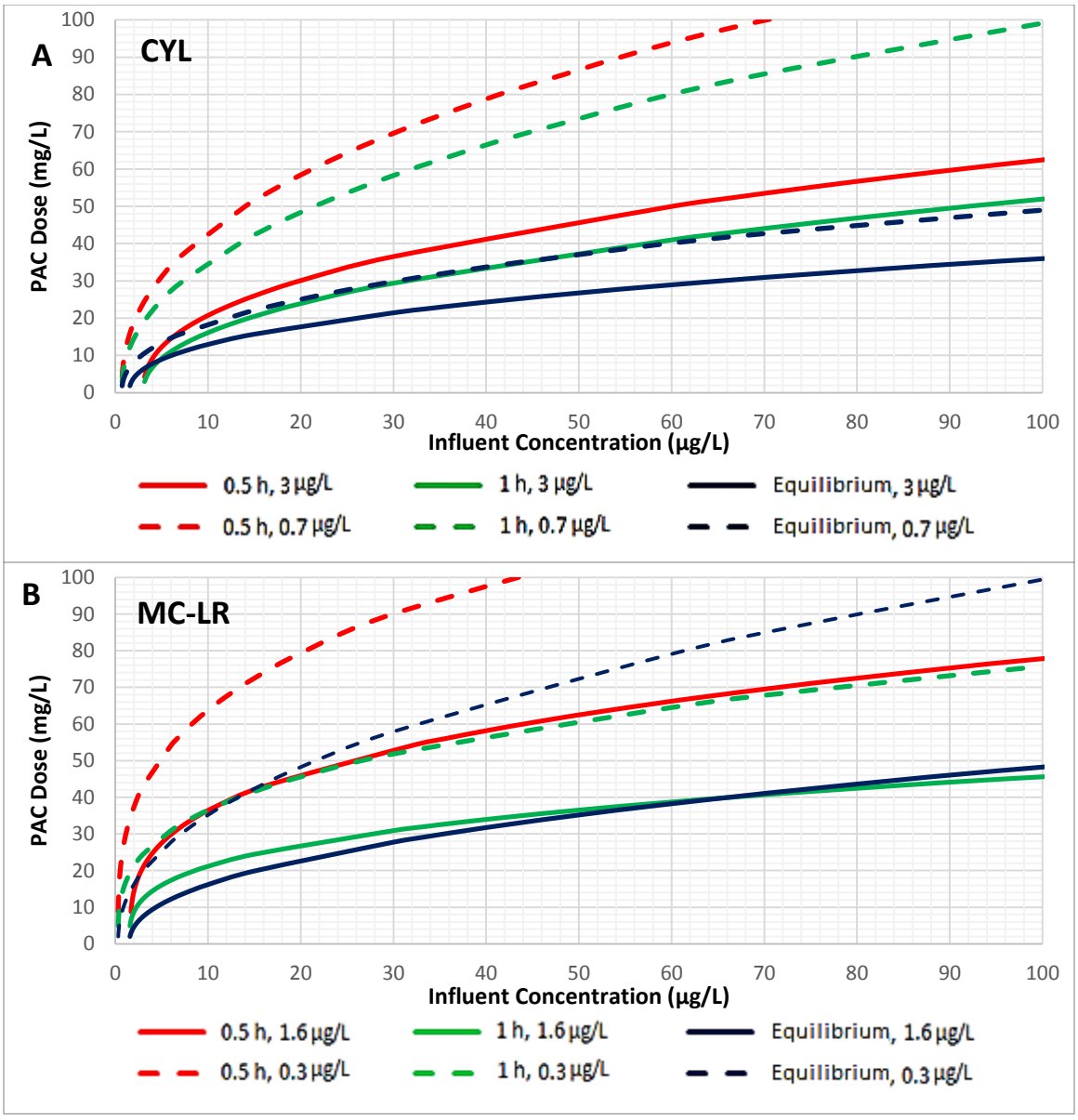

Figure 4.11 Evaluation of the effect of initial cyanotoxin concentration and PAC contact time on BG-HHM dose for CYL and MC-LR adsorption. A) CYL adsorption with initial concentrations of 0.7 µg/L and 3 µg/L at 0.5 h, 1 h, and equilibrium, and B) MC-LR adsorption at initial concentrations of 0.3 µg/L and 1.6 µg/L at 0.5 h, 1 h, and equilibrium

4.4.6 Comparison with Literature Values

The equilibrium Freundlich isotherms obtained in this study for removal of CYL, MC-LR, and ANTA from Lake Erie water were compared with available literature values. While only a portion of the DOC in Lake Erie water is able to compete with cyanotoxins for adsorption sites, the DOC content of the surface water in other studies was provided as an indicator of water quality, since

only DOC information is readily available in most studies. The comparison was broken down by PAC source material, as Figure 4.12 A showing the coal-based PAC isotherms and Figure 4.12 B with the wood-based PAC isotherms. The trade names or carbon codes of PACs, if trade names were not available, are indicated. The isotherms determined for different concentration ranges in other studies were extrapolated to be in the range of 1 - 100 µg/L used in this study. These limitations for isotherm comparison should be noted – as with limited information on NOM composition and PAC properties, PAC performance is subject to variability.

With respect to the coal-based PAC isotherms (Figure 4.12A), the 1/n values (indicating model slopes) obtained in this study were greater than those in other studies for both ANTA and CYL studies, resulting in lower capacities at low equilibrium concentrations but greater capacities at high equilibrium concentrations. In this study, CYL was somewhat better adsorbed by COL-PL60-800 than was ANTA. However, the performance of the coal-based Watercarb-800 to adsorb ANTA (Vlad et al., 2015) and PAC A to adsorb CYL (Ho et al., 2008) were quite similar, which is possibly related to the higher DOC content in the CYL study (5.4 mg/L vs. 10.2 mg/L).

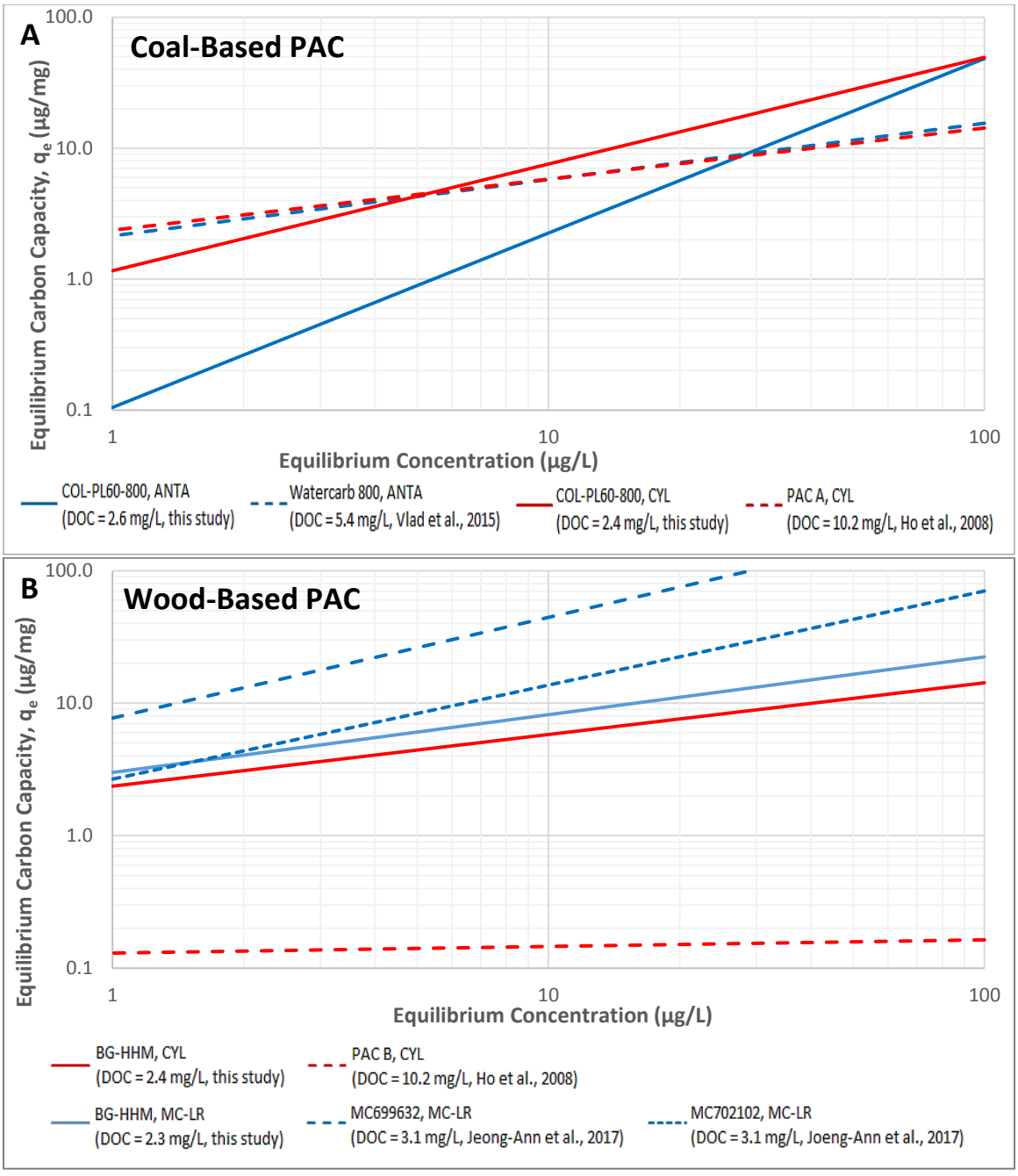

Figure 4.12 Comparison of Freundlich equilibrium isotherms in this study to literature values. A) CYL and ANTA isotherms for the coal-based COL-PL60-800 PAC are from the current study. The ANTA isotherm for coal-based Watercarb 800 PAC (Vlad, 2015), and the isotherm for CYL obtained using the coal-based PAC A (Ho et al., 2008) were plotted based on the Freundlich parameters obtained from these references. B) CYL and MC-LR isotherms for the wood-based BG-HHM PAC are from the current study. The CYL isotherm for the wood-based PAC B (Ho et al., 2008) and MC-LR isotherms for the wood-based MC699632 abd MC702102 (Joeng-Ann et al., 2017) were plotted based on the Freundlich parameters observed from these references.

In terms of the wood-based PAC isotherms (Figure 4.12 B), CYL was much better adsorbed by the BG-HHM used in this study with 2.4 mg/L of DOC than PAC B applied by Ho et al. (2008) with 10.2 mg/L of DOC, likely due at least in part to the high DOC content resulting in far more competition for adsorption sites. In addition, PAC properties, such as pore volume and size, might also play a role, while various factors other than source material could alter PAC properties, such as the activation method. Although the DOC contents were higher, MC699632 performed similarly to the BG-HHM at low equilibrium concentrations, and both mesoporous carbon, MC699632 and MC702102, outperformed BG-HHM for MC-LR adsorption, as reported by Jeong-Ann et al. (2017) who used these two mesoporous carbons particularly targeting the molecular dimensions of MC-LR. In the present study, CYL was slightly less well adsorbed than MC-LR by BG-HHM at environmentally relevant cyanotoxin concentrations.

4.5 Conclusions

The adsorption of CYL, MC-LR, and ANTA by the coal-based COL-PL60-800, wood-based BG-HHM, and coconut-based WPC PACs was investigated in Lake Erie water using the bottle-point technique.

With respect to CYL adsorption, the BG-HHM (wood) adsorbed it the fastest, achieving equilibrium after 6 h of contact, while the COL-PL60-800 (coal) and WPC (coconut) performed similarly reaching equilibrium after 10 h. At equilibrium, COL-PL60-800 (coal) performed much better with a higher capacity than BG-HHM (wood) and WPC (coconut), with 2.9 µg/mg adsorbent at an aqueous CYL concentration of 1 µg/L (vs. 2.3 µg/mg for BG-HHM and 2.1 µg/mg for WPC). Carbon loading was also determined at 0.5 h and 1.0 h contact, mimicking the competitive adsorption of CYL in NOM-containing water under realistic drinking water treatment conditions. In this study, the Freundlich model was also used to evaluate PAC capacity under non-equilibrium conditions. Assessment of non-equilibrium carbon loading revealed substantial differences

compared to the equilibrium isotherms, with significant reductions in adsorption capacities of COL-PL60-800 (coal) and WPC (coconut), but with only a slight decrease in capacity for BG-HHM (wood). This effect was mainly due to the faster rate of adsorption of BG-HHM (wood), as BG-HHM (wood), unlike the other PACs, was very close to having reached equilibrium at 0.5 h and 1.0 h.

In terms of MC-LR adsorption, BG-HHM (wood) adsorbed it the fastest, achieving equilibrium in approximately 1.5 h, followed by COL-PL60-800 (coal), and finally WPC (coconut) which took 10 h and 60 h respectively. At equilibrium, the COL-PL60-800 (coal) and BG-HHM (wood) performed similarly with the highest capacities (3.0 µg/mg adsorbent for both carbons at an aqueous microcystin-LR concentration of 1 µg/L), followed by WPC (2.7 µg/mg adsorbent at MC-LR concentration of 1 µg/L). Under non-equilibrium circumstances, BG-HHM's capacity was somewhat reduced, whereas WPC (coconut) and COL-PL60-800 (coal) had severely reduced capacities.

ANTA adsorbed much more slowly than CYL and MC-LR. Of the 3 PACs, WPC (coconut) reached equilibrium most quickly (in about 72 h), while BG-HHM (wood) required 120 h and COL-PL60-800 (coal)over 221 h. WPC (coconut) and BG-HHM (wood) had the highest equilibrium capacities for ANTA (1.7 µg/mg and 1.4 µg/mg, respectively, at a 1 µg/L aqueous ANTA concentration), which was substantially higher than for COL-PL60-800 (coal) (0.6 µg/mg at 1 µg/L ANTA concentration). Under non-equilibrium conditions, all 3 PACs had substantially reduced adsorption capacities for ANTA, although WPC performed somewhat better than the others. As such, none of selected PACs in this study is an effective barrier for ANTA removal and for this reason other PAC products or other ANTA removal techniques, such as ozonation, should be considered if a water source is known to be particularly prone to ANTA formation.

The adsorption efficiency for all studied cyanotoxins was reduced in NOM-containing Lake Erie water, as the highly adsorbable NOM compounds competed for adsorption sites and blocked access

to the sites. Furthermore, in full-scale practice, PAC contact time is typically not long enough to reach the adsorption equilibrium.

The SEBCM was applied in this study using data sets obtained at short contact times to describe the competitive adsorption of cyanotoxins and NOM under non-equilibrium conditions and hence, to more accurately reflect full-scale plant practice. PAC dose and corresponding costs for each PAC used to removal each selected cyanotoxin were determined under 0.5 h and 1 h non-equilibrium conditions, given a target effluent concentration of 1.5 µg/L as the model input. The results revealed that at high initial concentrations (> 3 µg/L for CYL and > 2 µg/L for MC-LR), the wood-based BG-HHM was the most cost-effective alternative for both CYL and MC-LR removal, whereas at low initial concentrations, not much difference could be discerned among the 3 PACs. Although the coconut-based WPC outperformed the other 2 PACs for ANTA adsorption, none of the selected PACs was a cost-effective barrier when initial concentrations were higher than 6 µg/L. It should be noted that the SEBCM parameters are only valid for the investigated circumstances, with the specific PAC, contact time, cyanotoxin, and water source. These findings confirm that the SEBCM can be a useful tool to determine the PAC dose required to reduce cyanotoxin concentrations to below regulatory maximum accepted concentrations/limits.

Chapter 5

Cylindrospermopsin Adsorption by Granular Activated Carbon in Ultrapure Water

5.1 Summary

The adsorption of CYL onto three virgin GACs (coal-, wood- and coconut-based) and one preloaded GAC in ultrapure water was investigated at bench-scale using the bottle-point technique at potential environmental CYL levels. Of the virgin GACs, the wood-based C Gran had the fastest adsorptive rate, followed by the coconut-based Aqua Carb, while the coal-based F-300 removed CYL the slowest. Conversely, the F-300 had the highest overall capacity at equilibrium, while the C Gran had the lowest capacity among all virgin GACs investigated at an initial CYL concentration of 100 µg/L. Both the rate of CYL adsorption and capacity of the F-300 deteriorated substantially as a result of NOM adsorption during preloading.

5.2 Introduction

Cyanobacteria were amongst the earliest primary organisms responsible for providing an oxygen-rich atmosphere on Earth through photosynthesis reactions, by converting atmospheric nitrogen to ammonia. Cyanobacteria have long been known to be potent producers of a variety of toxins (cyanotoxins) causing human and animal illness and in some cases death, and their presence in drinking water is a potential risk to public health (Carmichael et al., 1997; Svrcek & Smith, 2004; Westrick et al., 2010; Merel et al., 2013; Vlad, 2015). While the environmental factors required for cyanobacterial growth and bloom of an individual species are not completely understood, the formation of a cyanobacterial bloom is generally affected by a combination of three primary environmental variables, including temperature, light and nutrients (Merel et al., 2013). Eutrophication resulting from excess nutrient loading and storage in lakes and reservoirs is often considered as the primary cause of dominance of cyanobacteria over competing organisms in

aquatic ecosystems, and global climate change may be creating conditions favouring cyanobacterial blooms (Merel et al., 2013).

Cylindrospermopsin (CYL) has emerged as one of the most important cyanotoxins worldwide from the perspective of source water protection, due to its multiple toxicity endpoints, the severity of health impacts, and frequency of occurrence (de la Cruz et al., 2013). It mainly inhibits protein translation and binds to DNA, leading to strand breakage and in turn causing hepatotoxicity, cytotoxicity, neurotoxicity and genotoxicity (Svrcek & Smith, 2004; Westrick et al., 2010). CYL was named based on *Cylindrospermopsis raciborskii*, but other CYL-producing cyanobacteria species are also known, including *Aphanizomenon ovalisporum*, *Raphidiopsis curvata*, and *Umezakia natans* (Merel et al., 2003). CYL is a zwitterion in the typical pH range of natural waters, resulting in high water solubility with a half-life exceeding ten days in ultrapure water (Chiswell et al., 1999; Westrick et al., 2010).

At present, there are no official guidelines or regulations for CYL in drinking water worldwide, however, the USEPA has included CYL on the third iteration of the Contaminant Candidate List (CCL 3) as well as on the draft CCL 4 (USEPA, 2016). In addition, the USEPA issued "10-Day Drinking Water Health Advisories (HAs)" for CYL in 2015, which indicated 0.7 µg/L for bottle-fed infants and pre-school children and 3 µg/L for all others (USEPA, 2015). A CYL drinking water guideline of 1 µg/L was proposed by Humpage & Falconer (2003).

CYL was initially considered a tropical toxin, as it was only detected in warm climates, such as Australia and New Zealand (Chiswell et al., 1999), until it was discovered in temperate countries, such as Germany (Fastner et al., 2003). In North America, CYL has been reported in Florida and Louisiana at concentrations as high as 202 µg/L (Yilmaz & Phlips, 2011), and it has also been reported in the state of New York and the Lower Great Lakes (Boyer, 2008). Therefore, it would be prudent to assume it could be present in most temperate regions, and drinking water treatment plants should be designed or assessed for the removal or inactivation of CYL and other cyanotoxins.

Some drinking water oxidants/disinfectants, including chloramines, chlorine dioxide, and potassium permanganate have been shown to be ineffective for CYL treatment (Cheng et al., 2009; Westrick et al., 2010). Although chlorine is able to oxidize CYL, two hepatotoxic chlorination by-products have been identified including 5-chloro-cylindrospermopsin (Senogles et al., 2000) and cylindrospermic acid (Banker et al., 2001) (Westrick et al., 2010) so this potentially restricts its use. Ozone and advanced oxidation processes (AOPs) are highly effective for CYL inactivation, however, ozone oxidation of CYL is pH-dependent and AOPs are not widely employed.

To date, it does not appear as if any adsorption data have been published on the removal of CYL by granular activated carbon (GAC). However, powdered activated carbon (PAC) has been demonstrated to be an effective treatment barrier for extracellular CYL (Donati et al., 1994; Newcombe & Nicholson, 2004; Westrick et al., 2010; Merel et al., 2013). Ho et al. (2008) predicted that a PAC dose of 25 mg/L is required to lower a CYL concentration from 5 µg/L to somewhere below 1 µg/L, at a contact time of 60 min in natural water, using the homogenous surface diffusion model (HSDM).

Adsorption is a complex process and is governed by a wide range of factors which affect transport and access of an adsorbate to adsorption sites, and attachment mechanisms between adsorbate and adsorption sites, such as hydrophobic and electrostatic interactions (Delgado et al., 2012; Vlad, 2015). Typically, multiple factors and mechanisms are at play, and the complex interactions between those factors are difficult to investigate. Capacity (as described by isotherms) and rate of adsorption are good indicators of adsorptive behavior and were used in this study.

As with most activated carbon, capacity is diminished by competitive adsorption with dissolved natural organic carbon (NOM). This is a result of two potential mechanisms: 1) pore blockage by NOM, as larger NOM molecules block the small pores or access to the pores limiting the access of smaller cyanotoxin molecules; and 2) direct competition, as small NOM molecules directly compete with cyanotoxin molecules for access to the adsorption sites (Donati et al., 1994;

Campinas & Rosa, 2006; Ratnayake et al., 2011; Zoschke et al., 2011). In addition, preloading of GAC with natural water has been shown to change the surface properties of carbons, particularly the surface charge, which might significantly alter the adsorption behavior of carbons (de Ridder et al., 2011). Thus, GAC kinetics and capacity are usually substantially impacted by preloading effects, and is dependent on contact time, water quality, preloading duration, and carbon type (Crittenden et al., 2012). To date, the effects of carbon preloading for CYL have not been reported.

The objectives of this chapter are to: 1) investigate CYL adsorption by a variety of GACs in ultrapure water; and 2) investigate the impact of preloading on GAC adsorption of CYL. Performing GAC adsorption studies in ultrapure water can provide a baseline measure to better understand CYL adsorption behavior.

CYL adsorption studies were conducted at bench-scale using the bottle-point technique. Three virgin GACs (coal-based Calgon F-300®, wood-based Norit C Gran®, coconut-based Evoqua Aqua Carb CX®), and one preloaded coal-based GAC (Calgon F-300®, prepared by Vlad, 2015) were selected. All four selected carbons were investigated with respect to their performance of CYL adsorption in ultrapure water in batch experiments under controlled conditions, and performance was evaluated based on kinetics and equilibrium capacity (or isotherms).

5.3 Materials and Methods

5.3.1 Materials

Coal-based F-300® GAC was provided by Calgon Carbon (PA, USA), wood-based C Gran® GAC was provided by Norit (TX, USA), and coconut-based Aqua Carb CX® GAC was provided by Evoqua (PA, USA). All GACs were donated by the manufacturers at no charge. These GACs were originally acquired for use in an anatoxin-a study (Vlad, 2015).

The CYL standard (> 95% purity) was acquired from GreenWater Laboratories (FL, USA), and HPLC-grade 1,9-diaminononane, HPLC-grade acetonitrile and formic acid were acquired from Sigma-Aldrich (WI, USA). Ultrapure water was produced using a Millipore Milli-Q® UV PLUS water system (MA, USA).

A 100 mg/L CYL stock solution of was prepared by dissolving 1 mg of solid CYL into 10 mL of Milli-Q water. A CYL working solution of 1 mg/L was then diluted from the stock solution. 100 mg/L of 1,9-diamininonane stock solution was prepared using Milli-Q water, and was diluted to a working solution of 1 mg/L. The CYL and IS stock solutions were prepared monthly, whereas working solutions for both compounds were refreshed weekly. All stock and working solutions described above were stored in amber vials at -20 °C.

5.3.2 Sample Preparation and Handling

The bottle-point method was applied to investigate the adsorption of CYL by virgin GACs in Milli-Q® water at bench-scale (Droste, 1997). As recommended by Worch (2012), adapted from Sontheimer et al. (1988), virgin GACs were rinsed with Milli-Q® water to remove fine particles, dried at 110 °C for 24-36 h, and finally stored in desiccators. In an effort to standardize the test protocol, all GAC products were sieved to capture particles ranging from 420 µm to 2.38 mm using ASTM C 136-06 Standard Test Method for Sieve Analysis of Fine and Coarse Aggregates (ASTM International, 2014).

The freeze-dried preloaded GAC sample was prepared by Vlad (2015). The coal-based Calgon F-300® GAC was preloaded with post-sedimentation water from the Mannheim Water Treatment in Southwestern Ontario, which uses the Grand River as a source.

Milli-Q® water was produced and collected as a batch, and then stored to equilibrate overnight with no pH adjustment. The pH of equilibrated Milli-Q® water stabilized to pH values between 6.2 to 6.6. The selected GACs in this study were not crushed in an effort to more accurately simulate

GAC conditions in a full-scale plant. Furthermore, this study intended to compare adsorption behavior between virgin and preloaded carbons. Preloaded GAC cannot be crushed, as crushing would open previously inaccessible pores and in turn change properties of the preloaded carbon. Based on the sieve size analysis (Table 5.1), the median diameter is 0.84 - 1.19 nm for both the F-300 (coal) and C Gran (wood), and 0.60 - 0.84 nm for Aqua Carb (coconut). Given GAC particle size may affect its adsorption performance, particles in median size range were used in this study for adsorption experiments to represent the particle size of each product. For each GAC test, eight 500 mL bottles were filled with 500 mL of 100 µg/L CYL solution and uncrushed GAC was added to each with the initial dose being 4 mg followed by 6, 9, 12, 15, 18, 21 and 25 mg). One positive 100 µg/L CYL control in Milli-Q water without GAC was included in each batch to monitor potential CYL degradation over time. Four negative controls (one for each GAC) containing 500 mL of Milli-Q® water and 50 mg/L of GAC, and one blank containing only 500 mL of Milli-Q® water were included to exclude any compounds that could be possibly misidentified as CYL.

Table 5.1 Carbon properties (Vlad, 2015)

Product name	Manufacturer	Base material	Activation	Median Effective size[1] (mm)	pH_{PZC}[2]	BET surface area[3] (m^2/g)	DFT method pore volume[3] (cm^3/g)	DFT pore size distribution[3]			% of pore volume in micropores[3, 4]
								Primary Micropores <0.8 nm (cm^3/g)	Secondary Micropores 0.8-2 nm (cm^3/g)	Mesopores 2-24 nm (cm^3/g)	
F300	Calgon	Coal	Steam	0.84 – 1.19	9.2	1057	0.551	0.23	0.19	0.14	74%
Aqua Carb	Siemens (now Evoqua Water Technologies)	Coconut	Enhanced	0.60 – 0.84	10.1	1568	0.672	0.33	0.31	0.08	94%
C Gran	Norit	Wood	Chemical	0.84-1.19	4.6	1813	1.444	0.12	0.40	0.89	36%

[1] experimentally determined at the University of Waterloo; [2] pH point of zero charge - experimentally determined at the University of Waterloo; [3] experimentally determined at external lab; [4] micropores defined as <2 nm (Rouquerol *et al*., 1994)
BET – Brunauer–Emmett–Teller adsorption theory

DFT – density functional theory

All samples and controls were placed onto 3 orbital shakers at 150 rpm with an opaque cover to minimize light exposure. The CYL concentrations in the sample bottles containing the highest GAC doses (50 mg/L) were monitored regularly by taking 1 mL aliquot from the bottles and measuring it directly by LC-MS/MS without any further sample pretreatment. Equilibrium was defined as less than 1% of daily change in aqueous concentration (Vlad, 2015). CYL concentrations in each of the sample and control bottles were determined at equilibrium, and then used to generate Freundlich adsorption isotherms. Equilibrium was reached at Day 12, 10, and 11 for F-300, C Gran, and Aqua Carb, respectively. The positive controls remained relatively stable throughout the contact period with less than 10% loss in any sample.

5.3.3 CYL Analysis by LC-MS/MS

CYL concentrations were measured using a Shimadzu 8030 liquid chromatography tandem mass spectrometer (LC-MS/MS), composed of a Shimadzu DGU-20A3R degassing unit and a Shimadzu LC-20 ADXR pump with a 100 µL looping system. The system contained a tandem quadrupole mass spectrometer analyzing various analytes via a multiple reaction monitoring (MRM) technique, which monitored a specific precursor ion and corresponding product ion(s) for each analyte. A 50 mm x 2.1 mm Pinnacle DB C18 analytical column with 1.9 µm packing (Restek, PA, USA) was used and heated to 35℃for analysis. This CYL method was based on those of Bogialli et al. (2006) and Oehrle et al. (2010). An internal standard, 1,9-diaminononane at a concentration of 10 mg/L, was selected for analysis based on the Bogialli et al. (2006) study. The binary eluent employed an aqueous (with 0.1% formic acid) and an acetonitrile (with 0.1% formic acid) mobile phase at a flow rate of 0.3 mL/min, adapted from Oehrle et al. (2010). The binary eluent was run isocratically, by employing 98% aqueous and 2% acetonitrile mobile phase. Injection volume was 20 µL. MRM monitored 415.95>194.10 and 415.95>336.25 transitions for CYL, and the 159.10>142.15 transition for 1,9-dianinononane. An eight-point linear calibration was established in the range of

0.5-100 µg/L CYL, with a method detection limit (MDL) of 0.23 µg/L. Internal standard quantification was performed using 1,9-diaminononane.

5.3.4 Data Analysis

5.3.4.1 Pseudo-First Order Model

The empirical pseudo-first order model is described in Section 3.3.4.1 of this thesis.

5.3.4.2 Pseudo-Second Order Model

The empirical pseudo-second order model is described in Section 3.3.4.2.

5.3.4.3 Freundlich Isotherm Model

The Freundlich isotherm model was used to describe CYL adsorption in this chapter, the model is described in detail in Section 3.3.4.3.

5.3.4.4 Equilibrium Column Model

In water treatment, time to breakthrough or the bed life of carbon is critical for the application of GAC in the form of fixed-bed adsorbers.

The equilibrium column model (ECM) is a simple model which simplifies the ideal 'S' shaped breakthrough curve into a single breakthrough estimate using only the single-solute solution Freundlich isotherm data as input. The model assumes that the input adsorbate solution is of constant concentration and the mass transfer zone (MTZ) is of negligible depth, eliminating resistance to mass transfer and minimizing dispersion (Worch, 2012). Notwithstanding its limitations, the ECM can effectively approximate the bed life of a theoretical fix-bed adsorber (Hand et al., 1997), and the steps of preliminary calculation are discussed below.

In a single-solute system, the ECM calculation is similar to the "carbon usage rate". Given negligible MTZ depth, the carbon column is completely saturated when adsorbate reaches the base

of the column, representing the largest specific throughput or smallest carbon usage rate (CUR). The total volume of water treated prior to exhaustion is calculated as:

$$V = \frac{q_i * m_A}{C_i} \quad (5.1)$$

Where q_i is the carbon loading at equilibrium, C_i represents the influent adsorbate concentration, and m_A is the mass of adsorbent in use. By applying the Freundlich equation to obtain q_i, Equation 5.1 yields:

$$V = \frac{K_F * C_i^{1/n} * m_A}{C_i} \quad (5.2)$$

where K_F and 1/n are Freundlich isotherm parameters for adsorbate (or CYL in this case).

By rearranging Equation 5.2, the carbon usage rate or CUR prior to exhaustion at initial concentration of C_i yields:

$$CUR = \frac{m_A}{V} = \frac{C_i}{K_F * C_i^{1/n}} \quad (5.3)$$

Based on Equation 5.3, the specific throughout is calculated as:

$$Specific\ throughout = \frac{1}{CUR} \quad (5.4)$$

5.4 Results and Discussion

5.4.1 Carbon Properties

Three virgin GACs were selected to represent a variety of available products for drinking water treatment, including source material, porosities, activation methods, and particle sizes. Carbon properties of the selected GACs are presented in Table 5.1. This table was prepared based on Vlad (2015), as the GAC products used in this study were those examined in Vlad's ANTA research.

One coal-based steam-activated GAC, one wood-based chemically activated GAC, and one coconut-based GAC with enhanced activation were tested.

The wood-based C Gran had more than twice the pore volume (DFT) than the coconut-based Aqua Carb, which in turn had about 14% more pore volume than the coal-based F-300. The BET surface area followed the same pattern. It is notable that C Gran had the largest volume of secondary micropores in the range of 0.8 - 2 nm and substantially more mesopore volume (2 - 24 nm). The molecular dimensions of CYL were determined to be 1.573 nm in length and 0.901 nm in width, using MarvinSketch® chemical editor (ChemAxon®, Budapest, Hungary). The dimensions suggest that CYL is potentially adsorbed on the cusp of secondary micropores and would fit within mesopores at the operating pH level (pH = 6.5), F-300 and Aqua Carb are positively charged whereas C Gran is negatively charged, based on their points of zero charge (pH_{PZC}) (Table 5.1). CYL appears approximately neutrally charged in the range of drinking water pH (6.0 - 8.5) and as such a positively or negatively charged surface of the carbons will likely not result in additional interactions (attraction or repulsion) between CYL and the adsorbent (Table 2.2).

5.4.2 Rate of CYL Adsorption in Ultrapure Water

The rate of CYL adsorption in ultrapure water using three virgin GACs and one preloaded GAC are shown in Figure 5.1 (initial CYL concentration was 100 µg/L). All three virgin GACs reached equilibrium by Day 13 but at significantly different rates. The wood-based C Gran adsorbed CYL the fastest in the first 3 days; however, the adsorption rates of the coal-based F-300 and the coconut-based Aqua Carb overtook C Gran from Day 4 until equilibrium. F-300 and Aqua Carb performed similarly throughout the experiment, with Aqua Carb reaching equilibrium about 1 day faster.

To investigate carbon preloading effects on CYL adsorption, preloaded F-300 GAC was tested. The F-300 was preloaded with post-sedimentation water from a full-scale surface water treatment plant, as described by Vlad (2015). A sample of preloaded GAC from Vlad (2015) had been freeze-dried and stored in desiccator until use in this study. The preloaded F-300 reached equilibrium in

23 days and its CYL adsorption was substantially slower than that of the virgin F-300, which achieved equilibrium in 12 days.

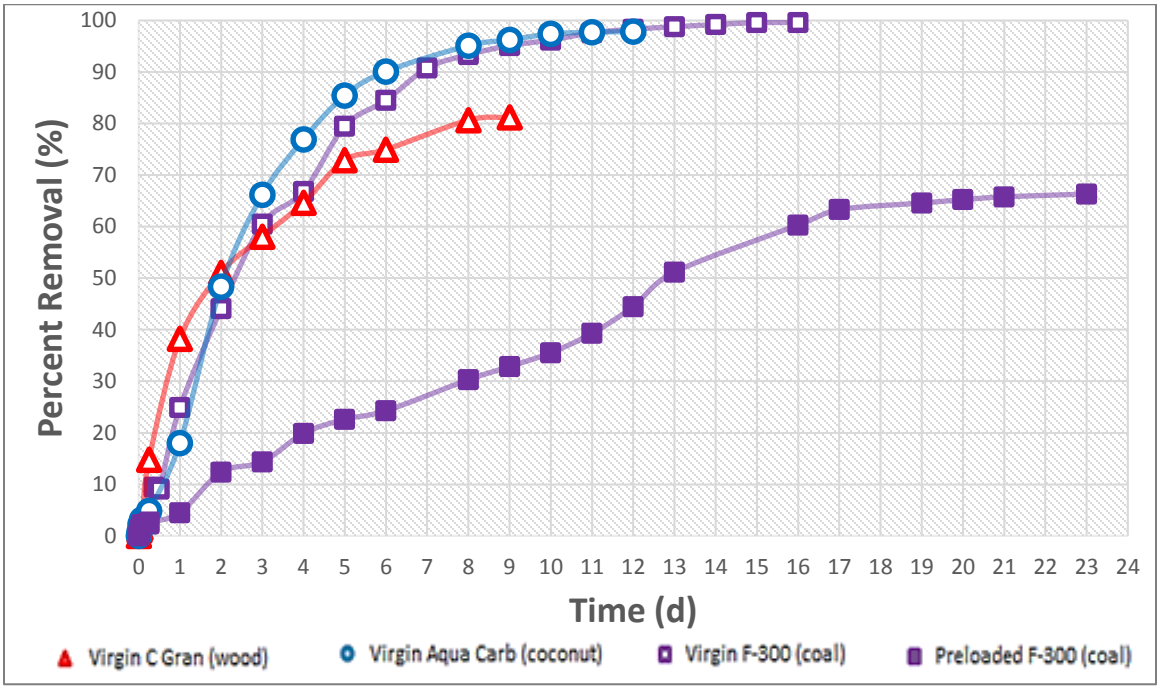

Figure 5.1 CYL removal in ultrapure water by virgin and preloaded GACs as a function of time; initial CYL concentration = 100 µg/L, GAC dose = 50 mg/L.

The pseudo-first and -second order models were applied to describe (fit) the rate of adsorption of CYL in ultrapure water using three virgin GACs and one preloaded GAC (Figure 5.2, Table 5.2, and Appendix C.1).

Based on the virgin GAC results, the R^2 values for the pseudo-first order model were either lower than or very similar to those of pseudo-second order model, indicating that the pseudo-second order model is better suited to describe the adsorption behavior of CYL using virgin GAC. Therefore, only this model was used to describe the adsorption of the selected carbons. The results of pseudo-first order model are documented in Appendix C.1. As shown in Figure 5.2, the pseudo-second order kinetic curves have higher R^2 values for the virgin F-300 (coal) and the virgin C Gran (wood) than the pseudo-first order curves, while the R^2 values calculated from both kinetic models are similar for the virgin Aqua Carb (coconut) and the preloaded F-300 (coal). Yet, the adsorption

behavior of the preloaded GAC was not very well described by both kinetic models, as the experimental data points did not line up on the kinetic model curve very well (Figure 5.2 and Appendix C.1). Pseudo-second order model is able to provide more accurate prediction for the F-300 (coal) adsorption, with much higher R^2 value. Therefore, pseudo-second order model was discussed in this chapter. Pseudo-first order model data were summarized in Appendix C.1. Removal rates are described by the pseudo-second order rate constants shown in Table 5.2, with the wood-based C Gran adsorbing CYL more rapidly than the coconut-based Aqua Carb, which in turn adsorbed CYL a little faster than the coal-based F-300 GAC. Kinetics constants generated by this model can provide a good estimation of the kinetic behavior of the selected GACs in adsorbing CYL.

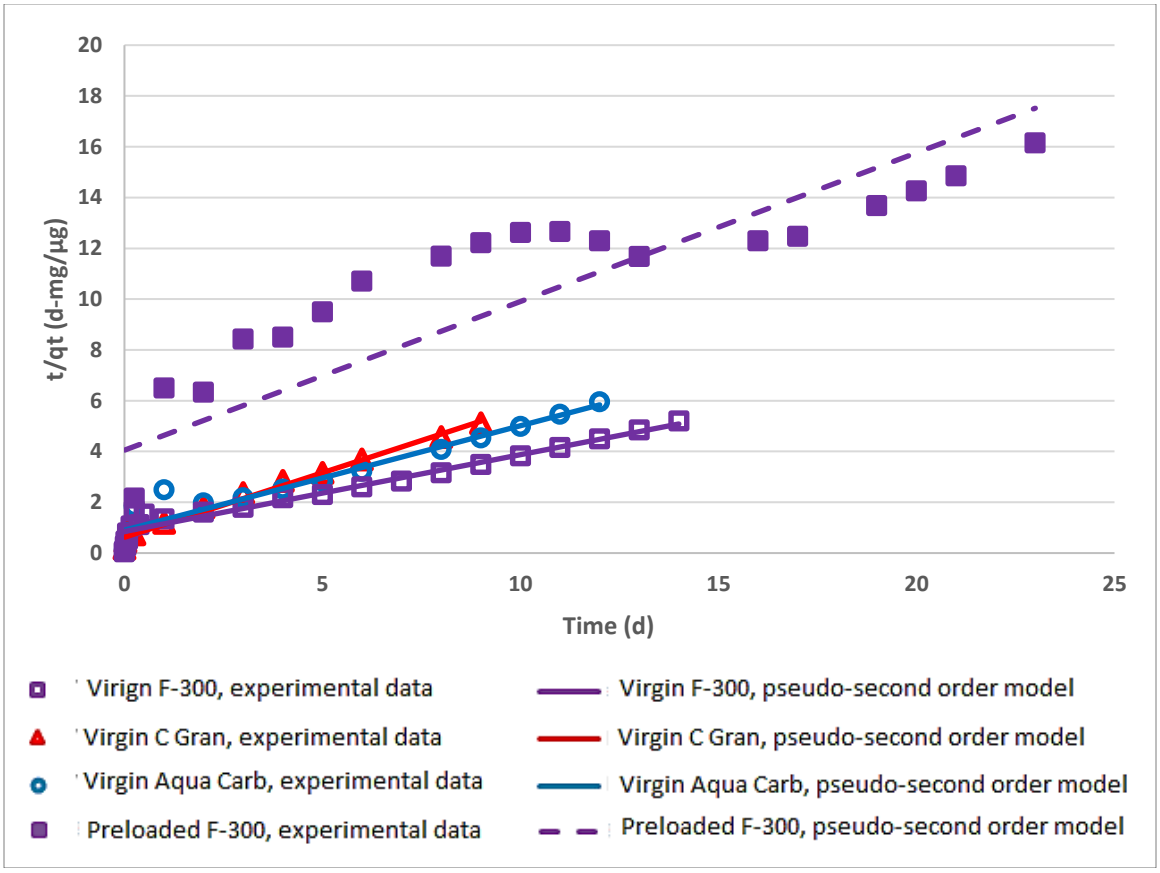

Figure 5.2 Pseudo-second order kinetic model fits using virgin and preloaded GACs in ultrapure water

Table 5.2 Pseudo-second order kinetic model fits using virgin and preloaded GACs in ultrapure water

GAC	Equilibrium Carbon Capacity, qe experimental (µg/mg)	Equilibrium Carbon Capacity, qe predicted (µg/mg)	k^2 (mg/µg/day)	R^2
Virgin F-300 (coal)	2.67	3.31	0.11	0.95
Virgin C Gran (wood)	1.76	1.97	0.41	0.99
Virgin Aqua Carb (coconut)	2.02	2.43	0.19	0.94
Pre-loaded F-300 (coal)	1.40	1.71	0.08	0.77

Both kinetic models yielded similar fits for the adsorptive behavior of preloaded F-300, but the R^2 values for both models were lower than those obtained in virgin F-300 experiments. As shown in Table 5.2 and Appendix C.1, the kinetics constants for preloaded F-300 obtained by both models are somewhat smaller than those for the virgin GACs, indicating slower rates of adsorption. This agrees with the rates of adsorption shown in Figure 5.1. Nevertheless, preloaded F-300 demonstrates two-phase kinetic behavior described by both models, as the kinetic curves behaved differently in the first 10 days and the period afterwards in both models. The two-phase kinetic behavior indicates systematic errors for both models. This was confirmed in the residual plots (Appendix C.1), with systemic errors being associated with both models. Therefore, none of the kinetic models can accurately describe CYL adsorption by GAC in this study. Further investigation is required to identify a more suitable fitting model for this carbon and to explore the different adsorptive behavior in those two phases.

5.4.3 Isotherms

The Freundlich isotherms (Equation 6, Section 3.3.5.3) are plotted in Figure 5.4 using equilibrium data obtained by the bottle-point technique for CYL adsorption by each GAC in ultrapure water. The Freundlich parameters were determined using non-linear least square regression (Table 5.3).

5.4.3.1 Freundlich Parameter Joint Confidence Region

Given the mathematical structure of the Freundlich equation (Equation 6, Section 3.3.5.3), the two Freundlich isotherm parameters (K_F and 1/n) are highly correlated, which means the estimated value of one parameter is substantially impacted by the estimation of the other. Thus, the simple confidence interval for each independent parameter cannot accurately describe the range of model fits using equilibrium data obtained from this study. A joint confidence region (JCR), on the other hand, takes the correlation of the two Freundlich parameters into consideration, providing estimates for each model parameter at the 95% confidence level. As presented in Figure 5.3, the JCRs of two Freundlich parameters for each of the four selected GACs used for CYL adsorption in ultrapure water appear in the shape of ellipses, indicating the two model parameters are highly correlated. The calculation details for the JCRs are summarized in Appendix C.3. The virgin F-300 and Aqua Carb were distinct from the other two carbons, with relatively higher capacity but lower 1/n values. The JCR of the virgin F-300 overlaps the JCR of the virgin Aqua Carb, indicating that the adsorptive performance of those two GACs are not statistically different from each other. The virgin C Gran and the preloaded F-300 have less capacity but high 1/n values, with quite small JCRs, indicating excellent model fitting with high R^2 values. This also agrees with the toxin removal data obtained from this study, with the wood-based C Gran and the preloaded F-300 achieving only 80% and 65% of toxin removal, respectively, whereas the other two GACs removed virtually all the toxin at equilibrium.

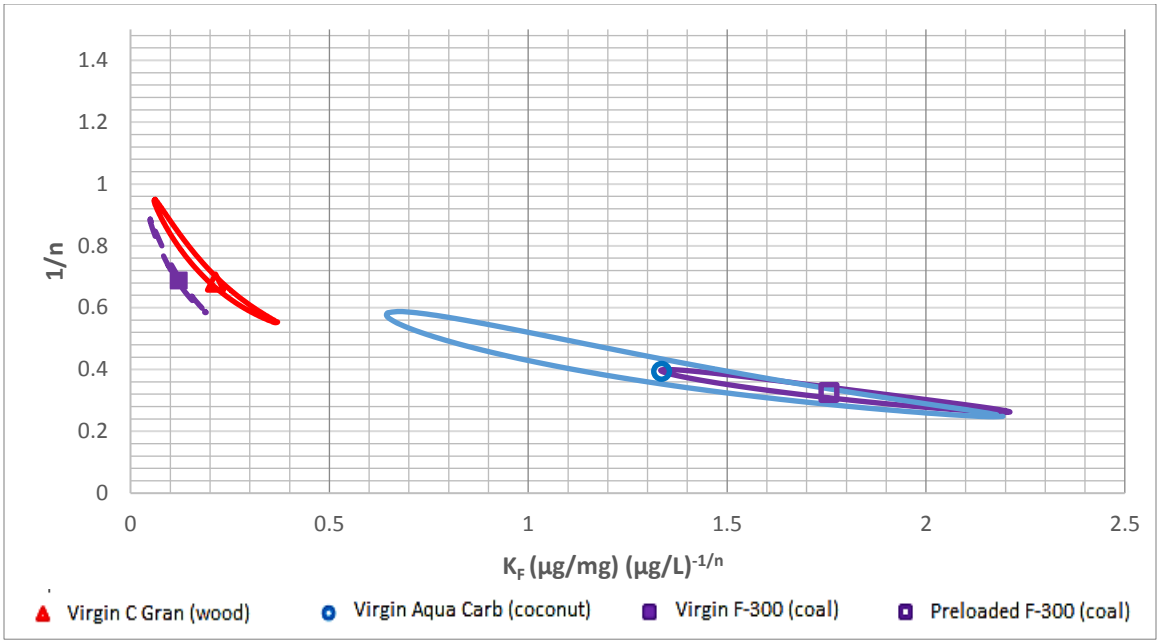

Figure 5.3 The 95% joint confidence region and point estimates for the Freundlich isotherm paramters generated with virgin and preloaded GACs in ultrapure water (ellipses in figure represent JCRs and symbols represent point estimates)

However, no obvious relationships between the selected GAC capacities and their carbon properties were identified. In general, adsorption is a complex process which is governed by the transport and access of adsorbate to adsorption sites, and attachment mechanisms between adsorbate and adsorption sites, such as hydrophobic and electrostatic interactions (Delgaso et al., 2012). Complex interactions among a variety of factors are at play making it difficult to draw conclusions. As with the kinetics results, no direct relationship was found between carbon capacity and BET surface area (Table 5.1). Based on molecular dimensions, CYL, at 1.572 x 0.901 nm, should be able to enter mesopores (2 - 50 nm), and the wood-based C Gran with the larger volume of mesopores (0.89 cm^3/g) would theoretically be expected to perform the best (Table 1). CYL is approximately neutrally charged in the range of drinking water pH (6.0 - 8.5) and as such the positively or negatively charged surface of the carbons will likely not result in additional interactions (attraction or repulsion) between CYL and the adsorbent (Table 2.2). However, the wood-based GAC had the lowest adsorption capacity, whereas the coal-based virgin GAC with smaller mesopore volume had the highest capacity. The isotherm results indicate that additional factors were involved.

5.4.3.2 Freundlich Isotherms

Of the virgin GACs, the coal-based F-300 had the highest K_F value (1.76 (µg/mg)(µg/L)$^{-1/n}$), while the wood-based BG-HHM GAC had the lowest K_F value (0.21 (µg/mg)(µg/L)$^{-1/n}$), as presented in Table 5.3. The 1/n values were quite low for both the F-300 and the coconut-based WPC (0.33-0.39), which were much lower than that of the BG-HHM (0.68). Residual plots for each of the isotherms are provided in Appendix C.2. No residual trends were found.

To investigate preloading on GAC adsorption in terms of capacity, the Freundlich isotherm parameters of virgin and preloaded F-300 were compared. As shown in Table 5.3, the preloaded F-300 has a much lower K_F value (0.12 (µg/mg)(µg/L)$^{-1/n}$), as compared to that of the virgin F-300 (1.76 (µg/mg)(µg/L)$^{-1/n}$). The capacity reduction of the preloaded GAC might be attributed to NOM that reduced the GAC capacity by directly occupying adsorption sites during preloading process (Yu et al., 2009; Crittenden et al., 2012). Nevertheless, the 1/n value of the preloaded F-300 (0.69) was much higher than that of the virgin F-300 made from the same material (0.33).

Figure 5.4 plots CYL isotherms for three virgin GACs and one preloaded GAC in ultrapure water, along with Freundlich isotherm model fitting for each data set. Among the selected virgin GACs, the F-300 and the WPC had the highest CYL adsorption capacity at equilibrium concentrations of 0 - 100 µg/L, while BG-HHM had much less capacity. As discussed in Section 5.4.3.1, the Freundlich isotherm parameters of the F-300 and the WPC were not statistically different from each other. The preloaded F-300 had a much lower capacity than all selected virgin GACs, due to the preloading effects described previously.

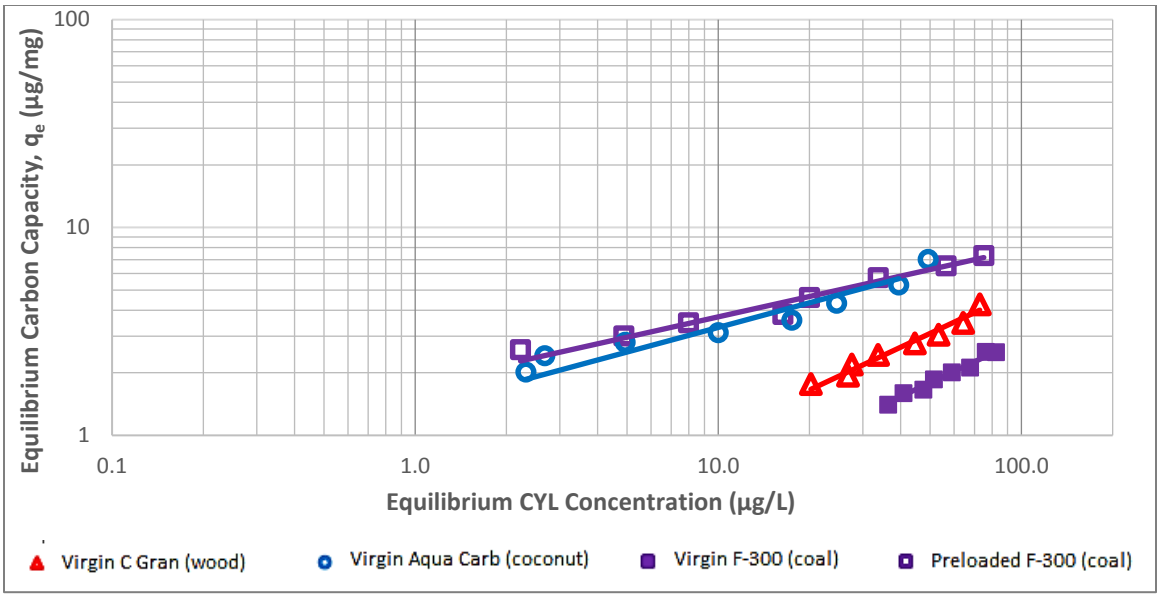

Figure 5.4 CYL Freundlich isotherms for virgin and preloaded GACs in ultrapure water (symbols represent experimental data and straight lines represent Freundlich isotherm fitting curves)

Table 5.3 Freundlich isotherm parameters for virgin and preloaded GACs in ultrapure water

GAC	Number of samples (n)	K_f (µg/mg)(µg/L)$^{-1/n}$	1/n
Coal-based	8	1.76 *(1.33,2.21)*	0.33 *(0.26,0.40)*
Wood-based	8	0.21 *(0.06,0.37)*	0.68 *(0.55,0.95)*
Coconut-based	8	1.34 *(0.64,2.19)*	0.39 *(0.25,0.59)*
Preloaded Coal-based	8	0.12 *(0.05,0.19)*	0.69 *(0.58,0.89)*

(*95% confidence interval*)

5.4.3.3 Comparison with Literature Values

To date, no Freundlich isotherm data have been previously published for CYL adsorption in ultrapure water. Thus, to investigate its relative adsorbability, CYL adsorption isotherms were compared with those in the literature for other microcontaminants under similar experimental conditions as used in this study (virgin coal-based GAC in ultrapure water). Figure 5.5 compares the F-300 GAC CYL adsorption isotherm obtained in this study with published Freundlich isotherms using F-300 and F-400 for two other cyanotoxins, ANTA (Vlad, 2015) and MC-LR (Chennette, 2017), and F-400 isotherms (Pirbazari et al., 1993) for two cyanobacterial taste and

odor compounds, geosmin and 2-methylisoborneol (MIB). F-300 and F-400 are similar coal-based products produced by Calgon Carbon. F-300 has a larger effective size (0.80 - 1.00 mm) than that of F-400 (0.55 - 0.75 mm). F-400 is widely used in drinking water treatment research and is commonly regarded as a benchmark in adsorption studies.

Based on Vlad et al. (2014), the molecular size of cyanotoxins are remarkably different, as ANTA (MW = 165 Da) is a much smaller molecule than CYL (415 Da) and MC-LR (995 Da), but CYL is somewhat closer in size to geosmin (182 Da) and MIB (168 Da) than it is to the regulated MC-LR. All of the above microcontaminants are produced by cyanobacteria and can co-occur in isolation or in combinations with each other in natural environmental scenarios. As geosmin and MIB are typically detected at lower concentrations (0.01 - 1 µg/L, Pirbazari et al., 1993 and 0.001 - 1 µg/L, Chen, Dussert & Suffet, 1997), the Freundlich model curves of these were extrapolated to compare with cyanotoxin results (Figure 5.5).

The cyanotoxins, CYL, MC-LR, and ANTA were less well adsorbed than the taste and odor compounds, geosmin and MIB, by virgin coal-based GAC in ultrapure water with equilibrium concentrations ranging from 1 to 100 µg/L (Figure 5.5). In terms of cyanotoxin adsorption by F-300, ANTA was better adsorbed than CYL, while MC-LR was well less adsorbed than the other two toxins, again at equilibrium concentrations of 1 - 100 µg/L. F-300 had the highest capacity for CYL adsorption among the GACs investigated in this study. F-400 performed better for ANTA adsorption throughout the equilibrium concentration range of 1 - 100 µg/L, with the two isotherm curves diverging at high equilibrium concentrations.

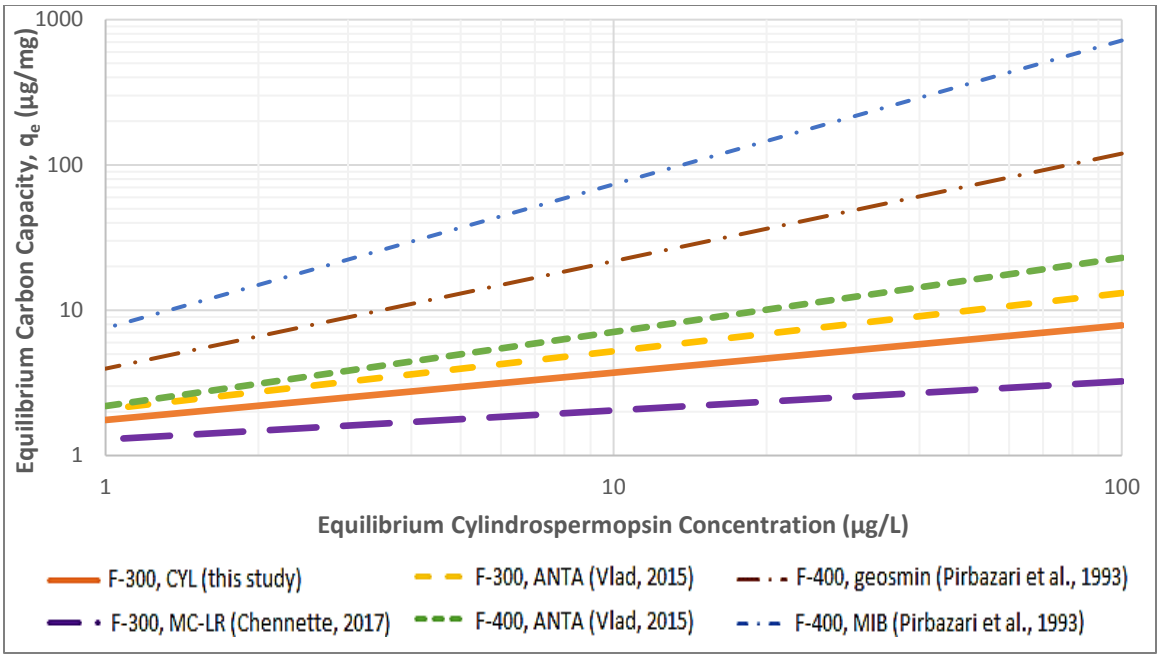

Figure 5.5 Comparison of Freundlich isotherms for CYL, ANTA, MC-LR, MIB, and geosmin by virgin coal-based GACs in ultrapure water. CYL isotherms were prepared using data from the current study, and ANTA, MC-LR, MIB and geosmin isotherms were plot based on the Freundlich parameters obtained from the literature using equilibrium CYL concentrations in the current study, F-300 & F-400 ANTA from Vlad (2015); F-300 MC-LR from Chennette (2017); F-400 geosmin and MIB from Pirbazari et al. (1993).

5.4.4 Equilibrium Column Model (ECM)

As presented in Figure 5.6, the bed lives of the fixed-bed adsorber were calculated for both virgin and preloaded coal-based GAC at three influent CYL concentrations (1, 5 and 20 µg/L) by the application of ECM, assuming a flow rate of 378.5 L/min (100 gal/min), F-300 density of 478.8 g/L, and an empty bed contact time (EBCT) of 10 min. Under these conditions, virgin carbon was predicted to treat more than ten times the bed volumes than the preloaded carbon. The treated bed volumes substantially declined with increasing influent CYL concentrations for both the virgin and preloaded GAC. The ECM was applied as a single-solute analysis in this case, implying no compounds other than CYL were present in the influent and no adsorption competition was considered. Thus, the bed life findings obtained in this case are the approximate maximum values, which would be reduced significantly in the presence of NOM.

Table 5.4 Comparison of ECM results for a fixed-bed adsorber filled with virgin and preloaded coal-based GAC (assuming a flowrate of 378.5 L/min and F-300 density of 478.8 g/L)

	Virgin Coal-Based GAC				Preloaded Coal-Based GAC			
Influent Concentration (µg/L)	1	5	20	100	1	5	20	100
Minimum CUR (mg/L)	0.57	1.69	4.29	12.71	8.24	13.61	20.96	34.62
Maximum Specific Throughput (L/mg)	1.76	0.59	0.23	0.08	0.12	0.07	0.05	0.03
Volume of Water Treated (10^6 m^3)	3.20	1.10	0.42	0.14	0.22	0.13	0.09	0.05
Bed-Life (10^3 d)	5.84	1.97	0.77	0.26	0.43	0.24	0.16	0.10

CUR = carbon usage rate

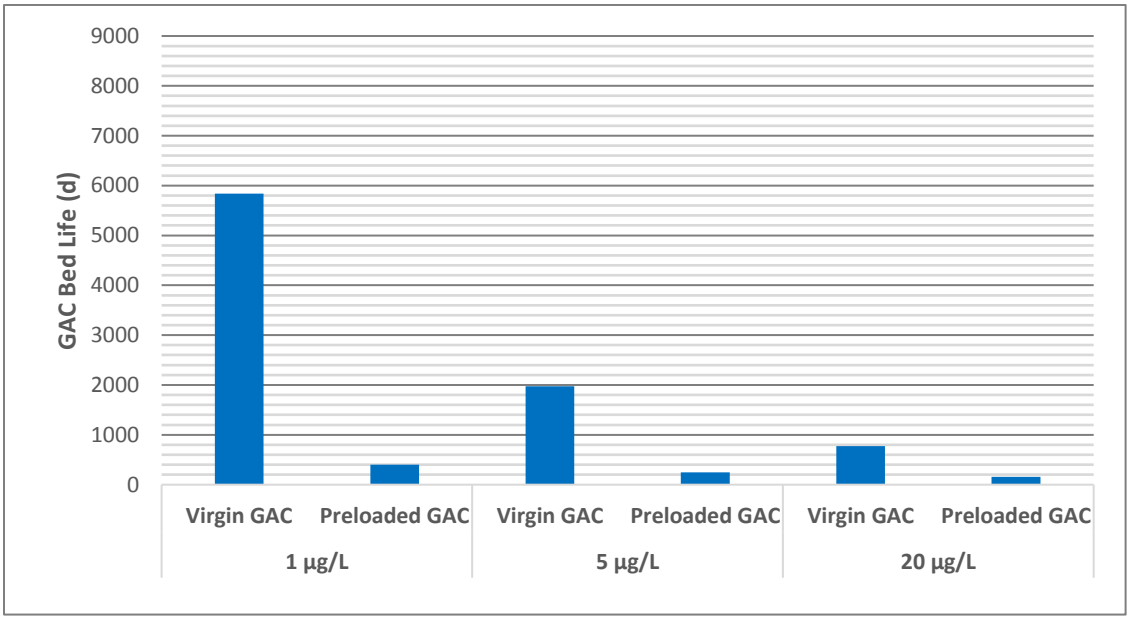

Figure 5.6 ECM predicted GAC bed-life for virgin and preloaded coal-based GAC in a single-solute system with influent CYL concentrations of 1, 5 and 20 µg/L for an EBCT of 10 min.

5.5 Conclusions and Recommendations

The adsorption of CYL in ultrapure water was investigated at bench-scale using three virgin GACs of different base material (coal, wood, and coconut) and one preloaded coal-based GAC. Of the virgin GACs, the wood-based C Gran adsorbed CYL the fastest, followed by the Aqua Carb (coconut), and finally the F-300 (coal). Based on JCR analysis, the Freundlich isotherms for the virgin F-300 and the virgin WPC could not be statistically distinguished from each other, while the

performance of the other GACs was quite different from one another. Among all the selected virgin GACs, the F-300 and WPC had the highest adsorptive capacity at equilibrium at a conservative estimate of potential environmental CYL levels, while C Gran had the lowest. By comparing the adsorptive performance of the virgin F-300 with the preloaded F-300, it was observed that both the rate of CYL adsorption and capacity of F-300 were substantially deteriorated after preloading, in which NOM occupied the adsorption sites for CYL and blocked the access to the sites. This study provides important CYL adsorption data in ultrapure water which can be compared between laboratories and suggests that GAC adsorption is a promising treatment barrier for CYL removal.

The following recommendations should be considered for further study.

- This study only examined CYL adsorption in ultrapure water with limited time and material. It will be important reproduce this work using natural waters to explore the effects of competitive adsorption attributable to the presence of dissolved NOM.
- Batch-scale experiments were conducted for CYL adsorption investigations using GACs of varying base material. Further natural water studies using pilot-scale GAC filters/contactors could help to optimize the operational conditions in natural water. Large scale studies will be severely constrained by the cost and availability of the cyanotoxins. Such studies would likely have to take advantage of an ongoing bloom to be feasible.

Chapter 6
Conclusions and Recommendations

6.1 Summary and Conclusions

Following a thorough literature review of the properties of cyanotoxins and appropriate drinking water treatment barriers for such toxins, activated carbon adsorption emerged as a promising treatment process for cylindrospermopsin (CYL), microcystin-LR (MC-LR), and anatoxin-a (ANTA). However, there are substantial knowledge gaps and further studies are needed. This research had two main foci: 1) powdered activated carbon (PAC) adsorption for CYL, MC-LR, and ANTA, and 2) granular activated carbon (GAC) adsorption for CYL. Initially, an LC-MS/MS analytical method was developed to simultaneously detect the aqueous concentrations of CYL, MC-LR, and ANTA. The method was later optimized to increase throughput when quantifying a single cyanotoxin concentration. As it pertains to PAC adsorption, this study examined the adsorptive behavior of three cyanotoxins with three commercially available PAC products: the coal-based COL-PL60-800, the wood-based BG-HHM, and the coconut-based WPC in both ultrapure water (Chapter 3) and Lake Erie water (Chapter 4). The adsorptive performance of each PAC was evaluated based on the rate of adsorption (kinetics) and capacity (isotherms) for each selected cyanotoxin. Isotherms were not only evaluated under equilibrium conditions, as is typically done, but also non-equilibrium conditions. Contact times of 0.5 h and 1 h were used in this study, which represent typical PAC contact times during drinking water treatment. Two water matrices were investigated in this experiment. A single-solute batch test in ultrapure water established a baseline of adsorption behavior with which other studies can compare when done, whereas the Lake Erie water batch test focused on the competitive adsorption influenced by dissolved NOM. A competitive model, the simplified equivalent background compound model (SEBCM), was utilized to predict the PAC dose required to achieve certain percentage cyanotoxin

removals. This model has been successfully applied to predict PAC dosage for the taste and odor compounds, geosmin and MIB, under non-equilibrium conditions (Zoschke et al., 2011).

With respect to GAC adsorption, three virgin GAC products including coal-based Calgon F-300, wood-based Norit C Gran, and coconut-based Siemens Aqua Carb CX were studied. One preloaded GAC, the coal-based Calgon F-300, was also included in this study. This GAC was preloaded in a pilot-scale setup with post-sedimentation Grand River water (Ontario, Canada) by Vlad et al. (2015). The adsorptive rate and equilibrium capacity were examined for CYL adsorption onto the three virgin GACs in Milli-Q water to establish a baseline for CYL adsorption. The preloading GAC experiment confirmed that, as with other organic compounds of concern, NOM preloading substantially affected CYL adsorption. The key findings and conclusions drawn from this study are summarized below.

6.1.1 Adsorption of CYL, MC-LR, and ANTA by Three PACs in Ultrapure Water (Chapter 3)

- Using the bottle-point method, the wood-based BG-HHM PAC had the fastest removal of all three cyanotoxins, achieving equilibrium in the first 6 h for CYL and MC-LR, while it took 3 days for ANTA. The faster adsorptive rates of BG-HHM are partially attributable to the higher proportion of mesopores in the wood-based carbon as compared to the coal-based COL-PL60-800 and the coconut-based WPC, providing shorter diffusion paths to the adsorption sites.
- ANTA was substantially slower adsorbed onto the selected PACs than the other cyanotoxins, while CYL was adsorbed slightly more quickly than MC-LR.
- Both pseudo-first and -second order kinetics models were generated to describe cyanotoxin adsorption by PACs over time, with the pseudo-second order model providing a slightly better fit.

- At equilibrium, the adsorptive capacity of the three PACs was very different. The BG-HHM (wood) had the highest capacity for CYL, the COL-PL60-800 (coal) retained the highest capacity for MC-LR, and the WPC (coconut) had the highest capacity for ANTA.
- Adsorptive capacities of the selected PACs at equilibrium varied significantly from their non-equilibrium capacities. Under non-equilibrium conditions, at contact times of 0.5 h and 1 h, the BG-HHM outperformed all other PACs evaluated, primarily due to it having the fastest rates of adsorption for all selected cyanotoxins.

6.1.2 Adsorption of CYL, MC-LR, and ANTA by Three PACs in Lake Erie Water (Chapter 4)

- In Lake Erie water, the BG-HHM adsorbed CYL and MC-LR the fastest, and along with the WPC, the two PACs were the fastest for ANTA adsorption, while ANTA was substantially less quickly adsorbed than all other cyanotoxins.
- At equilibrium, the COL-PL60-800 had the highest capacity for CYL adsorption, followed by the BG-HHM and the WPC with similar performance. Similarly, the COL-PL60-800 and the BG-HHM were shown to have the highest and similar capacity for MC-LR removal, while the WPC had the lowest capacity at equilibrium. ANTA was significantly less well adsorbed than CYL and MC-LR, with the WPC and the BG-HHM having the highest equilibrium capacity followed by the COL-PL60-800 with much lower capacity.
- Each of the tested PACs demonstrated substantially distinct adsorptive capacities under equilibrium and practical (or non-equilibrium) conditions. The BG-HHM had the highest non-equilibrium capacity for CYL and MC-LR removal. Again, the capacity of all PACs was substantially lower for ANTA adsorption under non-equilibrium conditions, with the WPC performing the best.
- Comparing the adsorption of cyanotoxins in ultrapure and surface water, a substantial reduction of adsorptive capacity and a slight decrease the rate of adsorption were observed in the surface water, resulting mainly from competitive adsorption caused by the presence

of dissolved NOM. Based on the DOC and SUVA data collected before and after adsorption experiments, the aromatic organic matter fraction of NOM was responsible for the competitive adsorption.

- A simplified competitive adsorption model, the SEBCM, was investigated to describe the competitive adsorption between the selected cyanotoxins and dissolved NOM in Lake Erie water. This model was applied to predict PAC dose to achieve target removal for each of CYL, MC-LR, and ANTA under practical (i.e. non-equilibrium) conditions for a typical WTP with 0.5 h and 1 h contact times.
- An economic analysis revealed that the BG-HHM was the most cost-effective alternative with the lowest dose required for CYL and MC-LR removal under environmentally relevant concentrations. However, none of the selected PACs tested in this study was an effective barrier for ANTA.

6.1.3 CYL Adsorption by Virgin and Preloaded GAC in Ultrapure Water (Chapter 5)

- Of the virgin GACs, the wood-based C Gran adsorbed CYL the fastest, followed by the coconut-based Aqua Carb, and the coal-based F-300.
- Among the virgin GACs, the coal-based Calgon F-300 had the highest capacity at equilibrium, while the C Gran had the lowest capacity (assuming a starting CYL concentration of 100 µg/L.
- Both the adsorptive rate and capacity of the GAC were substantially deteriorated by NOM preloading as compared the adsorption behavior of virgin and preloaded F-300.

6.1.4 Relevance to the Drinking Water Industry

The information presented in this thesis provides confirmation that PAC can be used to treat the cyanotoxins microcystin-LR and cylindrospermopsin in their free (extracellular) form in drinking water. Under realistic WTP conditions, PAC adsorption performance was examined using a Great Lakes water to quantify removal rates and capacities of the three most common of these toxins.

While these carbons are representative of three base materials (coal, wood, coconut) caution should be exercised in the selection of a particular PAC as it cannot necessarily be inferred that all carbons of a specific base material will perform similarly. The simplified competitive adsorption model, SEBCM, was utilized in this study to predict PAC dose for extracellular cyanotoxin removal under non-equilibrium or practical conditions. This model was demonstrated to a useful tool in the selection of a PAC for removal of various cyanotoxins in Lake Erie water. In addition, three commonly applied GACs representing three base materials (coal, wood, coconut) were used in this thesis proving that GAC is effective for extracellular CYL removal in ultrapure water. Although findings were not confirmed under realistic WTP conditions, GAC appears to be a potentially important technology for CYL removal from drinking water.

6.2 Recommendations for Future Research

The cost and availability of cyanotoxins can impose serve limitations for studies and in particular those involve large volumes. Over the course of this study, some areas demonstrated potential merit for further investigation. The following recommendations should be considered for further studies.

- Three commercially available PAC products were selected to investigate adsorptive performance from the perspective of being composed of distinct base materials. However, one product per material may be insufficient to draw a generalized conclusion. Additional PAC products should be evaluated.
- Comparisons with the rate of adsorption of other cyanobacterial metabolites, including the taste and odor compounds, geosmin and MIB, were conducted based on literature values. However, the conclusions are rather untenable as the isotherm parameters were determined under different experimental conditions in other studies. Since PAC is applied at the front end of a treatment process to achieve geosmin and MIB removal, those two cyanobacterial

metabolites could (and should) be investigated along with cyanotoxins for further differentiation of the most effective PAC alternatives.

- In this study, Lake Erie water was collected in the summer but at a time when no cyanobacterial bloom events were occurring. It would be useful to further investigate PAC performance for cyanotoxin removal during a cyanobacterial bloom event, since NOM composition may vary once a bloom occurs.
- Batch-scale experiments were conducted for CYL adsorption investigation using various virgin GACs and a preloaded GAC. Pilot-scale experiments using flow-through columns might be useful to further optimize operational conditions for full-scale GAC contactors/filters used in water treatment facilities.
- This study only included one preloaded GAC that was prepared previously using river water, due to a lack of time and material; as such, other preloaded GACs should be considered for further research.
- While CYL adsorption experiments were conducted using virgin GAC in ultrapure water, there wasn't sufficient time to investigate CYL adsorption onto virgin GAC and preloaded GAC in natural water, to explore the effects of competitive adsorption resulting from the presence of dissolved NOM.
- While PAC and GAC adsorption were investigated in this study, biofiltration (with GAC and/or anthracite and/or sand) might be a feasible treatment barrier for CYL, MC-LR, and ANTA. Biofiltration has been demonstrated to remove cyanobacterial metabolites such as geosmin and MIB under some conditions, but information on cyanotoxin removal in the refereed literature is lacking.

6.3 Disclaimer

Mention of commercial products and/or trade names does not constitute endorsement or recommendation for their use by the authors.

References

Aldridge, P., Thiel, P. & Richards, B. (2001). Ozonation of drinking water: Benefits to the Caloundra-Maroochy Water Supply. Proceedings of the Australian Water Association 19th Federal Convention. Canberra, Australia, CD ROM.

Anderson, W.B., Slawson, R.M., & Mayfield, C.I. (2002). A Review of Drinking Water-Associated Endotoxin Including Potential Routes of Human Exposure. *Canadian Journal of Microbiology, 48*(7), 567-587.

Andrews, R.C., (1990). Removal of low concentrations of chlorination by-products using activated carbon. PhD thesis, University of Alberta, Canada.

ASTM C136 / C136M-14. (2014). *Standard Test Method for Sieve Analysis of Fine and Coarse Aggregates*, ASTM International, West Conshohocken, PA, 2014, www.astm.org.

Bailey, D., Bowen, B., Goodwin, L. & Proctor, L. (1999). An organic removal strategy for Grahamstown WTP. Proceedings of the 18th AWWA Federal Convention, April 1999, Adelaide, Australia. CD ROM.

Banker, R., Carmeli, S., Werman, M., Teltsch, B., Porat, R., & Sukenik, A. (2001). Uracil moiety is required for toxicity of the cyanobacterial hepatotoxin cylindrospermopsin. *Journal of Toxicology and Environmental Health Part A, 62*(4), 281-288.

Bogialli, S., Bruno, M., Curini, R., Di Corcia, A., & Laganà, A. (2006). Simple and rapid determination of anatoxin-a in lake water and fish muscle tissue by liquid-chromatography-tandem mass spectrometry. *Journal of Chromatography*. A, *1122* (1-2), 180–185.

Boyer G.L., Watzin M.C., Shambaugh A.D., Satchwell M.F., Rosen B.H., Mihuc T. (2004). The Occurrence of Cyanobacterial Toxins in Lake Champlain. In Boyer, GL, Watzin, MC, Shambaugh, AD, Satchwell, MF, Rosen, BH, and Mihuc, T. (Ed.). *Lake Champlain: Partnerships and Research in the New Millennium* (pp. 241–57). New York, NY: Kluwer Academic/Plenum Publ.

Boyer, G. L. (2008). Cyanobacterial toxins in New York and the lower Great Lakes ecosystems. In Kenneth, H.K. (Ed.). *Cyanobacterial Harmful Algal Blooms: State of the Science and Research Needs* (pp. 153-165). New York, NY: Springer.

Burns, J. 2005. CyanoHABs – The Florida Experience. In International Symposium on Cyanobacterial Harmful Algal Blooms. Durham, NC, USA, 09/6–09/10.

Carmichael, W. W., Evans, W. R., Yin, Q. Q., Bell, P., & Moczydlowski, E. (1997). Evidence for paralytic shellfish poisons in the freshwater cyanobacterium *Lyngbya wollei* (Farlow ex Gomont) comb. nov. *Applied and Environmental Microbiology*, *63*(8), 3104-3110.

Carmichael, W.W. (2001). Health effects of toxin-producing cyanobacteria: the CyanoHABs. *Human and Ecological Risk Assessment: An International Journal*, *7*(5), 1393-1407.

Carmichael, W. W., Evans, W. R., Yin, Q. Q., Bell, P., & Moczydlowski, E. (1997). Evidence for paralytic shellfish poisons in the freshwater cyanobacterium *Lyngbya wollei* (Farlow ex Gomont) comb. nov. *Applied and Environmental Microbiology*, *63*(8), 3104-3110.

Carrière, A., Prévost, M., Zamyadi, A., Chevalier, P., & Barbeau, B. (2010). Vulnerability of Quebec drinking-water treatment plants to cyanotoxins in a climate change context. *Journal of Water and Health*, *8*(3), 455-465.

Chen, G., Dussert, B., Suffet, I. (1997). Evaluation of granular activated carbons for removal of methylisoborneol to below odor threshold concentration in drinking water. *Water Research*, *31*(5), 1155-1163.

Cheng, X., Maher, J., Chen, C., & Klaassen, C. D. (2005). Tissue distribution and ontogeny of mouse organic anion transporting polypeptides (Oatps). *Drug Metabolism and Disposition*, *33*(7), 1062-1073.

Cheng, X., Shi, H., Adams, C. D., Timmons, T., & Ma, Y. (2009). Effects of oxidative and physical treatments on inactivation of *Cylindrospermopsis raciborskii* and removal of CYL. *Water Science and Technology*, *60*(3), 689-697.

Chennette, V. (2017). *Granular Activated Carbon for the Removal of Seasonally Present Microcystin-LR* (Master's thesis, University of Waterloo).

Chiswell, R. K., Shaw, G. R., Eaglesham, G., Smith, M. J., Norris, R. L., Seawright, A. A., & Moore, M. R. (1999). Stability of cylindrospermopsin, the toxin from the cyanobacterium, *Cylindrospermopsis raciborskii*: effect of pH, temperature, and sunlight on decomposition. *Environmental Toxicology*, *14*(1), 155-161.

Chorus I. (2005). *Current Approaches to Cyanotoxin Risk Assessment, Risk Management and Regulations in Different Countries*. Berlin, Germany: Federal Environment Agency.

Chorus, I., & Bartram, J. (1999). Toxic cyanobacteria in water: a guide to their public health consequences, monitoring and management. *London: E & FN Spon*.

Codd, G.A. (1995). Cyanobacterial toxins: occurrence, properties and biological significance. *Water Science & Technology*, *34*(4), 149-156.

Crittenden, J. C., Trussell, R. R., Hand, D. W., Howe, K. J., Tchobanoglous, G. (2012). *MWH's Water Treatment Principles and Design*. 3rd Edition. New York, NY: John Wiley & Sons.

de la Cruz, A. A., Hiskia, A., Kaloudis, T., Chernoff, N., Hill, D., Antoniou, M. G., He, X., Loftin, K., O'Shea, K., Zhao, C. & Pelaez, M. (2013). A review on cylindrospermopsin: the global occurrence, detection, toxicity and degradation of a potent cyanotoxin. *Environmental Science. Processes & Impacts*, *15*(11), 1979-2003.

de Maagd, P. G. J., Hendriks, A. J., Seinen, W., & Sijm, D. T. (1999). pH-dependent hydrophobicity of the cyanobacteria toxin microcystin-LR. *Water Research, 33*(3), 677-680.

De Ridder, D.J., Verliefde, A.R.D., Heijman, S.G.J., Verberk, J.Q.J.C., Rietveld, L.C., van der Aa, L.T.J., Amy, G.L., & van Dijk, J.C. (2011). Influence of natural organic matter on equilibrium adsorption of neutral and charged pharmaceuticals onto activated carbon. *Water Science and Technology*. *63*(3), 416-423.

Delgado, L.F., Charles, P., Glucina, K., & Morlay, C., (2012). The removal of endocrine disrupting compounds, pharmaceutically activated compounds and cyanobacterial toxins during drinking water treatment preparation using activated carbon - a review. Science of the Total Environment. *435*, 509-525.

Department of Water Affairs and Forestry (DWAF) (1999). South African Water Quality Guidelines (Second Edition).

Devlin, J. P., Edwards, O. E., Gorham, P. R., Hunter, N. R., Pike, R. K., & Stavric, B. (1977). Anatoxin-a, a toxic alkaloid from *Anabaena flos-aquae* NRC-44h. *Canadian Journal of Chemistry*, *55*(8), 1367-1371.

Donati, C., Drikas, M., Hayes, R., & Newcombe, G. (1994). Microcystin-LR adsorption by powdered activated carbon. *Water Research*, *28*(8), 1735-1742.

Droste, R. L. (1997). *Theory and Practice of Water and Wastewater Treatment*. Hoboken, NJ: John Wiley & Sons, Inc.

Duy, T. N., Lam, P. K. S., Shaw, G. R., and Connell, D. W. (2000). Toxicology and risk assessment of freshwater cyanobacterial (blue-green algal) toxins in water. *Reviews of Environmental Contamination and Toxicology* (pp. 113-186). New York, NY: Springer.

Ebie, K., Li, F., Azuma, Y., Yuasa, A., Hafishita, T. (2001). Pore distribution effect of activated carbon in adsorbing organic micropollutants from natural water. *Water Research, 35*(1), 167-179.

Faassen, E. J., Harkema, L., Begeman, L., Lurling, M. (2012). First report of (homo)anatoxin-a and dog neurotoxicosis after ingestion of benthic cyanobacteria in The Netherlands. *Toxicon, 60*(3), 378–384.

Falconer, I. R. (1991). Tumor promotion and liver injury caused by oral consumption of cyanobacteria. *Environmental Toxicology*, *6*(2), 177-184.

Fastner, J., Heinze, R., Humpage, A. R., Mischke, U., Eaglesham, G. K., & Chorus, I. (2003). CYL occurrence in two German lakes and preliminary assessment of toxicity and toxin production of *Cylindrospermopsis raciborskii* (Cyanobacteria) isolates. *Toxicon*, *42*(3), 313-321.

Federal-Provincial-Territorial Committee on Drinking Water. (2016). Cyanobacterial toxins in drinking water. Document for public consultation.

Francis, G. (1878). Poisonous Australian Lake. *Nature*, *18*, 11-12.

Fristachi, A., Sinclair, J. L., Hall, S., Berkman, J. A. H., Boyer, G., Burkholder, J., Carmichael, W., DuFour, A., Frazier, W., & Morton, S. L. (2008). Occurrence of cyanobacterial harmful algal blooms workgroup report. In *Cyanobacterial harmful algal blooms: state of the science and research needs* (pp. 45-103). New York, NY: Springer.

Gijsberten-Abrahamse, A.J., Schmidt, W., Chorus, I., & Heijman, S.G.J. (2006). Removal of cyanotoxins by ultrafiltration and nanofiltration. *Journal of Membrane Science, 276*(1-2), 252-259.

Gillogly, T.E.T. (1998). MIB adsorption in drinking water treatment. PhD dissertation, University of Illinois, Urbana, Illinois, USA

Graf, Karlheinz, and Michael Kappl. (2006). *Physics and chemistry of interfaces*. 2nd Edition. New York, NY: John Wiley & Sons.

Graham, J. L., Loftin, K. A., Meyer, M. T., & Ziegler, A. C. (2010). Cyanotoxin mixtures and taste-and-odor compounds in cyanobacterial blooms from the Midwestern United States. *Environmental Science & Technology*, *44*(19), 7361-7368.

Graham, M., Summers, R.S., Simpson, M.R., & Macleod, B.W. (2000). Modeling equilibrium adsorption of 2-methylisoborneol and geosmin in natural waters. *Water Research*, *34*(8), 2291-2300.

Grützmacher, G., Böttcher, G., Chorus, I., & Bartel, H. (2002). Removal of microcystins by slow sand filtration. *Environmental Toxicology*, *17*(4), 386-394.

Hand, D. W., Crittenden, J. C., Hokanson, D. R., & Bulloch, J. L. (1997). Predicting the performance of fixed-bed granular activated carbon adsorbers. *Water Science and Technology*, *35*(7), 235-241.

Hart, J. & Stott, P. (1993). *Microcystin-LR Removal from Water* (Report No. FR0367). Marlow, UK: Foundation for Water Research.

Hart, J., Fawell, J. K., Croll, B., Marsalek, B., Dolej, F., Stadeckova, A., Bruchet, A., Bernazeau, F., Baudin, I., & Pieronne, P. (1998). Algal toxins in surface waters: origins and removal during drinking water treatment processes. *Water Supply*, *16*(1-2), 611-623.

He, X., Liu, Y. L., Conklin, A., Westrick, J., Weavers, L. K, Dionysiou, D.D., Lenhart, J.J., Mouser, P.J., Szlag, D. & Walker, H.W. (2016). Toxic cyanobacteria and drinking water: Impacts, detection, and treatment. *Harmful Algae*, *54*, 174-193.

Health Canada (2017). Guidelines for Canadian Drinking Water Quality—Summary Table. Water and Air Quality Bureau, Healthy Environments and Consumer Safety Branch, Health Canada, Ottawa, Ontario. Retrieved on April 17, 2017 from http://www.hc-sc.gc.ca/ewh-semt/pubs/water-eau/sum_guide-res_recom/index-eng.php

Health Canada (2002). Guidelines for Canadian Drinking Water Quality: Supporting Documentation — Cyanobacterial Toxins — Microcystin-LR. Water Quality and Health Bureau, Healthy Environments and Consumer Safety Branch, Health Canada, Ottawa, Ontario. [Available at: https://www.canada.ca/content/dam/canada/health-

canada/migration/healthy-canadians/publications/healthy-living-vie-saine/water-cyanobacteria-cyanobacterie-eau/alt/water-cyanobacteria-cyanobacterie-eau-eng.pdf]

Hepplewhite, C., G. Newcombe, and D.R.U. Knappe, (2004). NOM and MIB, who wins in the competition for activated carbon adsorption sites? *Water Science and Technology, 49*(9), 257-265.

Ho, L, McDowall B, Wijesundara S, Shaw G, Saint C, Newcombe G. (2005). *Biological filtration processes for the removal of algal metabolite* (Research Report No. 64). Australia: The Cooperative Research Centre for Water Quality and Treatment.

Ho, L., & Newcombe, G. (2007). Evaluating the adsorption of microcystin toxins using granular activated carbon (GAC). *Journal of Water Supply: Research and Technology-Aqua*, *56*(5), 281-291.

Ho, L., Lambling, P., Bustamante, H., Duker, P., & Newcombe, G. (2011). Application of powdered activated carbon for the adsorption of cylindrospermopsin and microcystin toxins from drinking water supplies. *Water Research*, *45*(9), 2954-2964.

Ho, L., Meyn, T., Keegan, A., Hoefel, D., Brookes, J., Saint, C. P., & Newcombe, G. (2006). Bacterial degradation of microcystin toxins within a biologically active sand filter. *Water Research*, *40*(4), 768-774.

Ho, L., Onstad, G., Gunten, U.Von, Rinck-Pfeiffer, S., Craig, K., & Newcombe, G. (2006). Differences in the chlorine reactivity of four microcystin analogues. *Water Research*, *40*(6), 1200-1209.

Ho, L., Slyman, N., Kaeding, U., & Newcombe, G. (2008). Optimizing PAC and chlorination practices for cylindrospermopsin removal. *Journal American Water Works Association*, *100*(11), 88-96.

Ho, Y., McKay, G. (1999). Pseudo-second order model for sorption processes. *Process Biochemistry*, 34(5): 451-465

Hrudey, S., Burch, M., Drikas, M., & Gregory, R. (1999). Remedial measures. In Chorus, I., & Bartram, J. (Ed.). *Toxic cyanobacteria in water: a guide to their public health consequences, monitoring, and management* (pp. 275-312). London & New York: E & FN Spon.

Huang, W. J., Cheng, B. L., & Cheng, Y. L. (2007). Adsorption of microcystin-LR by three types of activated carbon. *Journal of Hazardous Materials*, *141*(1), 115-122.

Humpage, A. R., & Falconer, I. R. (2003). Oral toxicity of the cyanobacterial toxin cylindrospermopsin in male Swiss albino mice: determination of no observed adverse effect level for deriving a drinking water guideline value. *Environmental toxicology*, *18*(2), 94-103.

Keijola, A.M., Himberg, K., Esala, A.L., Sivonen, K., Hiisvirta, L. (1988). Removal of cyanobacterial toxins in water treatment processes: laboratory and pilot scale experiments. *Toxicity Assessment*, *3*(5), 643–656.

Kilduff, J. E., Karanfil, T., & Weber, W. J. (1998). Competitive effects of nondisplaceable organic compounds on trichloroethylene uptake by activated carbon. I. Thermodynamic predictions and model sensitivity analyses. *Journal of colloid and interface science*, *205*(2), 271-279.

Kingston, J. (2015). *Occurrence, Levels, and Distribution of Cyanobacterial Toxins in Municipal Drinking Water and Drinking Water Sources from Selected Drinking Water Systems in Ontario, 2004-2012*. Etobicoke, Ontario: Ministry of the Environment and Climate Change (MOECC).

Knappe, D. R. U., Matsui, Y., Snoeyink, V. L., Roche, P., Prados, M. J. & Bourbigot, M.-M. (1998). Predicting the capacity of powdered activated carbon for trace organic compounds in natural waters. *Environmental Science & Technology*. *32*(11), 1694–1698.

Knappe, D.R.U. (1996). Prediction of the removal of atrazine by powdered and granular activated carbon. Ph.D dissertation, University of Illinois, Urbana, Illinois, USA

Knappe, D.R.U., Snoeyink, V.L., Roche, P., Prados, M.J., Bourbigot, M.M. (1999). Atrazine removal by preloaded GAC. *Journal American Water Works Association*, *91*(10), 97-109.

Knappe, D.R.U., Matsui, Y., Snoeyink, V.L., Roche, P., Prados, M.J., Bourbigot, M.M. (1998). Predicting the capacity of powdered activated carbon for trace organic compounds in natural waters. *Environmental Science & Technology*, *32*(11), 1694-1698.

Manitoba Water Stewardship, 2011. State of Lake Winnipeg: 1999 to 2007. Environment Canada. p. 1– 209.

Matsui, Y., Fukuda, Y., Inoue, T. & Matsushita, T. (2003). Effect of natural organic matter on powdered activated carbon adsorption of trace contaminants: characteristics and mechanisms of competitive adsorption. *Water Research, 37*(18), 4413–4424.

Merel, S., Walker, D., Chicana, R., Snyder, S., Baures, E., & Thomas, O. (2013). State of knowledge and concerns on cyanobacterial blooms and cyanotoxins. *Environment International*, *59*, 303-327.

Michalak, Am. M., Anderson, E. J., Beletsky, D., Boland, S., Bosch, N. S., Bridgeman, T. B., Chaffin, J. D., Cho, K., Confesor, R., Daloglu, I., Depinto, J. V., Evans, M. A., Fahnenstiel, G. L., He, L., Ho, J. C., Jenkins, L., Johengen, T. H., Kuo, K. C., Laporte, E., Liu, X., McWilliams, M. R., Moore, M. R., Posselt, D. J., Richards, R. P., Scavia, D., Steiner, A. L., Verhamme, E., Wright, D. M., Zagorski, M. A. (2013). Record-setting algal bloom in Lake Erie caused by agricultural and meteorological trends consistent with expected future conditions. *Proceedings of the National Academy of Sciences of the U.S.A., 110*(16), 6448–6452.

Ministry of Health of China. (2006). Standards for drinking water quality. *GB5749-2006*. Retrieved on June 25, 2017 from http://www.iwa-network.org/filemanager-uploads/WQ_Compendium/Database/Selected_guidelines/016.pdf

Najm, I. N., Snoeyink, V. L. & Richard, Y. (1991). Effect of initial concentration of a SOC in natural water on its adsorption by activated carbon. *Journal American Water Works Association, 83*(8), 57–63.

New Zealand Ministry of Health (2016). *Guidelines for Drinking-water Quality Management for New Zealand* (2nd edition). Wellington, New Zealand: Ministry of Health.

Newcombe, G. (2002). *Removal of algal toxins from drinking water using ozone and GAC* (Report No. 90904). AWWA Research Foundation and American Water Works Association.

Newcombe, G., & Nicholson, B. (2004). Water treatment options for dissolved cyanotoxins. *Journal of Water Supply: Research and Technology-AQUA*, *53*(4), 227-239.

Newcombe, G., Cook, D., Brooke, S., Ho, L., & Slyman, N. (2003). Treatment options for microcystin toxins: similarities and differences between variants. *Environmental Technology*, *24*(3), 299-308.

Newcombe, G., Morrison, J., Hepplewhite, C., Knappe, D.R.U. (2002). Simultaneous adsorption of MIB and NOM onto activated carbon II. Competitive effects. *Carbon, 40*(12), 2147-2156

Newcombe, G., Morrison, J., Hepplewhite, C., & Knappe, D. R. U. (2002). In the (adsorption) competition between NOM and MIB, who is the winner, and why? *Water Science and Technology: Water Supply, 2*(2), 59-67.

NHMRC/NRMMC. (2004). *Australian Drinking Water Guidelines*. National Health and Medical Research Council/Natural Management Ministerial Council, Canberra.

Nicholson, B. C., Rositano, J., & Burch, M. D. (1994). Destruction of cyanobacterial peptide hepatotoxins by chlorine and chloramine. *Water Research*, *28*(6), 1297-1303.

NOAA (2015). Harmful algal blooms in Lake Erie—Experimental HAB bulletin archive. NOAA, Ann Arbor, MI. Retrieved on May 18, 2017 from https://www.glerl.noaa.gov/res/HABs_and_Hypoxia/lakeErieHABArchive/

O'Neil, J. M., Davis, T. W., Burford, M. A., & Gobler, C. J. (2012). The rise of harmful cyanobacteria blooms: the potential roles of eutrophication and climate change. *Harmful Algae*, *14*, 313-334.

Oehrle, S. A, Southwell, B., Westrick, J. (2010). Detection of various freshwater cyanobacterial toxins using ultra-performance liquid chromatography tandem mass spectrometry. *Toxicon, 55*(5), 965–972.

Onstad, G. D., Strauch, S., Meriluoto, J., Codd, G. A., & von Gunten, U. (2007). Selective oxidation of key functional groups in cyanotoxins during drinking water ozonation. *Environmental Science & Technology, 41*(12), 4397-4404.

Ontario Drinking Water Quality Standards (Standard No. O. Reg. 169/03). Retrieved on Apr. 15, 2017 from https://www.ontario.ca/laws/regulation/030169

Osswald, J., Rellán, S., Gago, A., Vasconcelos, V. (2007). Toxicology and detection methods of the alkaloid neurotoxin produced by cyanobacteria, anatoxin-a. *Environment International*, *33*(8), 1070–1089.

Park, J. A., Jung, S. M., Yi, I. G., Choi, J. W., Kim, S. B., & Lee, S. H. (2017). Adsorption of microcystin-LR on mesoporous carbons and its potential use in drinking water source. *Chemosphere*, *177*, 15-23.

Pirbazari, M., Ravindran, V., Badriyha, B. N., Craig, S., McGuire, M. J. (1993). GAC adsorber design protocol for the removal of off-flavors. *Water Research*, *27*(7), 1153-1166.

Poland Ministry of Health Regulation. (2002). Regulation of the Minister of Health of 19/11/02 om the requirements concerning the quality of drinking water. *Journal of Laws* No. 203/2002, item 1718.

Qi, S., Schideman, L., Mariñas, B. J., Snoeyink, V. L., & Campos, C. (2007). Simplification of the IAST for activated carbon adsorption of trace organic compounds from natural water. *Water Research*, *41*(2), 440-448.

Quinlivan, P.A., Li, L., Knappe, D.R.U. (2005). Effects of activated carbon characteristics on the simultaneous adsorption of aqueous organic micropollutants and natural organic matter. *Water Research, 39*(8), 1663–1673.

Rapala, J., Lahti, K., Sivonen, K., Niemela, S. I. (1994). Biodegradability and adsorption on lake sediments of cyanobacterial hepatotoxins and anatoxin-a. *Letters in Applied Microbiology, 19*(6), 423–428.

Reed, B. E., & Matsumoto, M. R. 1993. Modeling cadmium adsorption by activated carbon using the Langmuir and Freundlich isotherm expressions. *Separation Science and Technology*, *28*(13-14), 2179-2195.

Rodríguez, E., Sordo, A., Metcalf, J. S., & Acero, J. L. (2007). Kinetics of the oxidation of cylindrospermopsin and anatoxin-a with chlorine, monochloramine and permanganate. *Water Research*, *41*(9), 2048-2056.

Senogles, P., Shaw, G., Smith, M., Norris, R., Chiswell, R., Mueller, J., Sadler, R., & Eaglesham, G. (2000). Degradation of the cyanobacterial toxin cylindrospermopsin, from *Cylindrospermopsis raciborskii*, by chlorination. *Toxicon*, *38*(9), 1203-1213.

Shimabuku, K. K., Cho, H., Townsend, E. B., Rosario-Ortiz, F. L., & Summers, R. S. (2014). Modeling nonequilibrium adsorption of MIB and sulfamethoxazole by powdered activated carbon and the role of dissolved organic matter competition. *Environmental Science & Technology*, *48*(23), 13735-13742.

Sivonen, K., and Jones, G. (1999). Cyanobacterial toxins. *In Toxic cyanobacteria in water: a guide to their public health consequences, monitoring, and management*. (pp. 41–111). Edited by I. Chorus and J. Bartram. New York, NY: E & FN Spon.

Song, W., De La Cruz, A. A., Rein, K., & O'Shea, K. E. (2006). Ultrasonically induced degradation of microcystin-LR and-RR: Identification of products, effect of pH, formation and destruction of peroxides. *Environmental Science & Technology*, *40*(12), 3941-3946.

Sontheimer, H, Crittenden, J.C., Summers, R.S. (1988). *Activated carbon for water treatment* (2nd edition). American Water Works Association. Karlsruhe, Germany: DVWG Forschungsstelle.

Standard Methods. (2012). *Standard Methods for the Examination of Water and Wastewater* (22nd edition). American Public Health Association, American Water Works Association, Water Environment Federation.

Stevens, D. K., & Krieger, R. I. (1991). Stability studies on the cyanobacterial nicotinic alkaloid anatoxin-A. *Toxicon*, *29*(2), 167-179.

Summers, R.S. (1986). Activated carbon adsorption of humic substances: Effect of molecular size and heterodispersity. PhD thesis, Department of Civil Engineering, Stanford University.

Svrcek, C., & Smith, D. W. (2004). Cyanobacteria toxins and the current state of knowledge on water treatment options: a review. *Journal of Environmental Engineering and Science*, *3*(3), 155-185.

Szlag, D. C., Sinclair, J. L., Southwell, B., & Westrick, J. A. (2015). Cyanobacteria and cyanotoxins occurrence and removal from five high-risk conventional treatment drinking water plants. *Toxins*, *7*(6), 2198-2220.

Teixeira, M. R., & Rosa, M. J. (2006). Comparing dissolved air flotation and conventional sedimentation to remove cyanobacterial cells of *Microcystis aeruginosa*: part I: the key operating conditions. *Separation and Purification Technology*, *52*(1), 84-94.

Tsuji, K., Naito, S., Kondo, F., Ishikawa, N., Watanabe, M. F., Suzuki, M., & Harada, K. I. (1994). Stability of microcystins from cyanobacteria: effect of light on decomposition and isomerization. *Environmental Science & Technology*, *28*(1), 173-177.

UKWIR (1996). *Pilot Scale GAC Tests to Evaluate Toxin Removal* (Report No. 96/DW/07/1). London, UK: UK Water Industry Research Limited.

USEPA (2015). Drinking Water Health Advisory for the Cyanobacteria Microcystin Toxins. Retrieved July 23, 2016 from https://www.epa.gov/sites/production/files/201506/documents/microcystinsreport-2015.pdf

USEPA (2016). Drinking Water Contaminant Candidate List 4 (CCL4) and Regulatory Determination. Retrieved on December 12, 2016 from https://www.epa.gov/ccl

USEPA (2017). Guidelines and Recommendations. Retrieved May 12, 2017 from https://www.epa.gov/nutrient-policy-data/guidelines-and-recommendations

Valentine, W. M., Schaeffer, D. J., Beasley, V. R. (1991). Electromyographic assessment of the neuromuscular blockade produced in vivo by anatoxin-a in the rat. *Toxicon*, *29*(3), 347–357.

Van Apeldoorn, M. E., Van Egmond, H. P., Speijers, G. J., & Bakker, G. J. (2007). Toxins of cyanobacteria. *Molecular Nutrition & Food Research*, *51*(1), 7-60.

Vlad, S. (2015). *Treatment of the Cyanotoxin Anatoxin-a via Activated Carbon Adsorption.* Master's thesis, University of Waterloo. UWSpace. *http://hdl.handle.net/10012/9392*

Vlad, S., Anderson, W. B., Peldszus, S., & Huck, P. M. (2014). Removal of the cyanotoxin anatoxin-a by drinking water treatment processes: a review. *Journal of Water and Health*, *12*(4), 601-617.

Von Gunten, U., & Hoigné, J. (1994). Bromate formation during ozonization of bromide-containing waters: interaction of ozone and hydroxyl radical reactions. *Environmental Science & Technology*, *28*(7), 1234-1242.

Watson, S. B., Miller, C., Arhonditsis, G., Boyer, G. L., Carmichael, W., Charlton, M. N., Confesor, R., Depew, D.C., Höök, T.O., Ludsin, S.A. & Matisoff, G. (2016). The re-eutrophication of Lake Erie: Harmful algal blooms and hypoxia. *Harmful Algae*, 56, 44-66.

Westrick, J. A., Szlag, D. C., Southwell, B. J., & Sinclair, J. (2010). A review of cyanobacteria and cyanotoxins removal/inactivation in drinking water treatment. *Analytical and* bioanalytical chemistry, *397*(5), 1705-1714.

WHO (2004). *Guidelines for Drinking-Water Quality.* 3rd edition, Volume 1 Recommendations. World Health Organization, Geneva, 515 pp.

Worch, E. (2010). Competitive adsorption of micropollutants and NOM onto activated carbon: comparison of different model approaches. *Journal of Water Supply: Research and Technology-AQUA*, *59*(5), 285-297.

Worch, E. (2012). *Adsorption technology in water treatment: fundamentals, processes, and modeling*. Germany: Walter de Gruyter.

Yang, X. (2007). Occurrence of the cyanobacterial neurotoxin, Anatoxin-a, in the Lower Great Lakes. PhD Thesis. Statue University of New York.

Yilmaz, M., & Phlips, E. J. (2011). Toxicity and genetic diversity of *Cylindrospermopsis raciborskii* in Florida, USA. *Lake and Reservoir Management*, *27*(3), 235-244.

Yu, Z. (2007). *Analysis of Selected Pharmaceuticals and Endocrine Disrupting Compounds and their Removal by Granular Activated Carbon in Drinking Water Treatment.* PhD thesis, University of Waterloo. UWSpace. http://hdl.handle.net/10012/3309

Yu, Z., Peldszus, S., Huck, P. M. (2009). Adsorption of Selected Pharmaceuticals and an Endocrine Disrupting Compound by Granular Activated Carbon. *Environmental Science and Technology, 29*(5), 1467-1473.

Zhu, S., Yin, D., Gao, N., Zhou, S., Wang, Z., & Zhang, Z. (2016). Adsorption of two microcystins onto activated carbon: equilibrium, kinetic, and influential factors. *Desalination and Water Treatment*, *57*(50), 23666-23674.

Zietzschmann, F., Aschermann, G., & Jekel, M. (2016). Comparing and modeling organic micro-pollutant adsorption onto powdered activated carbon in different drinking waters and WWTP effluents. *Water Research, 102*, 190-201.

Zoschke, K., Engel, C., Börnick, H., & Worch, E. (2011). Adsorption of geosmin and 2-methylisoborneol onto powdered activated carbon at non-equilibrium conditions: Influence of NOM and process modelling. *Water Research, 45*(15), 4544-4550.

Appendix A
Supporting Information for Chapter 3

Appendix A.1 LC-MS/MS Method

A gradient LC-MS/MS method was developed to measure CYL, MC-LR, and ANTA, simultaneously. In this method, the acidified acetonitrile was initially running at 4% for 4 min and then increased to 70% over 6 min, then washed with 80% acetonitrile for one min, and finally returned to 4% for 2 min prior to the next injection.

Appendix A.2 PAC Pore Distribution Data

Table A.1 Pore volume and surface area data for COL-PL60-800 (coal)

Half pore width (Å)	Cumulative Pore Volume (cc/g)	Cumulative Surface Area (m^2/g)
2.8	5.6E-02	2.3E+02
3.0	6.6E-02	2.6E+02
3.1	7.4E-02	2.9E+02
3.2	8.2E-02	3.1E+02
3.3	8.8E-02	3.3E+02
3.5	8.9E-02	3.4E+02
3.6	8.9E-02	3.4E+02
3.8	8.9E-02	3.4E+02
3.9	8.9E-02	3.4E+02
4.1	9.1E-02	3.4E+02
4.3	9.2E-02	3.4E+02
4.4	9.2E-02	3.4E+02
4.6	9.2E-02	3.4E+02
4.8	9.2E-02	3.4E+02
5.0	9.2E-02	3.4E+02
5.3	9.3E-02	3.4E+02
5.5	9.7E-02	3.5E+02
5.7	1.0E-01	3.6E+02
6.0	1.1E-01	3.7E+02
6.2	1.1E-01	3.8E+02
6.5	1.2E-01	3.9E+02
6.8	1.3E-01	4.0E+02
7.1	1.3E-01	4.0E+02
7.4	1.4E-01	4.2E+02
7.7	1.9E-01	4.8E+02
8.1	2.5E-01	5.6E+02
8.4	3.2E-01	6.4E+02
8.8	4.0E-01	7.3E+02
9.2	4.6E-01	8.0E+02
9.6	5.1E-01	8.5E+02
10.0	5.5E-01	8.9E+02
10.6	5.6E-01	9.1E+02
6.5	2.2E-01	5.1E+02
6.8	2.3E-01	5.2E+02
7.1	2.4E-01	5.3E+02

Half pore width (Å)	Cumulative Pore Volume (cc/g)	Cumulative Surface Area (m^2/g)
7.4	2.4E-01	5.4E+02
7.7	2.4E-01	5.4E+02
8.1	2.4E-01	5.4E+02
8.4	2.5E-01	5.4E+02
8.8	2.5E-01	5.5E+02
9.2	2.5E-01	5.5E+02
9.6	2.5E-01	5.5E+02
10.0	2.5E-01	5.5E+02
10.6	2.5E-01	5.5E+02
11.0	2.6E-01	5.6E+02
11.4	2.6E-01	5.7E+02
11.8	2.7E-01	5.8E+02
12.2	2.8E-01	5.9E+02
12.6	2.8E-01	6.1E+02
13.0	2.9E-01	6.2E+02
13.5	3.0E-01	6.3E+02
14.0	3.1E-01	6.4E+02
14.5	3.2E-01	6.6E+02
15.0	3.3E-01	6.7E+02
15.5	3.4E-01	6.8E+02
16.0	3.5E-01	6.9E+02
16.6	3.5E-01	7.0E+02
17.2	3.6E-01	7.1E+02
17.8	3.6E-01	7.1E+02
18.4	3.7E-01	7.2E+02
19.0	3.7E-01	7.2E+02
19.7	3.7E-01	7.2E+02
20.4	3.8E-01	7.3E+02
21.1	3.8E-01	7.3E+02
21.8	3.8E-01	7.3E+02
22.6	3.8E-01	7.3E+02
23.4	3.8E-01	7.3E+02
24.2	3.8E-01	7.3E+02
25.1	3.9E-01	7.4E+02
25.9	3.9E-01	7.4E+02
26.8	3.9E-01	7.4E+02
27.8	3.9E-01	7.4E+02
28.8	4.0E-01	7.5E+02
29.8	4.0E-01	7.5E+02

Half pore width (Å)	Cumulative Pore Volume (cc/g)	Cumulative Surface Area (m^2/g)
30.8	4.0E-01	7.5E+02
31.9	4.0E-01	7.5E+02
33.0	4.1E-01	7.5E+02
34.2	4.1E-01	7.6E+02
35.3	4.1E-01	7.6E+02
36.6	4.1E-01	7.6E+02
37.9	4.1E-01	7.6E+02
39.2	4.1E-01	7.6E+02
40.6	4.1E-01	7.6E+02
42.0	4.1E-01	7.6E+02
43.5	4.1E-01	7.6E+02
45.0	4.1E-01	7.6E+02
46.5	4.1E-01	7.6E+02
48.2	4.2E-01	7.6E+02
49.9	4.2E-01	7.6E+02
51.6	4.2E-01	7.6E+02
53.4	4.2E-01	7.6E+02
55.3	4.2E-01	7.6E+02
57.2	4.2E-01	7.6E+02
59.2	4.2E-01	7.6E+02
61.3	4.2E-01	7.6E+02
63.4	4.2E-01	7.6E+02
65.7	4.2E-01	7.6E+02
68.0	4.2E-01	7.6E+02
70.3	4.2E-01	7.7E+02
72.8	4.2E-01	7.7E+02
75.3	4.2E-01	7.7E+02
78.0	4.2E-01	7.7E+02
80.7	4.2E-01	7.7E+02
83.5	4.2E-01	7.7E+02
86.5	4.2E-01	7.7E+02
89.5	4.2E-01	7.7E+02
92.6	4.2E-01	7.7E+02
95.9	4.2E-01	7.7E+02
99.2	4.2E-01	7.7E+02
102.7	4.3E-01	7.7E+02
106.3	4.3E-01	7.7E+02
110.0	4.3E-01	7.7E+02
113.8	4.3E-01	7.7E+02

Half pore width (Å)	Cumulative Pore Volume (cc/g)	Cumulative Surface Area (m^2/g)
117.8	4.3E-01	7.7E+02
122.0	4.3E-01	7.7E+02
126.2	4.3E-01	7.7E+02
130.6	4.3E-01	7.7E+02
135.2	4.3E-01	7.7E+02
139.9	4.3E-01	7.7E+02
144.8	4.3E-01	7.7E+02
149.9	4.3E-01	7.7E+02
155.2	4.3E-01	7.7E+02
160.6	4.3E-01	7.7E+02
166.2	4.3E-01	7.7E+02
172.0	4.3E-01	7.7E+02
178.1	4.3E-01	7.7E+02
184.3	4.3E-01	7.7E+02
190.7	4.3E-01	7.7E+02
197.4	4.3E-01	7.7E+02
204.3	4.3E-01	7.7E+02
211.5	4.3E-01	7.7E+02
218.9	4.3E-01	7.7E+02
226.5	4.3E-01	7.7E+02
234.5	4.3E-01	7.7E+02
242.7	4.3E-01	7.7E+02
251.2	4.4E-01	7.7E+02

Table A.2 Pore volume and surface area data for BG-HHM (wood)

Half pore width (Å)	Cumulative Pore Volume (cc/g)	Cumulative Surface Area (m^2/g)
2.8	5.5E-02	2.4E+02
3.0	7.4E-02	3.0E+02
3.1	9.2E-02	3.6E+02
3.2	1.0E-01	4.0E+02
3.3	1.1E-01	4.1E+02
3.5	1.1E-01	4.1E+02
3.6	1.1E-01	4.1E+02
3.8	1.1E-01	4.1E+02
3.9	1.1E-01	4.1E+02
4.1	1.1E-01	4.1E+02
4.3	1.2E-01	4.3E+02
4.4	1.3E-01	4.7E+02
4.6	1.5E-01	5.0E+02

Half pore width (Å)	Cumulative Pore Volume (cc/g)	Cumulative Surface Area (m^2/g)
4.8	1.6E-01	5.3E+02
5.0	1.7E-01	5.5E+02
5.3	1.9E-01	5.8E+02
5.5	2.0E-01	6.1E+02
5.7	2.2E-01	6.4E+02
6.0	2.4E-01	6.6E+02
6.2	2.5E-01	6.8E+02
6.5	2.6E-01	7.0E+02
6.8	2.7E-01	7.2E+02
7.1	2.7E-01	7.2E+02
7.4	2.9E-01	7.4E+02
7.7	3.2E-01	7.9E+02
8.1	3.6E-01	8.4E+02
8.4	4.0E-01	8.8E+02
8.8	4.3E-01	9.2E+02
9.2	4.6E-01	9.5E+02
9.6	5.0E-01	9.9E+02
10.0	5.5E-01	1.0E+03
10.6	5.7E-01	1.1E+03
6.5	3.6E-01	8.6E+02
6.8	3.7E-01	8.8E+02
7.1	3.8E-01	8.9E+02
7.4	3.9E-01	9.0E+02
7.7	3.9E-01	9.1E+02
8.1	3.9E-01	9.1E+02
8.4	3.9E-01	9.1E+02
8.8	4.0E-01	9.2E+02
9.2	4.0E-01	9.2E+02
9.6	4.0E-01	9.2E+02
10.0	4.0E-01	9.2E+02
10.6	4.0E-01	9.2E+02
11.0	4.0E-01	9.3E+02
11.4	4.1E-01	9.3E+02
11.8	4.1E-01	9.4E+02
12.2	4.2E-01	9.5E+02
12.6	4.2E-01	9.6E+02
13.0	4.3E-01	9.7E+02
13.5	4.4E-01	9.8E+02
14.0	4.4E-01	9.9E+02
14.5	4.4E-01	9.9E+02
15.0	4.5E-01	1.0E+03
15.5	4.5E-01	1.0E+03

Half pore width (Å)	Cumulative Pore Volume (cc/g)	Cumulative Surface Area (m^2/g)
16.0	4.5E-01	1.0E+03
16.6	4.6E-01	1.0E+03
17.2	4.6E-01	1.0E+03
17.8	4.6E-01	1.0E+03
18.4	4.6E-01	1.0E+03
19.0	4.7E-01	1.0E+03
19.7	4.7E-01	1.0E+03
20.4	4.7E-01	1.0E+03
21.1	4.7E-01	1.0E+03
21.8	4.7E-01	1.0E+03
22.6	4.8E-01	1.0E+03
23.4	4.8E-01	1.0E+03
24.2	4.8E-01	1.0E+03
25.1	4.8E-01	1.0E+03
25.9	4.8E-01	1.0E+03
26.8	4.9E-01	1.0E+03
27.8	4.9E-01	1.0E+03
28.8	5.0E-01	1.0E+03
29.8	5.0E-01	1.1E+03
30.8	5.1E-01	1.1E+03
31.9	5.1E-01	1.1E+03
33.0	5.2E-01	1.1E+03
34.2	5.2E-01	1.1E+03
35.3	5.3E-01	1.1E+03
36.6	5.3E-01	1.1E+03
37.9	5.4E-01	1.1E+03
39.2	5.4E-01	1.1E+03
40.6	5.5E-01	1.1E+03
42.0	5.6E-01	1.1E+03
43.5	5.6E-01	1.1E+03
45.0	5.7E-01	1.1E+03
46.5	5.8E-01	1.1E+03
48.2	5.9E-01	1.1E+03
49.9	6.0E-01	1.1E+03
51.6	6.1E-01	1.1E+03
53.4	6.2E-01	1.1E+03
55.3	6.3E-01	1.1E+03
57.2	6.4E-01	1.2E+03
59.2	6.5E-01	1.2E+03
61.3	6.6E-01	1.2E+03
63.4	6.7E-01	1.2E+03
65.7	6.9E-01	1.2E+03

Half pore width (Å)	Cumulative Pore Volume (cc/g)	Cumulative Surface Area (m^2/g)
68.0	7.0E-01	1.2E+03
70.3	7.2E-01	1.2E+03
72.8	7.3E-01	1.2E+03
75.3	7.5E-01	1.2E+03
78.0	7.6E-01	1.2E+03
80.7	7.8E-01	1.2E+03
83.5	7.9E-01	1.2E+03
86.5	8.1E-01	1.2E+03
89.5	8.3E-01	1.2E+03
92.6	8.4E-01	1.2E+03
95.9	8.6E-01	1.2E+03
99.2	8.8E-01	1.2E+03
102.7	8.9E-01	1.2E+03
106.3	9.1E-01	1.3E+03
110.0	9.2E-01	1.3E+03
113.8	9.4E-01	1.3E+03
117.8	9.5E-01	1.3E+03
122.0	9.7E-01	1.3E+03
126.2	9.8E-01	1.3E+03
130.6	9.9E-01	1.3E+03
135.2	1.0E+00	1.3E+03
139.9	1.0E+00	1.3E+03
144.8	1.0E+00	1.3E+03
149.9	1.0E+00	1.3E+03
155.2	1.0E+00	1.3E+03
160.6	1.0E+00	1.3E+03
166.2	1.1E+00	1.3E+03
172.0	1.1E+00	1.3E+03
178.1	1.1E+00	1.3E+03
184.3	1.1E+00	1.3E+03
190.7	1.1E+00	1.3E+03
197.4	1.1E+00	1.3E+03
204.3	1.1E+00	1.3E+03
211.5	1.1E+00	1.3E+03
218.9	1.1E+00	1.3E+03
226.5	1.1E+00	1.3E+03
234.5	1.1E+00	1.3E+03
242.7	1.1E+00	1.3E+03
251.2	1.1E+00	1.3E+03

Table A.3 Pore volume and surface area data for WPC (coconut)

Half pore width (Å)	Cumulative Pore Volume (cc/g)	Cumulative Surface Area (m^2/g)
3.0	0.0E+00	0.0E+00
3.1	0.0E+00	0.0E+00
3.2	2.4E-03	7.6E+00
3.3	2.9E-02	8.9E+01
3.5	6.5E-02	1.9E+02
3.6	8.4E-02	2.4E+02
3.8	8.6E-02	2.5E+02
3.9	8.7E-02	2.5E+02
4.1	9.1E-02	2.6E+02
4.3	9.1E-02	2.6E+02
4.4	9.1E-02	2.6E+02
4.6	9.1E-02	2.6E+02
4.8	9.8E-02	2.8E+02
5.0	1.1E-01	2.9E+02
5.3	1.1E-01	3.0E+02
5.5	1.1E-01	3.0E+02
5.7	1.2E-01	3.2E+02
6.0	1.3E-01	3.4E+02
6.2	1.4E-01	3.5E+02
6.5	1.5E-01	3.6E+02
6.8	1.5E-01	3.7E+02
7.1	1.6E-01	3.8E+02
7.4	1.6E-01	3.9E+02
7.7	1.7E-01	3.9E+02
8.1	1.7E-01	3.9E+02
8.4	1.7E-01	3.9E+02
8.8	1.7E-01	3.9E+02
9.2	1.7E-01	3.9E+02
9.6	1.7E-01	3.9E+02
10.0	1.7E-01	3.9E+02
10.6	1.7E-01	3.9E+02
6.5	3.0E-01	7.4E+02
6.8	3.0E-01	7.4E+02
7.1	3.1E-01	7.5E+02
7.4	3.1E-01	7.5E+02
7.7	3.1E-01	7.5E+02
8.1	3.1E-01	7.5E+02
8.4	3.1E-01	7.5E+02
8.8	3.1E-01	7.5E+02
9.2	3.1E-01	7.5E+02
9.6	3.1E-01	7.5E+02

Half pore width (Å)	Cumulative Pore Volume (cc/g)	Cumulative Surface Area (m^2/g)
10.0	3.1E-01	7.5E+02
10.6	3.1E-01	7.5E+02
11.0	3.1E-01	7.6E+02
11.4	3.1E-01	7.6E+02
11.8	3.2E-01	7.6E+02
12.2	3.2E-01	7.7E+02
12.6	3.2E-01	7.7E+02
13.0	3.2E-01	7.7E+02
13.5	3.2E-01	7.8E+02
14.0	3.2E-01	7.8E+02
14.5	3.2E-01	7.8E+02
15.0	3.2E-01	7.8E+02
15.5	3.2E-01	7.8E+02
16.0	3.3E-01	7.8E+02
16.6	3.3E-01	7.8E+02
17.2	3.3E-01	7.8E+02
17.8	3.3E-01	7.8E+02
18.4	3.3E-01	7.8E+02
19.0	3.3E-01	7.8E+02
19.7	3.3E-01	7.8E+02
20.4	3.3E-01	7.8E+02
21.1	3.3E-01	7.8E+02
21.8	3.3E-01	7.8E+02
22.6	3.3E-01	7.8E+02
23.4	3.3E-01	7.8E+02
24.2	3.3E-01	7.8E+02
25.1	3.3E-01	7.8E+02
25.9	3.3E-01	7.8E+02
26.8	3.3E-01	7.8E+02
27.8	3.3E-01	7.8E+02
28.8	3.3E-01	7.8E+02
29.8	3.3E-01	7.8E+02
30.8	3.3E-01	7.8E+02
31.9	3.3E-01	7.8E+02
33.0	3.3E-01	7.8E+02
34.2	3.3E-01	7.8E+02
35.3	3.3E-01	7.8E+02
36.6	3.3E-01	7.8E+02
37.9	3.3E-01	7.8E+02
39.2	3.3E-01	7.8E+02
40.6	3.3E-01	7.8E+02
42.0	3.3E-01	7.8E+02

Half pore width (Å)	Cumulative Pore Volume (cc/g)	Cumulative Surface Area (m^2/g)
43.5	3.3E-01	7.8E+02
45.0	3.3E-01	7.8E+02
46.5	3.3E-01	7.8E+02
48.2	3.3E-01	7.8E+02
49.9	3.3E-01	7.8E+02
51.6	3.3E-01	7.8E+02
53.4	3.3E-01	7.8E+02
55.3	3.3E-01	7.8E+02
57.2	3.3E-01	7.8E+02
59.2	3.3E-01	7.8E+02
61.3	3.3E-01	7.8E+02
63.4	3.3E-01	7.8E+02
65.7	3.3E-01	7.8E+02
68.0	3.3E-01	7.8E+02
70.3	3.3E-01	7.8E+02
72.8	3.3E-01	7.8E+02
75.3	3.3E-01	7.8E+02
78.0	3.3E-01	7.8E+02
80.7	3.3E-01	7.9E+02
83.5	3.4E-01	7.9E+02
86.5	3.4E-01	7.9E+02
89.5	3.4E-01	7.9E+02
92.6	3.4E-01	7.9E+02
95.9	3.4E-01	7.9E+02
99.2	3.4E-01	7.9E+02
102.7	3.4E-01	7.9E+02
106.3	3.4E-01	7.9E+02
110.0	3.4E-01	7.9E+02
113.8	3.4E-01	7.9E+02
117.8	3.4E-01	7.9E+02
122.0	3.4E-01	7.9E+02
126.2	3.4E-01	7.9E+02
130.6	3.4E-01	7.9E+02
135.2	3.4E-01	7.9E+02
139.9	3.4E-01	7.9E+02
144.8	3.4E-01	7.9E+02
149.9	3.4E-01	7.9E+02
155.2	3.4E-01	7.9E+02
160.6	3.4E-01	7.9E+02
166.2	3.4E-01	7.9E+02
172.0	3.4E-01	7.9E+02
178.1	3.4E-01	7.9E+02

Half pore width (Å)	Cumulative Pore Volume (cc/g)	Cumulative Surface Area (m^2/g)
184.3	3.4E-01	7.9E+02
190.7	3.4E-01	7.9E+02
197.4	3.4E-01	7.9E+02
204.3	3.4E-01	7.9E+02
211.5	3.4E-01	7.9E+02
218.9	3.4E-01	7.9E+02
226.5	3.4E-01	7.9E+02
234.5	3.4E-01	7.9E+02
242.7	3.4E-01	7.9E+02
251.2	3.5E-01	7.9E+02

Appendix A.3 Rate of Adsorption in Ultrapure Water

Table A.4 CYL adsorption rate data determined with COL-PL60-800 (coal) in ultrapure water

Time (d)	IS-Area Count	CYL-Area Count	Response Ratio	Concentration (µg/L)
0	287773	139771	0.49	107.49
0.25	167772	67054	0.40	88.37
0.5	120335	24503	0.20	44.81
0.75	150255	10477	0.07	15.05
1	234537	7089	0.03	6.27
1.25	310231	3567	0.01	2.11
1.5	305109	2760	0.01	1.57
1.75	296349	2662	0.01	1.55
2	329709	1973	0.01	0.89
6	268278	563	0.00	0.02
25.5	233744	472	0.00	0.00

Table A.5 CYL adsorption rate data determined with BG-HHM (wood) in ultrapure water

Time (d)	IS-Area Count	CYL-Area Count	Response Ratio	Concentration (µg/L)
0	431659	209657	0.49	107.49
0.25	421113	45081	0.11	23.34
0.5	427766	8931	0.02	4.20
0.75	411802	4942	0.01	2.22
1	452887	4004	0.01	1.52
1.25	409583	2845	0.01	1.10
1.5	415012	2800	0.01	1.05
1.75	415031	2405	0.01	0.84
2	418427	2328	0.01	0.79
6	438774	2128	0.00	0.63

Table A.6 CYL adsorption rate data determined with WPC (coconut) in ultrapure water

Time (d)	IS-Area Count	CYL-Area Count	Response Ratio	Concentration (µg/L)
0	481848	237207	0.49	108.95
0.25	484874	56109	0.12	25.27
0.5	484211	15468	0.03	6.65
0.75	478611	11434	0.02	4.86
1	445491	7328	0.02	3.21
1.25	498143	6241	0.01	2.34
1.5	486134	4705	0.01	1.71
1.75	481369	3865	0.01	1.34
2	428642	1836	0.00	0.51
6	453396	1698	0.00	0.39

Table A.7 MC-LR adsorption rate data determined with COL-PL60-800 (coal) in ultrapure water

Time (d)	IS-Area Count	CYL-Area Count	Response Ratio	Concentration (µg/L)
0	364434	777286	2.13	104.42
0.25	348517	417652	1.20	58.61
0.5	347531	166184	0.48	23.31
0.75	342486	84829	0.25	12.01
1	393128	52181	0.13	6.37
1.25	362647	36439	0.10	4.79
1.5	381609	18860	0.05	2.29
1.75	374242	11529	0.03	1.38
2	345572	5669	0.02	0.67
6	330469	1913	0.01	0.15
25.5	394834	1519	0.00	0.06

Table A.8 MC-LR adsorption rate data determined with BG-HHM (wood) in ultrapure water

Time (d)	IS-Area Count	CYL-Area Count	Response Ratio	Concentration (µg/L)
0	291250	620468	2.13	104.30
0.25	291776	36381	0.12	5.98
0.5	294029	8438	0.03	1.27
0.75	275310	2436	0.01	0.30
1	294482	2476	0.01	0.28
1.25	301460	2496	0.01	0.27
1.5	318197	2121	0.01	0.19

Table A.9 MC-LR adsorption rate data determined with WPC (coconut) in ultrapure water

Time (d)	IS-Area Count	CYL-Area Count	Response Ratio	Concentration (µg/L)
0	297448	621143	2.09	102.23
0.25	308241	305642	0.99	48.47
0.5	286359	145901	0.51	24.84
0.75	294597	71382	0.24	11.75
1	285968	45788	0.16	7.72
1.25	280827	32039	0.11	5.46
1.5	337693	28475	0.08	4.00
1.75	339468	16748	0.05	2.29
2	335044	7821	0.02	1.01
6	325705	1405	0.00	0.08
25.5	327573	284	0.00	-0.09

Table A.10 ANTA adsorption rate data determined with COL-PL60-800 (coal) in ultrapure water

Time (d)	IS-Area Count	CYL-Area Count	Response Ratio	Concentration (µg/L)
0	632569	1541230	2.44	101.98
0.25	584214	1405321	2.41	100.70
0.5	618802	1458453	2.36	98.68
0.75	605892	1383079	2.28	95.60
1	599950	1330746	2.22	92.92
1.25	624558	1335762	2.14	89.63
1.5	624028	1237656	1.98	83.18
1.75	562148	1098132	1.95	81.94
2	662534	1258030	1.90	79.67
6	590872	944923	1.60	67.24
25.5	743417	767871	1.03	43.74
48	697336	542109	0.78	33.14
72	747411	400012	0.54	23.09
96	895093	300262	0.34	14.80
120	623123	131385	0.21	9.63
144	747445	121372	0.16	7.62
168	796456	122692	0.15	7.28

Table A.11 ANTA adsorption rate data determined with BG-HHM (wood) in ultrapure water

Time (d)	IS-Area Count	CYL-Area Count	Response Ratio	Concentration (µg/L)
0	665963	1741792	2.62	109.41
0.25	501695	492364	0.98	41.61
0.5	570656	363505	0.64	27.32
0.75	462451	289474	0.63	26.86
1	442161	259450	0.59	25.23
1.25	464819	274182	0.59	25.36
1.5	462571	242263	0.52	22.62
1.75	473363	213408	0.45	19.59
2	436854	184308	0.42	18.39
6	468484	132888	0.28	12.65
25.5	530168	71258	0.13	6.46
48	633381	49220	0.08	4.11
72	642328	44165	0.07	3.74

Table A.12 ANTA adsorption rate data determined with WPC (coconut) in ultrapure water

Time (d)	IS-Area Count	CYL-Area Count	Response Ratio	Concentration (µg/L)
0	403614	1025180.5	2.54	106.28
0.25	348023	566767	1.63	68.46
0.5	387536	533530	1.38	58.01
0.75	422386	569778	1.35	56.86
1	675886	784670	1.16	49.06
1.25	573339	615151	1.07	45.40
1.5	599745	638735	1.07	45.08
1.75	534908	522753	0.98	41.43
2	473285	446600	0.94	40.04
6	368075	234432	0.64	27.31
25.5	527947	152569	0.29	12.87
48	423477	87807	0.21	9.49
72	432499	82222	0.19	8.77

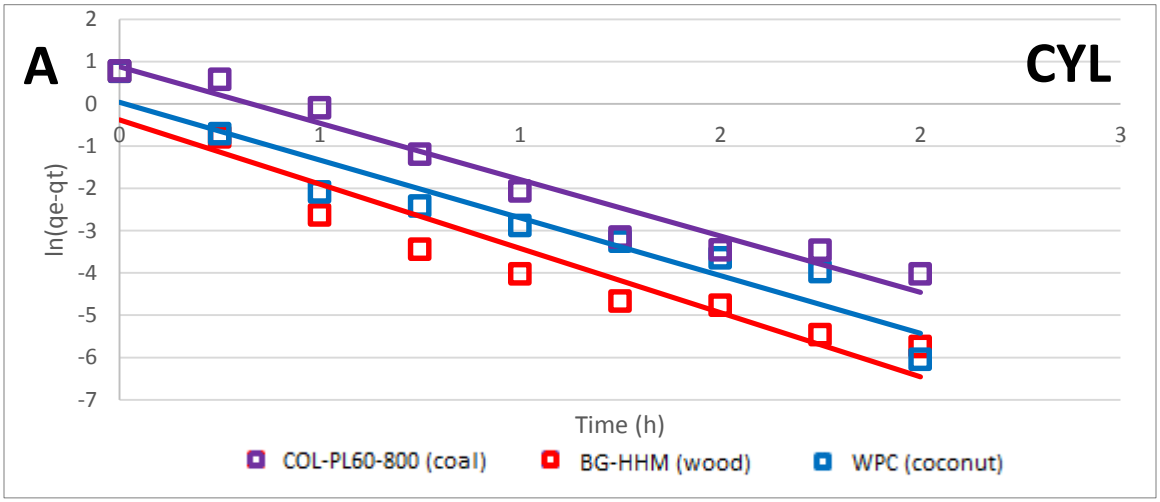

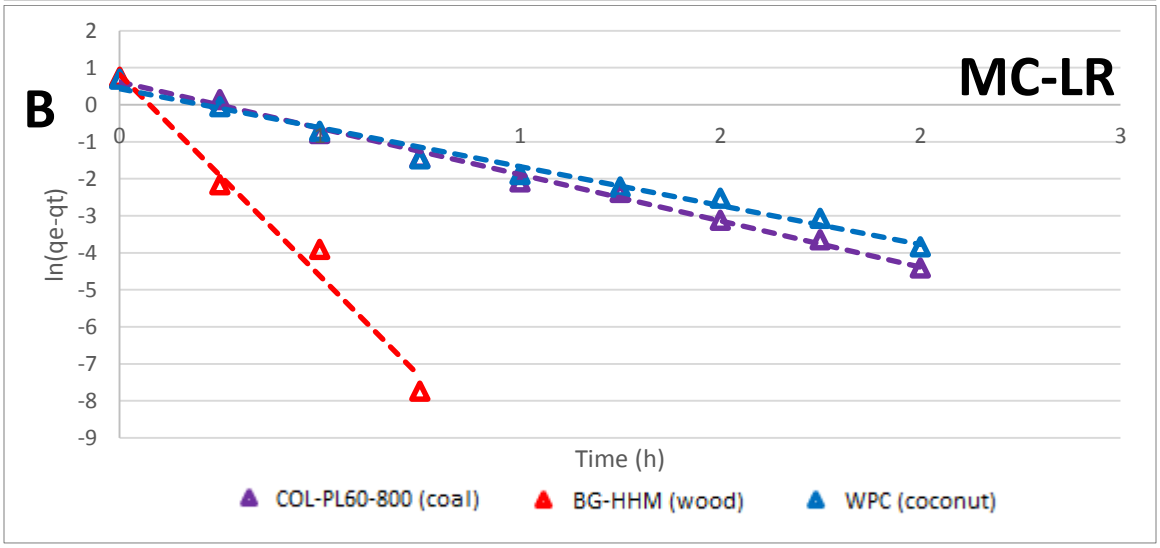

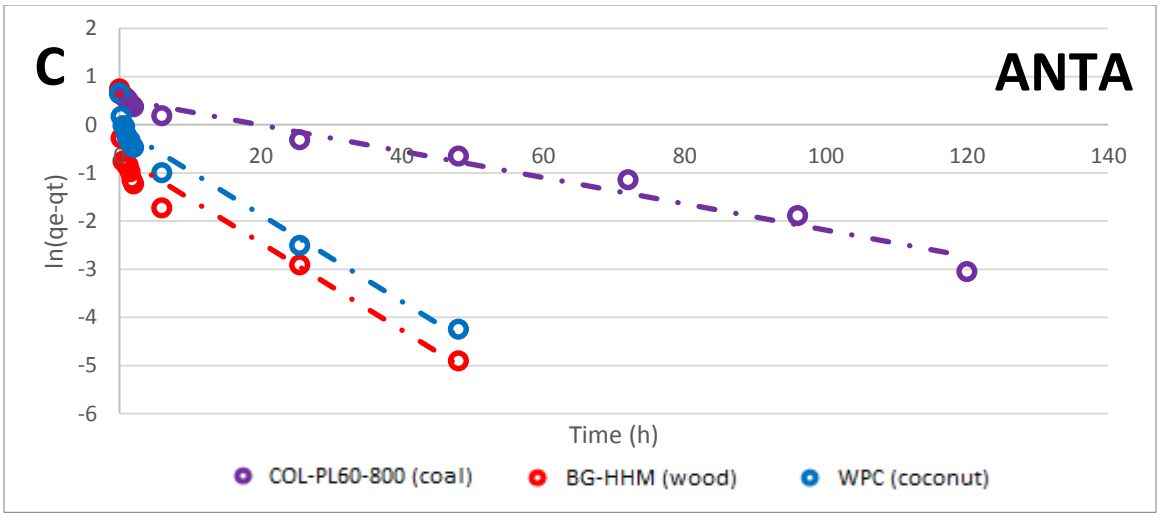

Figure A.1 Pseudo-first order kinetic model fits of cyanotoxin adsorption by three PACs in ultrapure water. A) CYL, B) MC-LR, and C) ANTA.

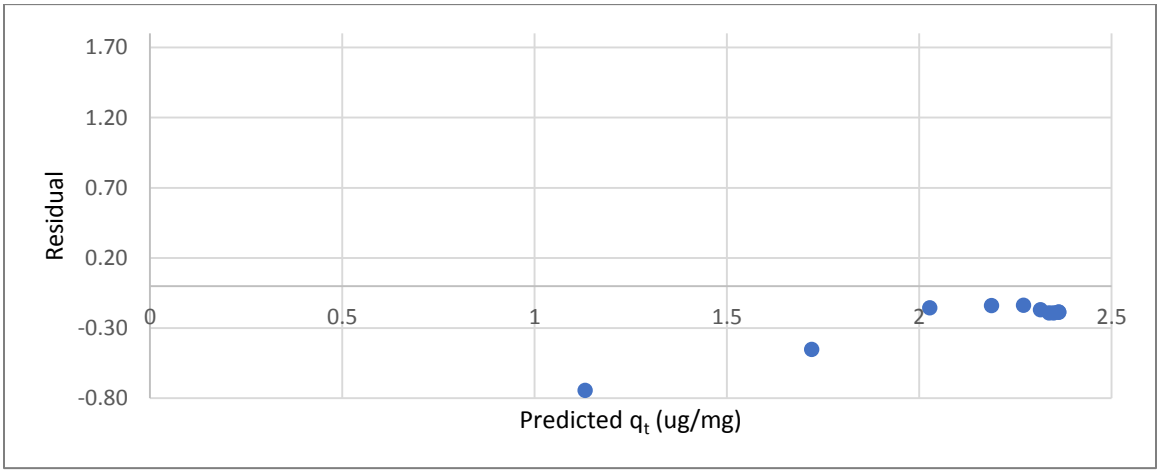

Figure A.2 Residual plot for pseudo-first order fit of CYL adsorption by the COL-PL60-800 (coal)

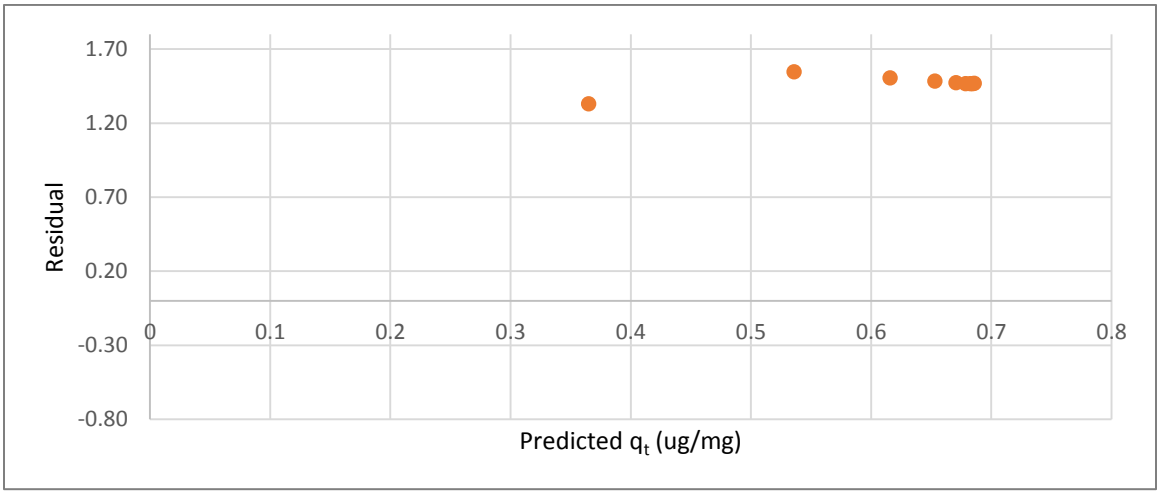

Figure A.3 Residual plot for pseudo-first order fit of CYL adsorption by the BG-HHM (wood)

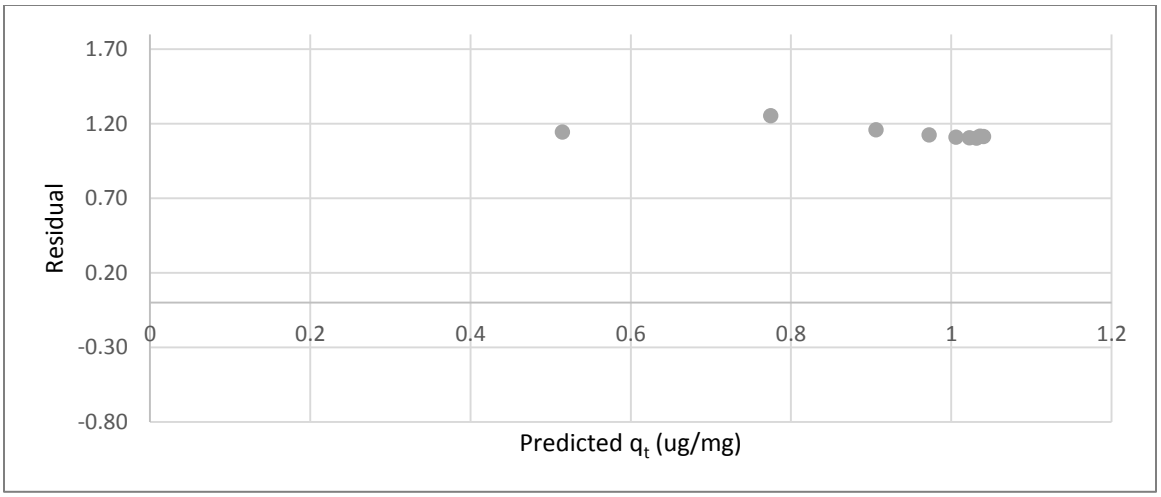

Figure A.4 Residual plot for pseudo-first order fit of CYL adsorption by the WPC (coconut)

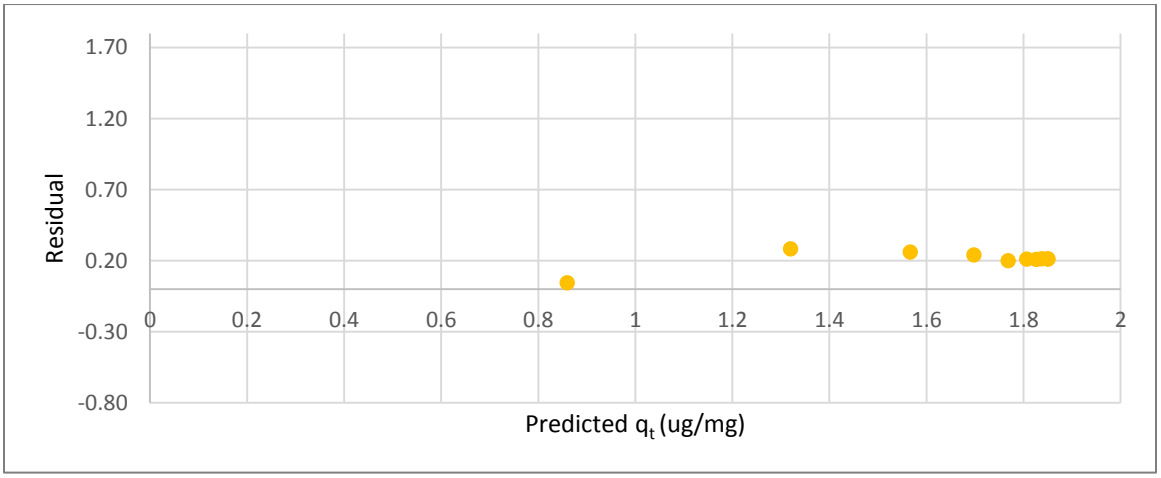

Figure A.5 Residual plot for pseudo-first order fit of MC-LR adsorption by the COL-PL60-800 (coal)

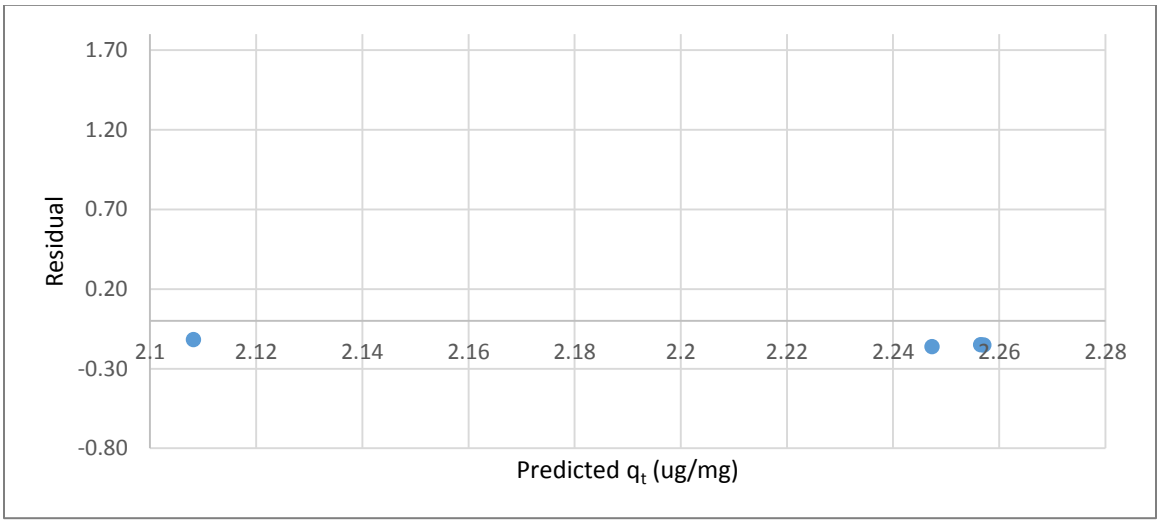

Figure A.6 Residual plot for pseudo-first order fit of MC-LR adsorption by the BG-HHM (wood)

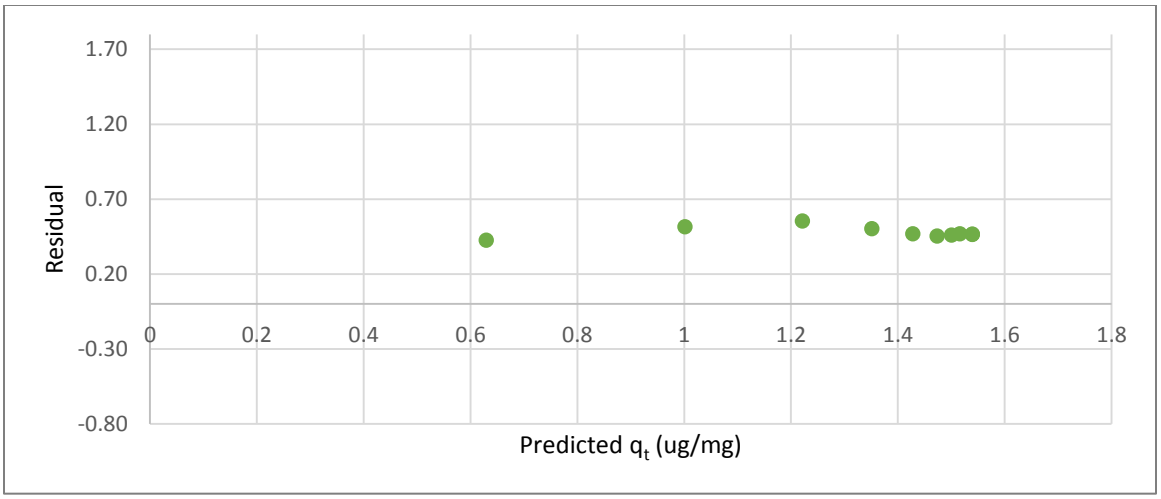

Figure A.7 Residual plot for pseudo-first order fit of MC-LR adsorption by the WPC (coconut)

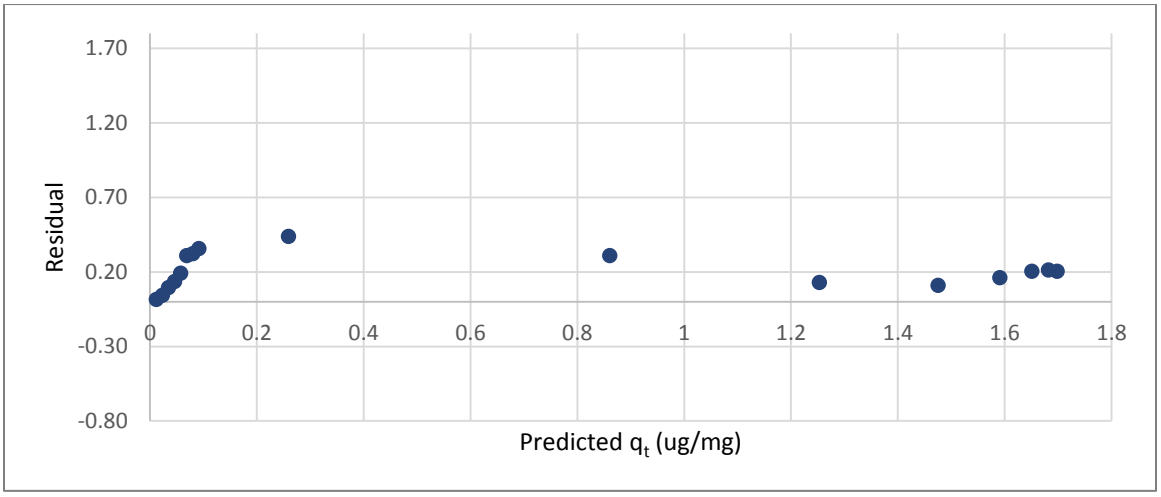

Figure A.8 Residual plot for pseudo-first order fit of ANTA adsorption by the COL-PL60-800 (coal)

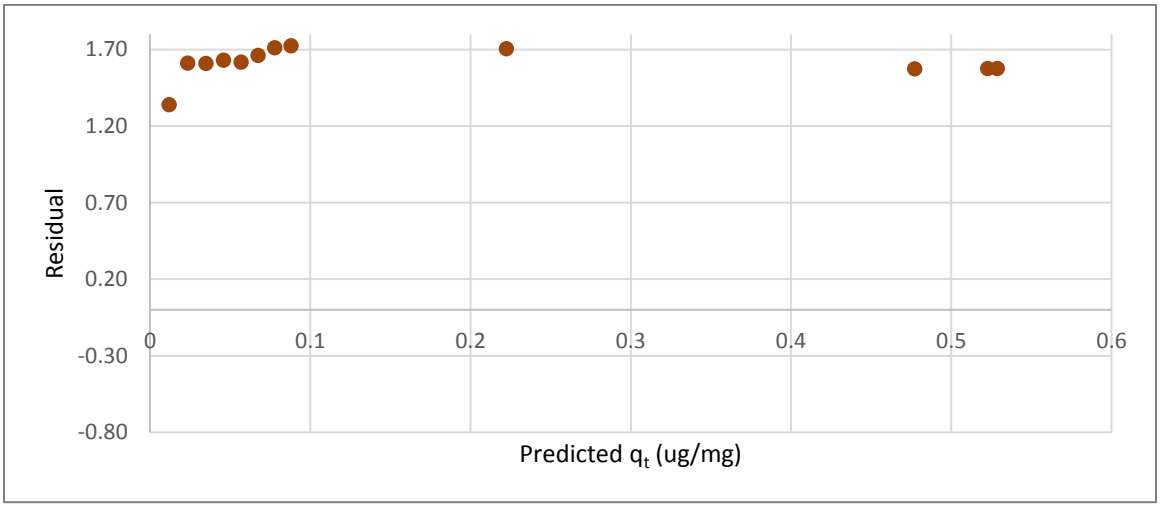

Figure A.9 Residual plot for pseudo-first order fit of ANTA adsorption by the BG-HHM (wood)

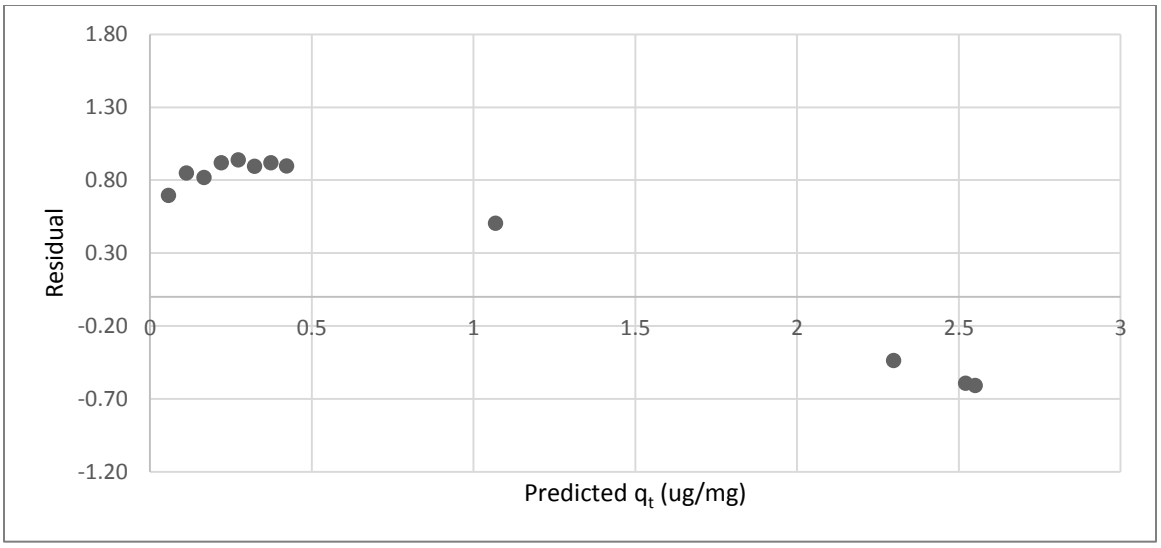

Figure A.10 Residual plot for pseudo-first order fit of ANTA adsorption by the WPC (coconut)

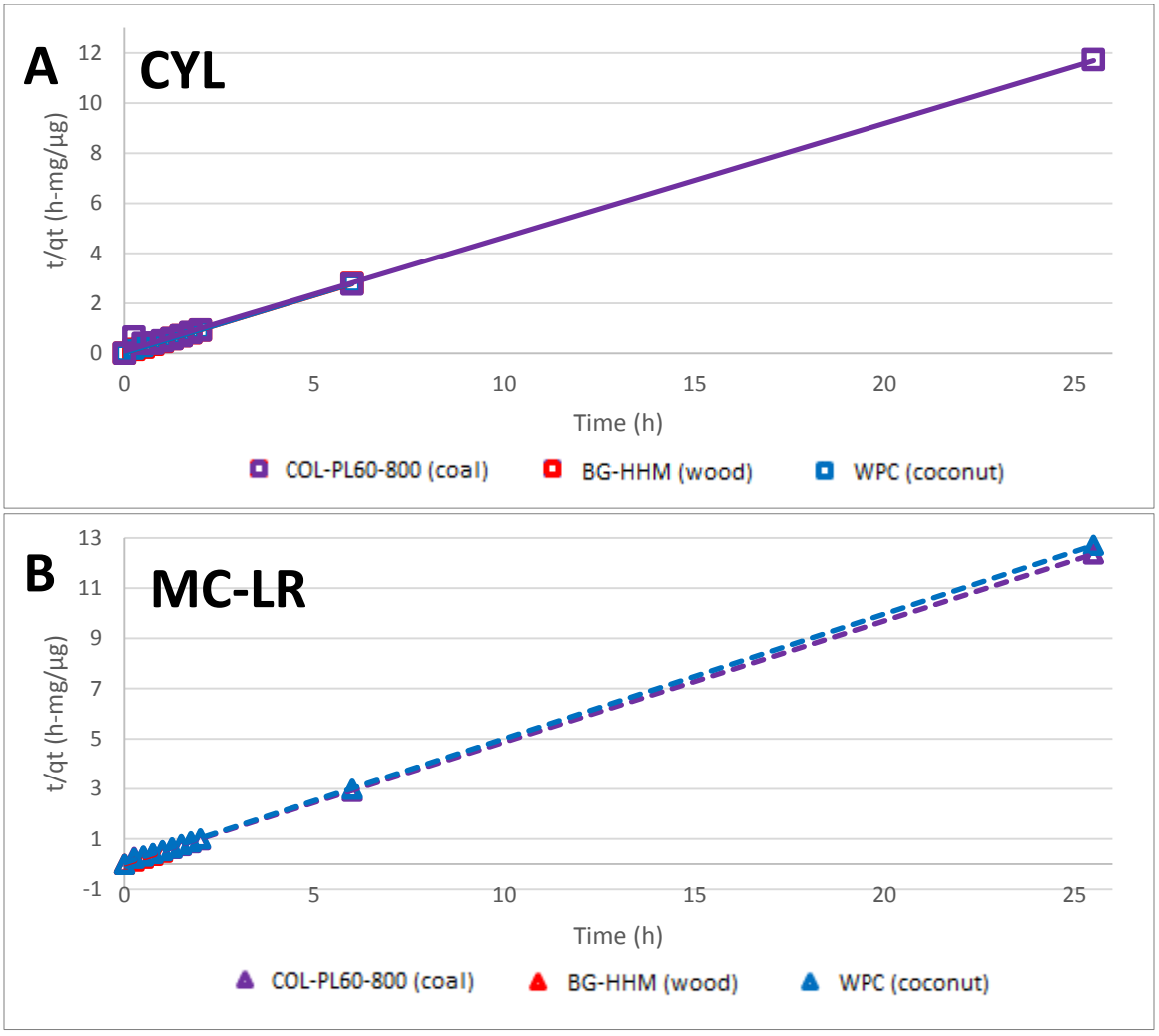

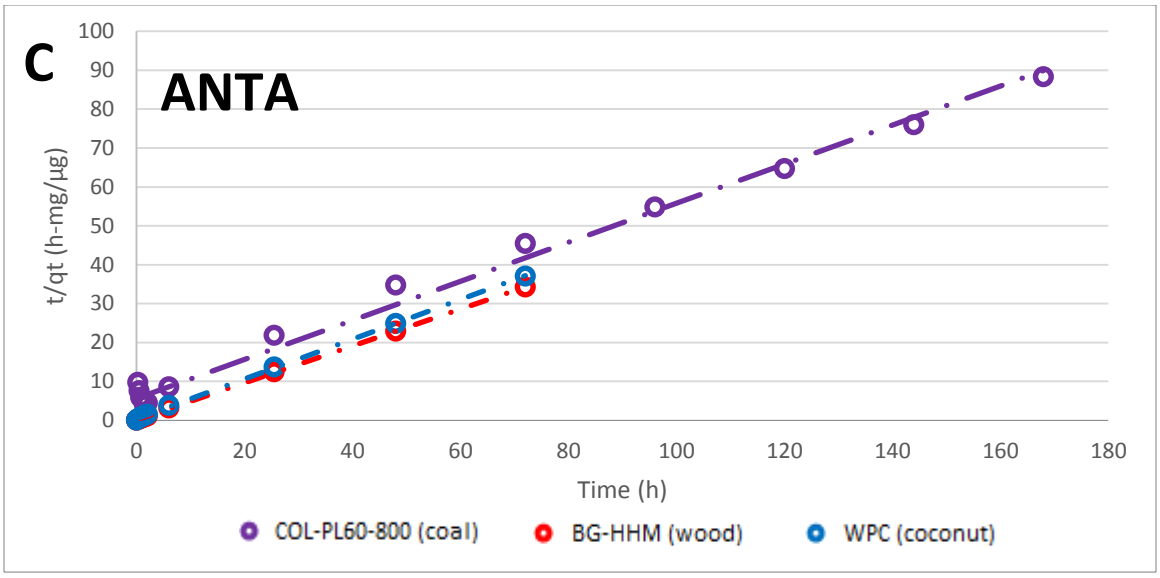

Figure A.11 Pseudo-second order kinetic model fits of cyanotoxin adsorption by three PACs in ultrapure water. A) CYL, B) MC-LR, and C) ANTA.

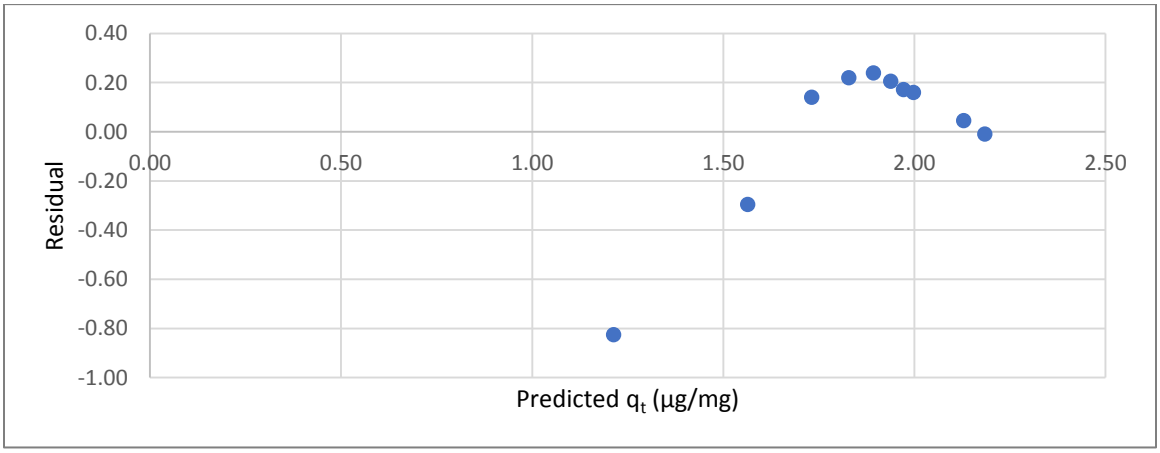

Figure A.12 Residual plot for pseudo-second order fit of CYL adsorption by the COL-PL60-800 (coal)

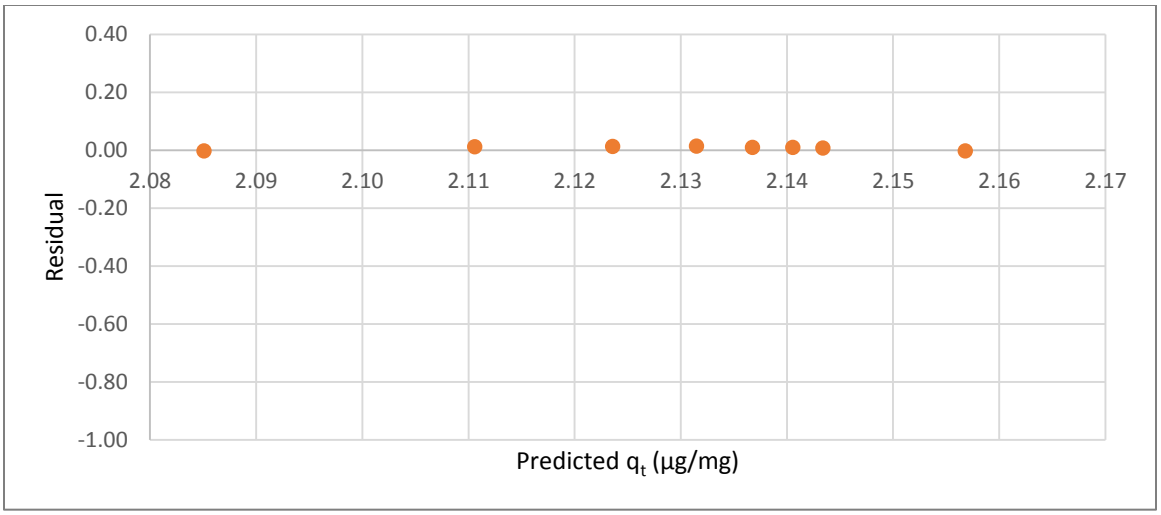

Figure A.13 Residual plot for pseudo-second order fit of CYL adsorption by the BG-HHM (wood)

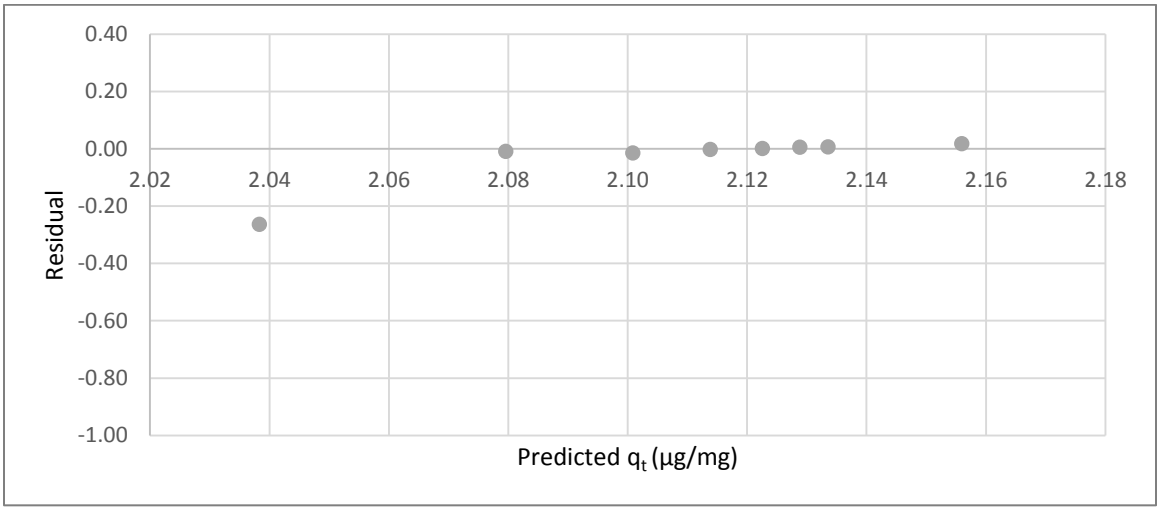

Figure A.14 Residual plot for pseudo-second order fit of CYL adsorption by the WPC (coconut)

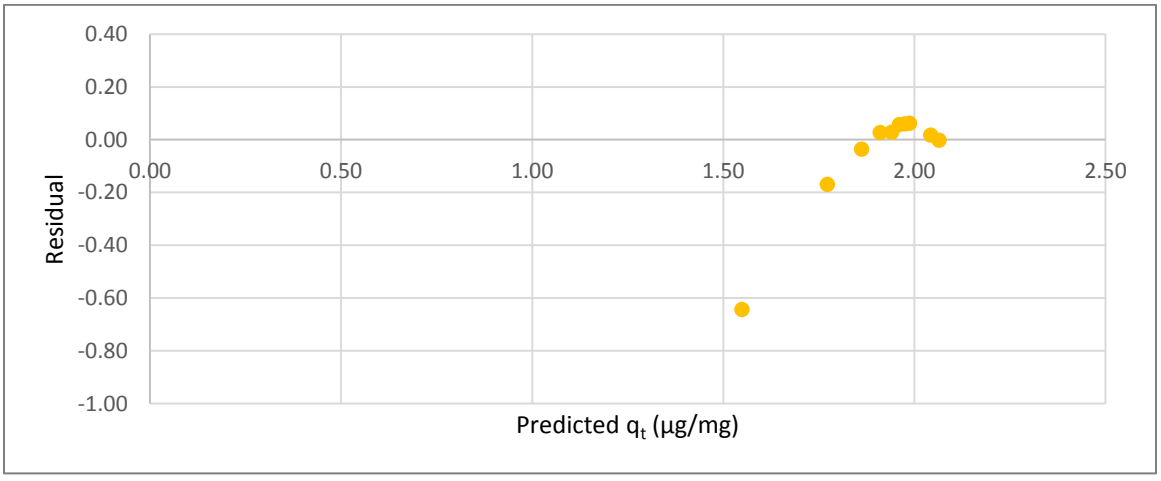

Figure A.15 Residual plot for pseudo-second order fit of MC-LR adsorption by the COL-PL60-800 (coal)

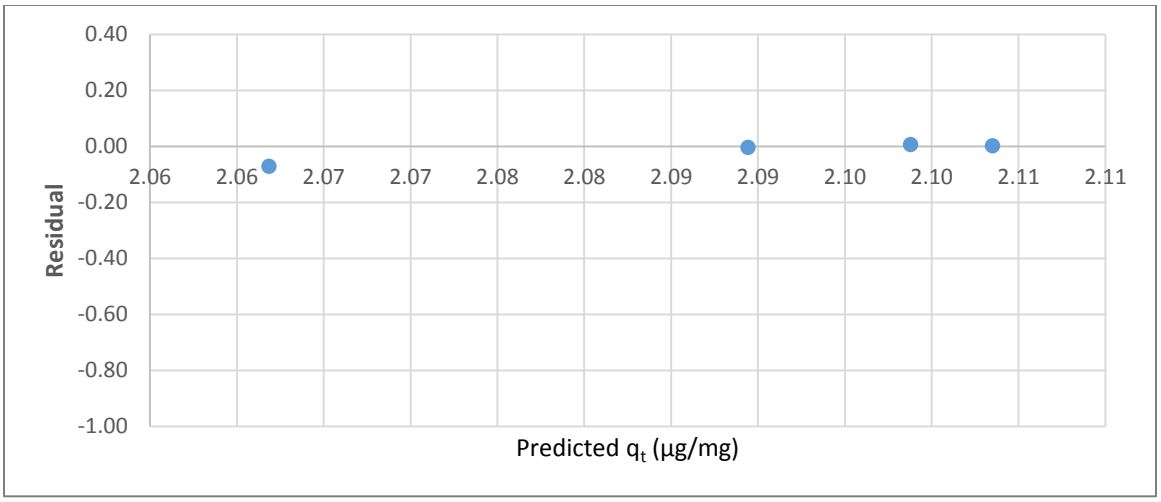

Figure A.16 Residual plot for pseudo-second order fit of MC-LR adsorption by the BG-HHM (wood)

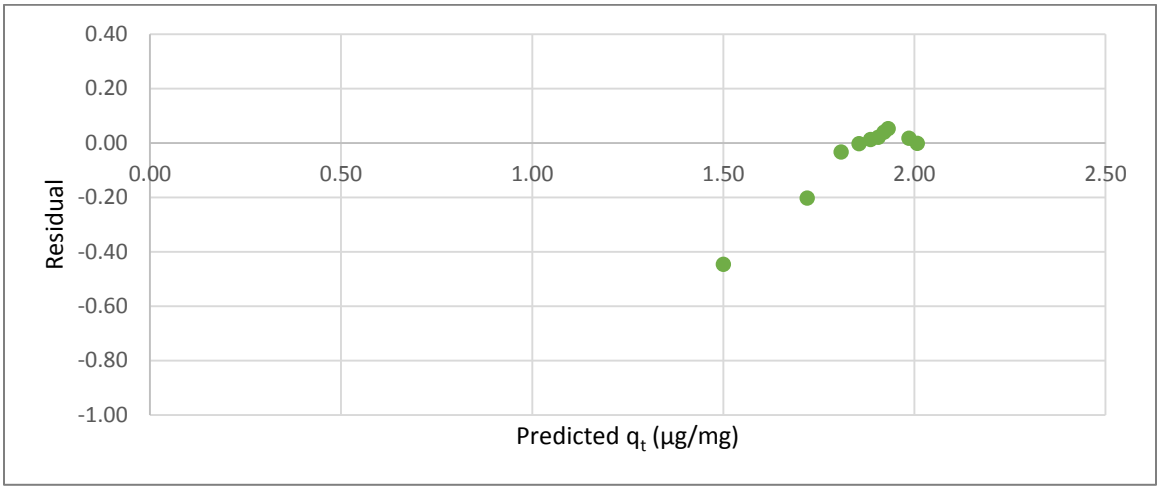

Figure A.17 Residual plot for pseudo-second order fit of MC-LR adsorption by the WPC (coconut)

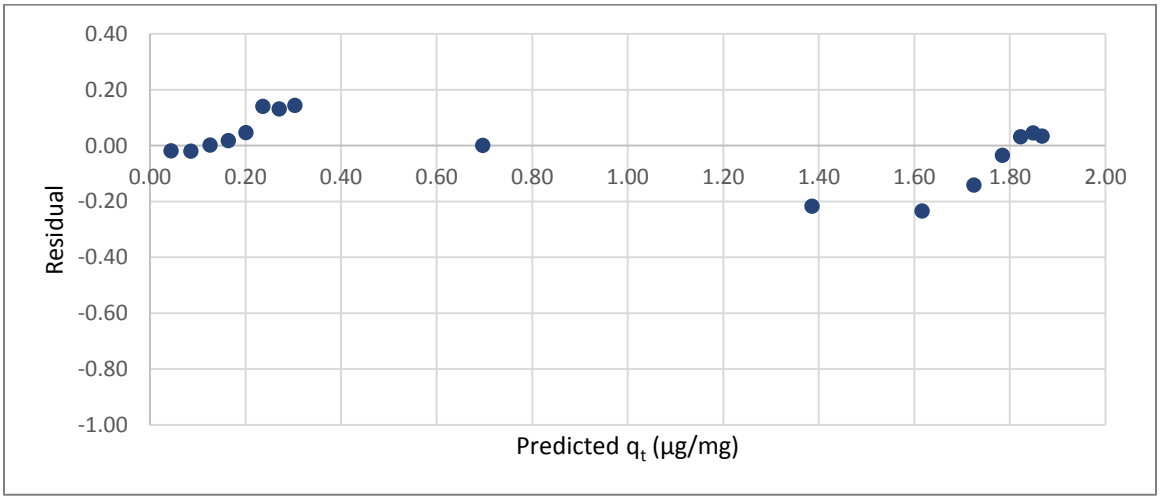

Figure A.18 Residual plot for pseudo-second order fit of ANTA adsorption by the COL-PL60-800 (coal)

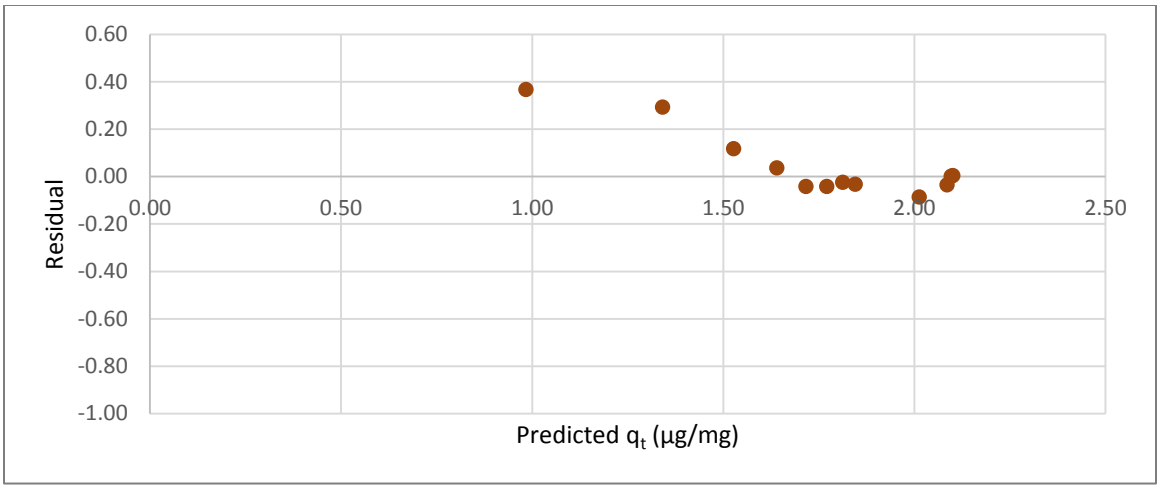

Figure A.19 Residual plot for pseudo-second order fit of ANTA adsorption by the BG-HHM (wood)

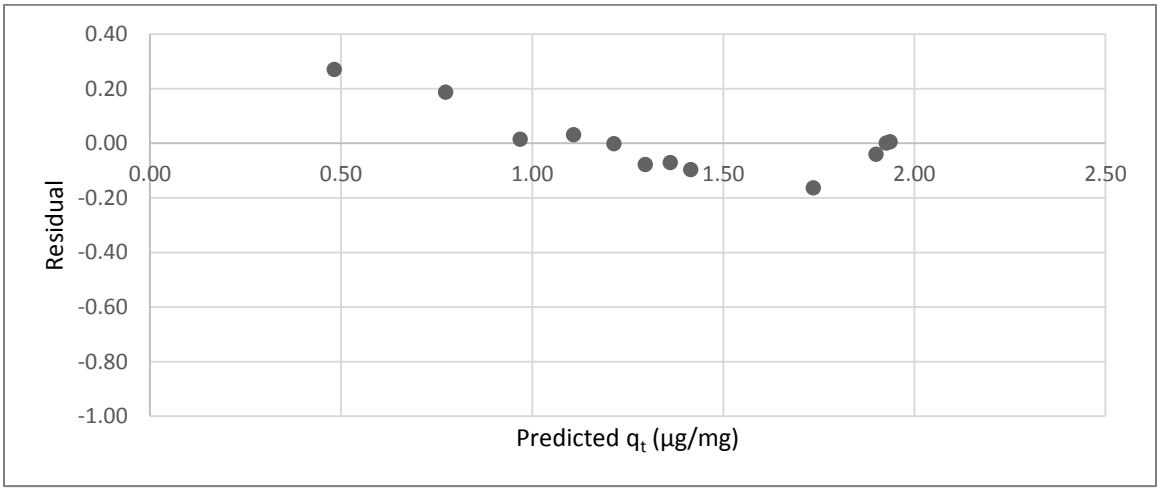

Figure A.20 Residual plot for pseudo-second order fit of ANTA adsorption by the WPC (coconut)

Table A.13 Pseudo-first order kinetic model parameters for PACs in ultrapure water

	Carbon	Equilibrium Carbon Capacity, qe experimental (µg/mg)	Equilibrium Carbon Capacity, qe predicted (µg/mg)	k_1 (h^{-1})	R^2
CYL	COL-PL60-800 (coal)	2.18	2.36	2.61	0.9525
CYL	BG-HHM (wood)	2.15	0.69	3.04	0.9014
CYL	WPC (coconut)	2.15	1.04	2.73	0.9186
MC-LR	COL-PL60-800 (coal)	2.06	1.85	2.50	0.9931
MC-LR	BG-HHM (wood)	2.11	2.26	10.88	0.9804
MC-LR	WPC (coconut)	2.01	1.54	2.10	0.9822
ANTA	COL-PL60-800 (coal)	1.90	1.72	0.03	0.0980
ANTA	BG-HHM (wood)	2.11	0.53	0.09	0.8765
ANTA	WPC (coconut)	1.94	2.55	0.09	0.9532

Appendix A.4 Ultrapure Water Isotherm

Table A.14 0.5 h carbon loading data for CYL adsorption by COL-PL60-800 (coal) in ultrapure water

Sample	Carbon dose (mg/L)	Equilibrium toxin concentration (µg/L)	Equilibrium Capacity, qe (µg/mg)
1	50.2	20.12	1.7
2	42.4	25.08	1.9
3	36.0	29.27	2.2
4	30.2	33.46	2.5
5	24.4	42.31	2.7
6	18.4	52.49	3.0
7	12.0	63.29	3.7
8	5.2	86.38	4.1

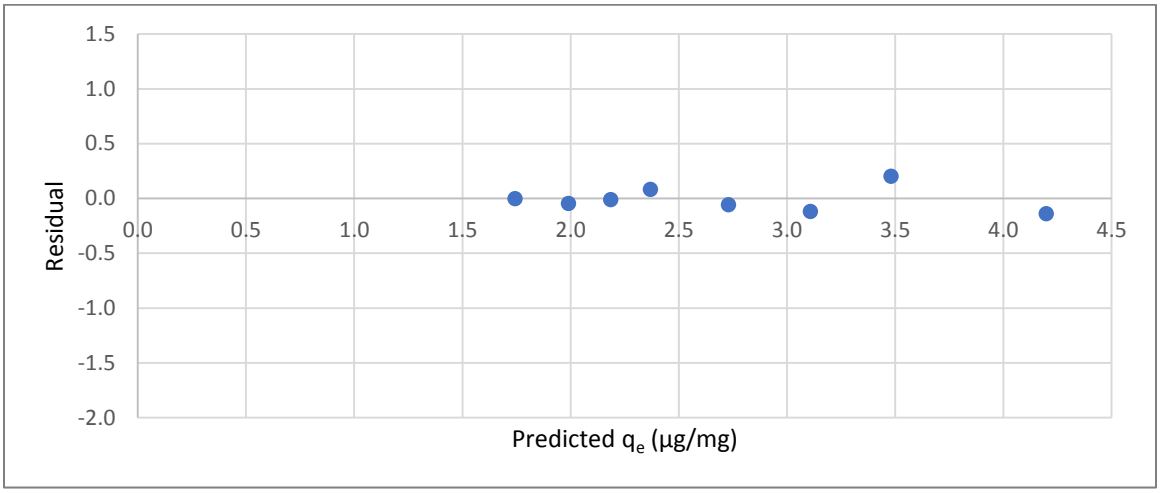

Figure A.21 Residual plot for 0.5 h isotherm of CYL adsorption by the COL-PL60-800 (coal)

Table A.15 1.0 h carbon loading data for CYL adsorption by COL-PL60-800 (coal) in ultrapure water

Sample	Carbon dose (mg/L)	Equilibrium toxin concentration (µg/L)	Equilibrium Capacity, qe (µg/mg)
1	50.2	6.27	2.0
2	42.4	8.47	2.3
3	36.0	13.15	2.6
4	30.2	16.65	3.0
5	24.4	26.97	3.3
6	18.4	38.78	3.7
7	12.0	53.68	4.5
8	5.2	76.66	5.9

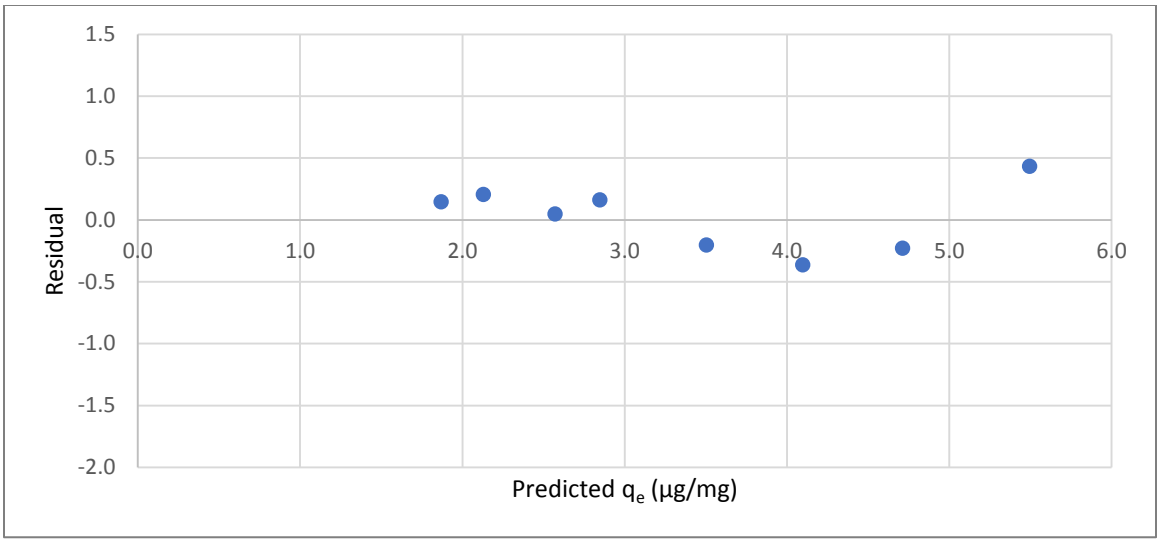

Figure A.22 Residual plot for 1.0 h isotherm of CYL adsorption by the COL-PL60-800 (coal)

Table A.16 Equilibrium carbon loading data for CYL adsorption by COL-PL60-800 (coal) in ultrapure water

Sample	Carbon dose (mg/L)	Equilibrium toxin concentration (µg/L)	Equilibrium Capacity, qe (µg/mg)
1	50.2	0.09	2.1
2	42.4	0.18	2.5
3	36.0	0.36	3.0
4	30.2	0.59	3.5
5	24.4	1.98	4.3
6	18.4	6.00	5.5
7	12.0	10.75	8.1
8	5.2	44.18	12.2

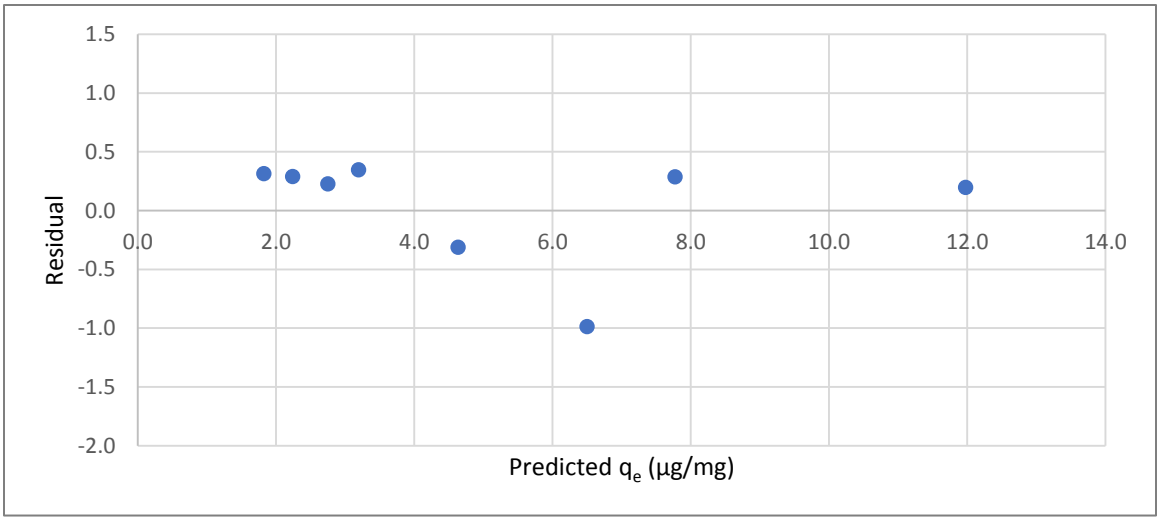

Figure A.23 Residual plot for equilibrium isotherm of CYL adsorption by the COL-PL60-800 (coal)

Table A.17 0.5 h carbon loading data for CYL adsorption by BG-HHM (wood) in ultrapure water

Sample	Carbon dose (mg/L)	Equilibrium toxin concentration (µg/L)	Equilibrium Capacity, qe (µg/mg)
1	50.2	3.42	2.1
2	36.2	5.43	2.8
3	30.4	7.35	3.3
4	24.2	12.57	3.9
5	21.6	15.25	4.3
6	17.8	26.37	4.6
7	11.8	41.61	5.6
8	4.8	72.42	7.3

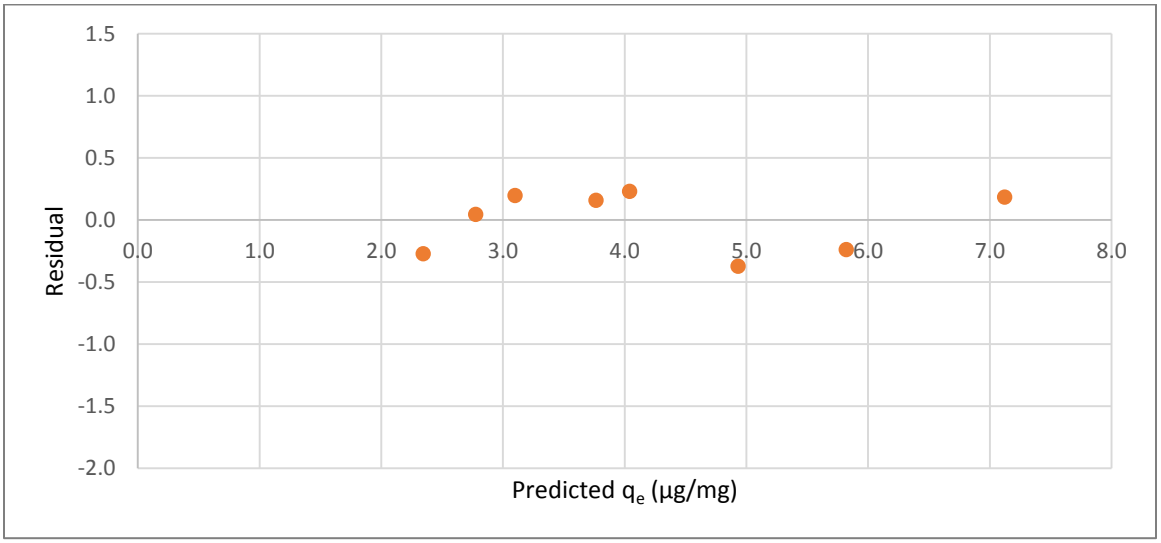

Figure A.24 Residual plot for 0.5 h isotherm of CYL adsorption by the BG-HHM (wood)

Table A.18 1.0 h carbon loading data for CYL adsorption by BG-HHM (wood) in ultrapure water

Sample	Carbon dose (mg/L)	Equilibrium toxin concentration (µg/L)	Equilibrium Capacity, qe (µg/mg)
1	50.2	1.52	2.1
2	36.2	1.86	2.9
3	30.4	2.57	3.5
4	24.2	4.08	4.3
5	21.6	5.51	4.7
6	17.8	10.20	5.5
7	11.8	22.57	7.2
8	4.8	42.83	13.5

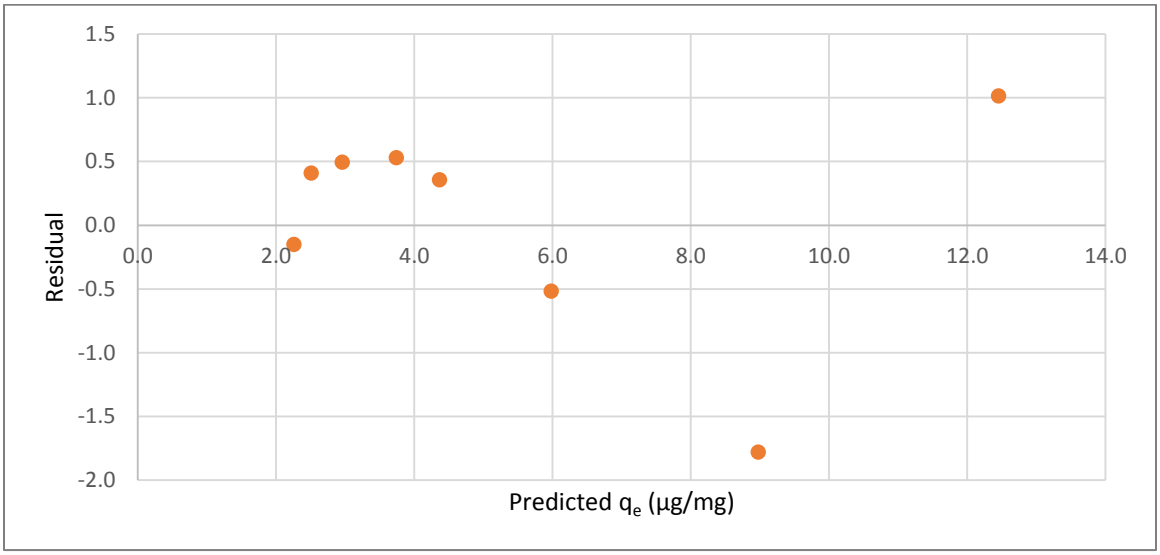

Figure A.25 Residual plot for 1.0 h isotherm of CYL adsorption by the BG-HHM (wood)

Table A.19 Equilibrium carbon loading data for CYL adsorption by BG-HHM (wood) in ultrapure water

Sample	Carbon dose (mg/L)	Equilibrium toxin concentration (µg/L)	Equilibrium Capacity, qe (µg/mg)
1	50.2	0.08	2.1
2	36.2	0.17	3.0
3	30.4	0.28	3.5
4	24.2	0.64	4.4
5	21.6	1.01	4.9
6	17.8	1.59	5.9
7	11.8	4.43	8.7
8	4.8	22.67	17.7

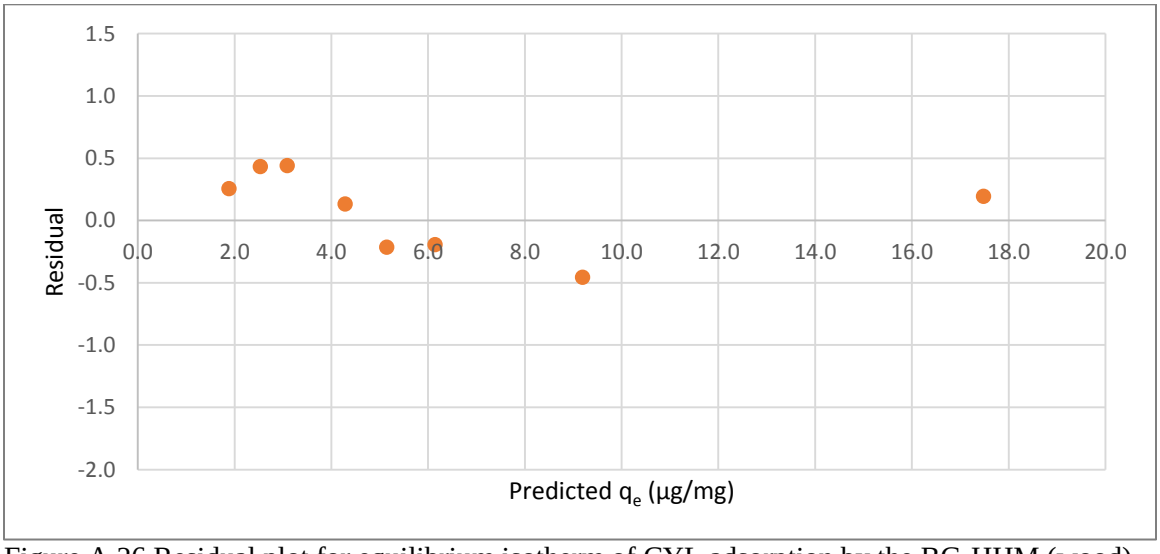

Figure A.26 Residual plot for equilibrium isotherm of CYL adsorption by the BG-HHM (wood)

Table A.20 0.5 h carbon loading data for CYL adsorption by WPC (coconut) in ultrapure water

Sample	Carbon dose (mg/L)	Equilibrium toxin concentration (µg/L)	Equilibrium Capacity, qe (µg/mg)
1	49.8	5.80	2.1
2	42.2	9.33	2.4
3	35.8	12.21	2.7
4	30.2	20.24	2.9
5	24.0	25.03	3.5
6	18.2	41.97	3.7
7	11.6	57.23	4.5
8	5.0	85.07	4.8

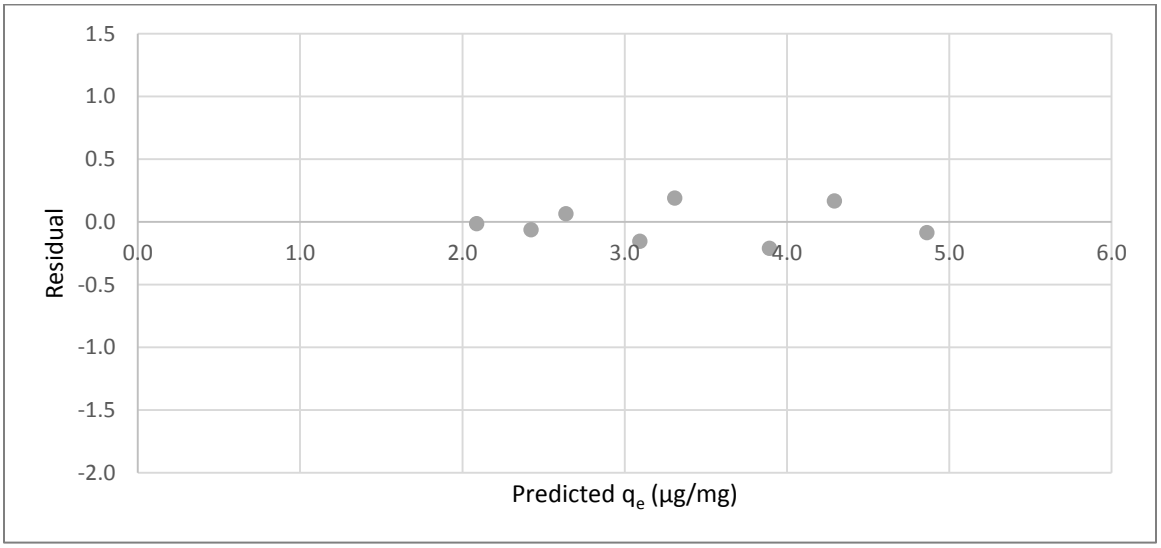

Figure A.27 Residual plot for 0.5 h isotherm of CYL adsorption by the WPC (coconut)

Table A.21 1.0 h carbon loading data for CYL adsorption by WPC (coconut) in ultrapure water

Sample	Carbon dose (mg/L)	Equilibrium toxin concentration (µg/L)	Equilibrium Capacity, qe (µg/mg)
1	49.8	1.75	2.2
2	42.2	2.64	2.5
3	35.8	3.35	2.9
4	30.2	4.59	3.5
5	24.0	8.04	4.2
6	18.2	14.84	5.2
7	11.6	30.59	6.8
8	5.0	57.35	10.3

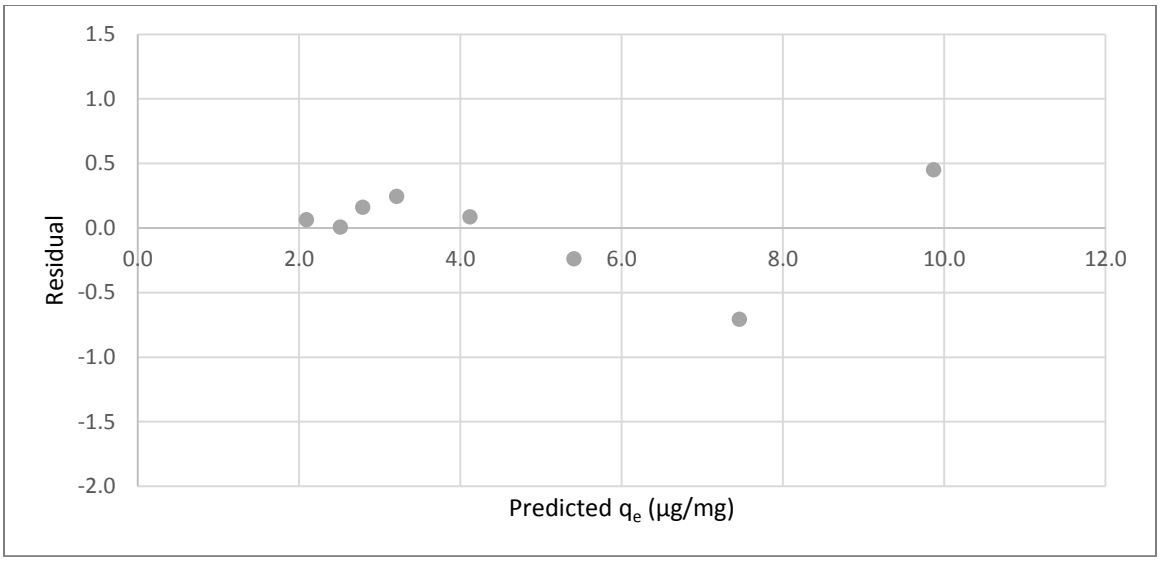

Figure A.28 Residual plot for 1.0 h isotherm of CYL adsorption by the WPC (coconut)

Table A.22 Equilibrium carbon loading data for CYL adsorption by WPC (coconut) in ultrapure water

Sample	Carbon dose (mg/L)	Equilibrium toxin concentration (µg/L)	Equilibrium Capacity, qe (µg/mg)
1	49.8	0.05	2.2
2	42.2	0.09	2.6
3	35.8	0.35	3.0
4	30.2	1.00	3.6
5	24.0	1.87	4.5
6	18.2	4.49	5.7
7	11.6	12.65	8.3
8	5.0	43.15	13.2

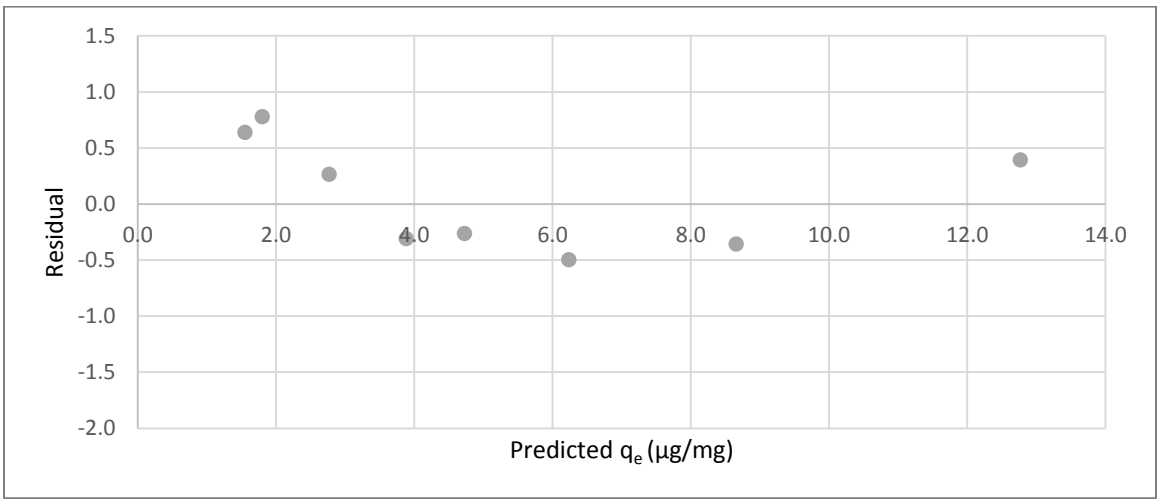

Figure A.29 Residual plot for equilibrium isotherm of CYL adsorption by the WPC (coconut)

Table A.23 0.5 h carbon loading data for MC-LR adsorption by COL-PL60-800 (coal) in ultrapure water

Sample	Carbon dose (mg/L)	Equilibrium toxin concentration (µg/L)	Equilibrium Capacity, qe (µg/mg)
1	50.2	33.35	1.4
2	42.0	37.62	1.6
3	36.0	42.98	1.7
4	30.4	50.09	1.8
5	24.0	54.08	2.1
6	18.2	62.32	2.3
7	12.2	73.12	2.6

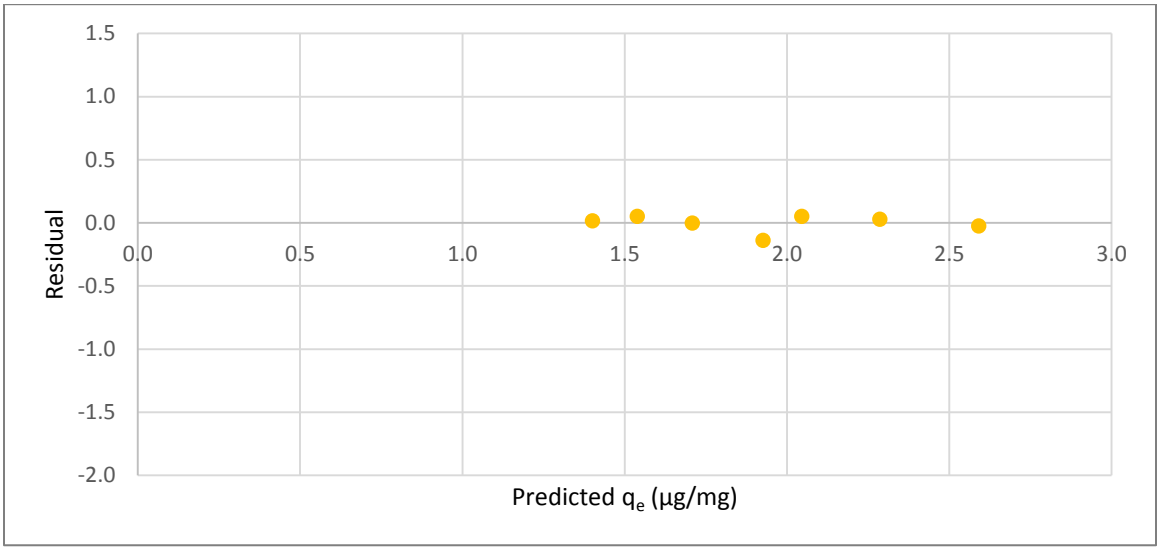

Figure A.30 Residual plot for 0.5 h isotherm of MC-LR adsorption by the COL-PL60-800 (coal)

Table A.24 1.0 h carbon loading data for MC-LR adsorption by COL-PL60-800 (coal) in ultrapure water

Sample	Carbon dose (mg/L)	Equilibrium toxin concentration (µg/L)	Equilibrium Capacity, qe (µg/mg)
1	50.2	10.60	1.9
2	42.0	18.03	2.1
3	36.0	28.00	2.1
4	30.4	33.86	2.3
5	24.0	44.03	2.5
6	18.2	56.01	2.7
7	12.2	68.13	3.0

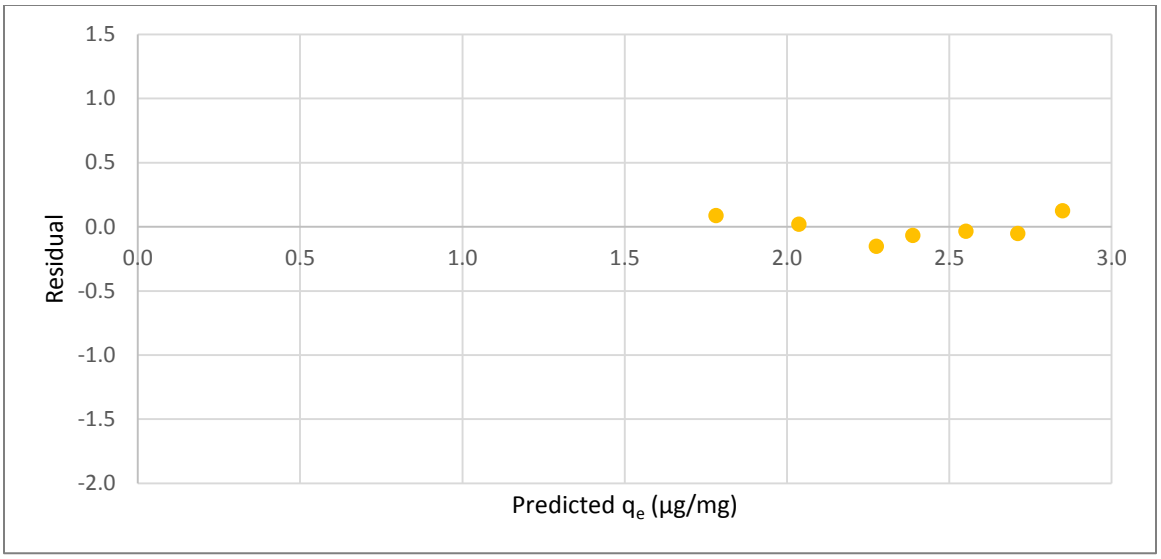

Figure A.31 Residual plot for 1.0 h isotherm of MC-LR adsorption by the COL-PL60-800 (coal)

Table A.25 Equilibrium carbon loading data for MC-LR adsorption by COL-PL60-800 (coal) in ultrapure water

Sample	Carbon dose (mg/L)	Equilibrium toxin concentration (µg/L)	Equilibrium Capacity, qe (µg/mg)
1	50.2	0.06	2.1
2	42.0	0.15	2.5
3	36.0	0.24	2.9
4	30.4	0.30	3.4
5	24.0	0.65	4.3
6	18.2	2.22	5.6
7	12.2	10.30	7.7

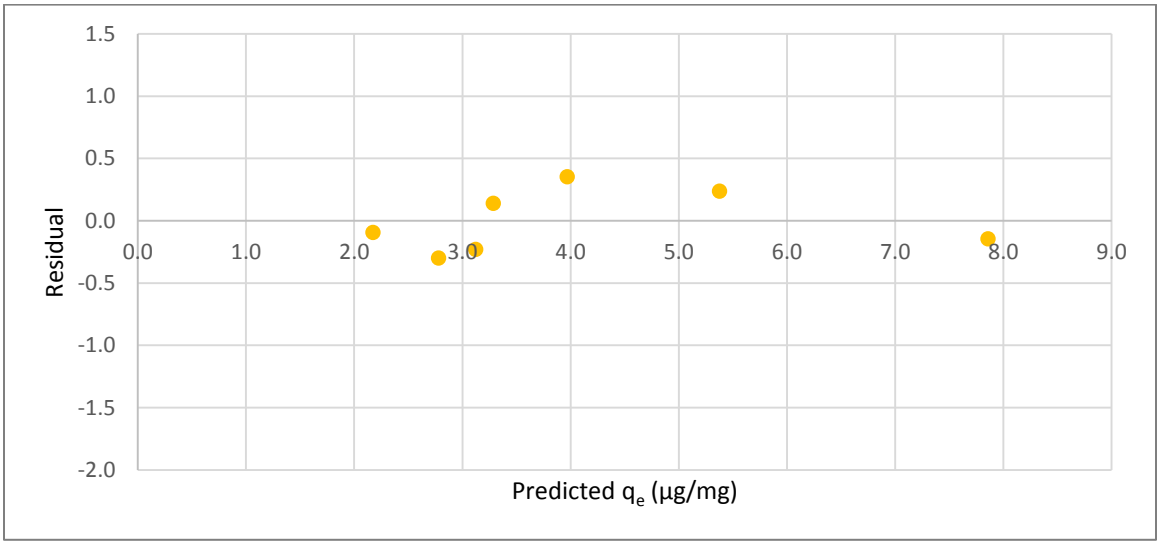

Figure A.32 Residual plot for equilibrium isotherm of MC-LR adsorption by the COL-PL60-800 (coal)

Table A.26 0.5 h carbon loading data for MC-LR adsorption by BG-HHM (wood) in ultrapure water

Sample	Carbon dose (mg/L)	Equilibrium toxin concentration (µg/L)	Equilibrium Capacity, qe (µg/mg)
1	50.4	1.27	2.0
2	42.0	1.77	2.4
3	36.0	3.14	2.8
4	30.2	5.08	3.3
5	24.0	8.59	4.0
6	18.0	22.20	4.6
7	11.8	45.23	5.0

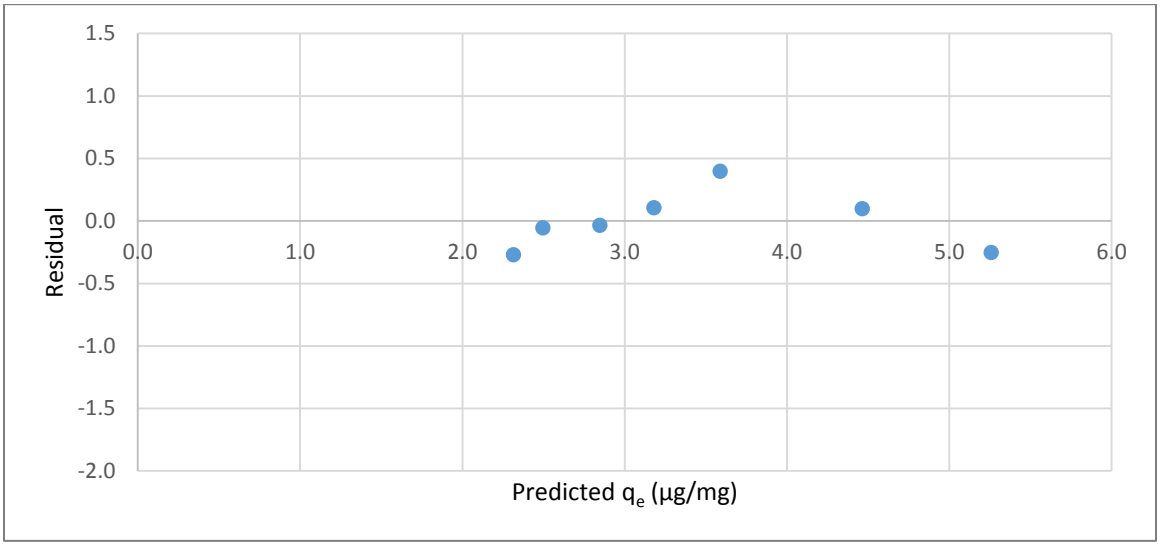

Figure A.33 Residual plot for 0.5 h isotherm of MC-LR adsorption by the BG-HHM (wood)

Table A.27 1.0 h carbon loading data for MC-LR adsorption by BG-HHM (wood) in ultrapure water

Sample	Carbon dose (mg/L)	Equilibrium toxin concentration (µg/L)	Equilibrium Capacity, qe (µg/mg)
1	50.4	0.09	2.1
2	42.0	0.33	2.5
3	36.0	0.68	2.9
4	30.2	2.08	3.4
5	24.0	3.25	4.2
6	18.0	16.41	4.9
7	11.8	40.73	5.4

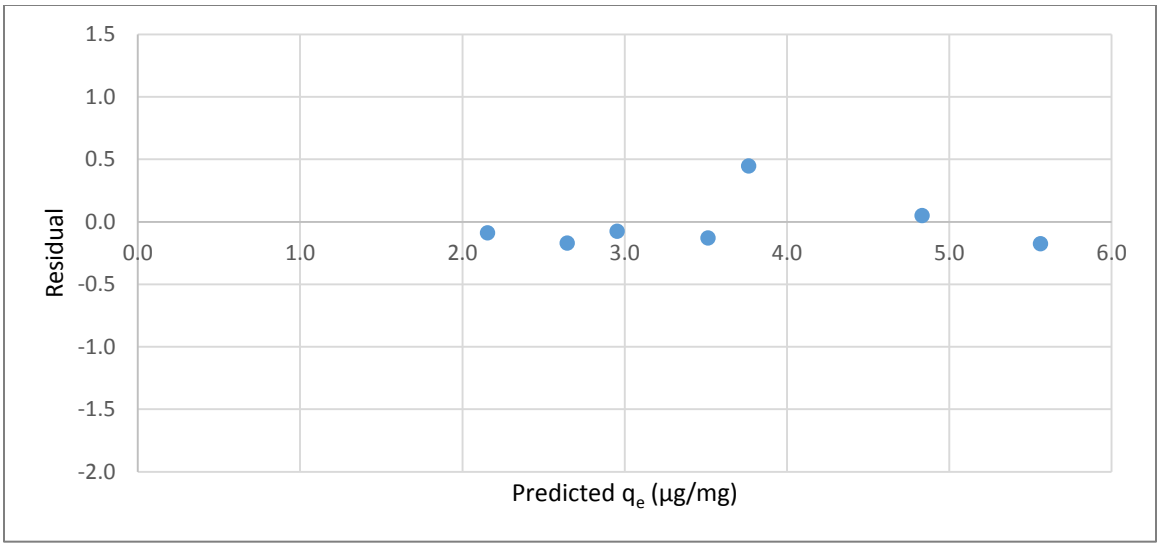

Figure A.34 Residual plot for 1.0 h isotherm of MC-LR adsorption by the BG-HHM (wood)

Table A.28 Equilibrium carbon loading data for MC-LR adsorption by BG-HHM (wood) in ultrapure water

Sample	Carbon dose (mg/L)	Equilibrium toxin concentration (µg/L)	Equilibrium Capacity, qe (µg/mg)
1	50.4	0.09	2.1
2	42.0	0.33	2.5
3	36.0	0.68	2.9
4	30.2	2.08	3.4
5	24.0	3.25	4.2
6	18.0	16.41	4.9
7	11.8	40.73	5.4

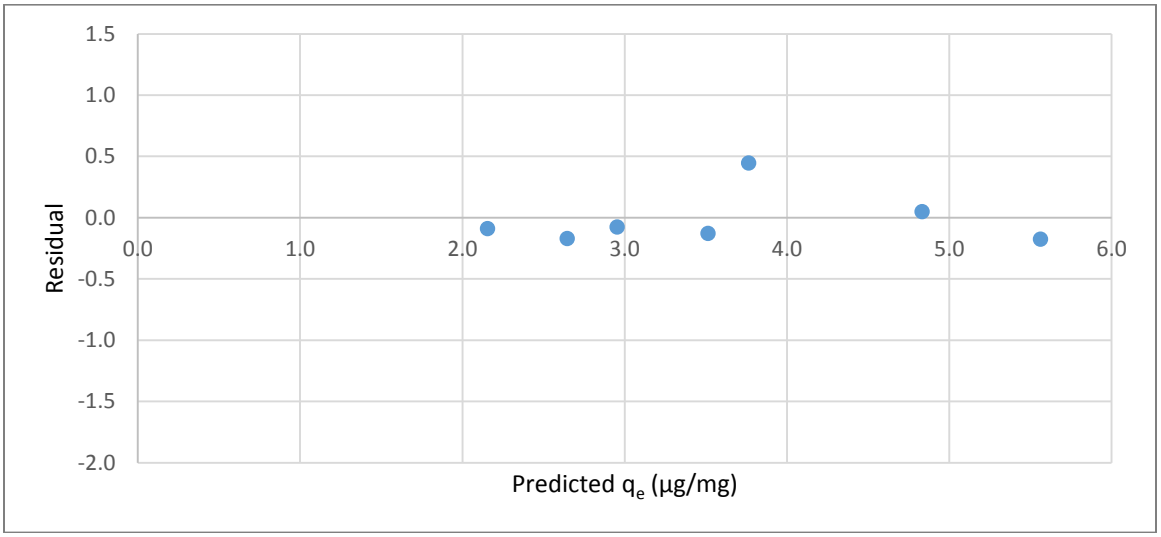

Figure A.35 Residual plot for equilibrium isotherm of MC-LR adsorption by the BG-HHM (wood)

Table A.29 0.5 h carbon loading data for MC-LR adsorption by WPC (coconut) in ultrapure water

Sample	Carbon dose (mg/L)	Equilibrium toxin concentration (µg/L)	Equilibrium Capacity, qe (µg/mg)
1	50.2	16.52	1.7
2	41.6	24.94	1.9
3	36.0	30.87	2.0
4	30.0	40.30	2.1
5	23.6	49.34	2.2
6	18.2	59.14	2.4
7	12.0	70.39	2.7

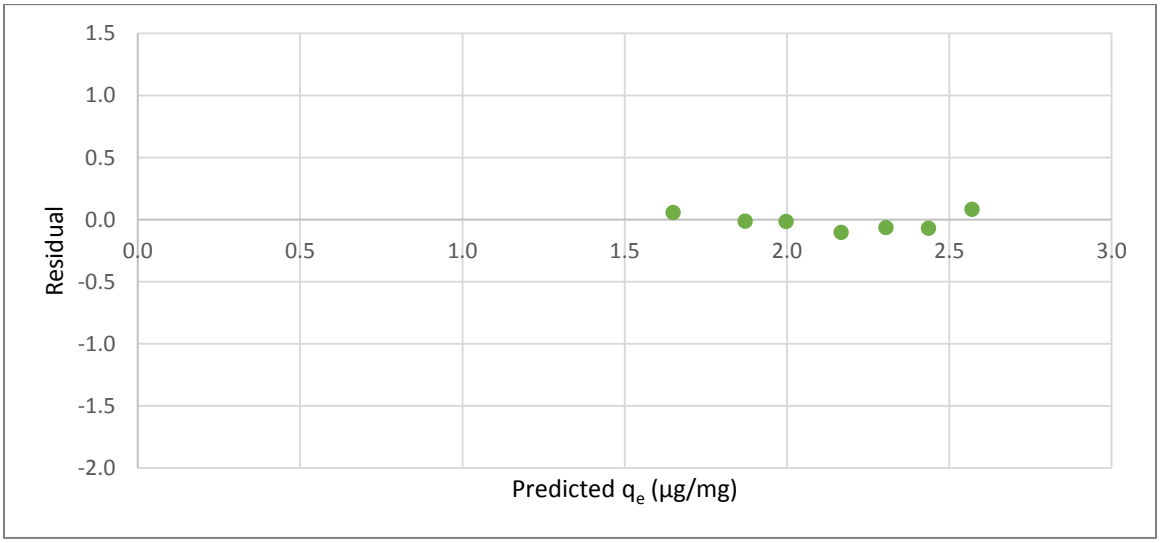

Figure A.36 Residual plot for 0.5 h isotherm of MC-LR adsorption by the WPC (coconut)

Table A.30 1.0 h carbon loading data for MC-LR adsorption by WPC (coconut) in ultrapure water

Sample	Carbon dose (mg/L)	Equilibrium toxin concentration (µg/L)	Equilibrium Capacity, qe (µg/mg)
1	50.2	10.33	1.8
2	41.6	21.03	2.0
3	36.0	28.11	2.1
4	30.0	35.68	2.2
5	23.6	42.99	2.5
6	18.2	52.99	2.7
7	12.0	68.80	2.8

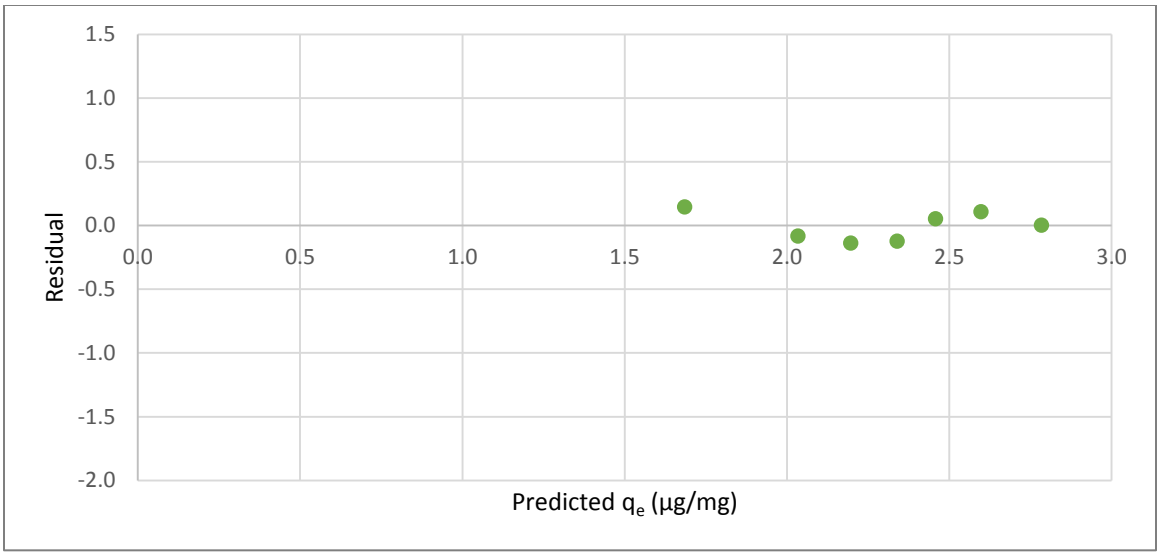

Figure A.37 Residual plot for 1.0 h isotherm of MC-LR adsorption by the WPC (coconut)

Table A.31 Equilibrium carbon loading data for MC-LR adsorption by WPC (coconut) in ultrapure water

Sample	Carbon dose (mg/L)	Equilibrium toxin concentration (µg/L)	Equilibrium Capacity, qe (µg/mg)
1	50.2	0.10	2.0
2	41.6	0.13	2.5
3	36.0	0.50	2.8
4	30.0	0.70	3.4
5	23.6	1.32	4.3
6	18.2	5.35	5.3
7	12.0	18.27	7.0

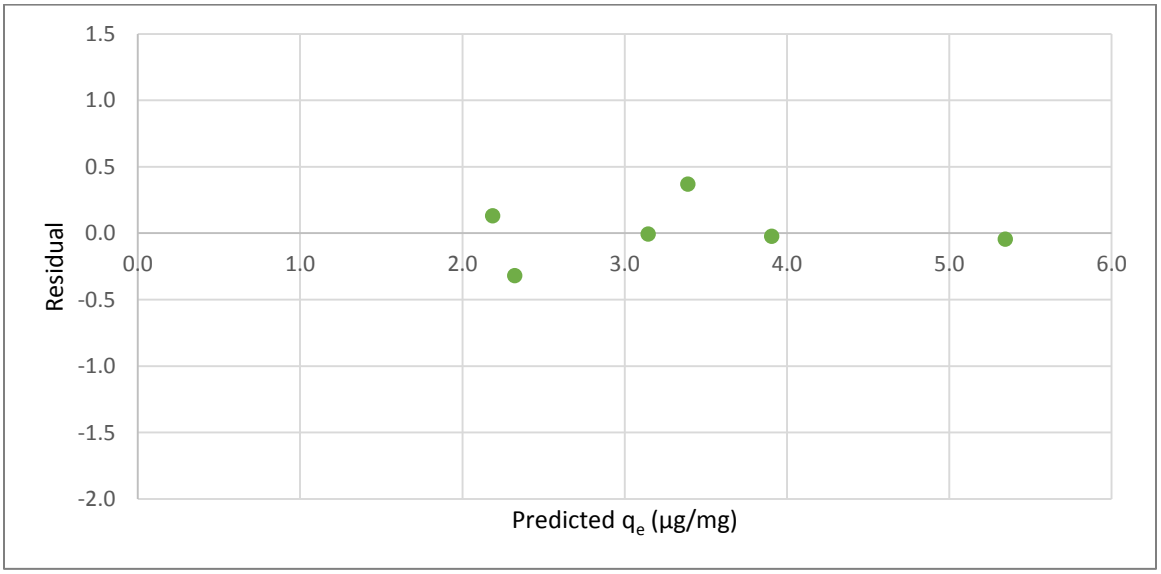

Figure A.38 Residual plot for equilibrium isotherm of MC-LR adsorption by the WPC (coconut)

Table A.32 0.5 h carbon loading data for ANTA adsorption by COL-PL60-800 (coal) in ultrapure water

Sample	Carbon dose (mg/L)	Equilibrium toxin concentration (µg/L)	Equilibrium Capacity, qe (µg/mg)
1	50.0	17.95	1.7
2	42.2	19.45	2.0
3	35.6	20.40	2.3
4	29.8	20.99	2.7
5	24.0	22.36	3.3
6	18.0	24.82	4.3
7	12.2	26.45	6.2
8	5.0	33.74	13.6

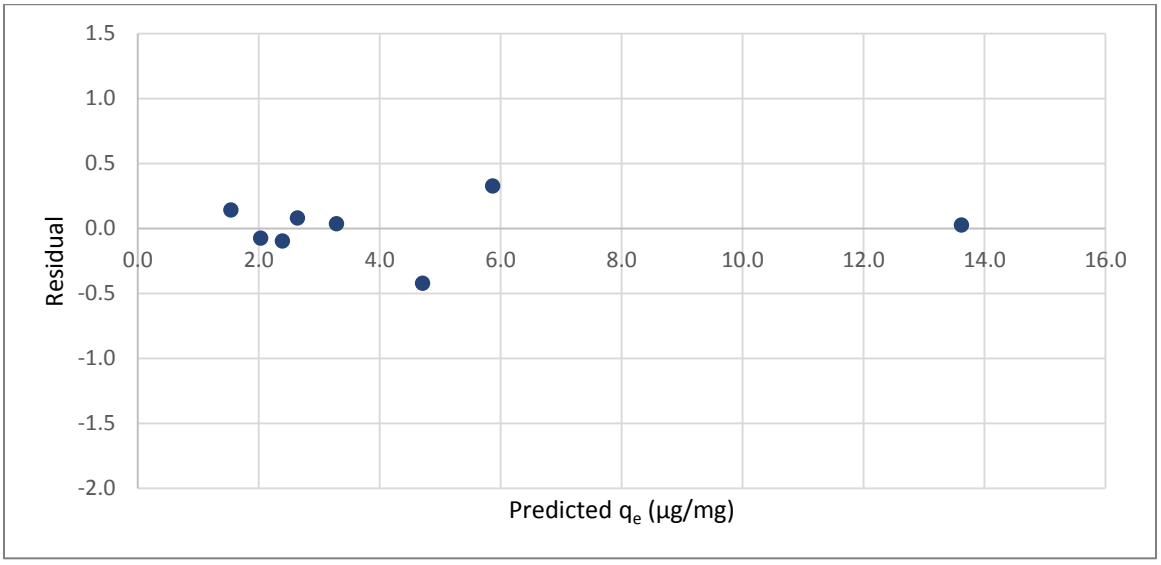

Figure A.39 Residual plot for 0.5 h isotherm of ANTA adsorption by the COL-PL60-800 (coal)

Table A.33 1.0 h carbon loading data for ANTA adsorption by COL-PL60-800 (coal) in ultrapure water

Sample	Carbon dose (mg/L)	Equilibrium toxin concentration (µg/L)	Equilibrium Capacity, qe (µg/mg)
1	50.0	16.42	1.7
2	42.2	18.65	2.0
3	35.6	19.39	2.3
4	29.8	19.98	2.8
5	24.0	21.84	3.3
6	18.0	22.45	4.4
7	12.2	25.13	6.3
8	5.0	29.53	14.5

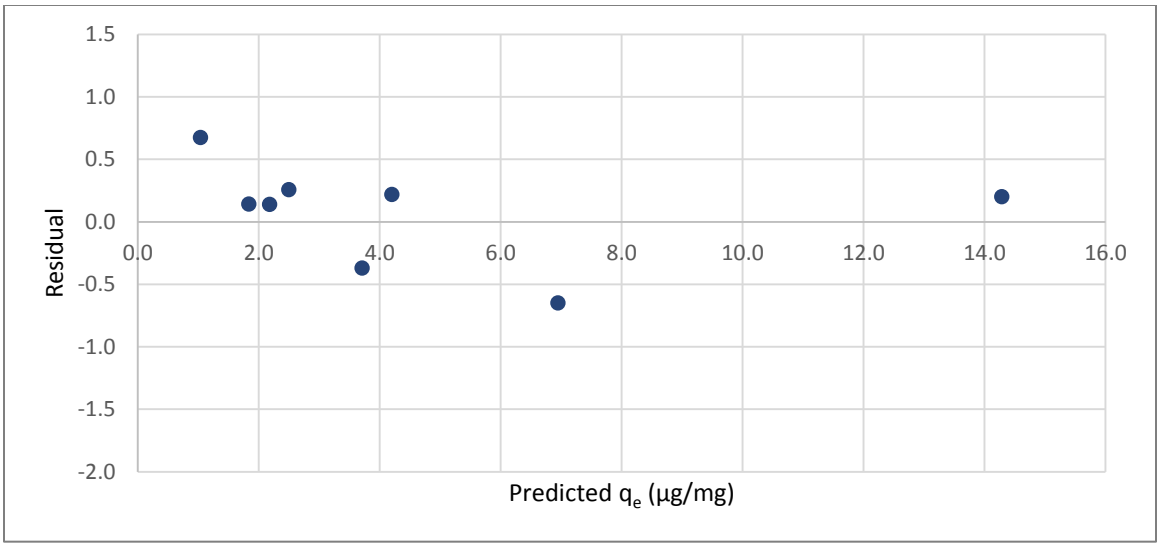

Figure A.40 Residual plot for 1.0 h isotherm of ANTA adsorption by the COL-PL60-800 (coal)

Table A.34 Equilibrium carbon loading data for ANTA adsorption by COL-PL60-800 (coal) in ultrapure water

Sample	Carbon dose (mg/L)	Equilibrium toxin concentration (µg/L)	Equilibrium Capacity, qe (µg/mg)
1	50.0	0.93	2.0
2	42.2	1.27	2.4
3	35.6	1.49	2.8
4	29.8	1.59	3.4
5	24.0	1.80	4.2
6	18.0	2.33	5.5
7	12.2	3.64	8.1
8	5.0	5.55	19.3

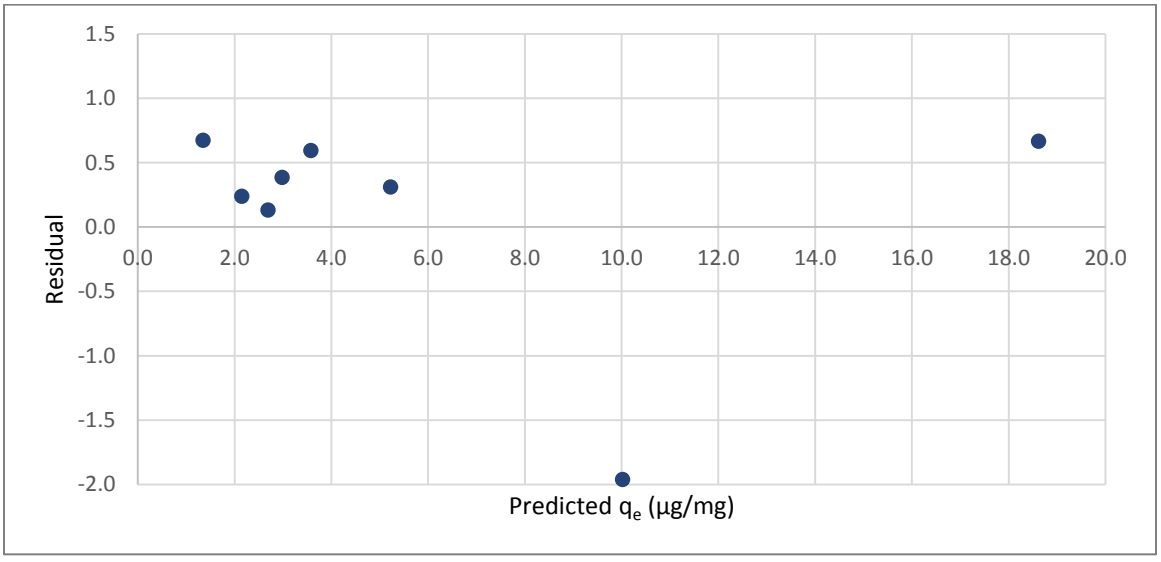

Figure A.41 Residual plot for equilibrium isotherm of ANTA adsorption by the COL-PL60-800 (coal)

Table A.35 0.5 h carbon loading data for ANTA adsorption by BG-HHM (wood) in ultrapure water

Sample	Carbon dose (mg/L)	Equilibrium toxin concentration (µg/L)	Equilibrium Capacity, qe (µg/mg)
1	50.0	32.60	1.5
2	42.4	39.14	1.7
3	36.2	44.52	1.8
4	29.8	51.13	2.0
5	24.0	58.16	2.1
6	17.8	66.87	2.4
7	12.0	76.10	2.8
8	5.0	92.68	3.3

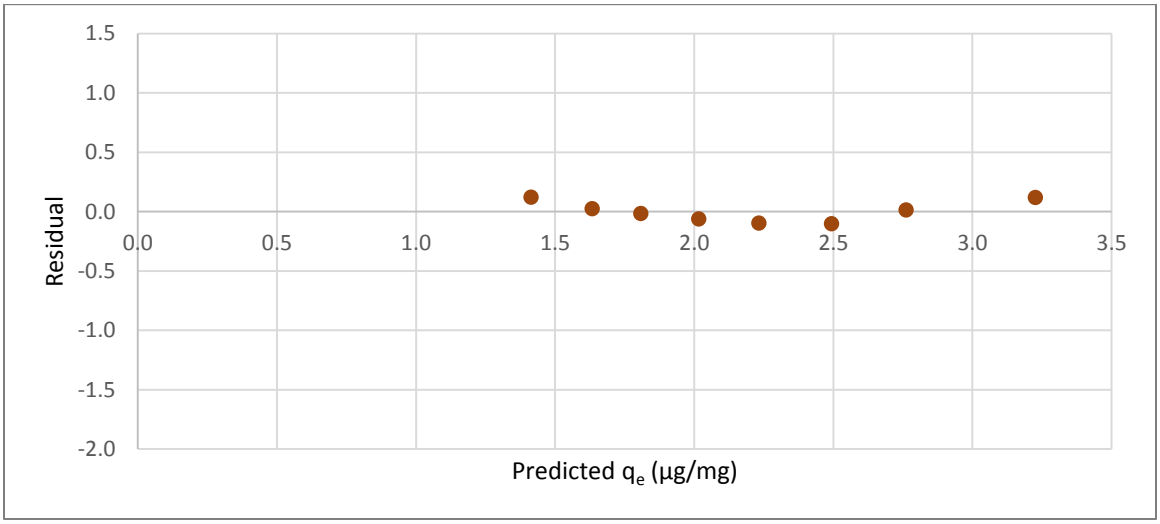

Figure A.42 Residual plot for 0.5 h isotherm of ANTA adsorption by the BG-HHM (wood)

Table A.36 1.0 h carbon loading data for ANTA adsorption by BG-HHM (wood) in ultrapure water

Sample	Carbon dose (mg/L)	Equilibrium toxin concentration (µg/L)	Equilibrium Capacity, qe (µg/mg)
1	50.0	25.23	1.7
2	42.4	30.77	1.9
3	36.2	36.36	2.0
4	29.8	44.47	2.2
5	24.0	51.65	2.4
6	17.8	61.34	2.7
7	12.0	73.90	3.0
8	5.0	91.87	3.5

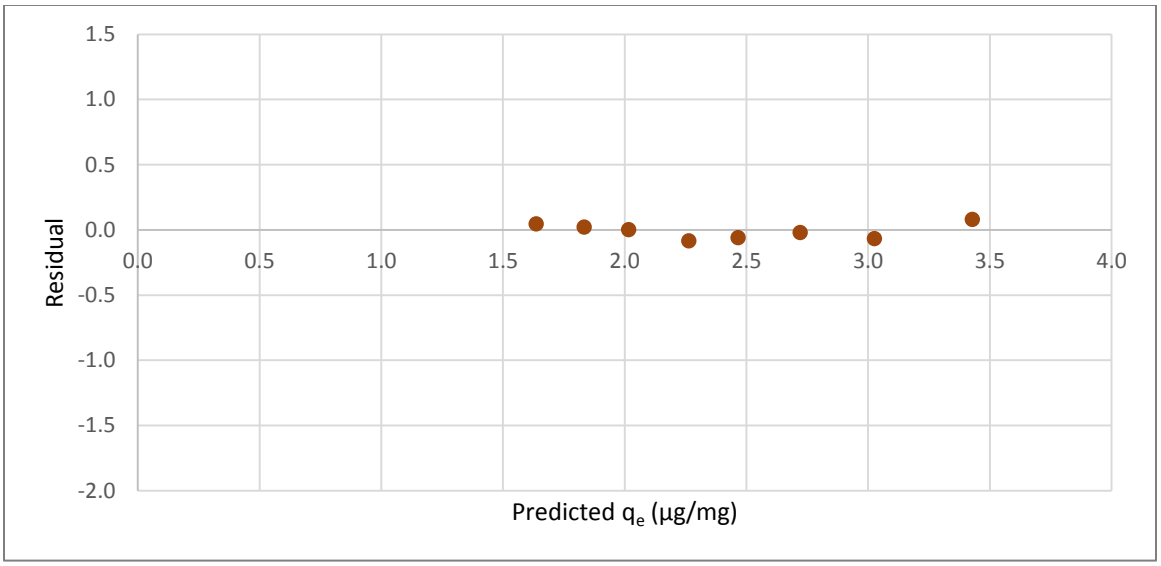

Figure A.43 Residual plot for 1.0 h isotherm of ANTA adsorption by the BG-HHM (wood)

Table A.37 Equilibrium carbon loading data for ANTA adsorption by BG-HHM (wood) in ultrapure water

Sample	Carbon dose (mg/L)	Equilibrium toxin concentration (µg/L)	Equilibrium Capacity, qe (µg/mg)
1	50.0	5.70	2.1
2	42.4	7.63	2.4
3	36.2	11.16	2.7
4	29.8	14.38	3.2
5	24.0	19.77	3.7
6	17.8	24.67	4.8
7	12.0	42.06	5.6
8	5.0	73.52	7.2

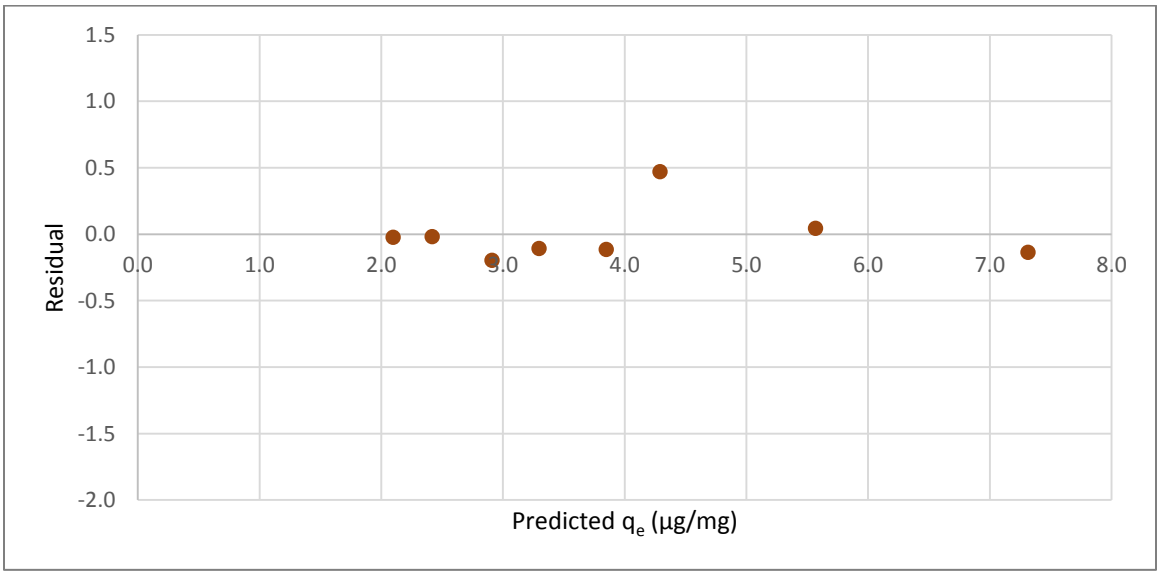

Figure A.44 Residual plot for equilibrium isotherm of ANTA adsorption by the BG-HHM (wood)

Table A.38 0.5 h carbon loading data for ANTA adsorption by WPC (coconut) in ultrapure water

Sample	Carbon dose (mg/L)	Equilibrium toxin concentration (µg/L)	Equilibrium Capacity, qe (µg/mg)
1	50.2	15.53	1.9
2	41.8	17.14	2.2
3	36.0	17.70	2.5
4	29.8	19.32	3.0
5	24.0	19.12	3.8
6	17.8	21.95	4.9
7	12.0	23.43	7.2
8	4.8	27.18	17.1

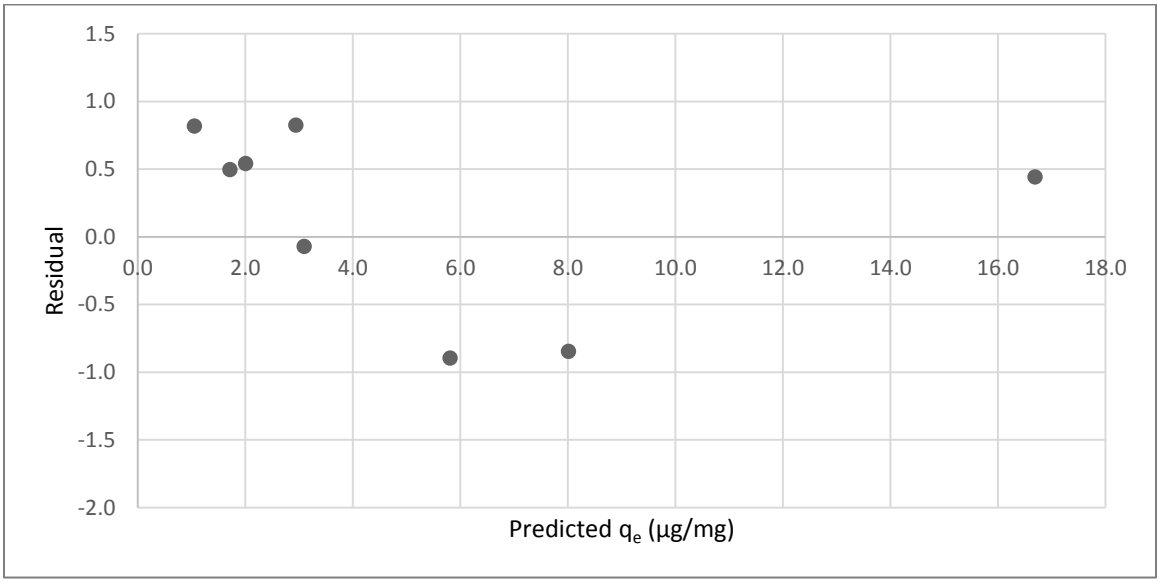

Figure A.45 Residual plot for 0.5 h isotherm of ANTA adsorption by the WPC (coconut)

Table A.39 1.0 h carbon loading data for ANTA adsorption by WPC (coconut) in ultrapure water

Sample	Carbon dose (mg/L)	Equilibrium toxin concentration (µg/L)	Equilibrium Capacity, qe (µg/mg)
1	50.2	14.37	1.9
2	41.8	16.17	2.2
3	36.0	15.72	2.6
4	29.8	16.89	3.1
5	24.0	18.39	3.8
6	17.8	19.32	5.1
7	12.0	21.13	7.4
8	4.8	25.97	17.4

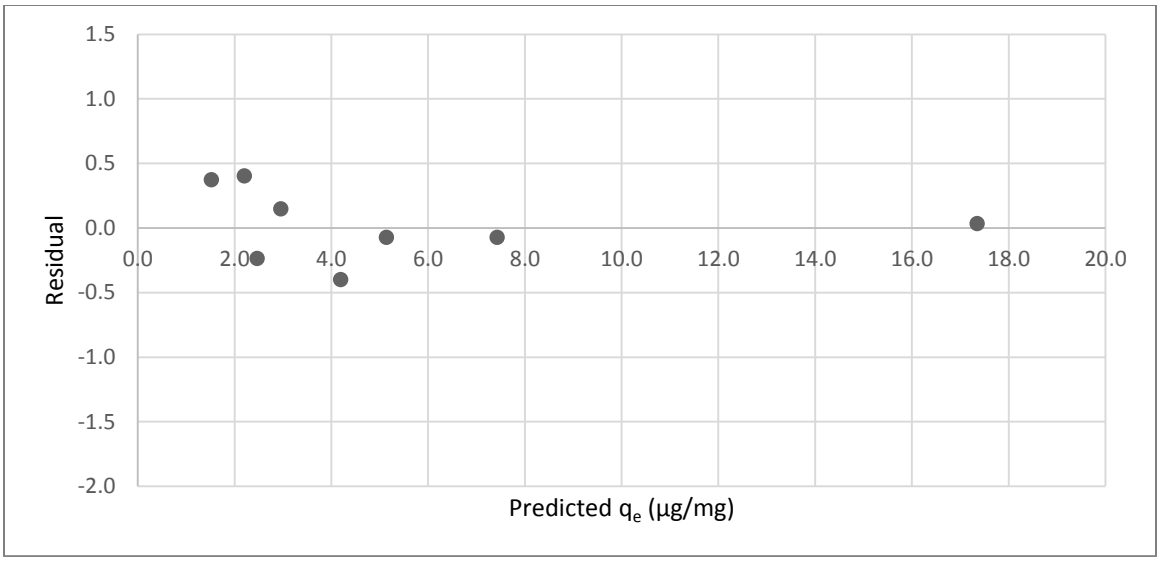

Figure A.46 Residual plot for 1.0 h isotherm of ANTA adsorption by the WPC (coconut)

Table A.40 Equilibrium carbon loading data for ANTA adsorption by WPC (coconut) in ultrapure water

Sample	Carbon dose (mg/L)	Equilibrium toxin concentration (µg/L)	Equilibrium Capacity, qe (µg/mg)
1	50.2	0.99	2.2
2	41.8	1.03	2.6
3	36.0	1.04	3.0
4	29.8	1.12	3.6
5	24.0	1.22	4.5
6	17.8	1.38	6.1
7	12.0	1.64	9.0
8	4.8	3.03	22.2

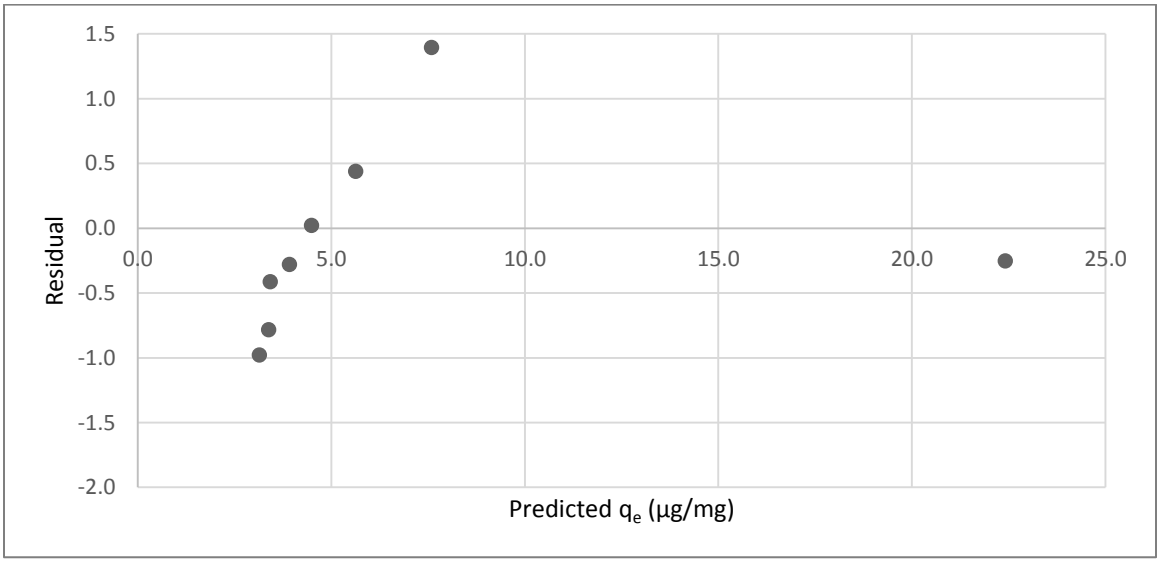

Figure A.47 Residual plot for equilibrium isotherm of ANTA adsorption by the WPC (coconut)

Table A.41 Freundlich 0.5-h non-equilibrium isotherm parameters for PAC adsorption in ultrapure water

Cyanotoxin	PAC	Number of Samples	K_F	1/n
CYL	COL-PL60-800 (coal)	8	0.28 (0.17,0.40)	0.60 (0.52,0.73)
CYL	BG-HHM (wood)	8	1.50 (1.16,1.85)	0.36 (0.30,0.43)
CYL	WPC (coconut)	8	1.20 (0.93,1.48)	0.32 (0.26,0.38)
MC-LR	COL-PL60-800 (coal)	7	0.09 (0.03,0.15)	0.78 (0.66,1.01)
MC-LR	BG-HHM (wood)	7	2.19 (1.75,2.64)	0.23 (0.16,0.31)
MC-LR	WPC (coconut)	7	0.70 (0.42,0.98)	0.31 (0.22,0.43)
ANTA	COL-PL60-800 (coal)	8	0.0000709 (0.000014,0.000132)	3.46 (3.29,3.82)
ANTA	BG-HHM (wood)	8	0.40 (0.20,0.61)	0.40 (0.30,0.55)
ANTA	WPC (coconut)	8	0.00000138 (-0.00000216,0.00000566)	4.94 (4.64,8.38)

Table A.42 Freundlich 1-h non-equilibrium isotherm parameters for PAC adsorption in ultrapure water

Cyanotoxin	PAC	Number of Sample	Kf	1/n
CYL	COL-PL60-800 (coal)	8	0.85 (0.49,1.23)	0.43 (0.33,0.57)
CYL	BG-HHM (wood)	8	1.82 (0.89,2.99)	0.51 (0.36,0.71)
CYL	WPC (coconut)	8	1.63 (1.24,2.05)	0.44 (0.38,0.52)
MC-LR	COL-PL60-800 (coal)	7	0.98 (0.51,1.41)	0.25 (0.16,0.39)
MC-LR	BG-HHM (wood)	7	3.14 (2.84,3.45)	0.15 (0.12,0.19)
MC-LR	WPC (coconut)	7	0.91 (0.58,1.26)	0.26 (0.18,0.38)
ANTA	COL-PL60-800 (coal)	8	0.00000387 (-0.0000037,0.0000115)	4.47 (4.21,6.31)
ANTA	BG-HHM (wood)	8	0.53 (0.26,0.82)	0.34 (0.24,0.51)
ANTA	WPC (coconut)	8	0.0000261 (0.0000016,0.0000508)	4.12 (3.92,4.61)

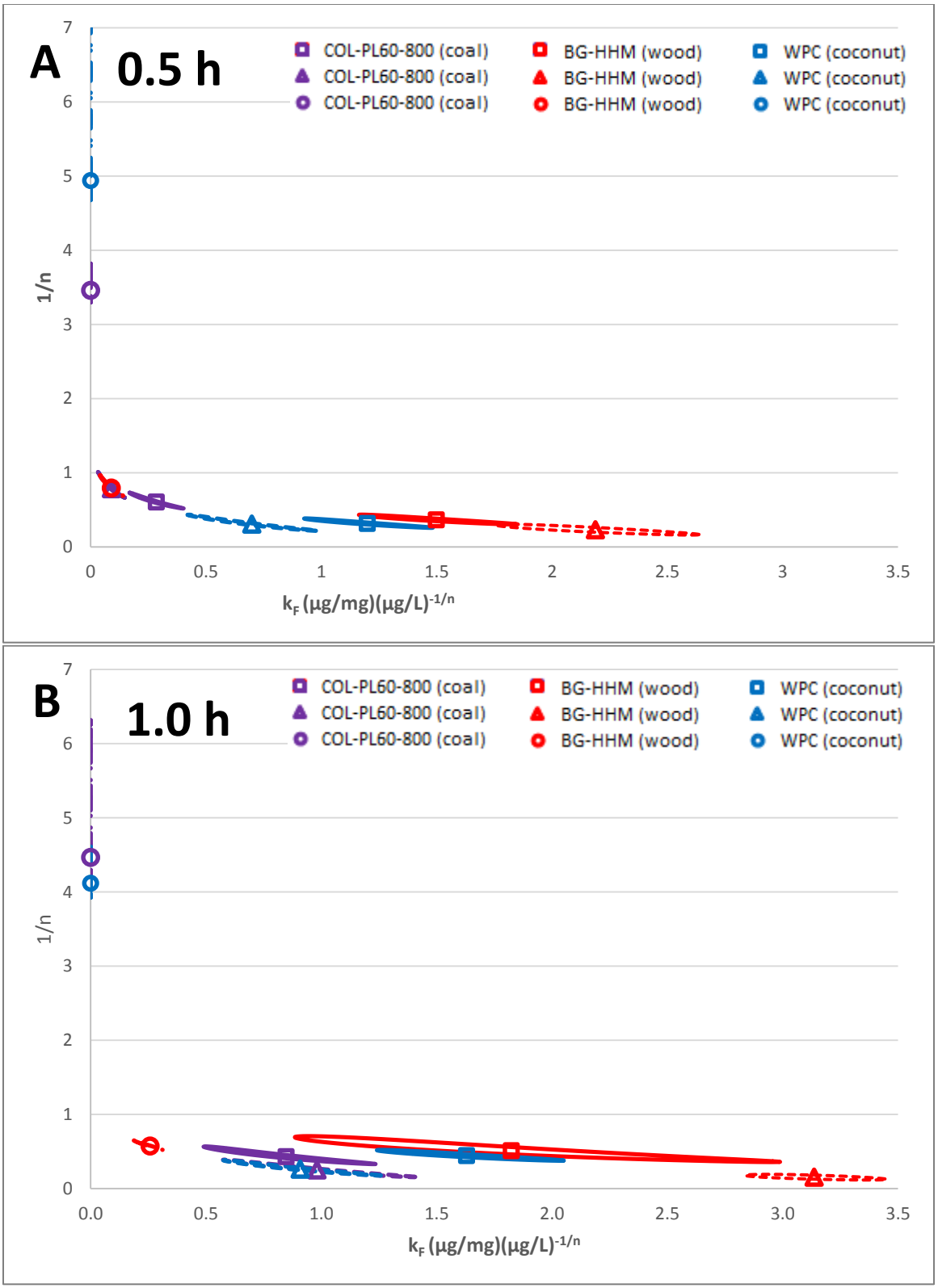

Figure A.48 95% joint confidence regions (ellipse in figures) and point of estimates (points in figures) for the Freundlich parameters of non-equilibrium isotherms generated with the adsorption of CYL, MC-LR and ANTA using the selected PACs in ultrapure water. A) 0.5 h, B) 1 h.

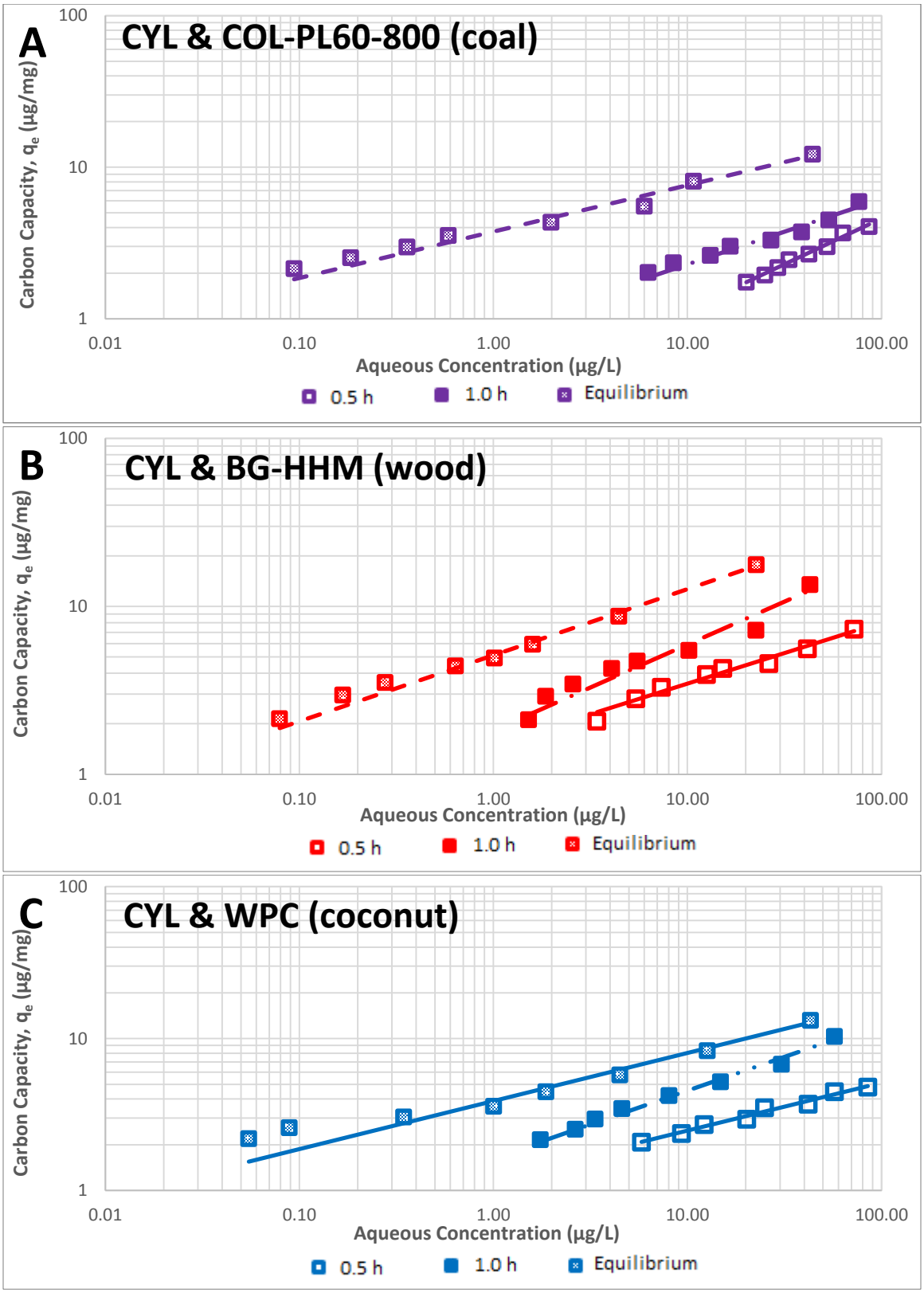

Figure A.49 Freundlich model plot demonstrating PAC adsorption of CYL at contact time of 0.5 h, 1 h and equilibrium (straight lines showing Freundlich fitting curves and symbols showing experimental data). A) Coal-based PAC; B) wood-based PAC; C) coconut-based PAC.

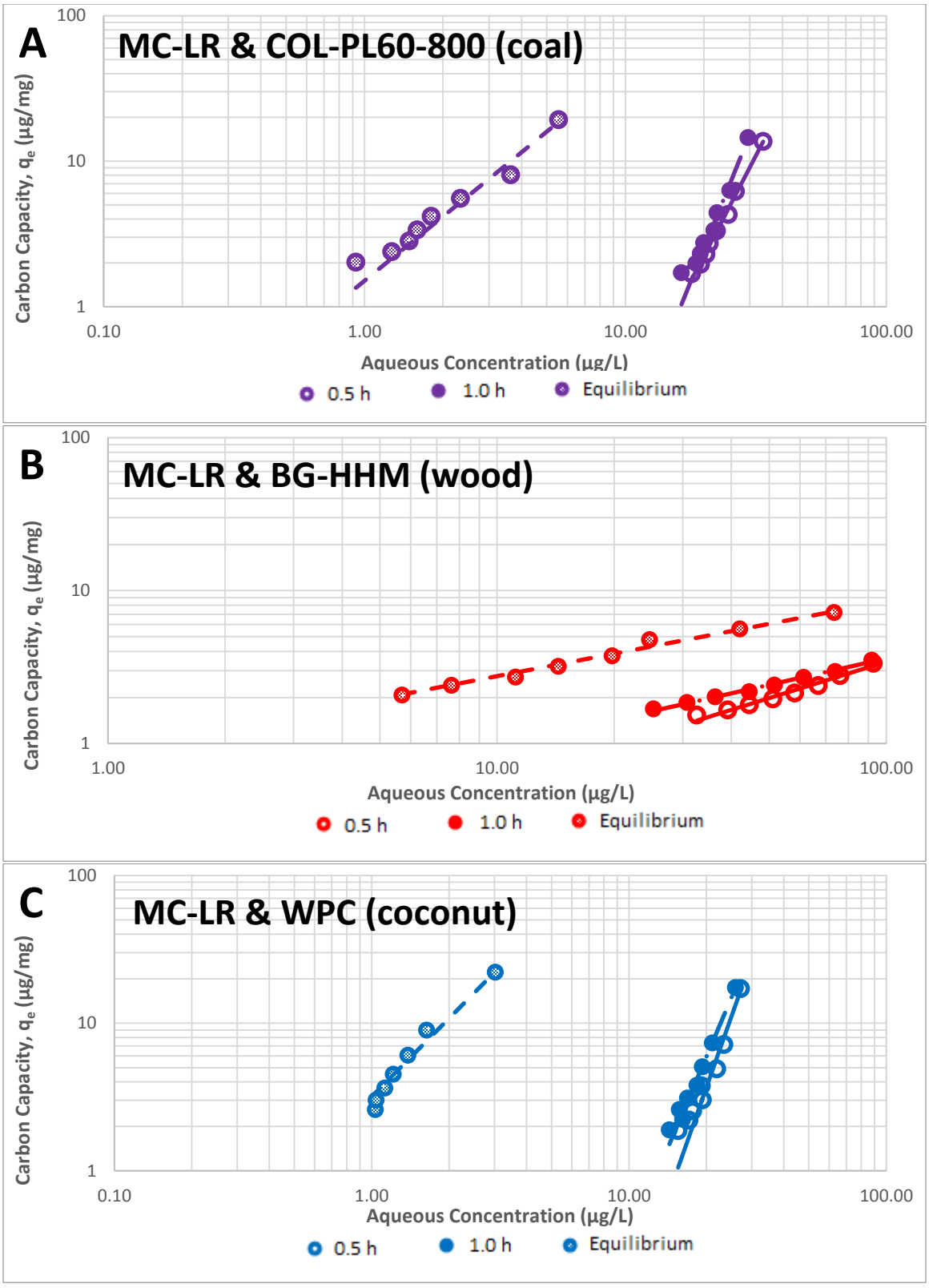

Figure A.50 Freundlich model plot demonstrating PAC adsorption of ANTA at contact time of 0.5 h, 1 h and equilibrium (straight lines showing Freundlich fitting curves and symbols showing experimental data). A) Coal-based PAC; B) wood-based PAC; C) coconut-based PAC.

Appendix A.5 MatLAB Code for JCRs

```
%JCR Plot Program
% this program is to plot the joint confidence region of the estimated
% parameters based on Freundlich model.
% input augments Ce, qe, kf, nrev
% ========================================================================
% program written by Y.Liu
% last modification Oct. 10, 2016
% ========================================================================
function jcrplot(Ce,qe, kf, nrev)
% Ce = independent variables
% qe = dependent variables
% kf = starting value of kf
% nrev = starting value of 1/n
clear
clc
Ce = input('input independent variables');
qe = input('input dependent variables');
kf = input('input starting value of kf');
nrev = input('input starting value of 1/n');

% calculate point of estimate for (Ce,kf)
kf1= 0;
nrev1 = 0;
w = qe - kf .* Ce.^nrev;
S = w'*w;
S1 = 0;
p = 2;
n = length(Ce);
   while or(or(abs(kf-kf1)>0.00001, abs(nrev-nrev1)>0.00001), abs(S-S1) >0.00001)
      pdkf = Ce.^nrev;
```

```
    pdCe = kf .* Ce.^nrev .* log(Ce);
    X = [pdkf, pdCe];
    w = qe - kf .* Ce.^nrev;
    theta = [kf,nrev] + (inv(X' * X) * X' * w)';
    kf1 = kf;
    kf = theta(1);
    nrev1 = nrev;
    nrev = theta(2);
    S1 = S;
    S = w'*w;
  end

% convert X to full matrix
X=full(X);

% calculate variance covariance matrix for parameters
vcm = inv(X'*X).* S./(n-p);

% calculate standard error of parameters
ss = sqrt(diag(vcm));

kf
nrev

% plot joint confidence regions of kf and 1/n
f = finv(0.95,2,n);
bdry = S*(1 + p/(n-p)*f);

% calculate equally spaced plotting values for the estimated parameters
r1 = 10 * ss(1);
r2 = 10 * ss(2);
```

```
b1s = [linspace((kf-r1),(kf+r1),200)];
b2s = [linspace((nrev-r2),(nrev+r2),200)];

% calculate ss matrix
k = 0;
for ba = b1s
   k = k+1;
   j = 0;
    for bb = b2s;
       j = j+1;
       a(k,j) = (qe - ba.*Ce.^bb)' * (qe - ba.*Ce.^bb);
    end
end

% plot contour as joint confidence region
JCR = contour(b1s,b2s,a,[bdry,bdry],'-b')'

% identify 95% confidence interval of each parameter
CI_kf = [min(JCR(2:end,1)),max(JCR(2:end,1))]
CI_nrev = [min(JCR(2:end,2)),max(JCR(2:end,2))]

hold on

plot(kf, nrev,'*r');

hold off

% calcluate SSE, SSR, and SST
SSR = sum((kf*Ce.^nrev - mean(qe)).^2)
SSE = sum((qe - kf*Ce.^nrev).^2)
SST = sum((qe - mean(qe)).^2)
```

SSR_SSE = SST + SSE

R2 = 1 - SSE/SST

Appendix B

Supplementary Material for Chapter 4

Appendix B.1 Rate of Adsorption in Natural Water

Table B.1 CYL adsorption rate data determined with COL-PL60-800 (coal) in natural water

Time (h)	IS-Area Count	CYL-Area Count	Response Ratio	Concentration (µg/L)
0.1	401879	415168	1.03	225.1
0.25	353776	168298	0.48	101.3
0.5	385610	173196	0.45	95.4
0.75	349728	106749	0.31	63.4
1	512778	167033	0.33	67.9
1.25	420479	65817	0.16	30.3
1.5	379557	54667	0.14	27.6
1.75	382713	51155	0.13	25.3
2	538009	64767	0.12	22.3
6	395230	13405	0.03	3.1
25.5	471531	13224	0.03	1.8

Table B.2 CYL adsorption rate data determined with BG-HHM (wood) in natural water

Time (h)	IS-Area Count	CYL-Area Count	Response Ratio	Concentration (µg/L)
0.1	600324.5	289536	0.48	102.7
0.25	546625	35807	0.07	10.1
0.5	536178	20346	0.04	4.0
0.75	430403.5	15994	0.04	3.8
1	394582	14203	0.04	3.6
1.25	376644.5	12213	0.03	2.8
1.5	225784	9359	0.04	4.8
1.75	225149	9045	0.04	4.5
2	238678.5	8763	0.04	3.7
6	264671.5	6726	0.03	1.2
25.5	497890.5	11245	0.02	0.6

Table B.3 CYL adsorption rate data determined with WPC (coconut) in natural water

Time (h)	IS-Area Count	CYL-Area Count	Response Ratio	Concentration (µg/L)
0.1	543405	249644	0.46	97.6
0.25	557267	151400	0.27	55.9
0.5	454901	92380	0.20	40.7
0.75	578198	85497	0.15	28.4
1	542660	83532	0.15	29.8
1.25	571263	55647	0.10	17.2
1.5	485856	46805	0.10	17.0
1.75	499759	44161	0.09	15.2
2	651399	47932	0.07	11.9
6	645272	17461	0.03	1.6
25.5	845356	20082	0.02	0.8

Table B.4 MC-LR adsorption rate data determined with COL-PL60-800 (coal) in natural water

Time (h)	IS-Area Count	CYL-Area Count	Response Ratio	Concentration (µg/L)
0.1	408140	257769	0.63	135.9
0.25	327584	151788	0.46	98.5
0.5	288494	119799	0.42	87.8
0.75	301877	99956	0.33	69.1
1	369881	114954	0.31	64.6
1.25	457255	85286	0.19	37.0
1.5	549178	78708	0.14	27.4
1.75	586276	63171	0.11	19.5
2	405737	36253	0.09	15.4
6	544973	13773	0.03	1.2
25.5	555514	13669	0.02	1.0

Table B.5 MC-LR adsorption rate data determined with BG-HHM (wood) in natural water

Time (h)	IS-Area Count	CYL-Area Count	Response Ratio	Concentration (µg/L)
0.1	489096	209778	0.43	90.9
0.25	463747	51739	0.11	20.3
0.5	481825	17420	0.04	3.6
0.75	502081	12668	0.03	1.2
1	522926	12938	0.02	1.1
1.25	427021	8751	0.02	0.1
1.5	508001.9048	10253	0.02	0.0

Table B.6 MC-LR adsorption rate data determined with WPC (coconut) in natural water

Time (h)	IS-Area Count	CYL-Area Count	Response Ratio	Concentration (µg/L)
0.1	630552	311574	0.49	105.4
0.25	586415	258908	0.44	93.7
0.5	546701	216214	0.40	83.4
0.75	511421	196737	0.38	81.0
1	457295	161508	0.35	74.0
1.25	487656	151558	0.31	64.6
1.5	530318	161599	0.30	63.3
1.75	489195	126298	0.26	52.9
2	440830	115044	0.26	53.5
6	577026	90864	0.16	30.5
25.5	564844	33528	0.06	8.7
48	467788	12771	0.03	1.6
72	508254	13592	0.03	1.5

Table B.7 ANTA adsorption rate data determined with COL-PL60-800 (coal) in natural water

Time (h)	IS-Area Count	CYL-Area Count	Response Ratio	Concentration (µg/L)
0.1	447246	2116307	4.73	174.6
0.25	455796	1380893	3.03	111.8
0.5	474204	1301011	2.74	101.3
0.75	452193	1115677	2.47	91.1
1	452852	1162949	2.57	94.8
1.25	452066	1098228	2.43	89.7
1.5	468795	1099523	2.35	86.6
1.75	459201	1012582	2.21	81.4
2	410267.8261	944246	2.30	85.0
6	433705.15	784529	1.81	66.8
25.5	356643	480340	1.35	49.7
48	317244.4	352967	1.11	41.1
72	296201.3043	235283	0.79	29.4
96	444398	282402	0.64	23.5
120	452292.381	213283	0.47	17.4
144	425255	144653	0.34	12.6
168	383959.0476	94372	0.25	9.1
221	457826	97767	0.21	7.9

Table B.8 ANTA adsorption rate data determined with BG-HHM (wood) in natural water

Time (h)	IS-Area Count	CYL-Area Count	Response Ratio	Concentration (µg/L)
0.1	467089	2092436	4.48	165.3
0.25	480521.3	1185882	2.47	91.1
0.5	482616	1179178	2.44	90.2
0.75	396828.3	895061	2.26	83.3
1	438516	931411	2.12	78.4
1.25	390679	633675	1.62	59.9
1.5	392290.8	616746	1.57	58.1
1.75	450107.6	685577	1.52	56.2
2	367285	548080	1.49	55.1
6	395344	241333	0.61	22.6
25.5	454577	206183	0.45	16.8
48	448346.4	112333	0.25	9.3
72	449703	96059	0.21	7.9
96	455667.8	53579	0.12	4.4
120	490652.8	48980	0.10	3.7

Table B.9 ANTA adsorption rate data determined with WPC (coconut) in natural water

Time (h)	IS-Area Count	CYL-Area Count	Response Ratio	Concentration (µg/L)
0.1	375205	2008915	5.35	197.6
0.25	463822	1107166	2.39	88.1
0.5	386372	900166	2.33	86.0
0.75	433982	600302	1.38	51.1
1	408516	559375	1.37	50.6
1.25	458186.4	625164	1.36	50.4
1.5	428554	580542	1.35	50.0
1.75	423084	570074	1.35	49.8
2	461729.8	496759	1.08	39.7
6	408612	262696	0.64	23.8
25.5	419939	151240	0.36	13.3
48	413741.9	67939	0.16	6.1
72	457095	68626	0.15	5.6

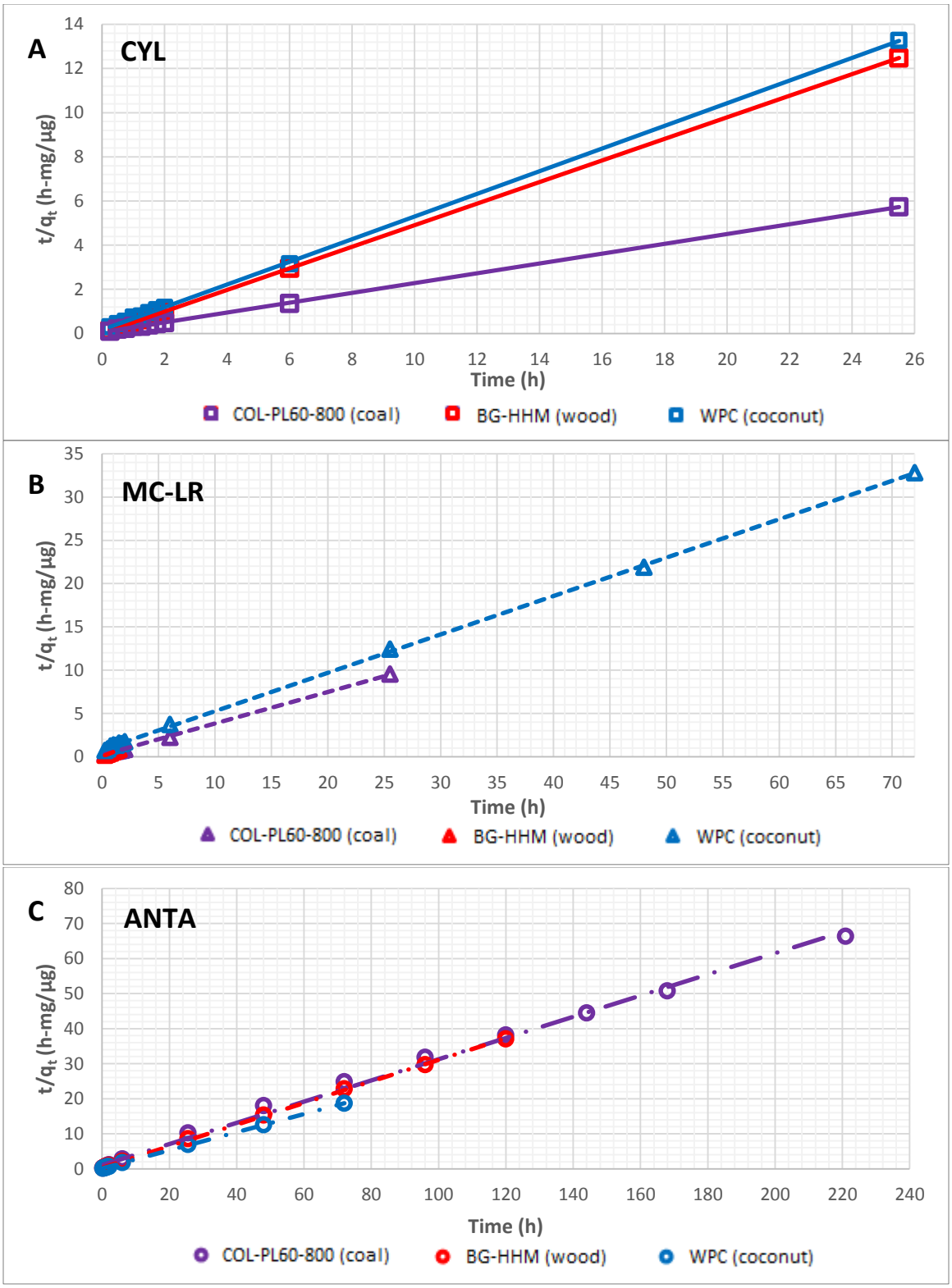

Figure B.1 Pseudo-second order kinetic model fits of CYL, MC-LR, and ANTA adsorption using coal-, wood-, and coconut-based PAC in Lake Erie Water: A) CYL adsorption, B) MC-LR adsorption, and C) ANTA adsorption.

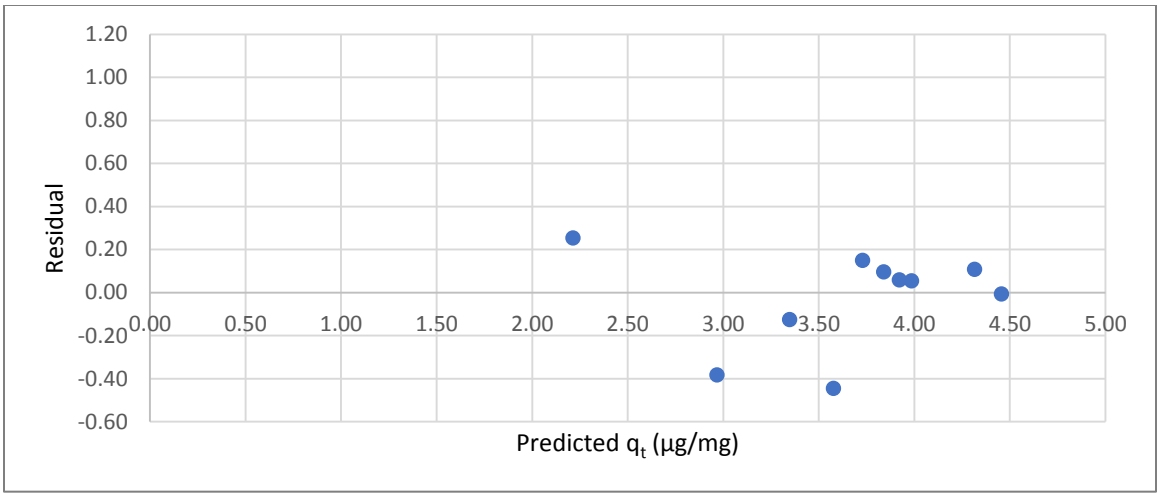

Figure B.2 Residual plot for pseudo-second order fit of CYL adsorption by the COL-PL60-800 (coal)

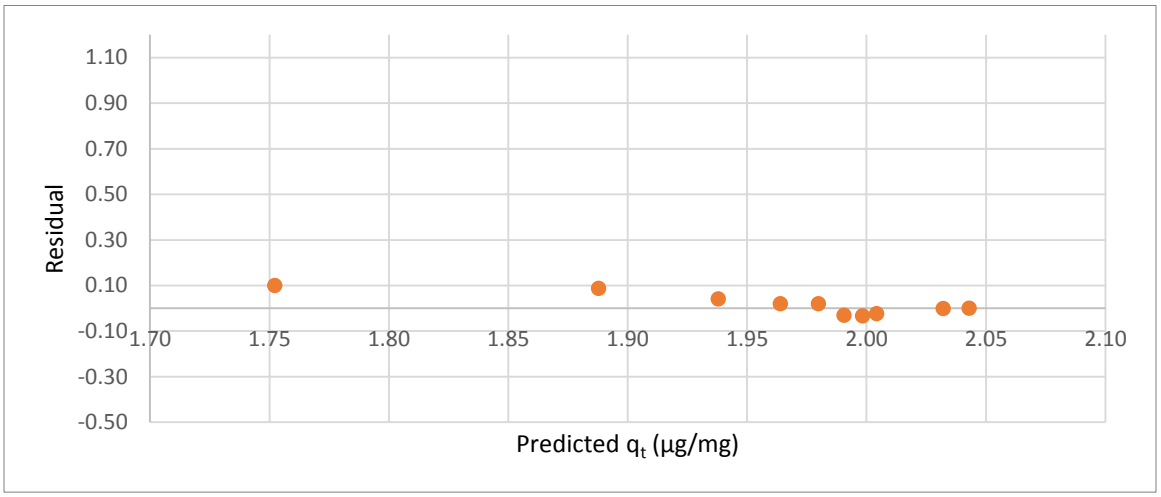

Figure B.3 Residual plot for pseudo-second order fit of CYL adsorption by the BG-HHM (wood)

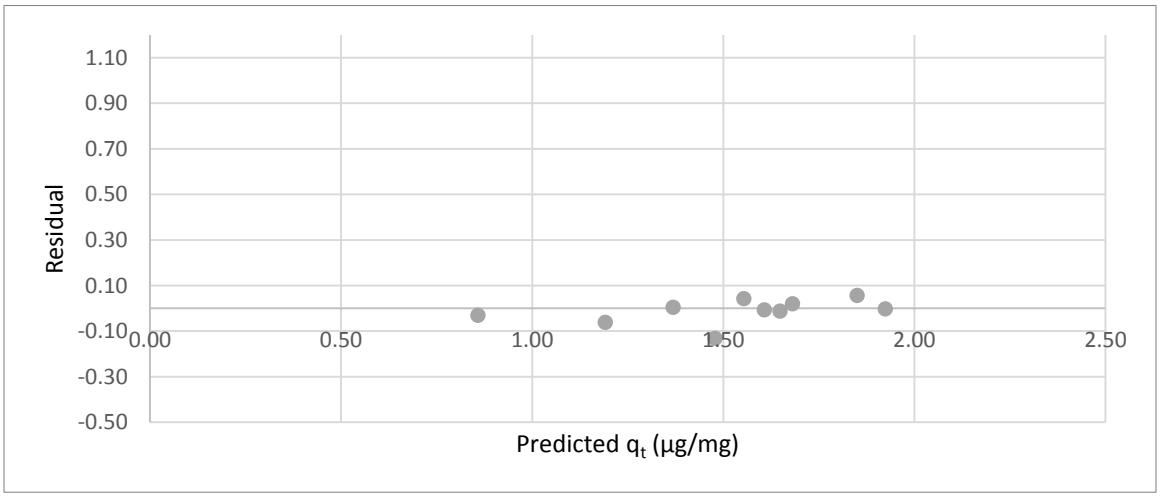

Figure B.4 Residual plot for pseudo-second order fit of CYL adsorption by the WPC (coconut)

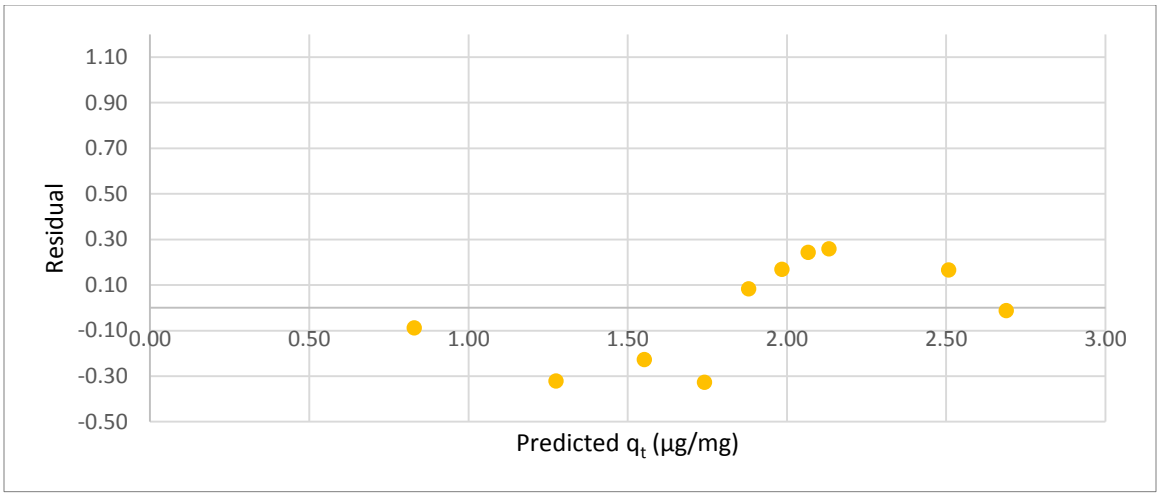

Figure B.5 Residual plot for pseudo-second order fit of MC-LR adsorption by the COL-PL60-800 (coal)

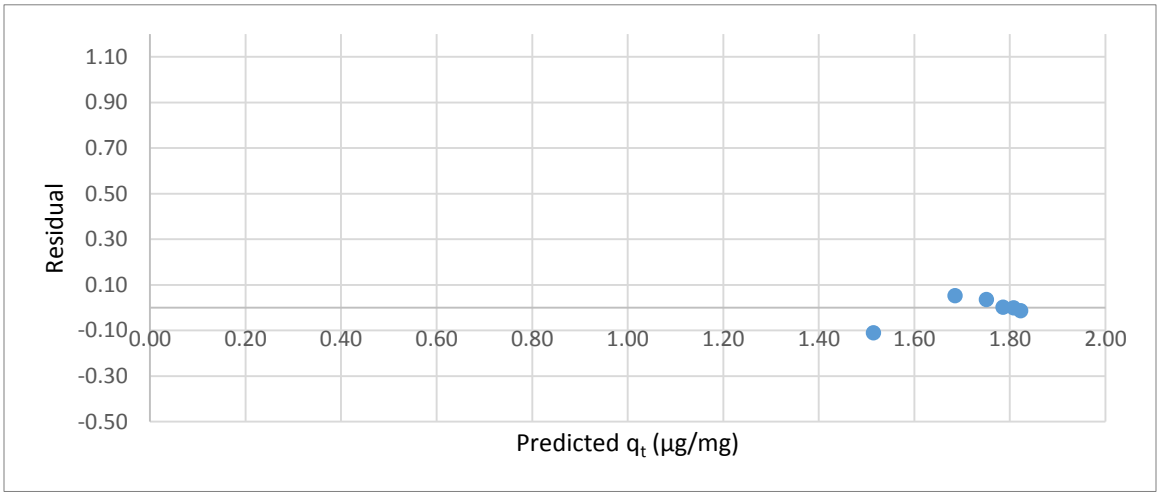

Figure B.6 Residual plot for pseudo-second order fit of MC-LR adsorption by the BG-HHM (wood)

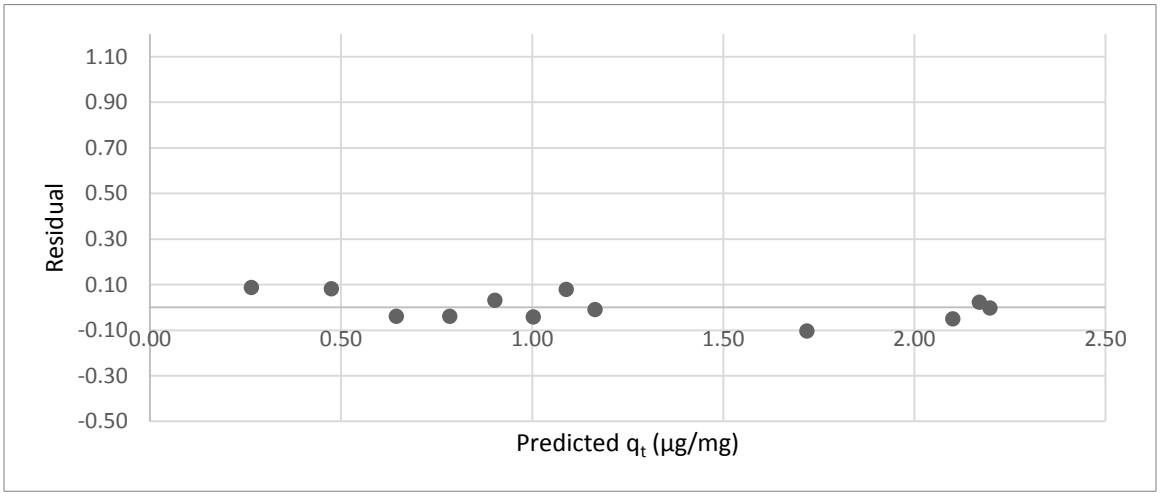

Figure B.7 Residual plot for pseudo-second order fit of MC-LR adsorption by the WPC (coconut)

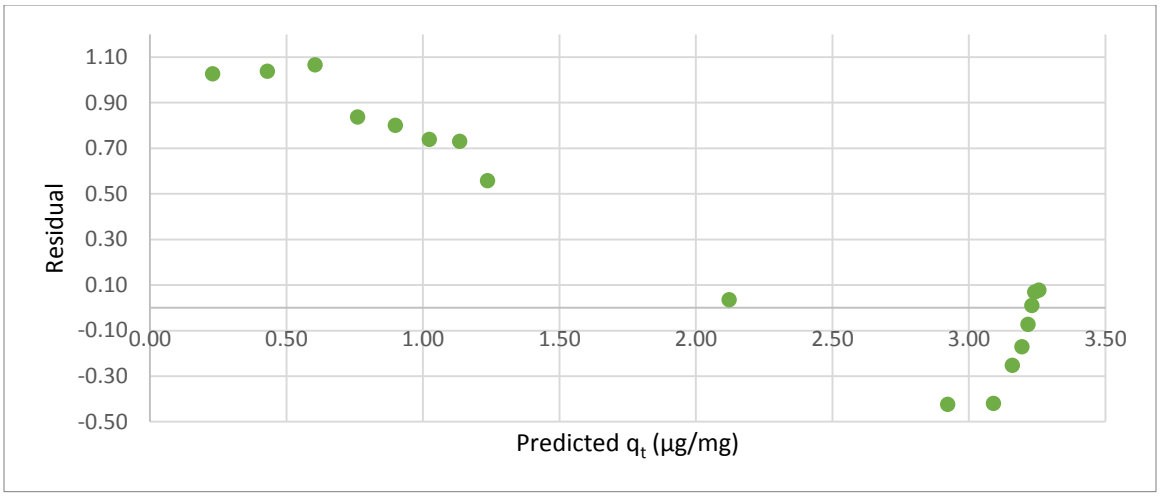

Figure B.8 Residual plot for pseudo-second order fit of ANTA adsorption by the COL-PL60-800 (coal)

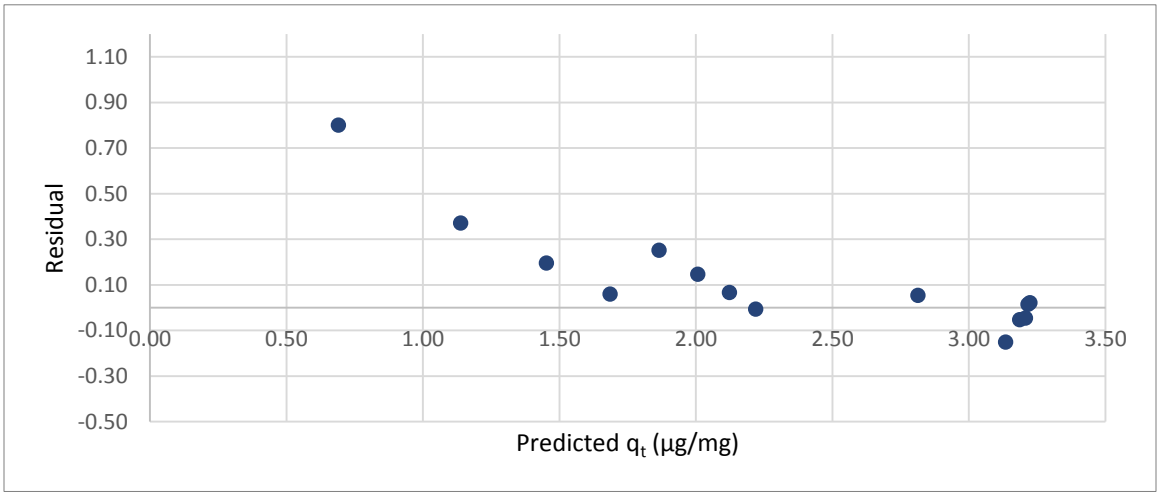

Figure B.9 Residual plot for pseudo-second order fit of ANTA adsorption by the BG-HHM (wood)

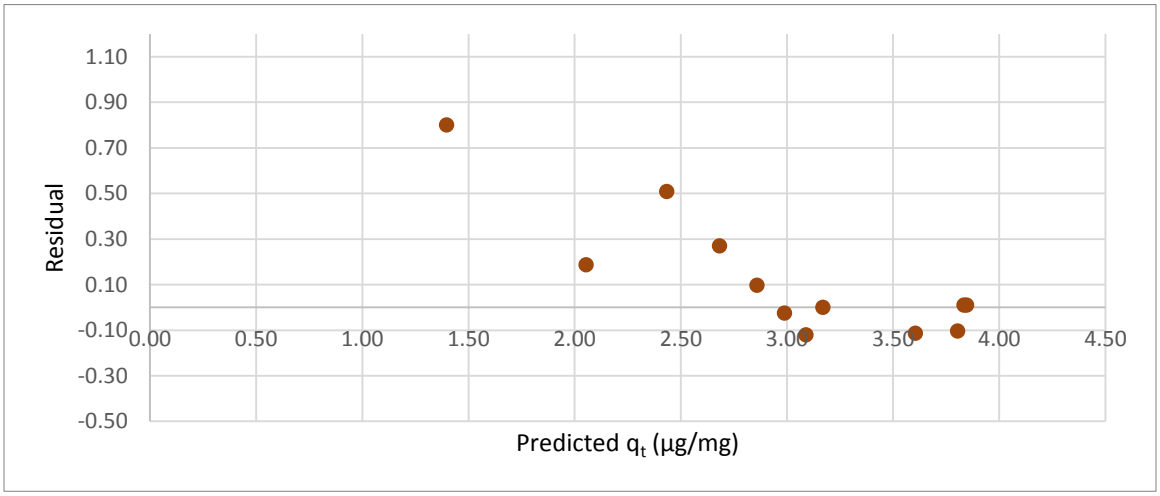

Figure B.10 Residual plot for pseudo-second order fit of ANTA adsorption by the WPC (coconut)

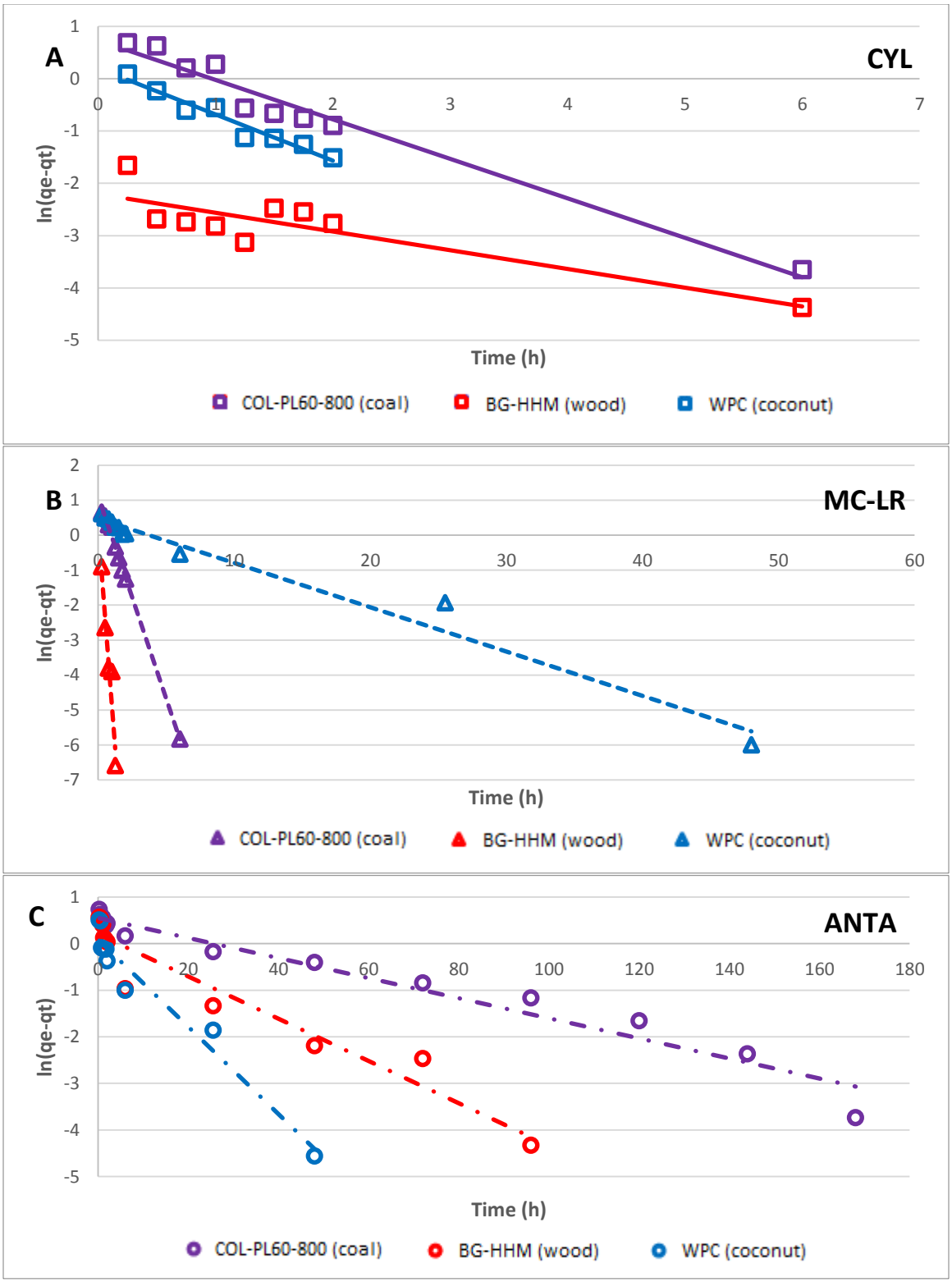

Figure B.11 Pseudo-first order kinetic model fits of CYL, MC-LR, and ANTA adsorption using coal-, wood-, and coconut-based PAC in Lake Erie Water: A) CYL adsorption, B) MC-LR adsorption, and C) ANTA adsorption.

Table B.10 Pseudo-first order kinetic model fits of CYL, MC-LR, and ANTA adsorption using coal-, wood-, and coconut-based PAC in Lake Erie Water: A) CYL adsorption, B) MC-LR adsorption, and C) ANTA adsorption.

Cyanotoxins	Carbon	Equilibrium Carbon Capacity, q_e Experimental (µg/mg)	Equilibrium Carbon Capacity, q_e Predicted (µg/mg)	k_1 (h^{-1})	R^2
CYL	COL-PL60-800 (coal)	4.45	2.07	0.75	0.9682
CYL	BG-HHM (wood)	2.03	0.11	0.36	0.7472
CYL	WPC (coconut)	1.91	1.22	0.88	0.9498
MC-LR	COL-PL60-800 (coal)	2.68	3.05	1.16	0.9963
MC-LR	BG-HHM (wood)	1.79	1.24	5.05	0.9246
MC-LR	WPC (coconut)	2.05	1.60	0.13	0.9725
ANTA	COL-PL60-800 (coal)	3.31	1.73	0.02	0.9617
ANTA	BG-HHM (wood)	3.16	1.22	0.05	0.9326
ANTA	WPC (coconut)	3.86	1.09	0.09	0.9526

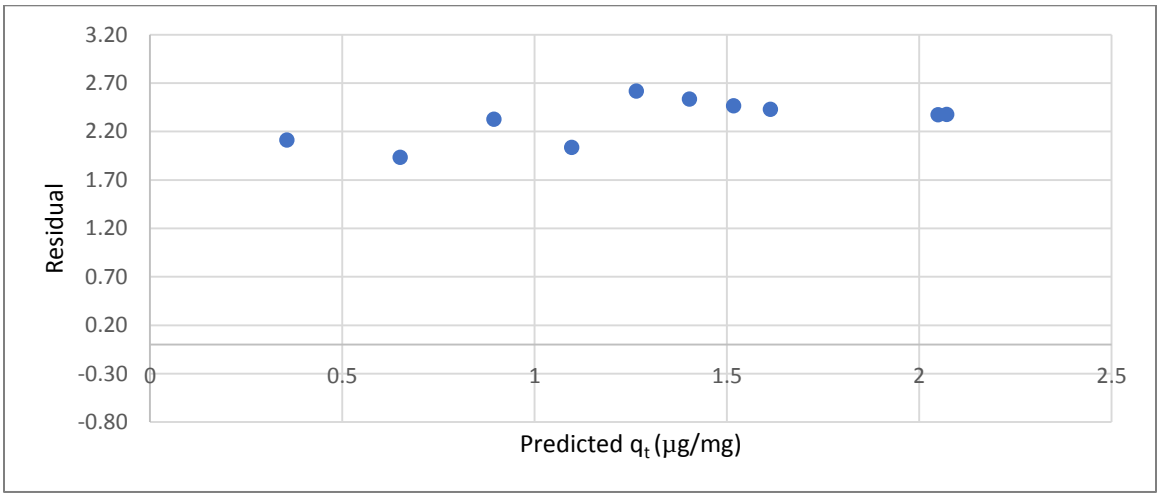

Figure B.12 Residual plot for pseudo-first order fit of CYL adsorption by the COL-PL60-800 (coal)

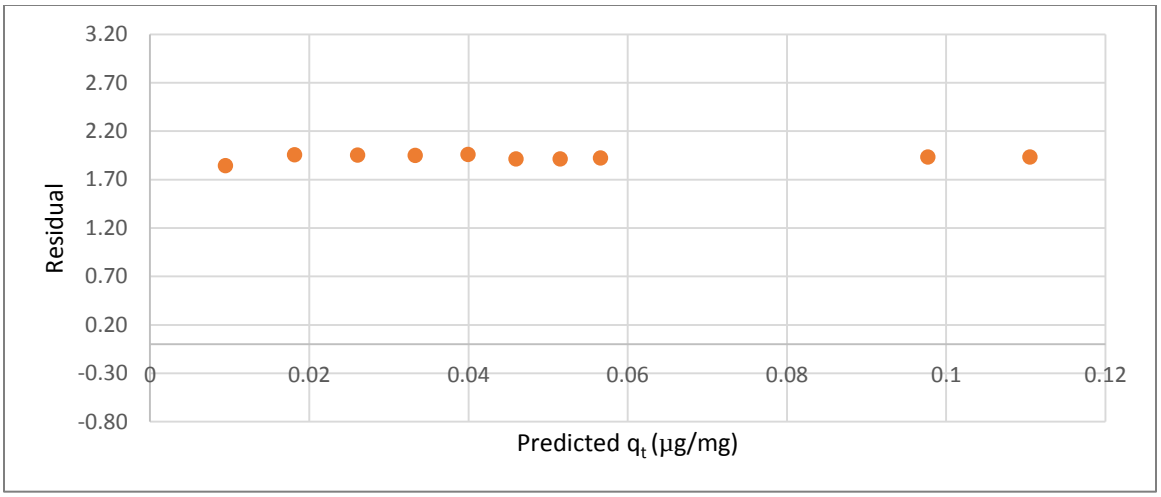

Figure B.13 Residual plot for pseudo-first order fit of CYL adsorption by the BG-HHM (wood)

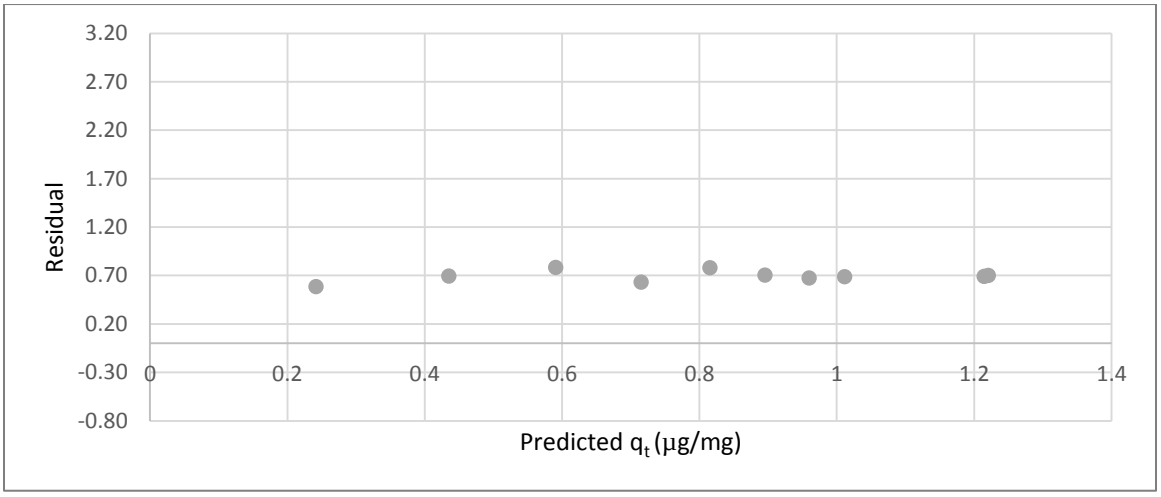

Figure B.14 Residual plot for pseudo-first order fit of CYL adsorption by the WPC (coconut)

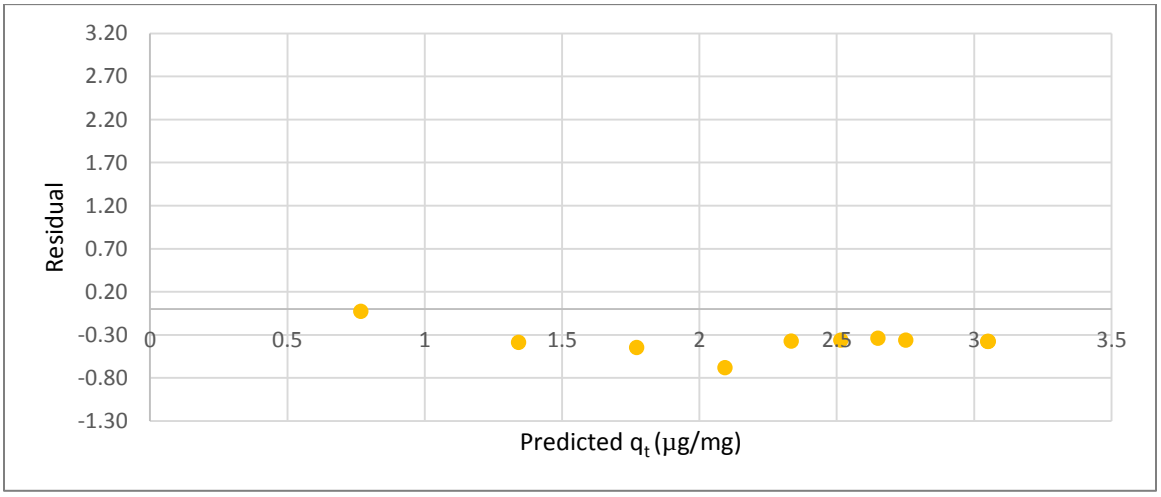

Figure B.15 Residual plot for pseudo-first order fit of MC-LR adsorption by the COL-PL60-800 (coal)

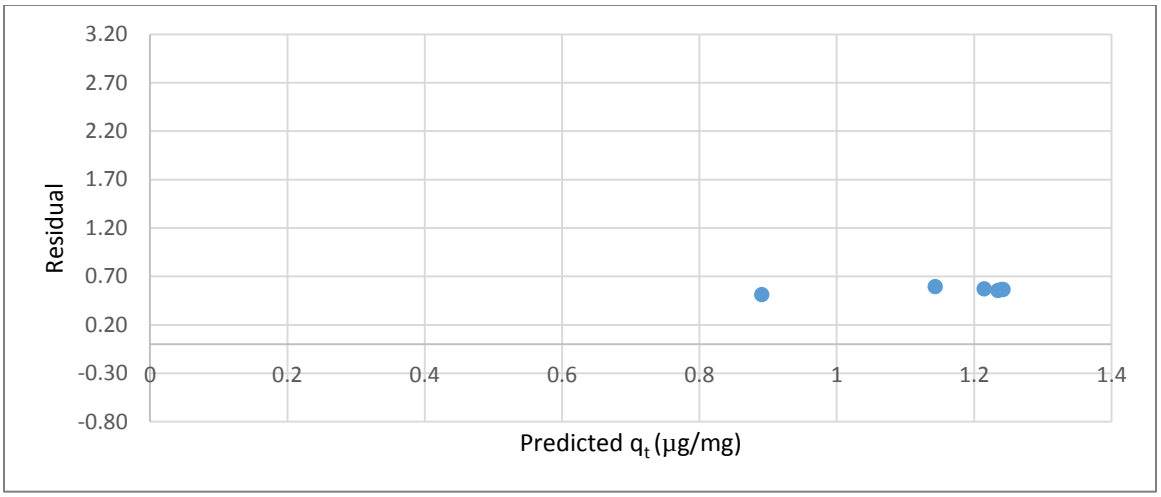

Figure B.16 Residual plot for pseudo-first order fit of MC-LR adsorption by the BG-HHM (wood)

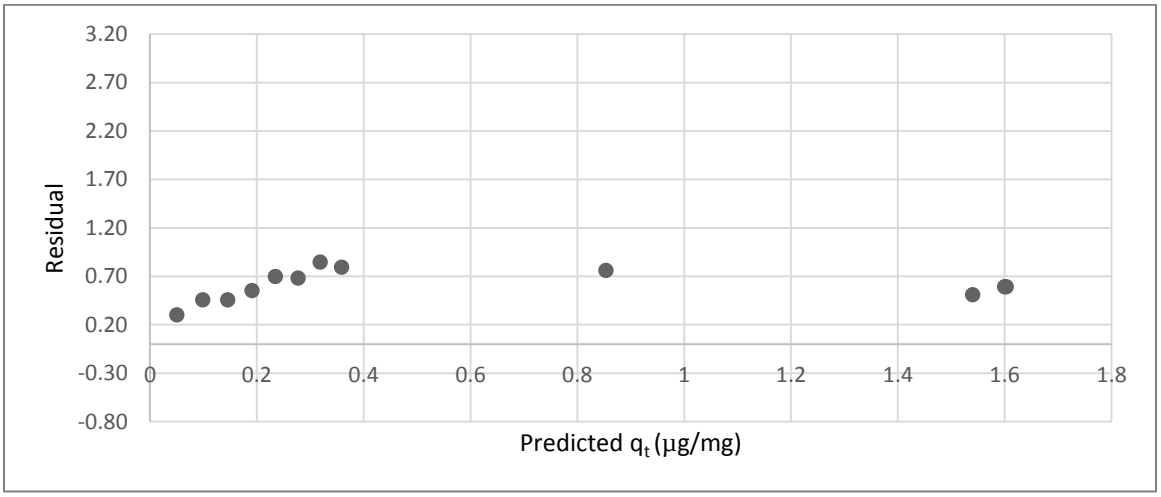

Figure B.17 Residual plot for pseudo-first order fit of MC-LR adsorption by the WPC (coconut)

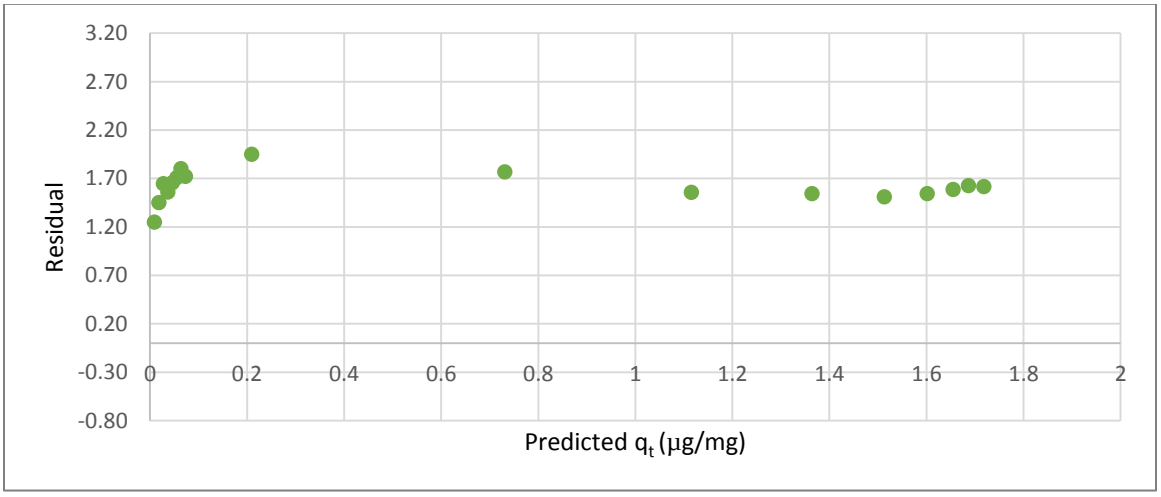

Figure B.18 Residual plot for pseudo-first order fit of ANTA adsorption by the COL-PL60-800 (coal)

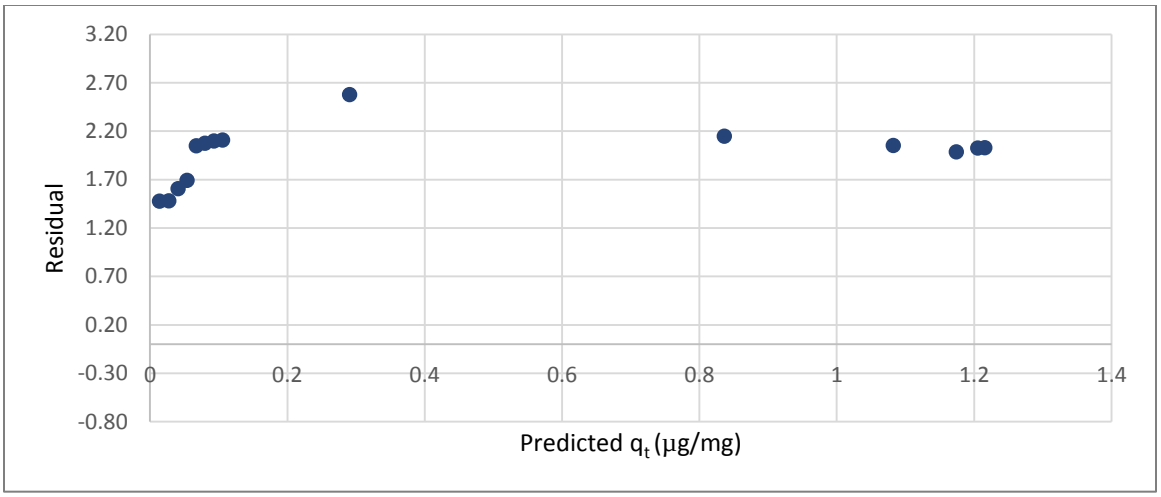

Figure B.19 Residual plot for pseudo-first order fit of ANTA adsorption by the BG-HHM (wood)

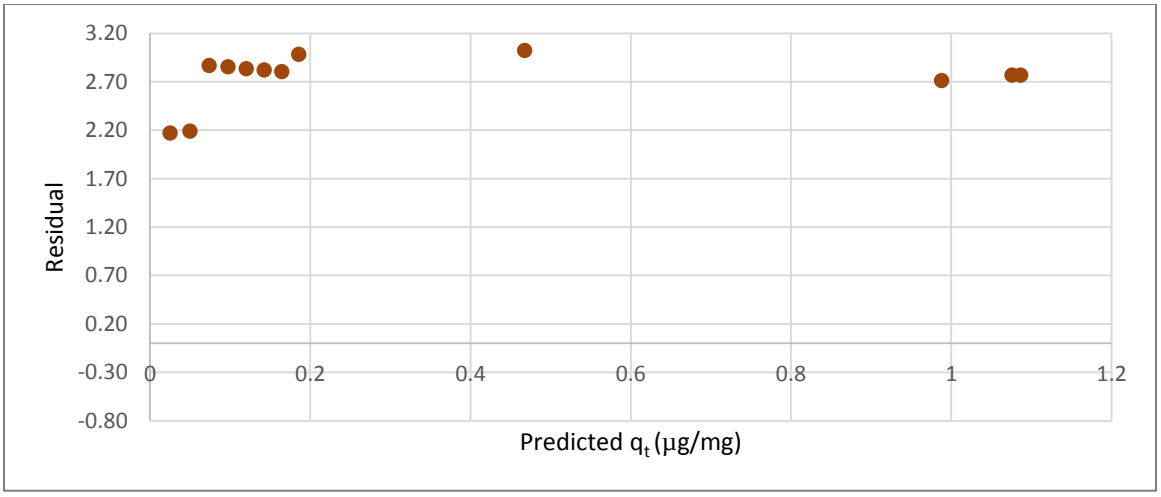

Figure B.20 Residual plot for pseudo-first order fit of ANTA adsorption by the WPC (coconut)

Appendix B.2 Natural Water Isotherms

Table B.11 0.5 h carbon loading data for CYL adsorption by COL-PL60-800 (coal) in Lake Erie water

Sample	Carbon dose (mg/L)	Equilibrium toxin concentration (µg/L)	Equilibrium Capacity, qe (µg/mg)
1	12.2	129.0	8.2
2	17.6	121.3	5.9
3	24.0	115.6	4.6
4	30.4	111.5	3.7
5	35.8	108.7	3.3
6	41.8	105.4	2.9
7	50.2	100.1	2.6

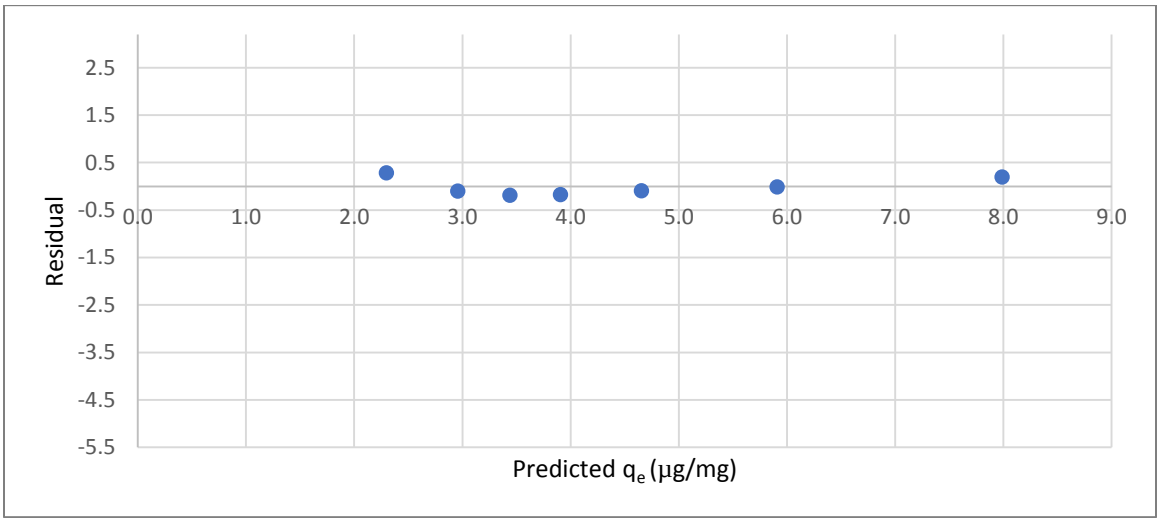

Figure B.21 Residual plot for the 0.5 h isotherm of CYL adsorption by the COL-PL60-800 (coal)

Table B.12 1.0 h carbon loading data for CYL adsorption by COL-PL60-800 (coal) in Lake Erie water

Sample	Carbon dose (mg/L)	Equilibrium toxin CYL conc. (µg/L)	Equilibrium Capacity, qe (µg/mg)
1	12.2	117.7	8.8
2	17.6	110.5	6.5
3	24	107.5	4.9
4	30.4	98.8	4.2
5	35.8	88.1	3.8
6	41.8	87.0	3.3
7	50.2	84.9	3.1

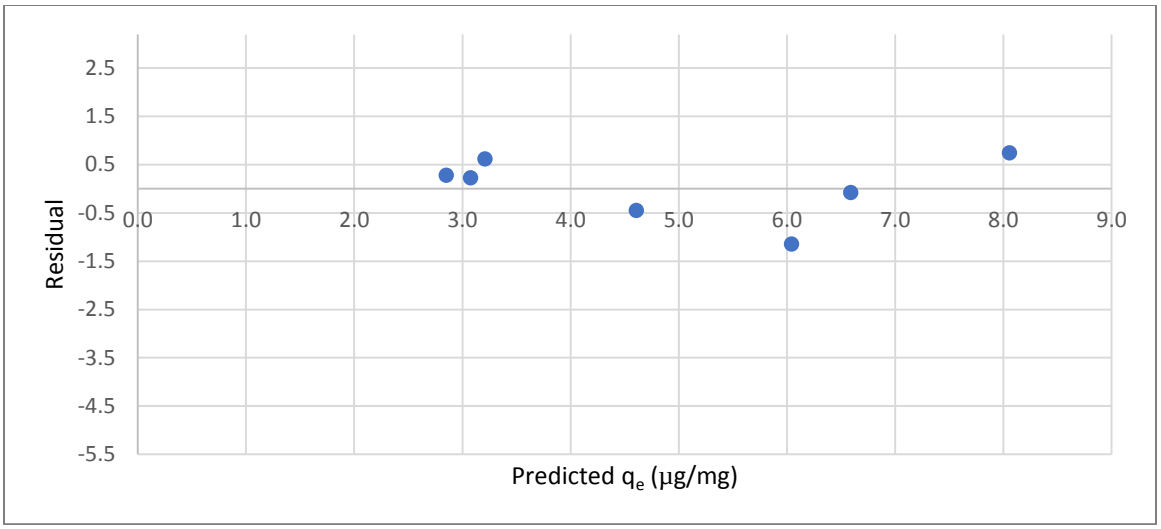

Figure B.22 Residual plot for the 1.0 h isotherm of CYL adsorption by the COL-PL60-800 (coal)

Table B.13 Equilibrium carbon loading data for CYL adsorption by COL-PL60-800 (coal) in Lake Erie water

Sample	Carbon dose (mg/L)	Equilibrium toxin concentration (µg/L)	Equilibrium Capacity, qe (µg/mg)
1	12.2	34.2	15.6
2	17.6	14.7	12.0
3	24.0	12.0	8.9
4	30.4	11.5	7.2
5	35.8	6.4	6.0
6	41.8	2.3	5.3
7	50.2	1.8	4.4

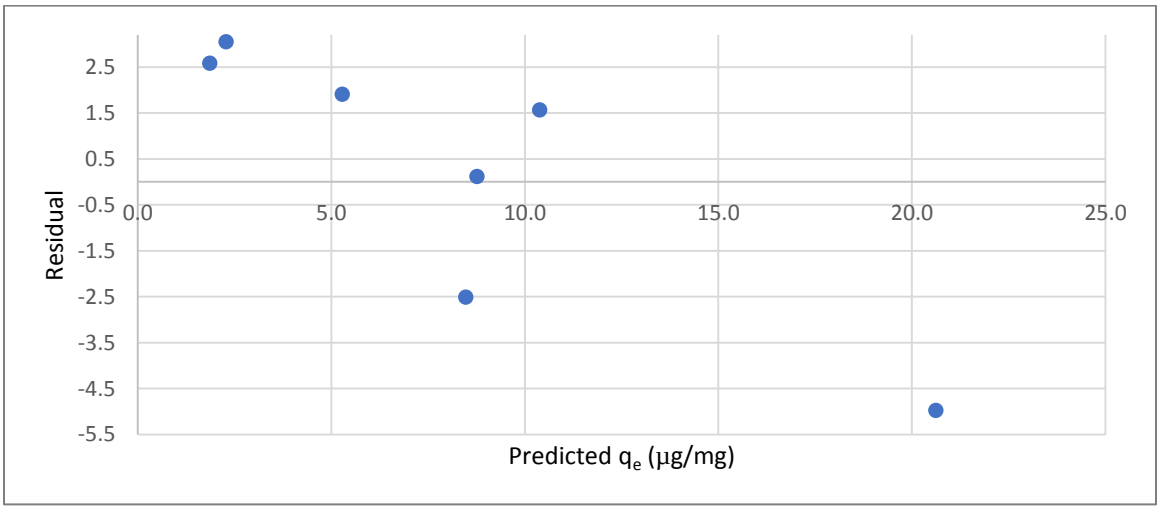

Figure B.23 Residual plot for the equilibrium isotherm of CYL adsorption by the COL-PL60-800 (coal)

Table B.14 0.5 h carbon loading data for CYL adsorption by BG-HHM (wood) in Lake Erie water

Sample	Carbon dose (mg/L)	Equilibrium toxin concentration (µg/L)	Equilibrium Capacity, qe (µg/mg)
1	12.2	59.5	3.5
2	18	37.9	3.6
3	24.4	24.6	3.2
4	30.4	16.3	2.8
5	35.8	11.9	2.5
6	42.2	8.1	2.2
7	50	4.0	2.0

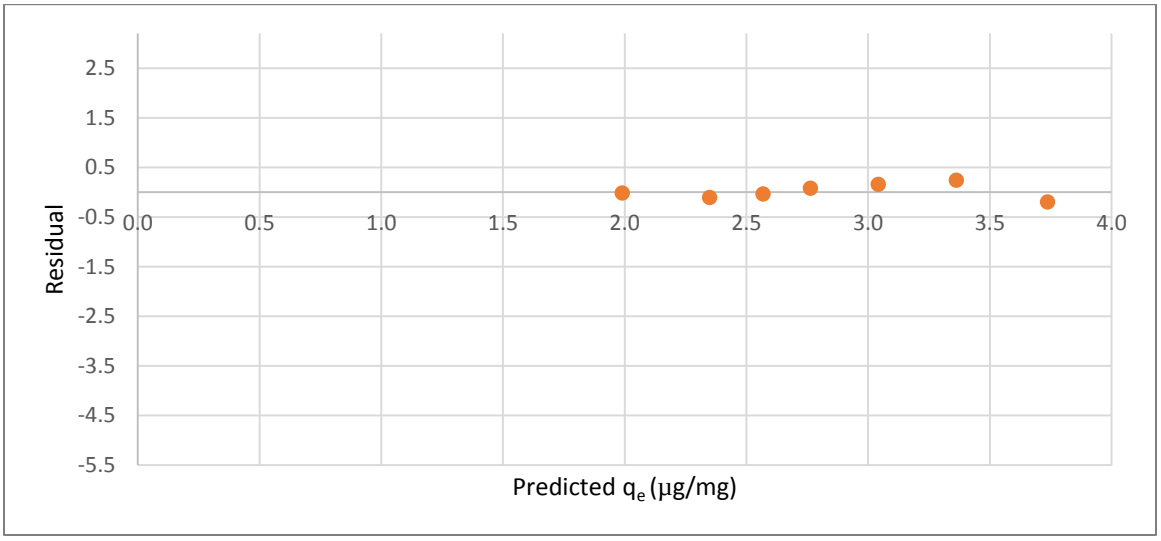

Figure B.24 Residual plot for the 0.5 h isotherm of CYL adsorption by the BG-HHM (wood)

Table B.15 1.0 h carbon loading data for CYL adsorption by BG-HHM (wood) in Lake Erie water

Sample	Carbon dose (mg/L)	Equilibrium toxin concentration (µg/L)	Equilibrium Capacity, qe (µg/mg)
1	12.2	41.2	5.0
2	18	27.7	4.2
3	24.4	15.4	3.6
4	30.4	8.7	3.1
5	35.8	10.0	2.6
6	42.2	5.4	2.3
7	50	2.3	2.0

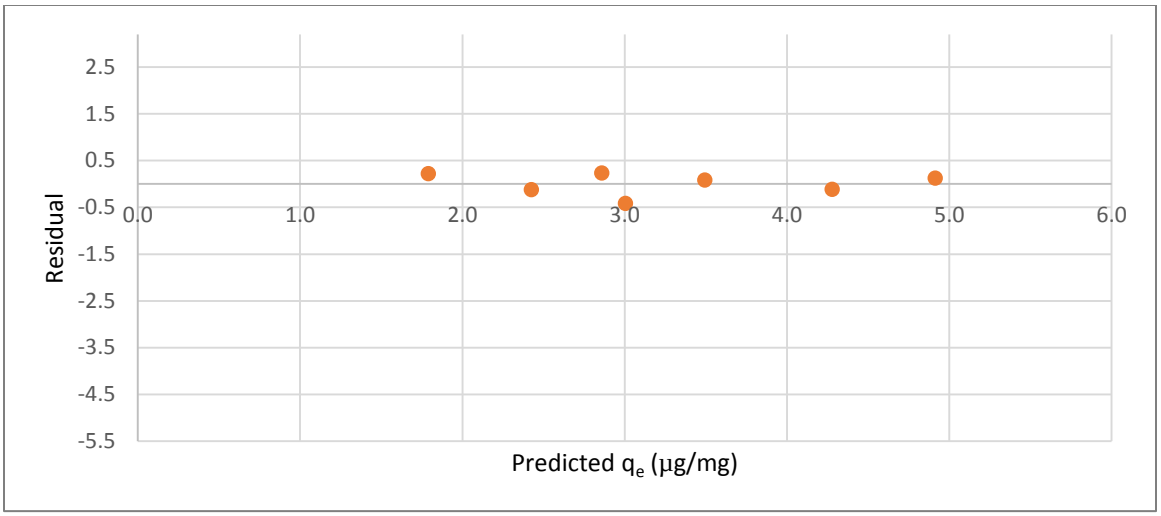

Figure B.25 Residual plot for the 1.0 h isotherm of CYL adsorption by the BG-HHM (wood)

Table B.16 Equilibrium carbon loading data for CYL adsorption by BG-HHM (wood) in Lake Erie water

Sample	Carbon dose (mg/L)	Equilibrium toxin concentration (µg/L)	Equilibrium Capacity, qe (µg/mg)
1	12.2	15.45	7.15
2	18	8.57	5.23
3	24.4	3.56	4.06
4	30.4	2.69	3.29
5	35.8	1.65	2.82
6	42.2	1.12	2.41
7	50	0.57	2.04

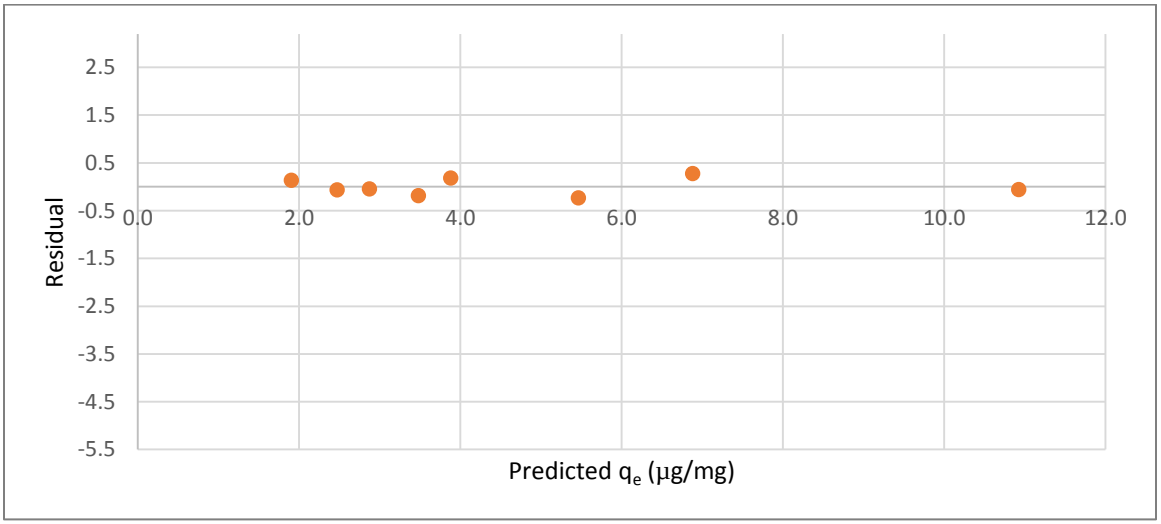

Figure B.26 Residual plot for the equilibrium isotherm of CYL adsorption by the BG-HHM (wood)

Table B.17 0.5 h carbon loading data for CYL adsorption by WPC (coconut) in Lake Erie water

Sample	Carbon dose (mg/L)	Equilibrium toxin concentration (µg/L)	Equilibrium Capacity, qe (µg/mg)
1	12.2	80.8	1.4
2	18.2	76.2	1.2
3	24.2	67.7	1.2
4	30.2	63.5	1.1
5	36.2	56.8	1.1
6	42.2	47.5	1.2
7	50.4	40.7	1.1

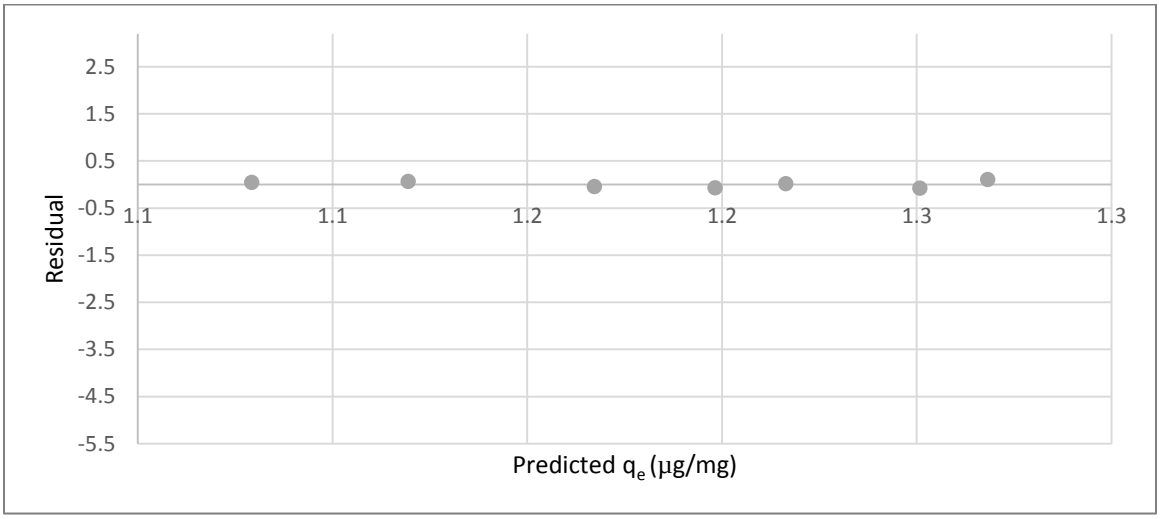

Figure B.27 Residual plot for the 0.5 h isotherm of CYL adsorption by the WPC (coconut)

Table B.18 1.0 h carbon loading data for CYL adsorption by WPC (coconut) in Lake Erie water

Sample	Carbon dose (mg/L)	Equilibrium toxin concentration (µg/L)	Equilibrium Capacity, qe (µg/mg)
1	12.2	75.3	1.8
2	18.2	63.5	1.9
3	24.2	55.1	1.8
4	30.2	52.8	1.5
5	36.2	48.5	1.4
6	42.2	39.2	1.4
7	50.4	29.8	1.3

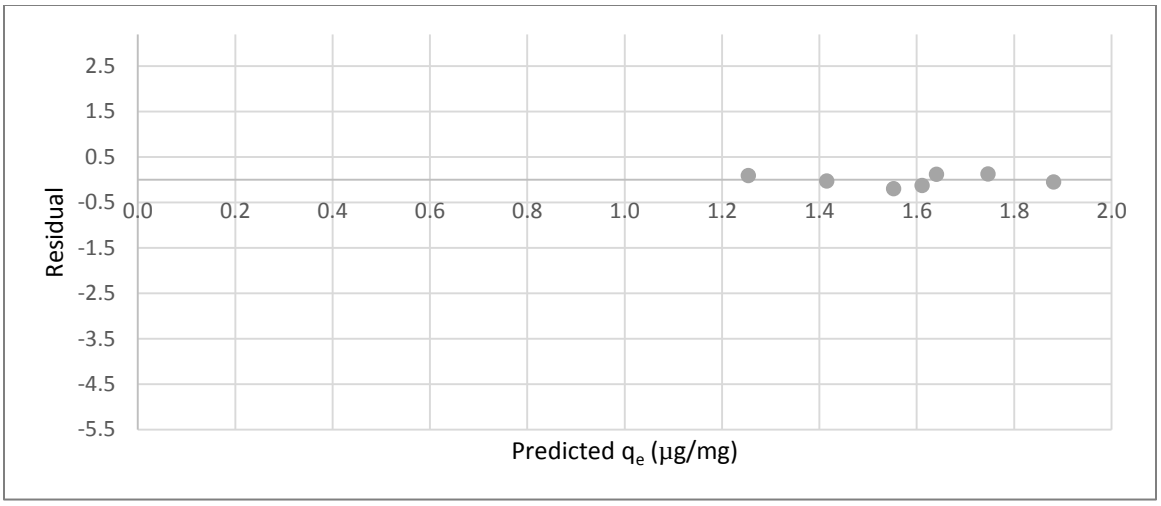

Figure B.28 Residual plot for the 1.0 h isotherm of CYL adsorption by the WPC (coconut)

Table B.19 Equilibrium carbon loading data for CYL adsorption by WPC (coconut) in Lake Erie water

Sample	Carbon dose (mg/L)	Equilibrium toxin concentration (µg/L)	Equilibrium Capacity, qe (µg/mg)
1	12.2	46.3	4.2
2	18.2	29.6	3.7
3	24.2	18.8	3.3
4	30.2	6.7	3.0
5	36.2	2.6	2.6
6	42.2	1.3	2.3
7	50.4	0.8	1.9

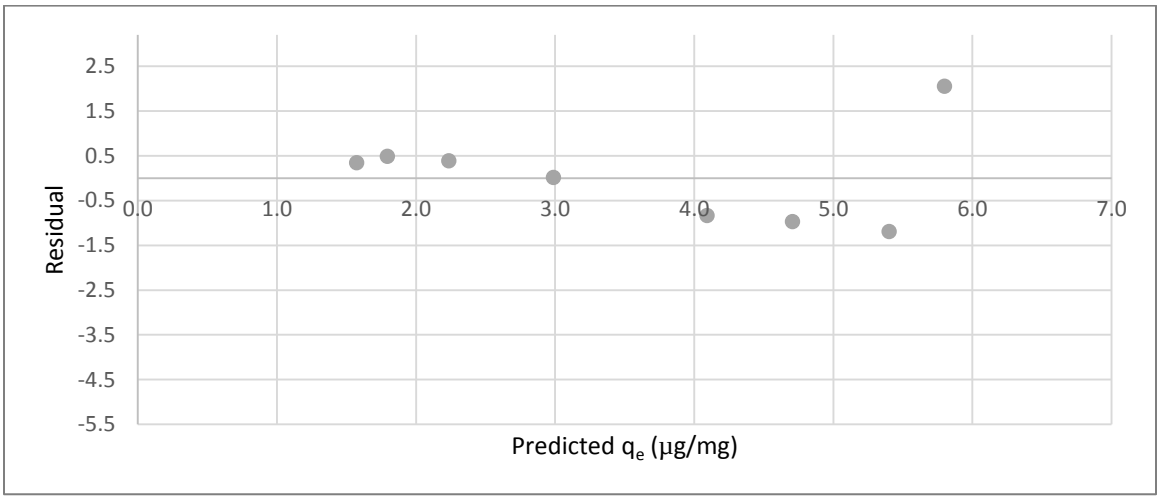

Figure B.29 Residual plot for the equilibrium isotherm of CYL adsorption by the WPC (coconut)

Table B.20 0.5 h carbon loading data for MC-LR adsorption by COL-PL60-800 (coal) in Lake Erie water

Sample	Carbon dose (mg/L)	Equilibrium toxin concentration (µg/L)	Equilibrium Capacity, qe (µg/mg)
1	12	113.6	2.3
2	18.4	105.1	1.7
3	24.4	101.6	1.4
4	30.4	96.7	1.1
5	36.4	95.6	1.0
6	42.2	95.3	1.0
7	50.4	92.2	1.0

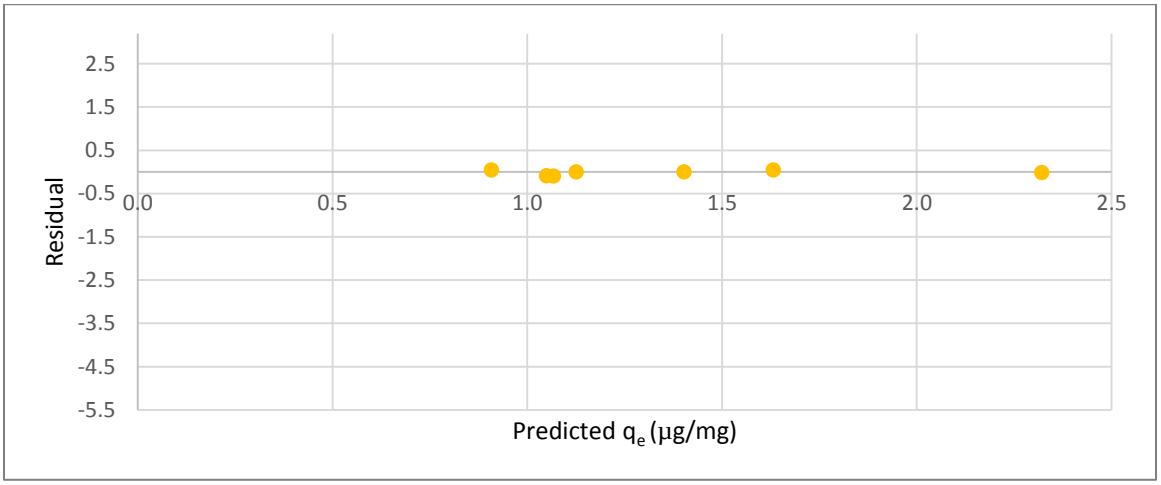

Figure B.30 Residual plot for the 0.5 h isotherm of MC-LR adsorption by the COL-PL60-800 (coal)

Table B.21 1.0 h carbon loading data for MC-LR adsorption by COL-PL60-800 (coal) in Lake Erie water

Sample	Carbon dose (mg/L)	Equilibrium toxin concentration (µg/L)	Equilibrium Capacity, qe (µg/mg)
1	12	103.4	2.7
2	18.4	96.5	2.1
3	24.4	89.1	1.9
4	30.4	84.5	1.7
5	36.4	77.1	1.6
6	42.2	72.1	1.5
7	50.4	64.6	1.4

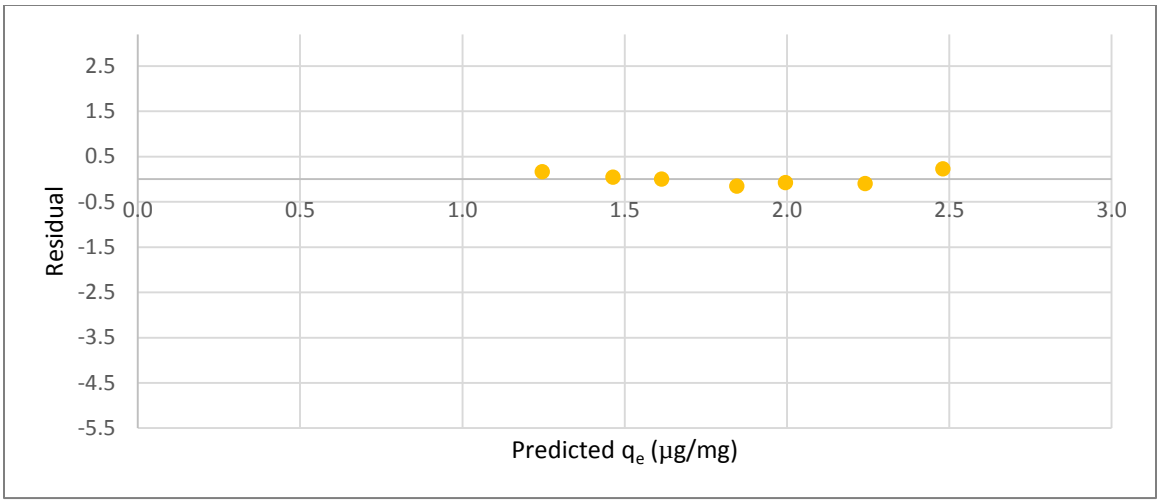

Figure B.31 Residual plot for the 1.0 h isotherm of MC-LR adsorption by the COL-PL60-800 (coal)

Table B.22 Equilibrium carbon loading data for MC-LR adsorption by COL-PL60-800 (coal) in Lake Erie water

Sample	Carbon dose (mg/L)	Equilibrium toxin concentration (µg/L)	Equilibrium Capacity, qe (µg/mg)
1	12	66.4	5.8
2	18.4	37.8	5.3
3	24.4	14.5	5.0
4	30.4	6.1	4.3
5	36.4	3.2	3.6
6	42.2	1.8	3.2
7	50.4	1.0	2.7

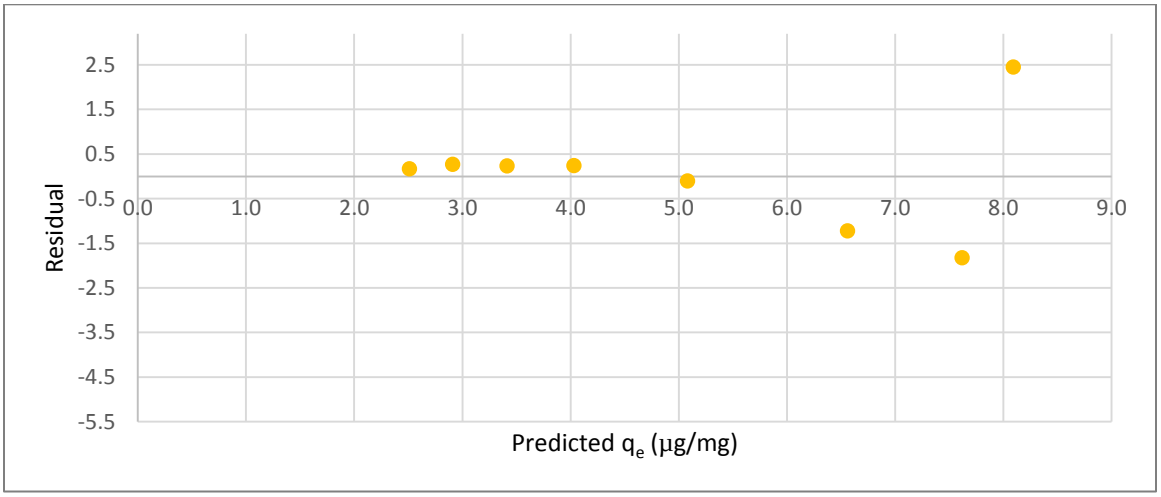

Figure B.32 Residual plot for the equilibrium isotherm of MC-LR adsorption by the COL-PL60-800 (coal)

Table B.23 0.5 h carbon loading data for MC-LR adsorption by BG-HHM (wood) in Lake Erie water

Sample	Carbon dose (mg/L)	Equilibrium toxin concentration (µg/L)	Equilibrium Capacity, qe (µg/mg)
1	12.0	79.6	7.0
2	17.8	60.2	5.8
3	24.2	35.9	5.3
4	30.0	22.7	4.7
5	35.8	18.1	4.1
6	42.0	8.9	3.7
7	50.2	3.6	3.2

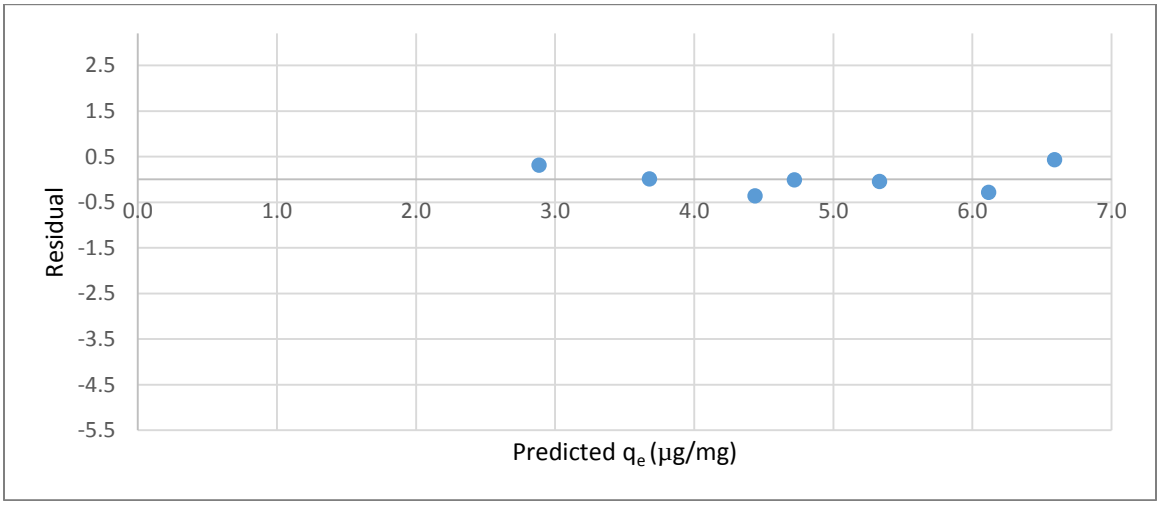

Figure B.33 Residual plot for the 0.5 h isotherm of MC-LR adsorption by the BG-HHM (wood)

Table B.24 1.0 h carbon loading data for MC-LR adsorption by BG-HHM (wood) in Lake Erie water

Sample	Carbon dose (mg/L)	Equilibrium toxin concentration (µg/L)	Equilibrium Capacity, qe (µg/mg)
1	12.0	42.4	10.1
2	17.8	24.6	7.8
3	24.2	9.9	6.4
4	30.0	5.8	5.3
5	35.8	2.8	4.5
6	42.0	1.4	3.9
7	50.2	1.1	3.2

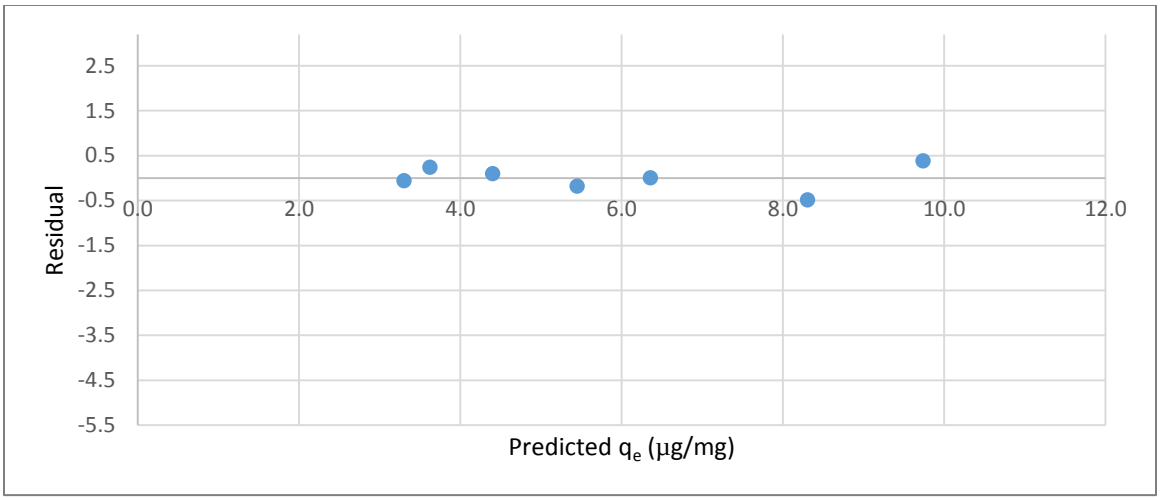

Figure B.34 Residual plot for the 1.0 h isotherm of MC-LR adsorption by the BG-HHM (wood)

Table B.25 Equilibrium carbon loading data for MC-LR adsorption by BG-HHM (wood) in Lake Erie water

Sample	Carbon dose (mg/L)	Equilibrium toxin concentration (µg/L)	Equilibrium Capacity, qe (µg/mg)
1	12.0	20.0	12.0
2	17.8	12.9	8.5
3	24.2	8.0	6.4
4	30.0	3.8	5.3
5	35.8	2.1	4.5
6	42.0	1.1	3.9

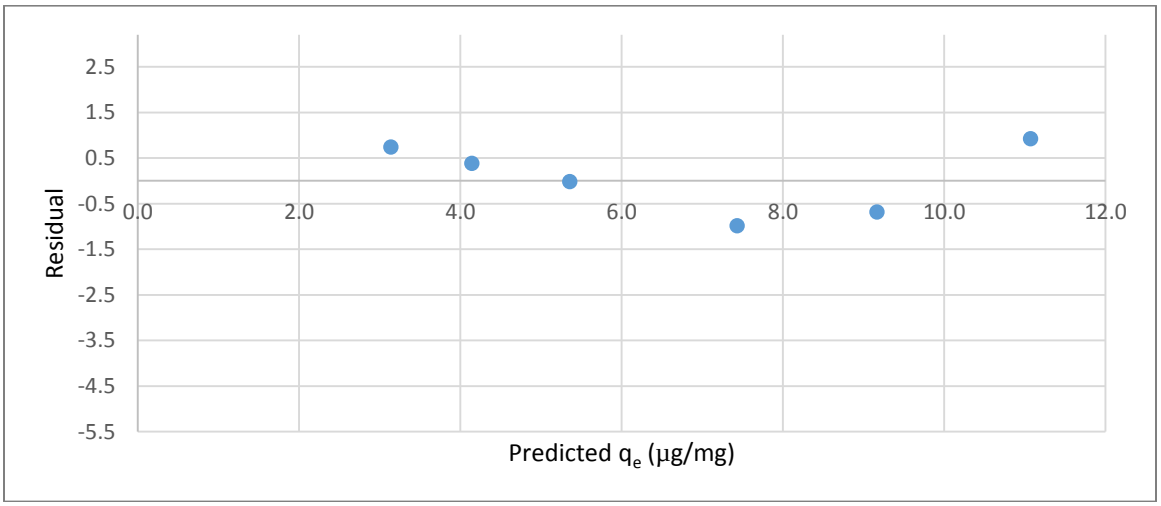

Figure B.35 Residual plot for the equilibrium isotherm of MC-LR adsorption by the BG-HHM (wood)

Table B.26 0.5 h carbon loading data for MC-LR adsorption by WPC (coconut) in Lake Erie water

Sample	Carbon dose (mg/L)	Equilibrium toxin concentration (µg/L)	Equilibrium Capacity, qe (µg/mg)
1	12.2	110.0	1.4
2	18.4	104.7	1.2
3	24.0	100.4	1.1
4	30.6	97.8	0.9
5	35.8	94.2	0.9
6	42.4	91.5	0.8
7	50.0	87.6	0.8

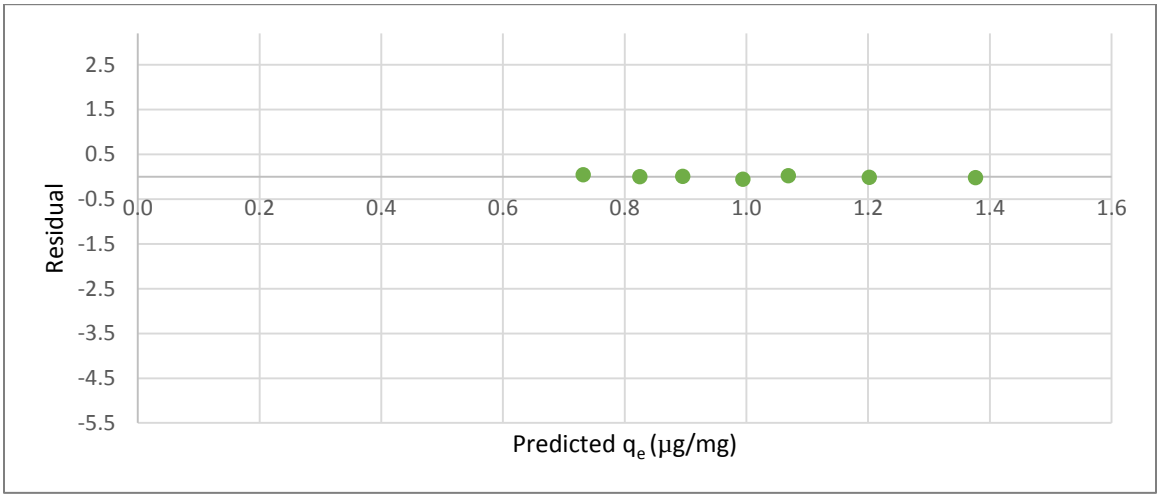

Figure B.36 Residual plot for the 0.5 h isotherm of MC-LR adsorption by the WPC (coconut)

Table B.27 1.0 h carbon loading data for MC-LR adsorption by WPC (coconut) in Lake Erie water

Sample	Carbon dose (mg/L)	Equilibrium toxin concentration (µg/L)	Equilibrium Capacity, qe (µg/mg)
1	12.2	103.1	1.9
2	18.4	96.6	1.6
3	24.0	92.5	1.4
4	30.6	85.5	1.3
5	35.8	83.6	1.2
6	42.4	78.6	1.1
7	50.0	74.0	1.0

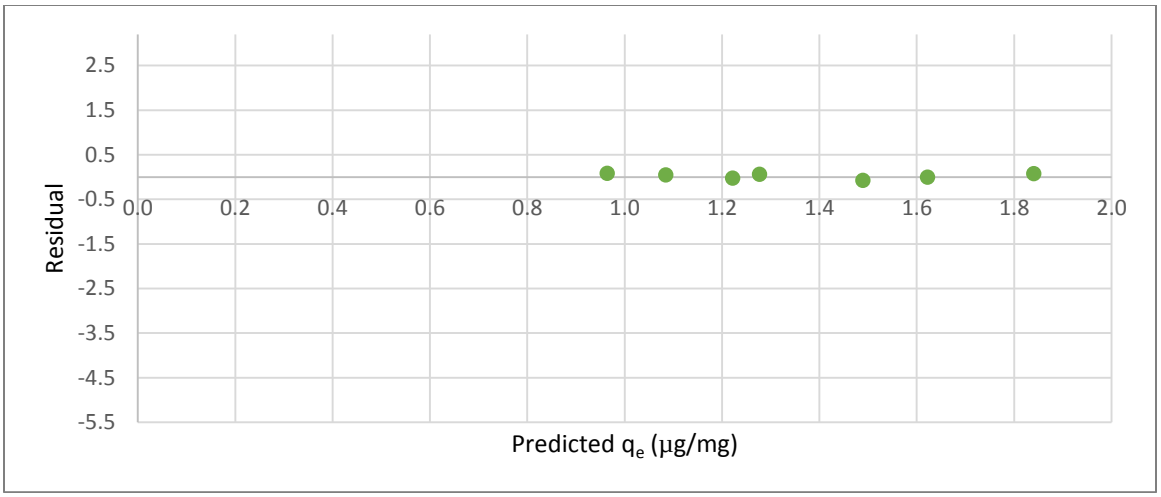

Figure B.37 Residual plot for the 1.0 h isotherm of MC-LR adsorption by the WPC (coconut)

Table B.28 Equilibrium carbon loading data for MC-LR adsorption by WPC (coconut) in Lake Erie water

Sample	Carbon dose (mg/L)	Equilibrium toxin concentration (µg/L)	Equilibrium Capacity, qe (µg/mg)
1	12.2	89.7	3.0
2	18.4	76.9	2.7
3	24.0	61.6	2.7
4	30.6	43.4	2.7
5	35.8	15.2	3.1
6	42.4	3.7	2.9
7	50.0	1.5	2.5

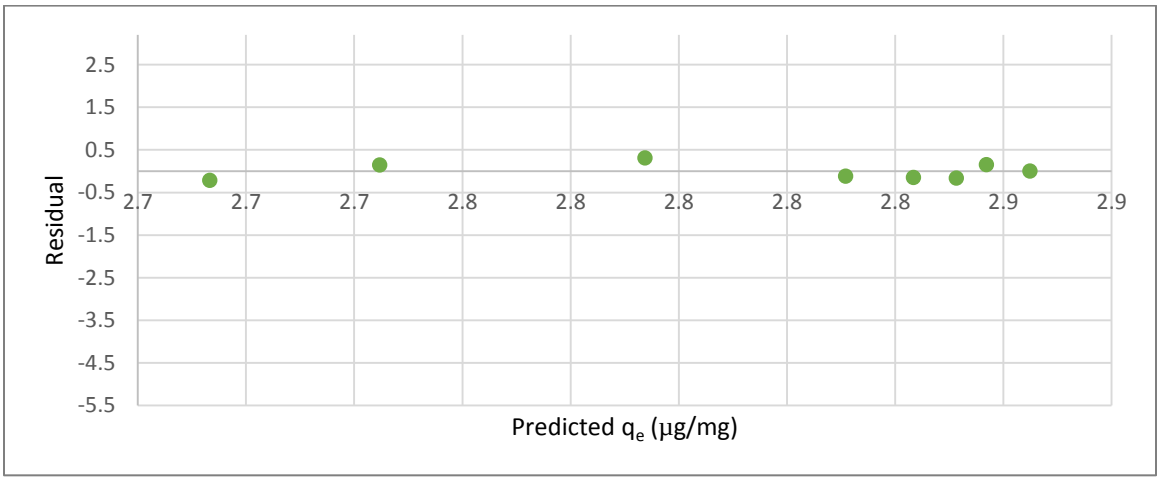

Figure B.38 Residual plot for the equilibrium isotherm of MC-LR adsorption by the WPC (coconut)

Table B.29 0.5 h carbon loading data for ANTA adsorption by COL-PL60-800 (coal) in Lake Erie water

Sample	Carbon dose (mg/L)	Equilibrium toxin concentration (µg/L)	Equilibrium Capacity, qe (µg/mg)
1	12.2	120.9	4.4
2	18.4	113.7	3.3
3	24	110.4	2.7
4	30.6	106.5	2.2
5	35.8	104.4	2.0
6	42.4	103.4	1.7
7	50	101.3	1.5

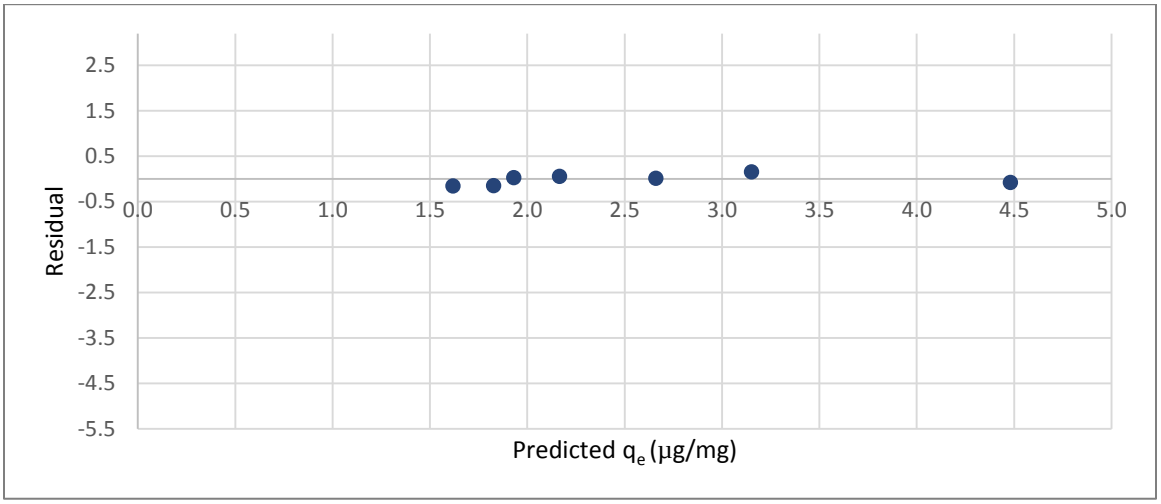

Figure B.39 Residual plot for the 0.5 h isotherm of ANTA adsorption by the COL-PL60-800 (coal)

Table B.30 1.0 h carbon loading data for ANTA adsorption by COL-PL60-800 (coal) in Lake Erie water

Sample	Carbon dose (mg/L)	Equilibrium toxin concentration (µg/L)	Equilibrium Capacity, qe (µg/mg)
1	12.2	114.9	4.9
2	18.4	107.9	3.6
3	24	102.7	3.0
4	30.6	101.4	2.4
5	35.8	99.4	2.1
6	42.4	98.3	1.8
7	50	94.8	1.6

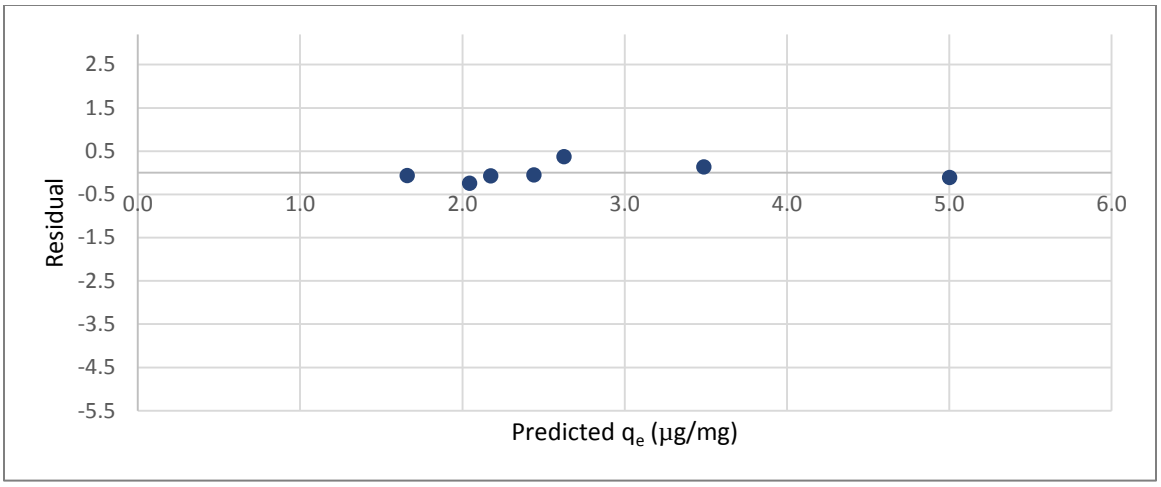

Figure B.40 Residual plot for the 1.0 h isotherm of ANTA adsorption by the COL-PL60-800 (coal)

Table B.31 Equilibrium carbon loading data for ANTA adsorption by COL-PL60-800 (coal) in Lake Erie water

Sample	Carbon dose (mg/L)	Equilibrium toxin concentration (µg/L)	Equilibrium Capacity, qe (µg/mg)
1	12.2	38.1	11.2
2	18.4	31.3	7.8
3	24	19.1	6.5
4	30.6	14.5	5.2
5	35.8	13.4	4.5
6	42.4	14.6	3.8
7	50	7.2	3.3

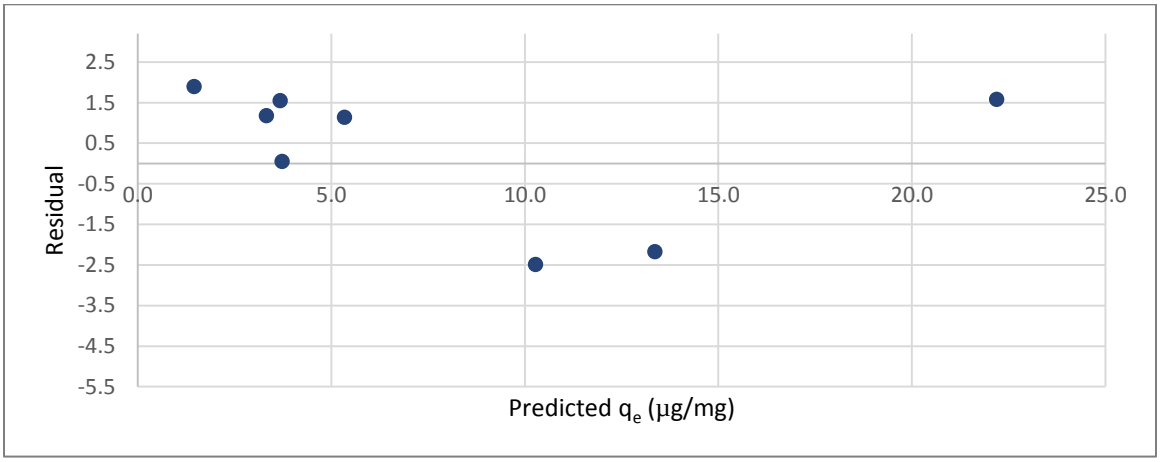

Figure B.41 Residual plot for the equilibrium isotherm of ANTA adsorption by the COL-PL60-800 (coal)

Table B.32 0.5 h carbon loading data for ANTA adsorption by BG-HHM (wood) in Lake Erie water

Sample	Carbon dose (mg/L)	Equilibrium toxin concentration (µg/L)	Equilibrium Capacity, qe (µg/mg)
1	12.2	109.6	4.6
2	17.8	105.8	3.3
3	24.0	101.7	2.7
4	30.0	97.0	2.3
5	36.4	96.1	1.9
6	41.8	92.6	1.7
7	49.8	90.2	1.5

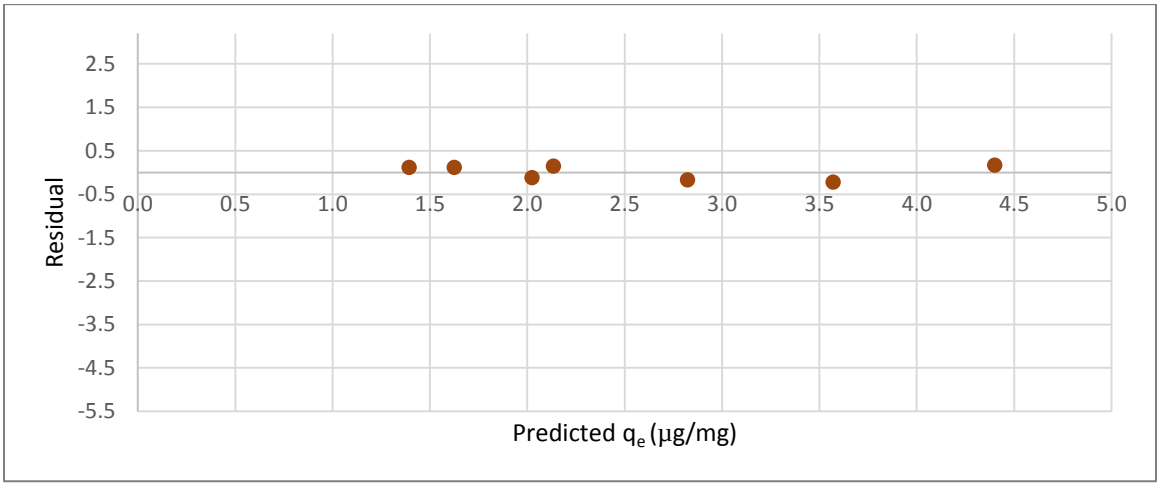

Figure B.42 Residual plot for the 0.5 h isotherm of ANTA adsorption by the BG-HHM (wood)

Table B.33 1.0 h carbon loading data for ANTA adsorption by BG-HHM (wood) in Lake Erie water

Sample	Carbon dose (mg/L)	Equilibrium toxin concentration (µg/L)	Equilibrium Capacity, qe (µg/mg)
1	12.2	101.8	5.2
2	17.8	94.0	4.0
3	24.0	89.6	3.2
4	30.0	86.1	2.6
5	36.4	83.7	2.2
6	41.8	81.8	2.0
7	49.8	78.4	1.7

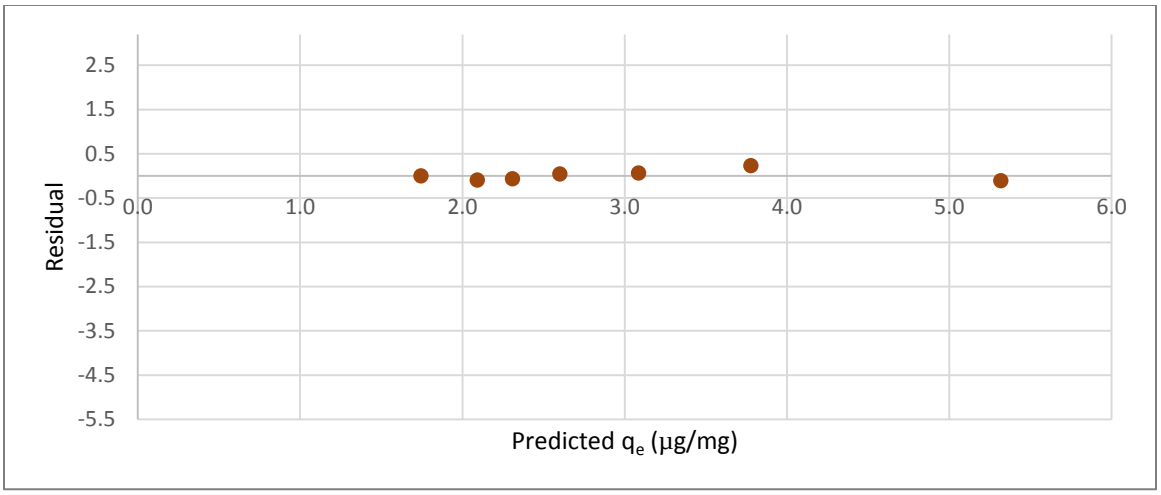

Figure B.43 Residual plot for the 1.0 h isotherm of ANTA adsorption by the BG-HHM (wood)

Table B.34 Equilibrium carbon loading data for ANTA adsorption by BG-HHM (wood) in Lake Erie water

Sample	Carbon dose (mg/L)	Equilibrium toxin concentration (µg/L)	Equilibrium Capacity, qe (µg/mg)
1	12.2	26.9	11.4
2	17.8	17.7	8.3
3	24.0	10.7	6.4
4	30.0	7.7	5.3
5	36.4	5.6	4.4
6	41.8	5.0	3.8
7	49.8	3.7	3.2

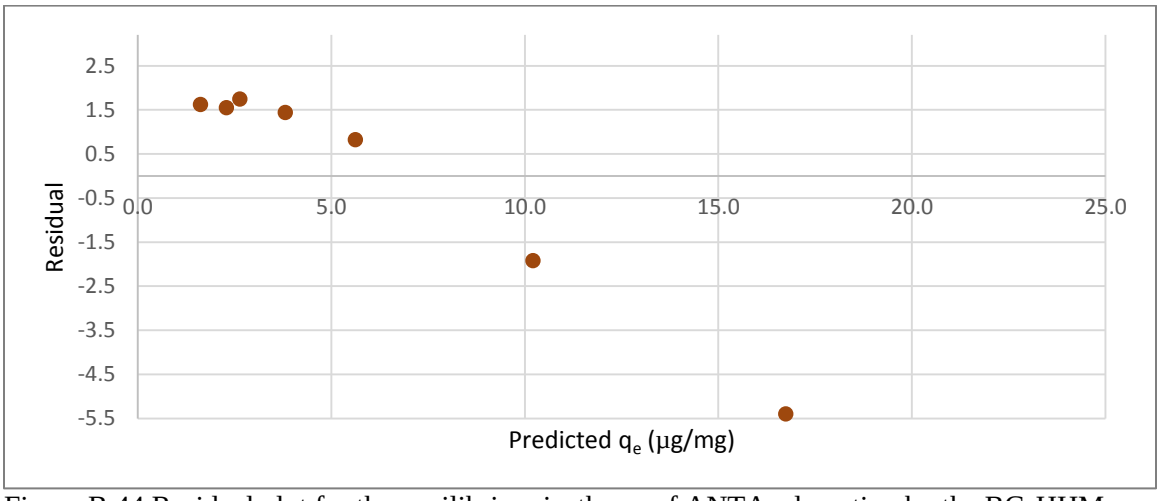

Figure B.44 Residual plot for the equilibrium isotherm of ANTA adsorption by the BG-HHM (wood)

Table B.35 0.5 h carbon loading data for ANTA adsorption by WPC (coconut) in Lake Erie water

Sample	Carbon dose (mg/L)	Equilibrium toxin concentration (µg/L)	Equilibrium Capacity, qe (µg/mg)
1	12.4	114.4	6.7
2	18.2	113.9	4.6
3	24.0	108.1	3.7
4	30.0	101.0	3.2
5	36.4	94.9	2.8
6	42.0	90.0	2.6
7	49.8	86.0	2.2

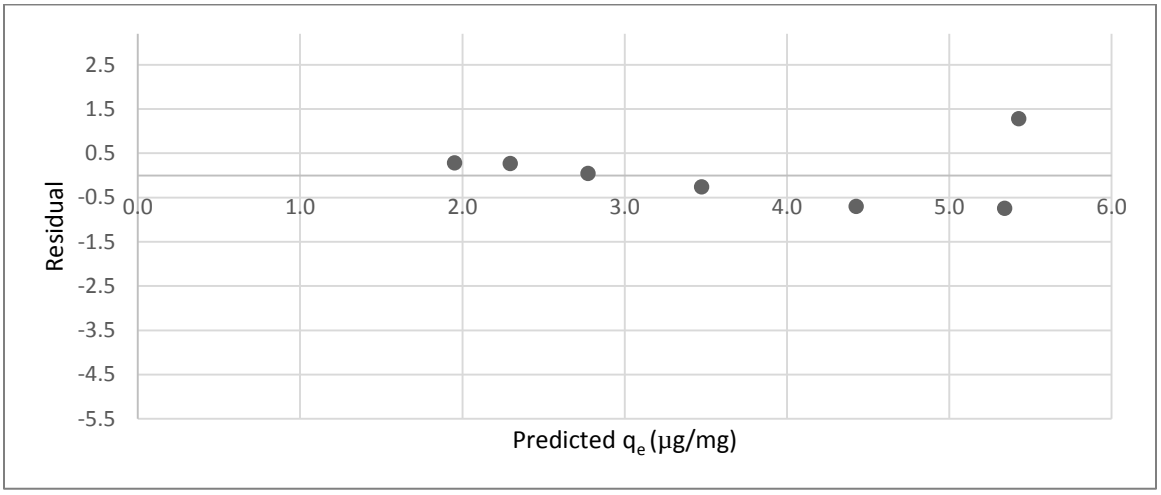

Figure B.45 Residual plot for the 0.5 h isotherm of ANTA adsorption by the WPC (coconut)

Table B.36 1.0 h carbon loading data for ANTA adsorption by WPC (coconut) in Lake Erie water

Sample	Carbon dose (mg/L)	Equilibrium toxin concentration (µg/L)	Equilibrium Capacity, qe (µg/mg)
1	12.4	112.6	6.9
2	18.2	96.3	5.6
3	24.0	88.8	4.5
4	30.0	73.5	4.1
5	36.4	63.9	3.7
6	42.0	57.2	3.3
7	49.8	50.6	3.0

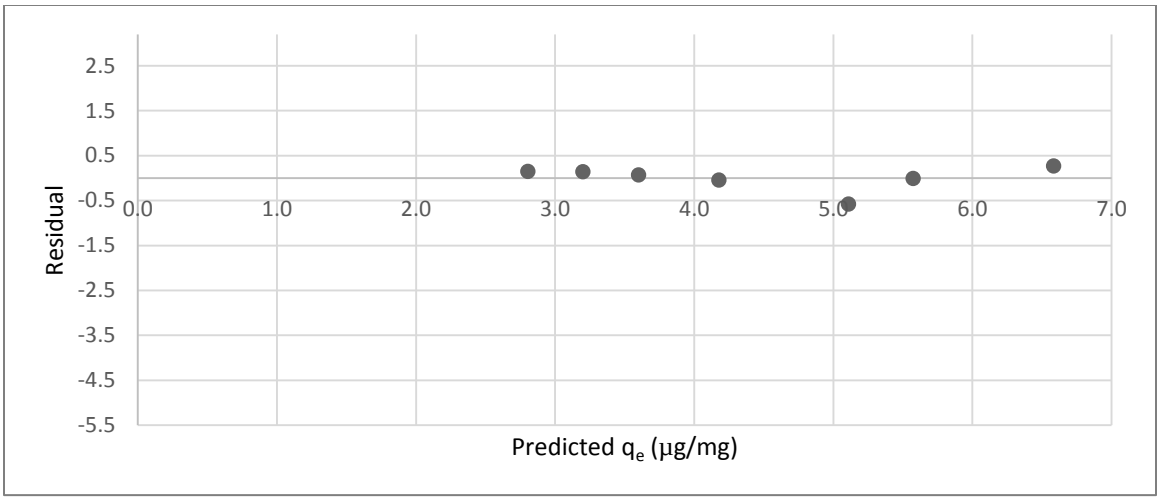

Figure B.46 Residual plot for the 1.0 h isotherm of ANTA adsorption by the WPC (coconut)

Table B.37 Equilibrium carbon loading data for ANTA adsorption by WPC (coconut) in Lake Erie water

Sample	Carbon dose (mg/L)	Equilibrium toxin concentration (µg/L)	Equilibrium Capacity, qe (µg/mg)
1	12.4	43.2	12.5
2	18.2	22.1	9.6
3	24.0	14.8	7.6
4	30.0	11.0	6.2
5	36.4	8.7	5.2
6	42.0	6.6	4.5
7	49.8	5.6	3.9

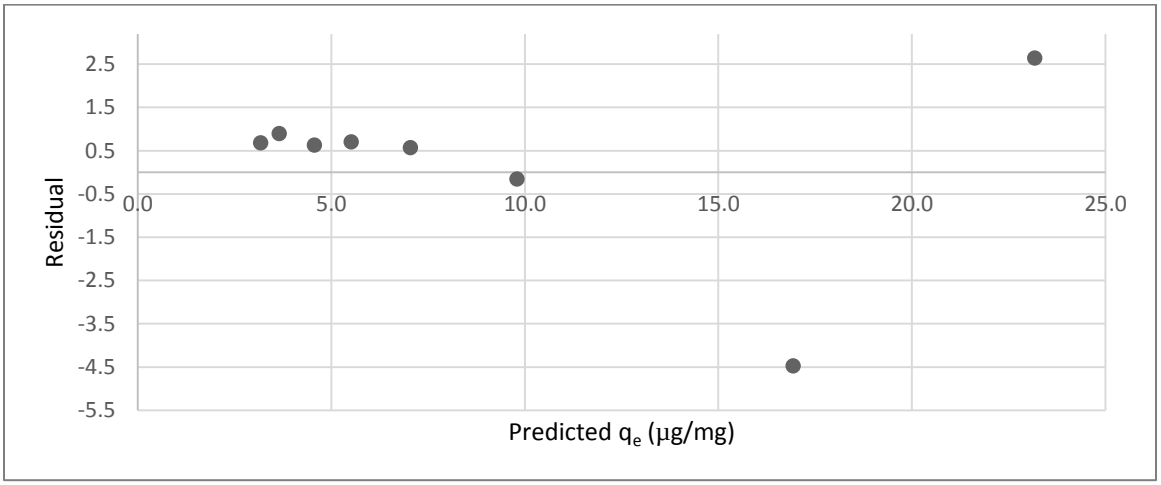

Figure B.47 Residual plot for the equilibrium isotherm of ANTA adsorption by the WPC (coconut)

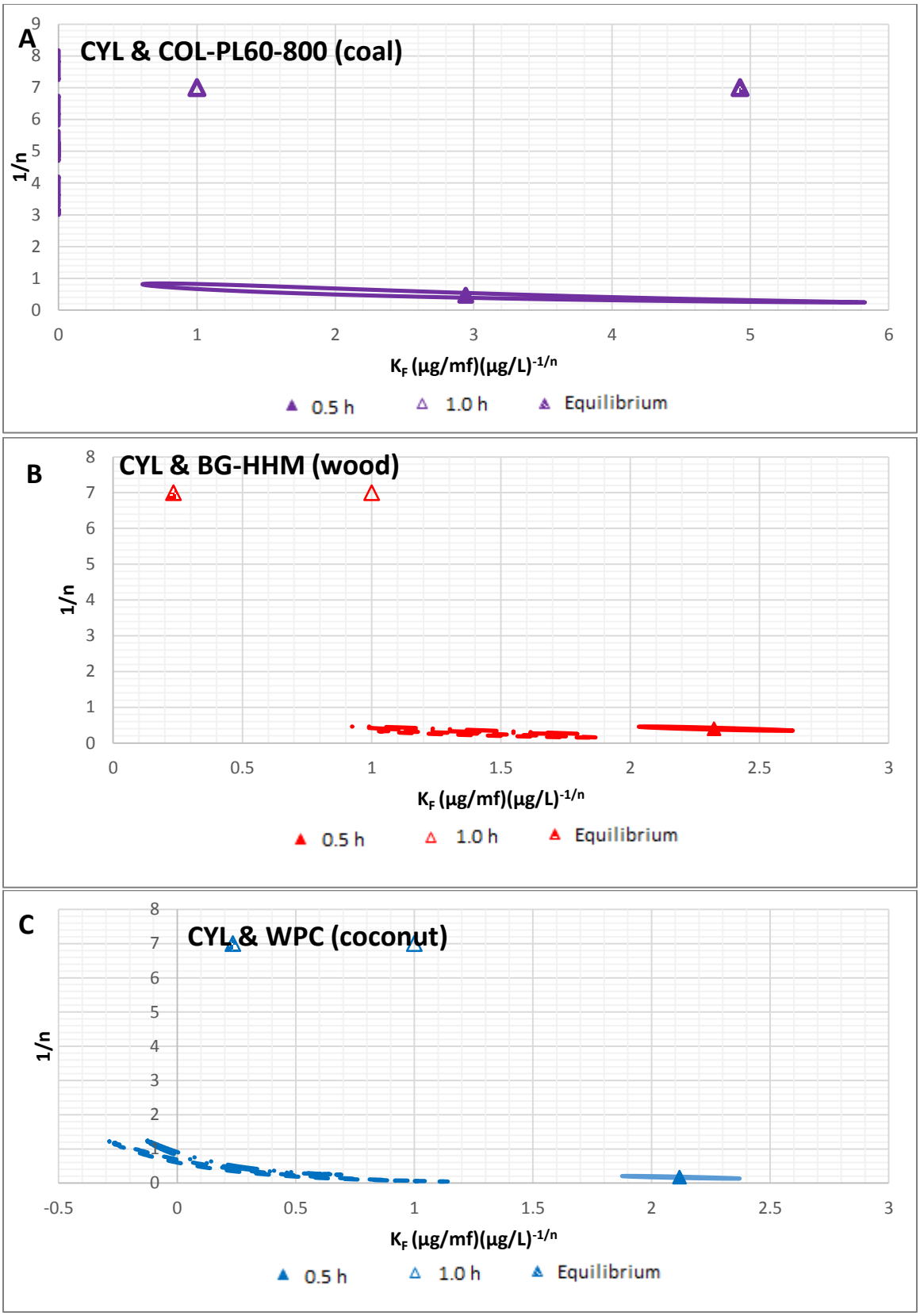

Figure B.48 JCRs of CYL adsorption in Lake Erie water under equilibrium and non-equilibrium conditions, using A) coal-, B) wood-, C) coconut-based PACs

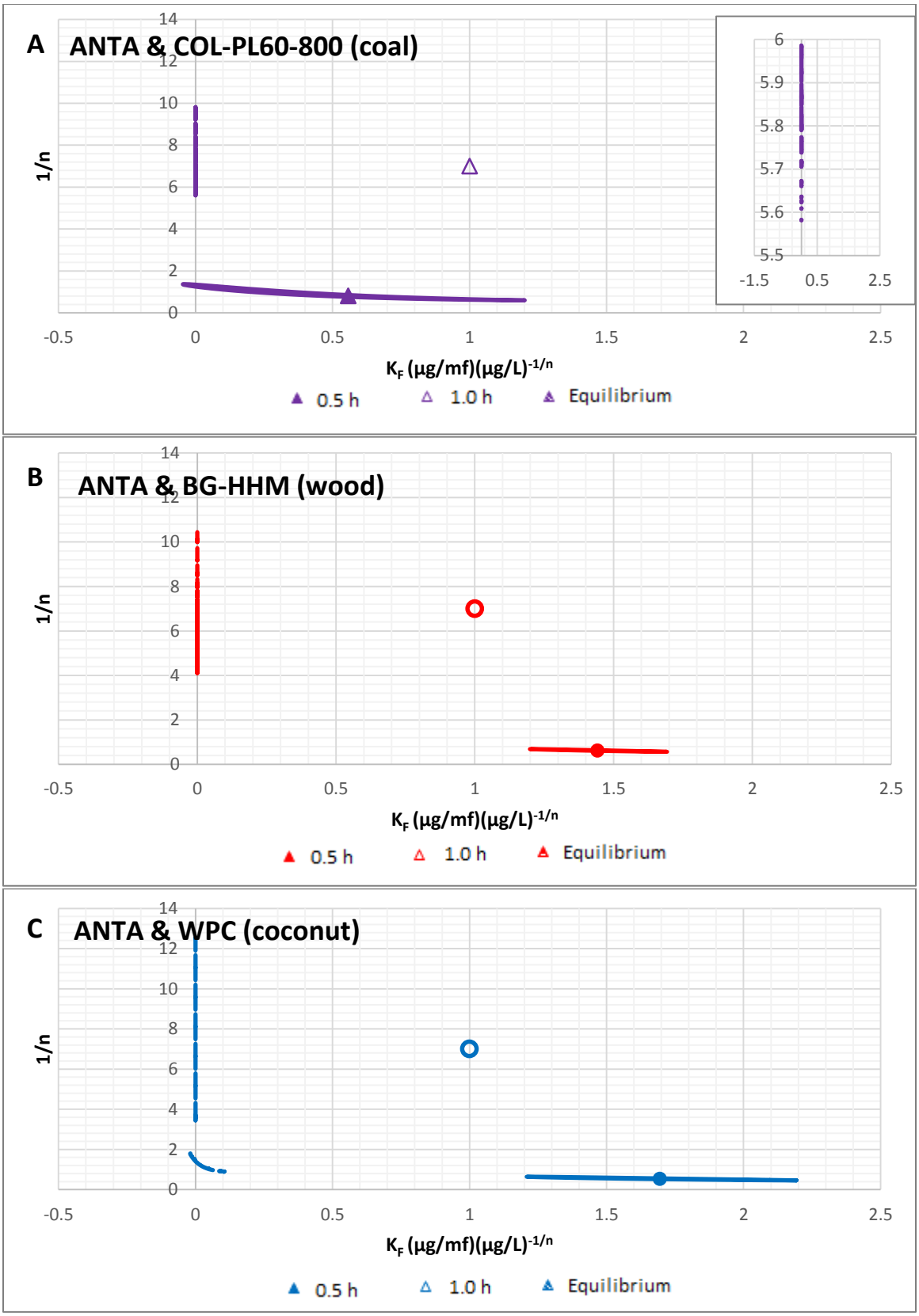

Figure B.49 JCRs of ANTA adsorption in Lake Erie water under equilibrium and non-equilibrium conditions, using A) coal-, B) wood-, C) coconut-based PACs

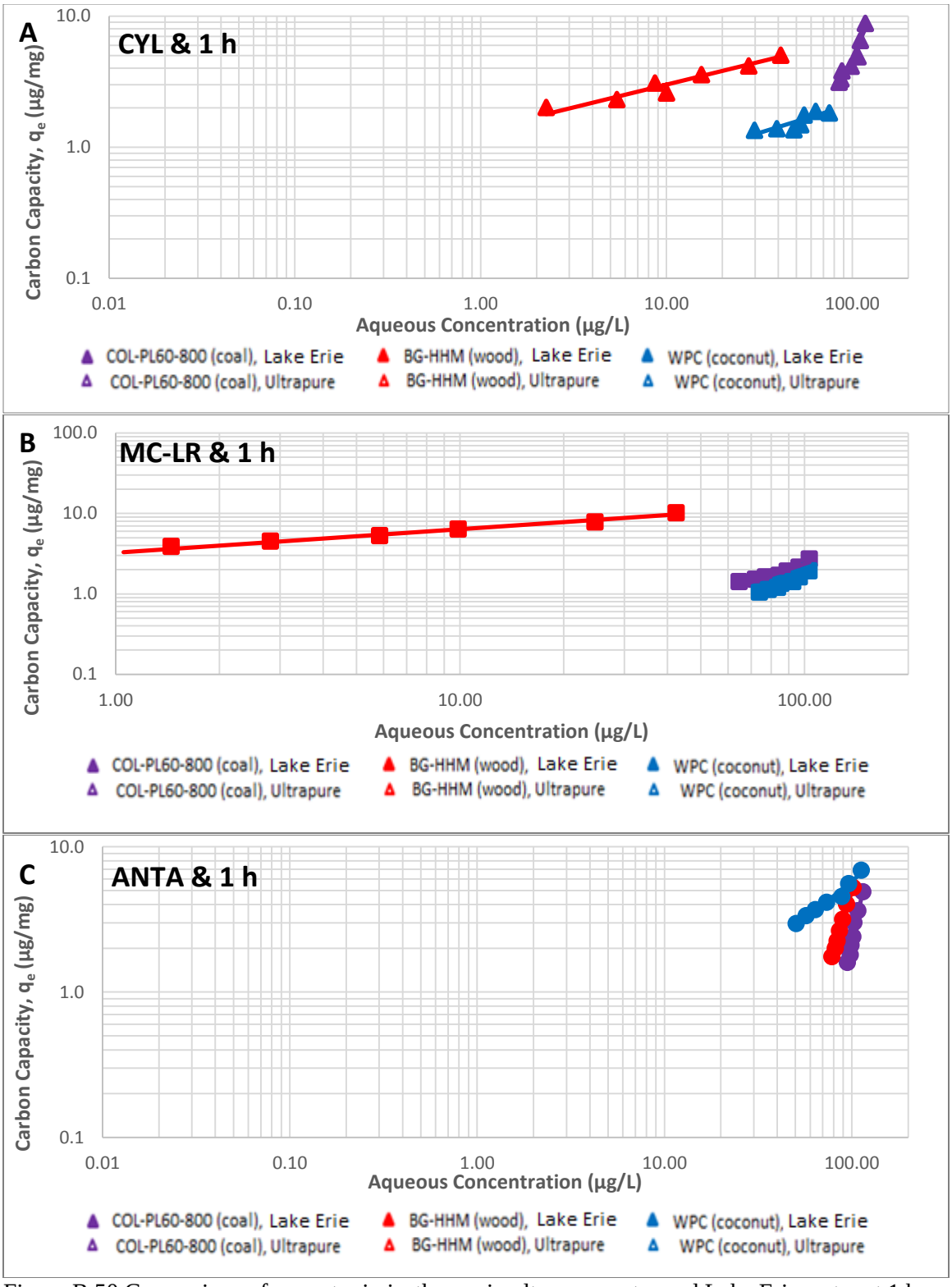

Figure B.50 Comparison of cyanotoxin isotherms in ultrapure water and Lake Erie water at 1 h. A) CYL, B) MC-LR, and C) ANTA

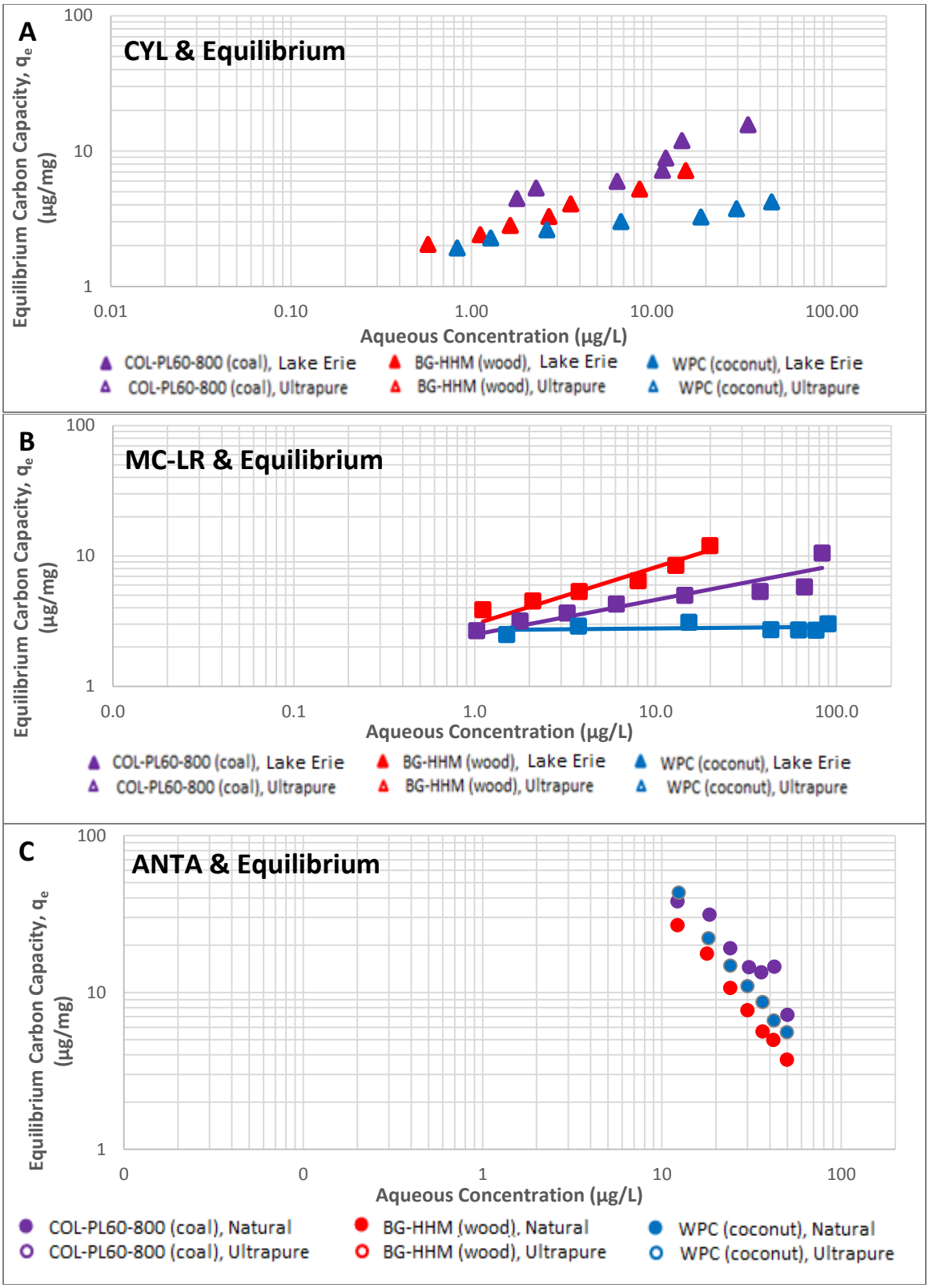

Figure B.51 Comparison of cyanotoxin isotherms in ultrapure and Lake Erie water at equilibrium. A) CYL, B) MC-LR, and C) ANTA

Appendix B.3 SEBCM

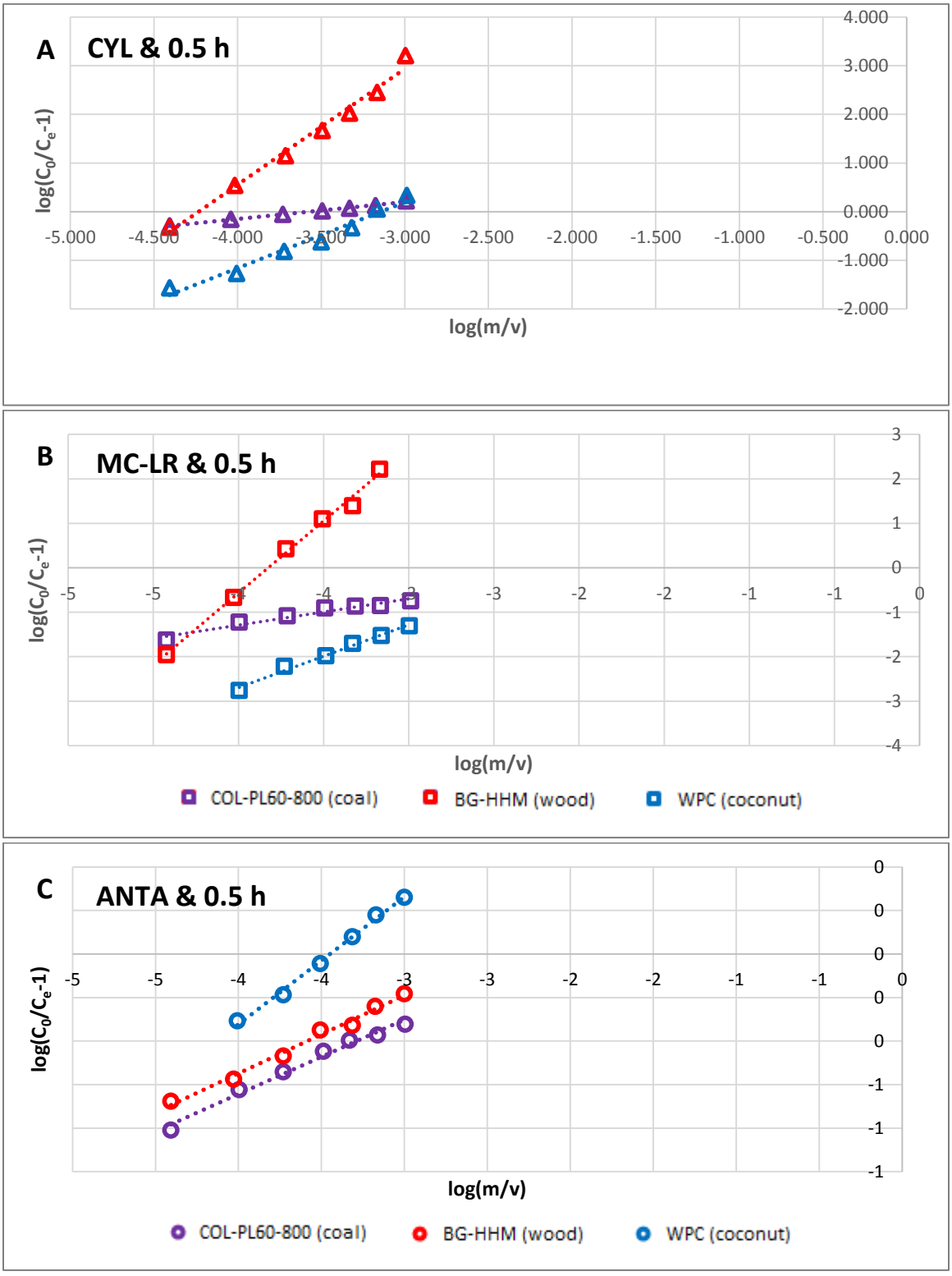

Figure B.52 SEBCM model fitting using the 0.5 h carbon loading data for the adsorption of A) CYL, B) MC-LR, and C) ANTA in Lake Erie water

Table B.38 SEBCM fitting parameters using the 0.5 h carbon loading data for the adsorption of CYL, MC-LR, and ANTA in Lake Erie Water

Cyanotoxin	PAC	lnA	$1/n_1$	R^2
CYL	COL-PL60-800 (coal)	-1.246	2.87	0.995
	BG-HHM (wood)	-10.086	0.42	0.986
	WPC (coconut)	-4.264	0.74	0.971
MC-LR	COL-PL60-800 (coal)	-1.082	1.69	0.951
	BG-HHM (wood)	-12.395	0.31	0.994
	WPC (coconut)	-2.959	0.71	0.987
ANTA	COL-PL60-800 (coal)	-0.725	2.92	0.985
	BG-HHM (wood)	-0.885	2.79	0.989
	WPC (coconut)	-2.020	1.71	0.995

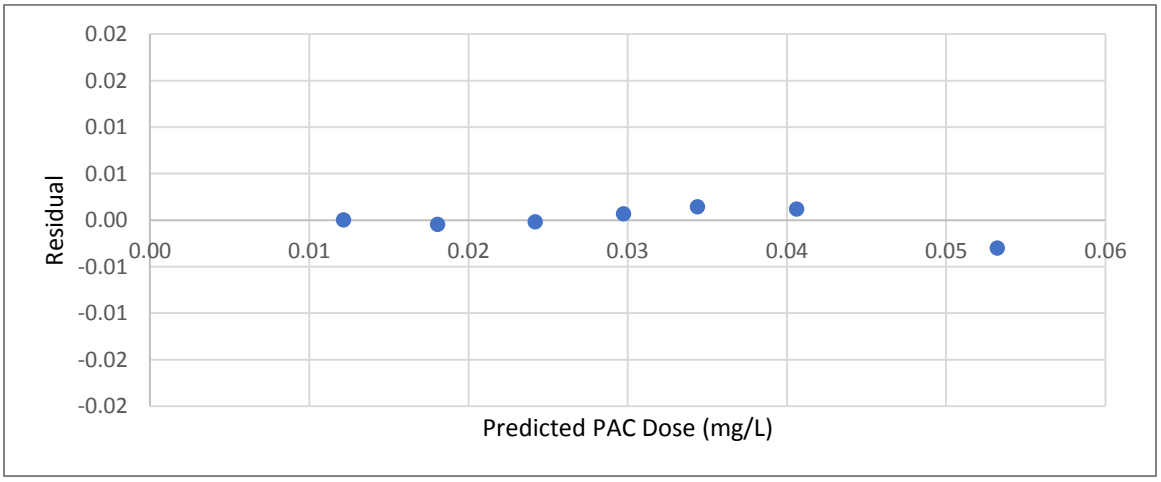

Figure B.53 Residual plot for 0.5 h SEBCM fitting of CYL adsorption by the COL-PL60-800 (coal)

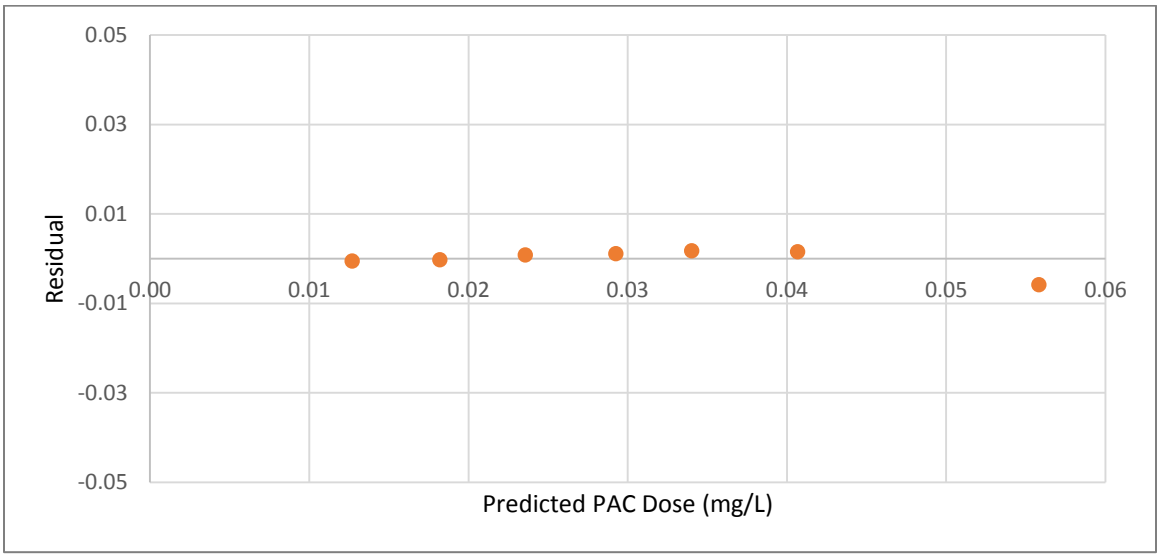

Figure B.54 Residual plot for 0.5 h SEBCM fitting of CYL adsorption by the BG-HHM (wood)

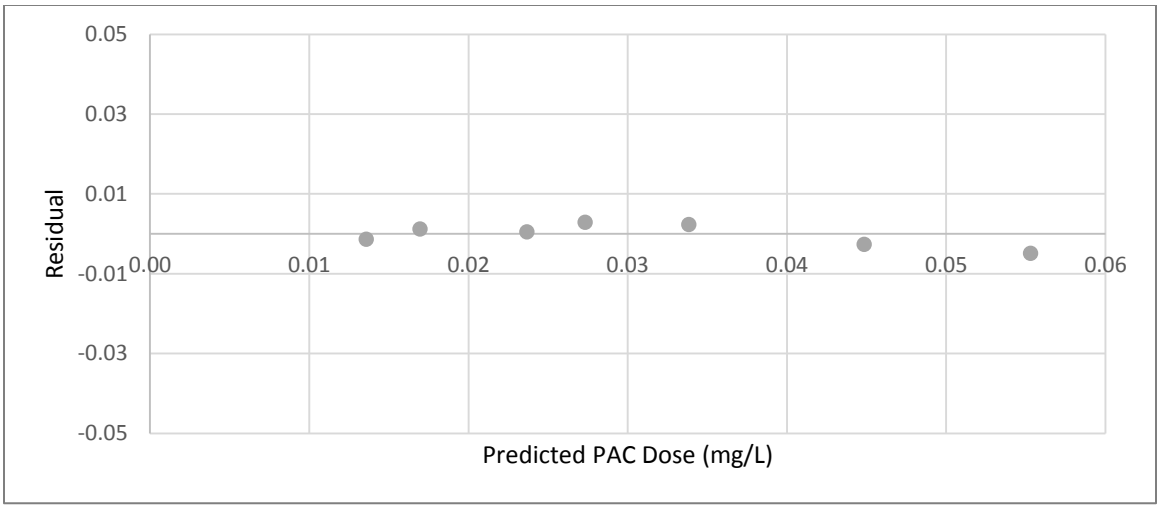

Figure B.55 Residual plot for 0.5 h SEBCM fitting of CYL adsorption by the WPC (coconut)

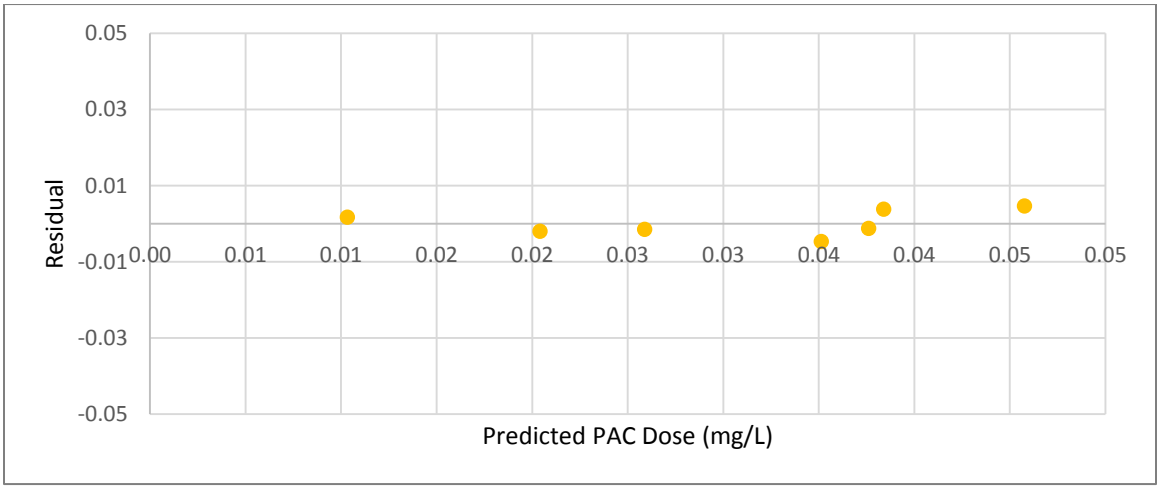

Figure B.56 Residual plot for 0.5 h SEBCM fitting of MC-LR adsorption by the COL-PL60-800 (coal)

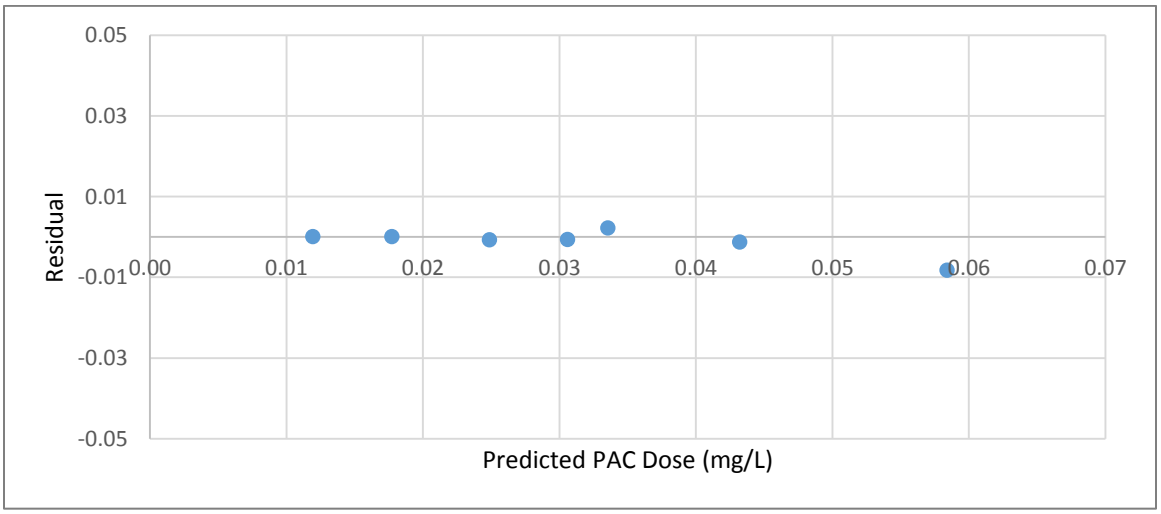

Figure B.57 Residual plot for 0.5 h SEBCM fitting of MC-LR adsorption by the BG-HHM (wood)

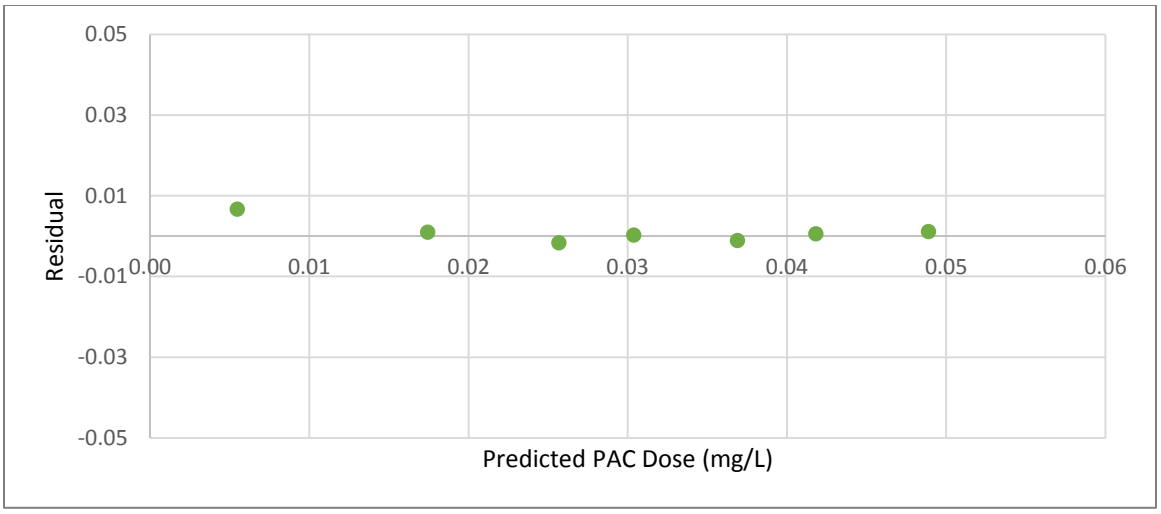

Figure B.58 Residual plot for 0.5 h SEBCM fitting of MC-LR adsorption by the WPC (coconut)

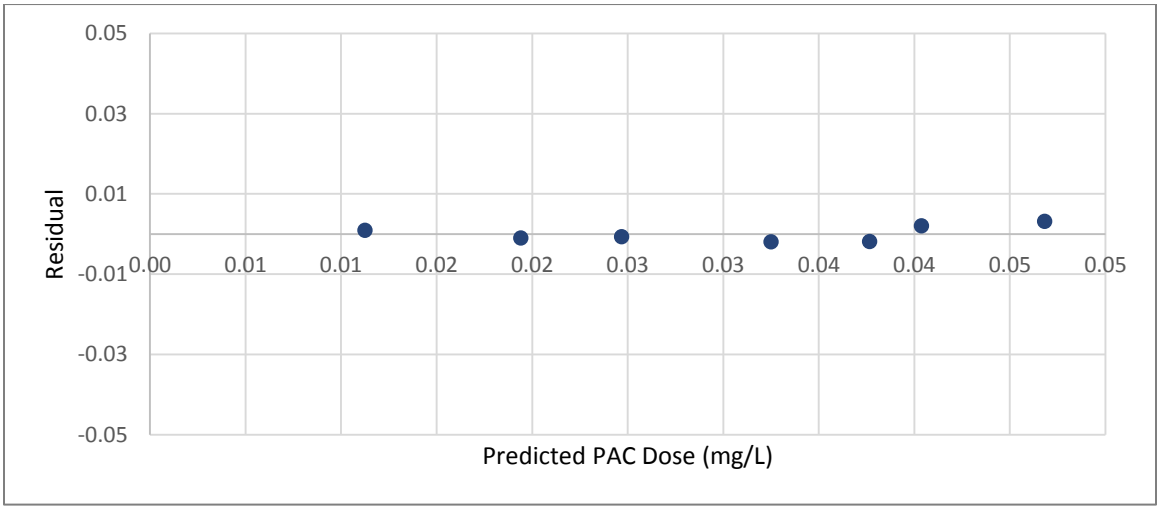

Figure B.59 Residual plot for 0.5 h SEBCM fitting of ANTA adsorption by the COL-PL60-800 (coal)

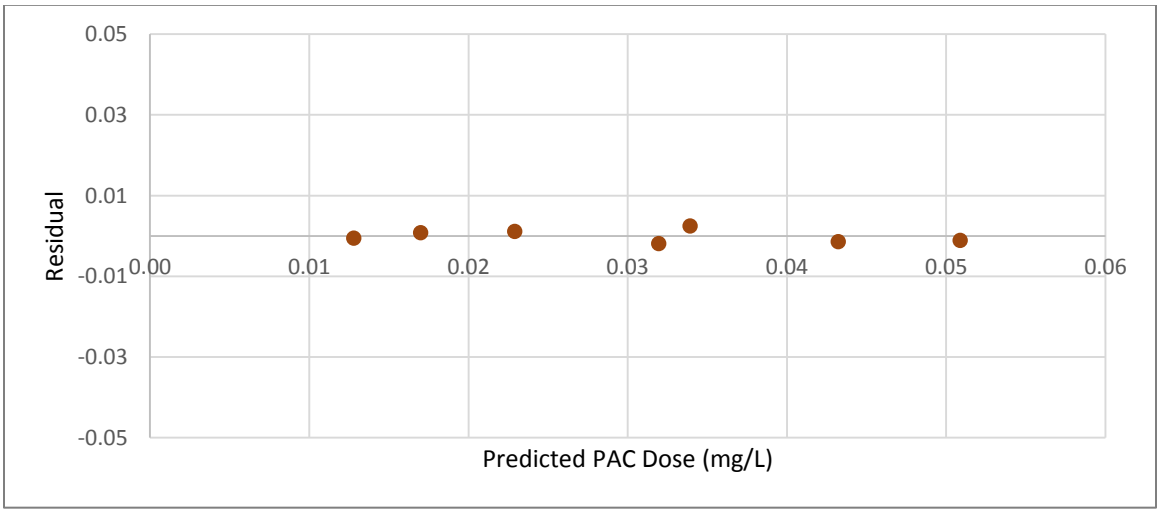

Figure B.60 Residual plot for 0.5 h SEBCM fitting of ANTA adsorption by the BG-HHM (wood)

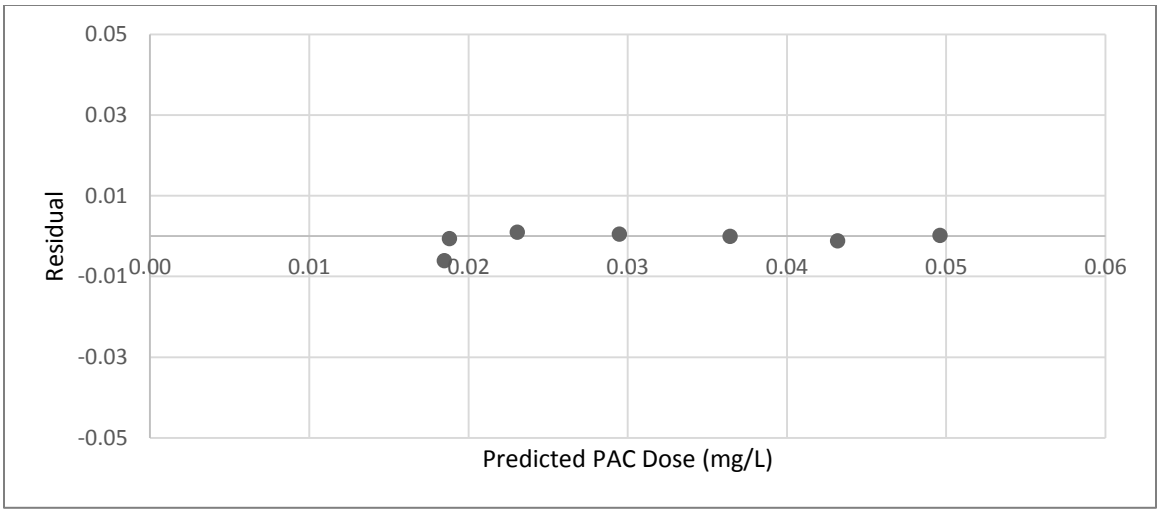

Figure B.61 Residual plot for 0.5 h SEBCM fitting of ANTA adsorption by the WPC (coconut)

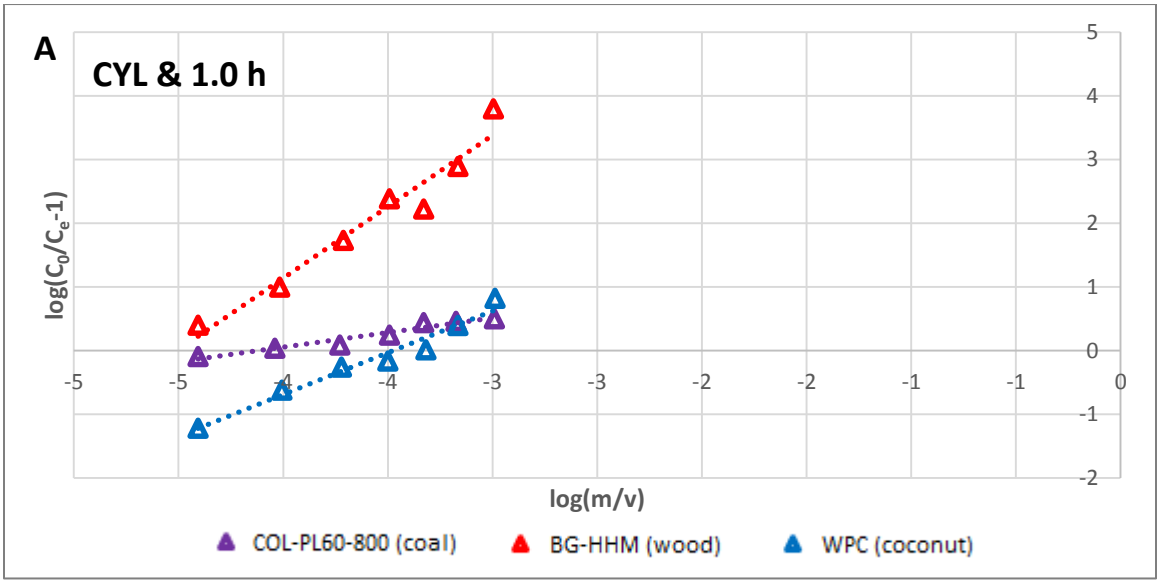

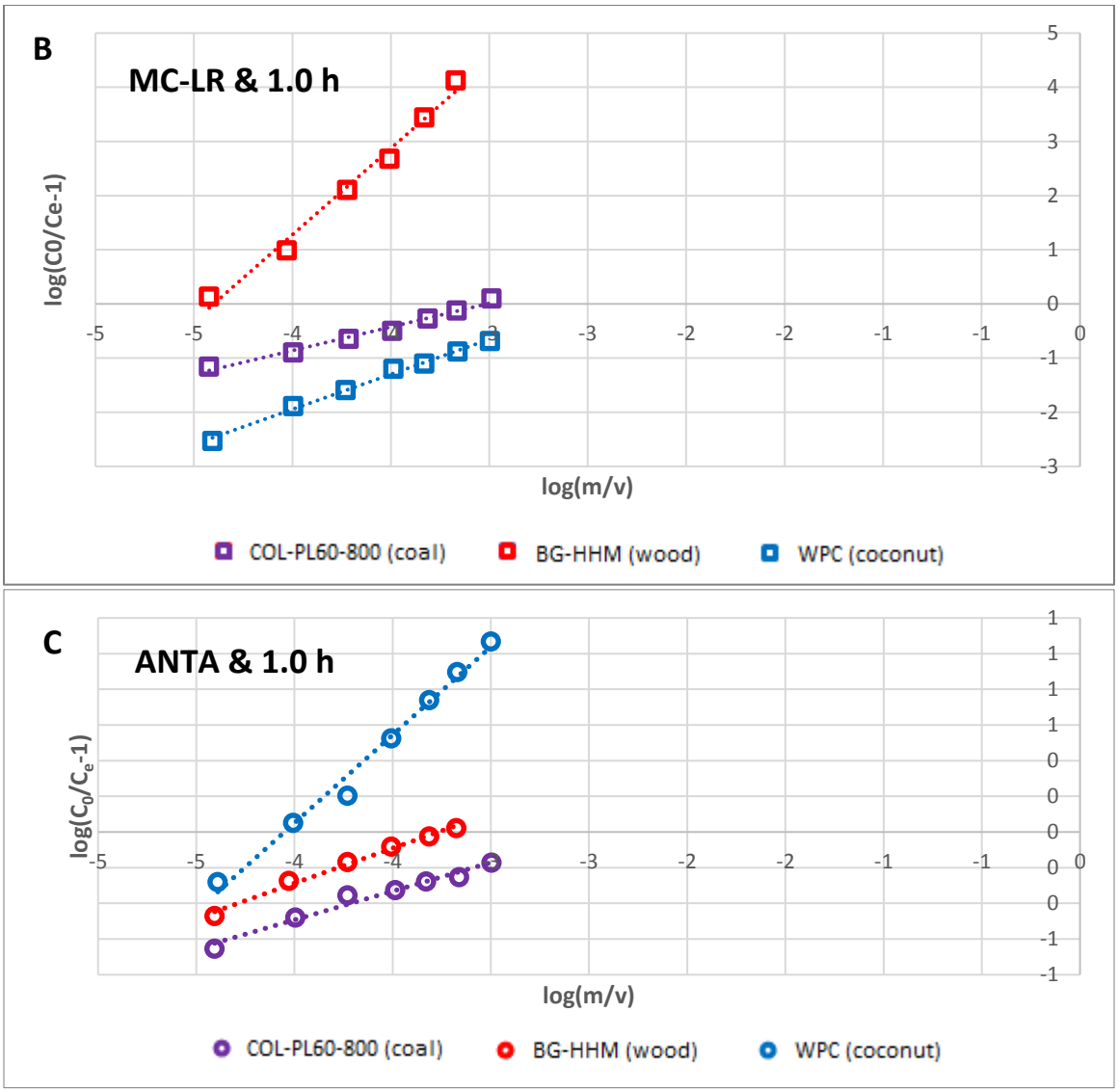

Figure B.62 SEBCM model fitting on the 1h carbon loading data for the adsorption of A) CYL, B) MC-LR, and C) ANTA in Lake Erie water

Table B.39 SEBCM fitting parameters using the 1.0 h carbon loading data for the adsorption of CYL, MC-LR, and ANTA in Lake Erie Water

Cyanotoxin	PAC	lnA	$1/n_1$	R^2
CYL	COL-PL60-800 (coal)	-1.888	2.18	0.944
	BG-HHM (wood)	-10.114	0.45	0.948
	WPC (coconut)	-4.555	0.76	0.963
MC-LR	COL-PL60-800 (coal)	-2.627	1.15	0.983
	BG-HHM (wood)	-14.040	0.31	0.986
	WPC (coconut)	-3.224	0.77	0.993
ANTA	COL-PL60-800 (coal)	-0.794	3.11	0.971
	BG-HHM (wood)	-1.282	2.55	0.990
	WPC (coconut)	-4.002	1.01	0.988

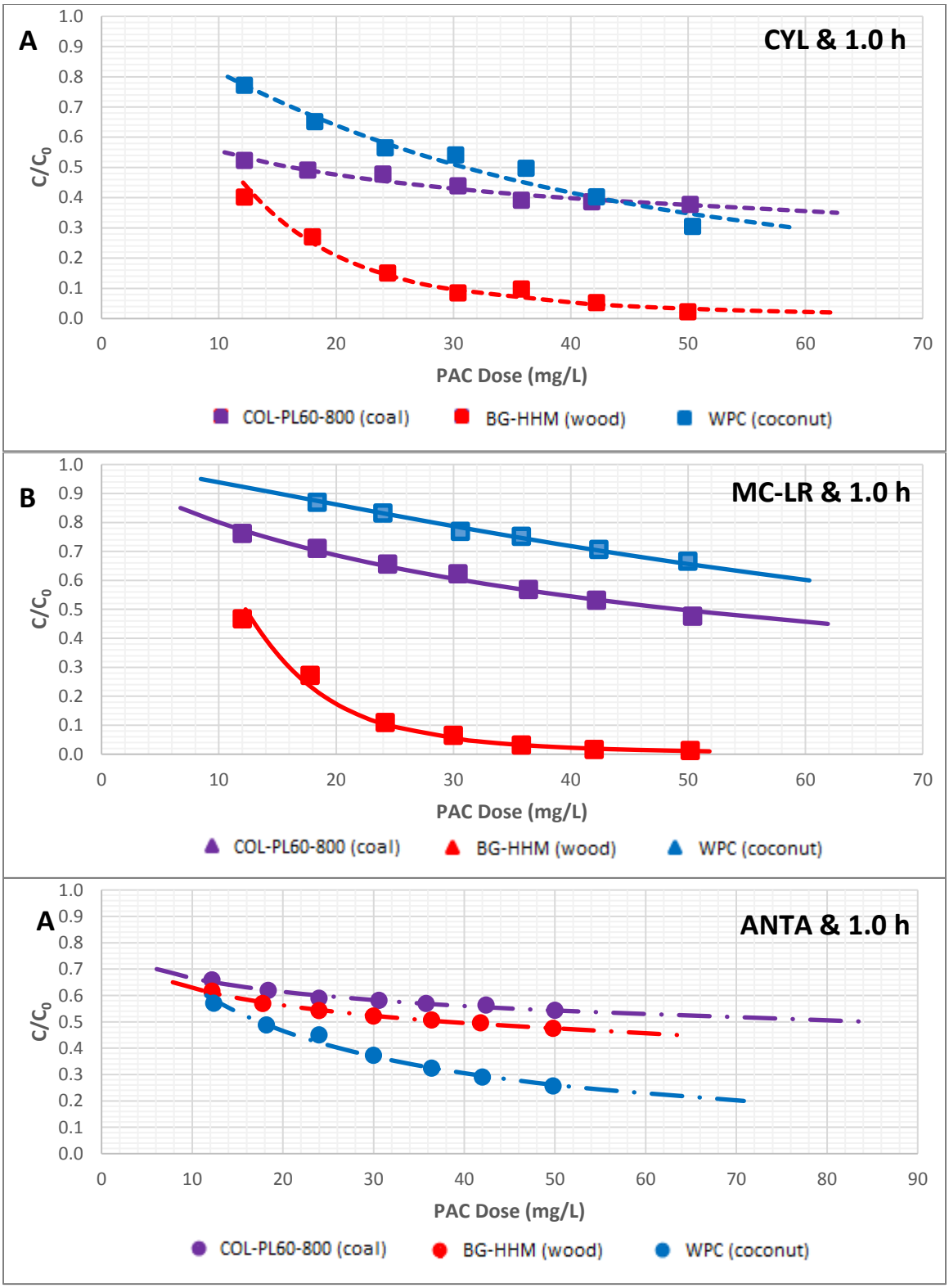

Figure B.63 Cyanotoxin adsorption in the presence of NOM in Lake Erie water using coal-, wood-, and coconut-based PACs, based on the 1 h non-equilibrium data. A) CYL adsorption, B) MC-LR adsorption, C) ANTA adsorption

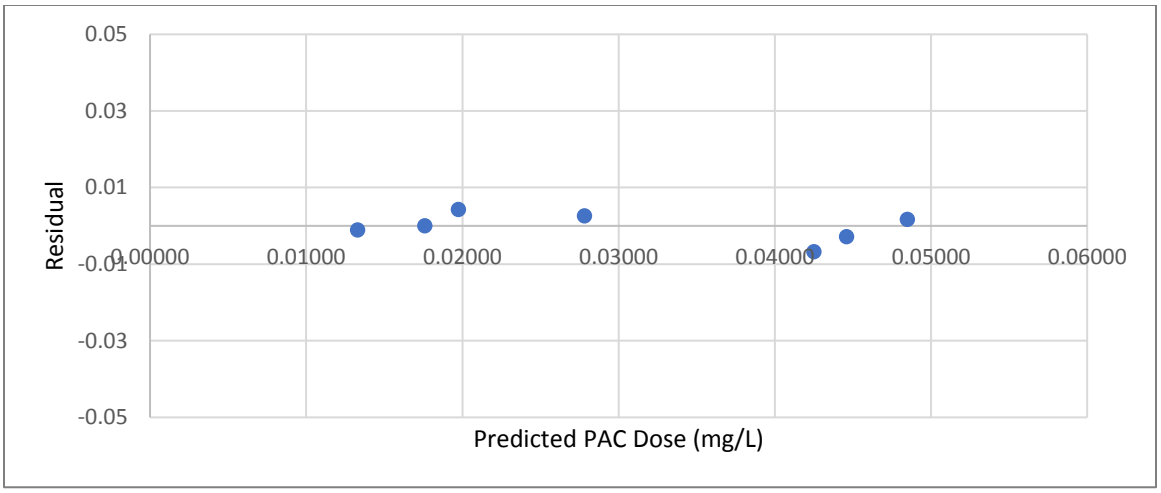

Figure B.64 Residual plot for 1.0 h SEBCM fitting of CYL adsorption by the COL-PL60-800 (coal)

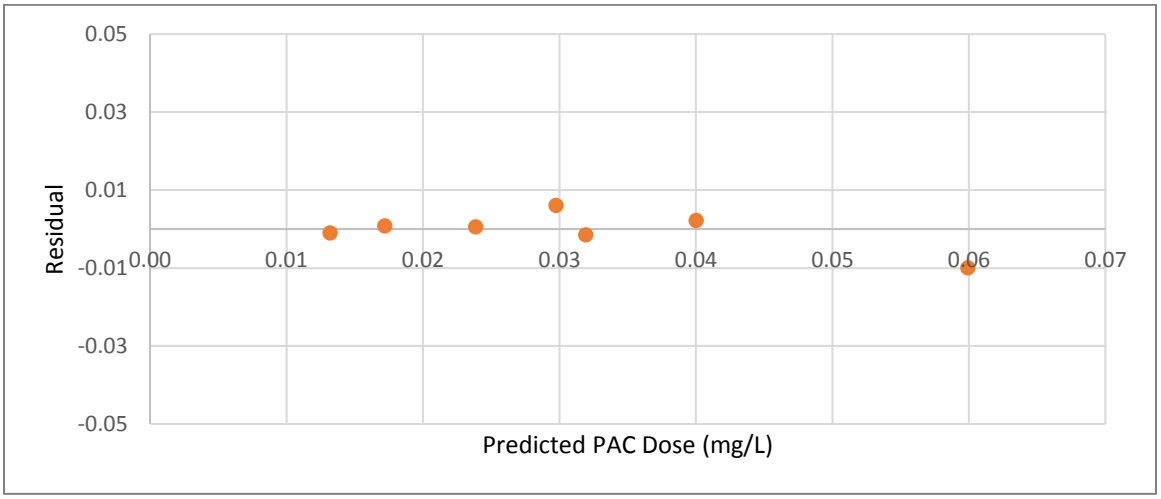

Figure B.65 Residual plot for 1.0 h SEBCM fitting of CYL adsorption by the BG-HHM (wood)

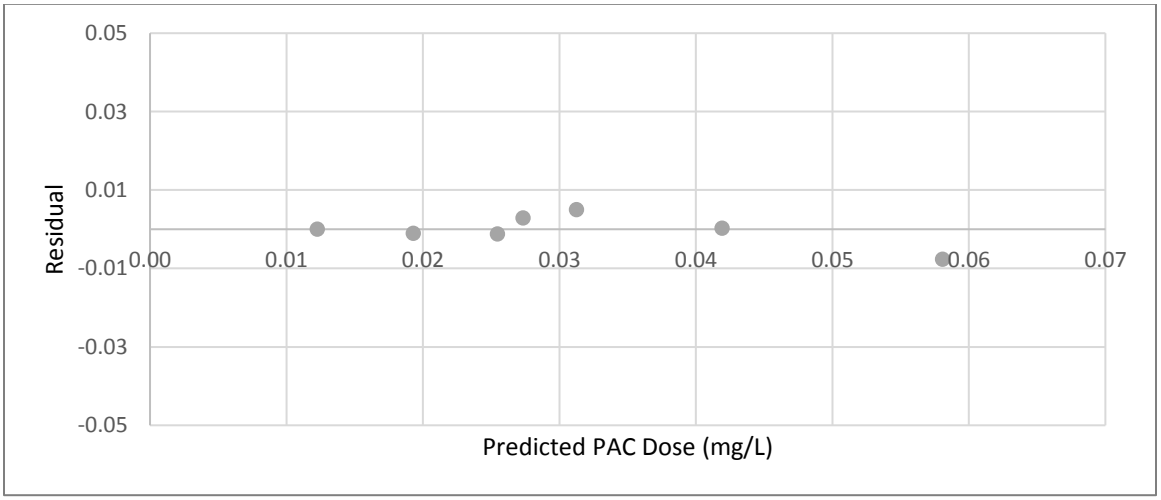

Figure B.66 Residual plot for 1.0 h SEBCM fitting of CYL adsorption by the WPC (coconut)

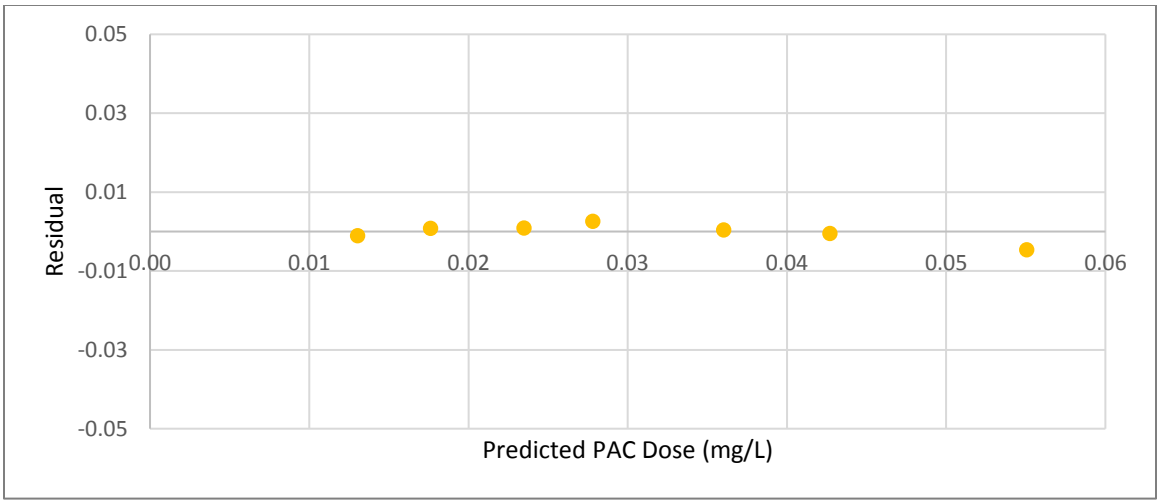

Figure B.67 Residual plot for 1.0 h SEBCM fitting of MC-LR adsorption by the COL-PL60-800 (coal)

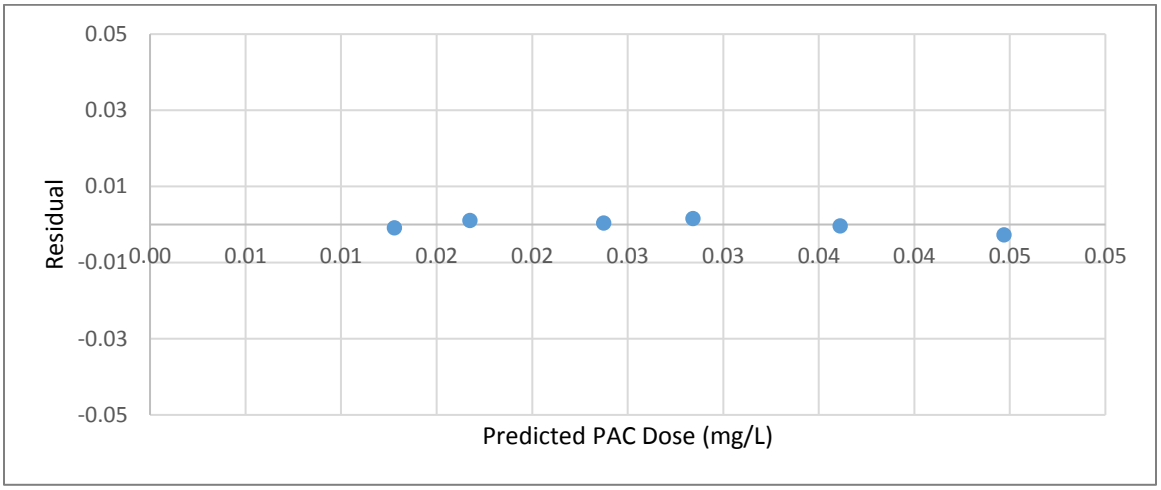

Figure B.68 Residual plot for 1.0 h SEBCM fitting of MC-LR adsorption by the BG-HHM (wood)

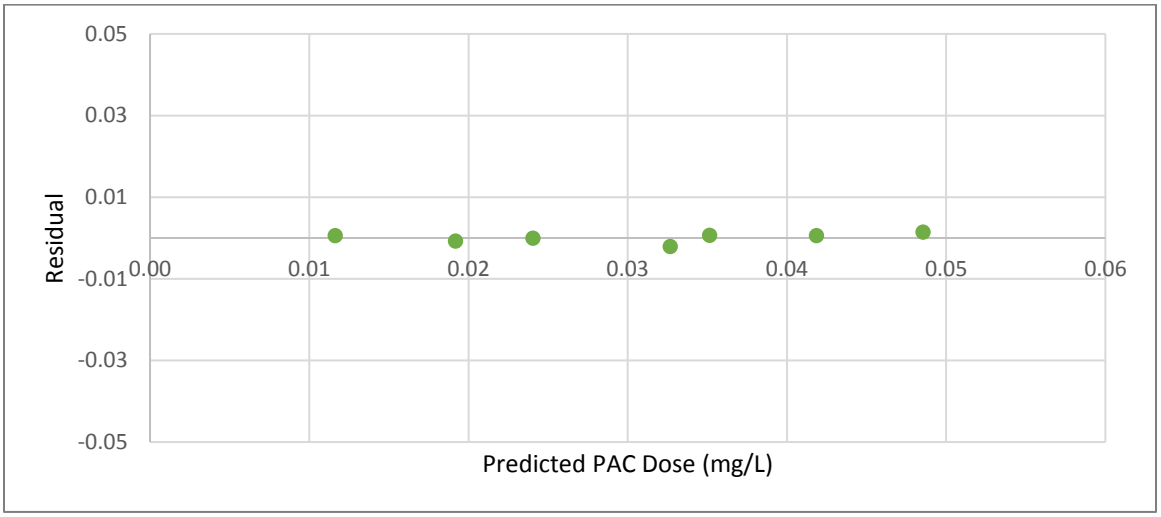

Figure B.69 Residual plot for 1.0 h SEBCM fitting of MC-LR adsorption by the WPC (coconut)

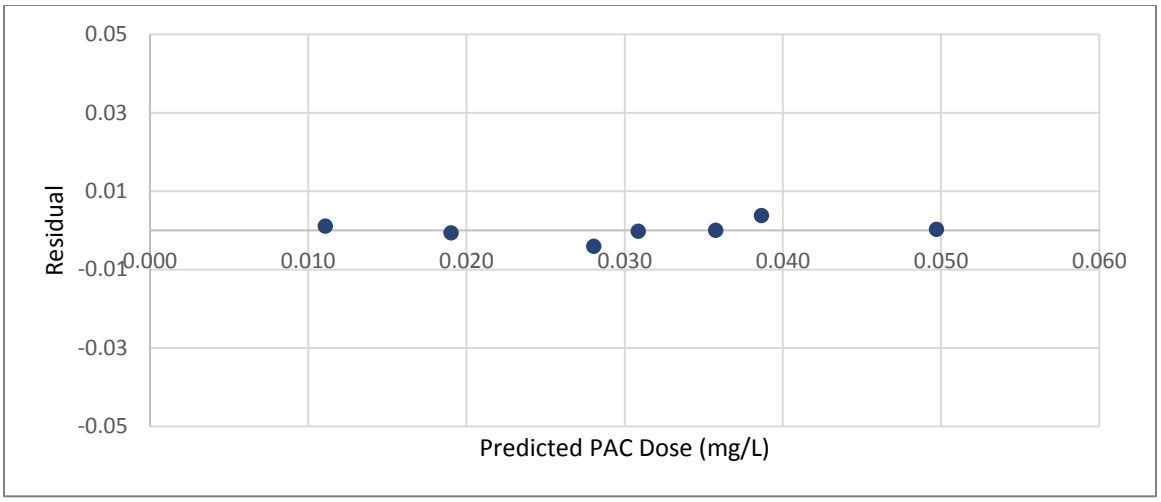

Figure B.70 Residual plot for 1.0 h SEBCM fitting of ANTA adsorption by the COL-PL60-800 (coal)

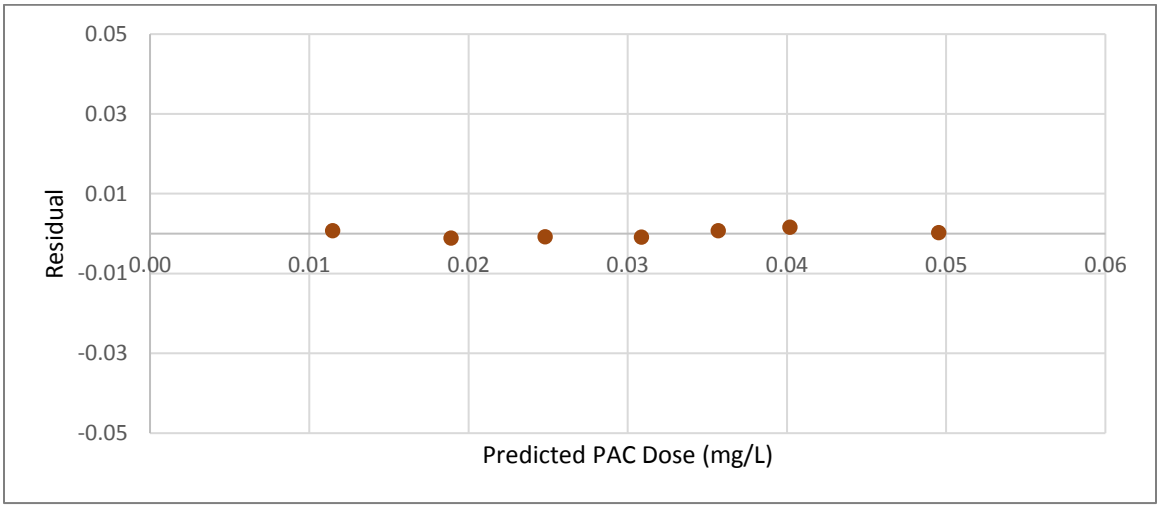

Figure B.71 Residual plot for 1.0 h SEBCM fitting of ANTA adsorption by the BG-HHM (wood)

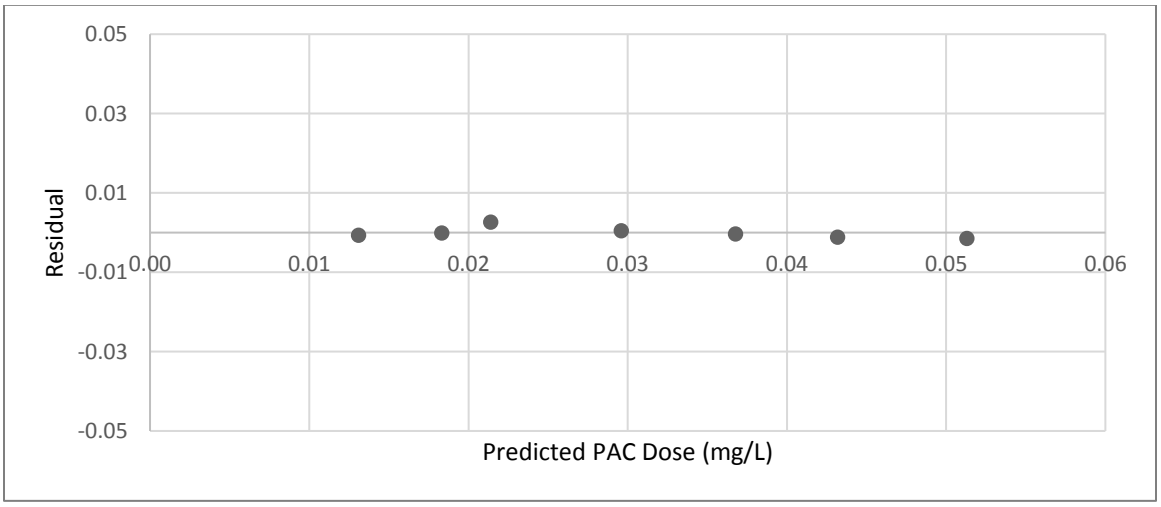

Figure B.72 Residual plot for 1.0 h SEBCM fitting of ANTA adsorption by the WPC (coconut)

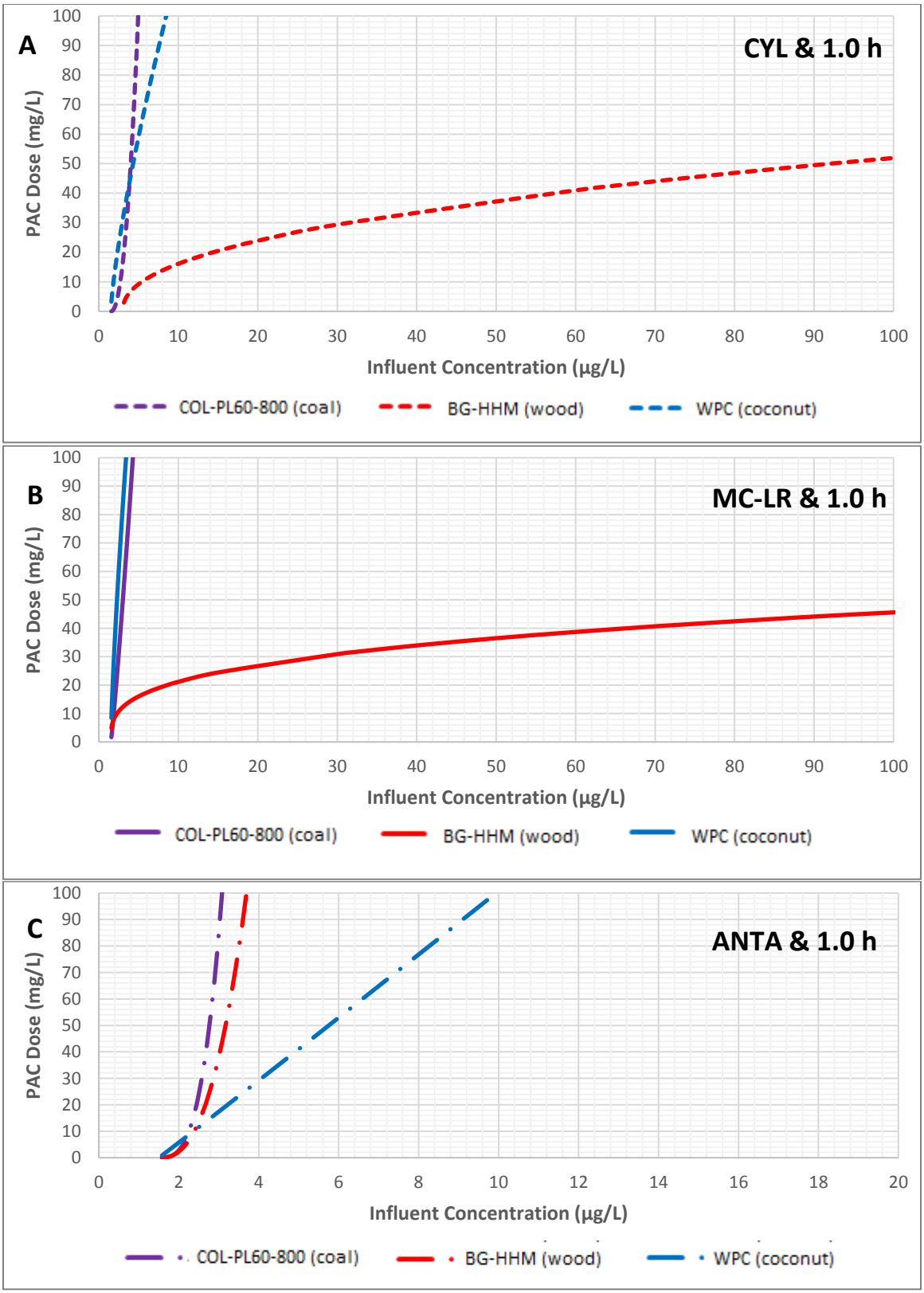

Figure B.73 Estimates of PAC dose for coal-, wood-, and coconut-based PACs for adsorption of A) CYL, B) MC-LR, and C) ANTA adsorption in Lake Erie water, based on SEBCM under 1 h non-equilibrium condition, given target concentration of 1.5 µg/L

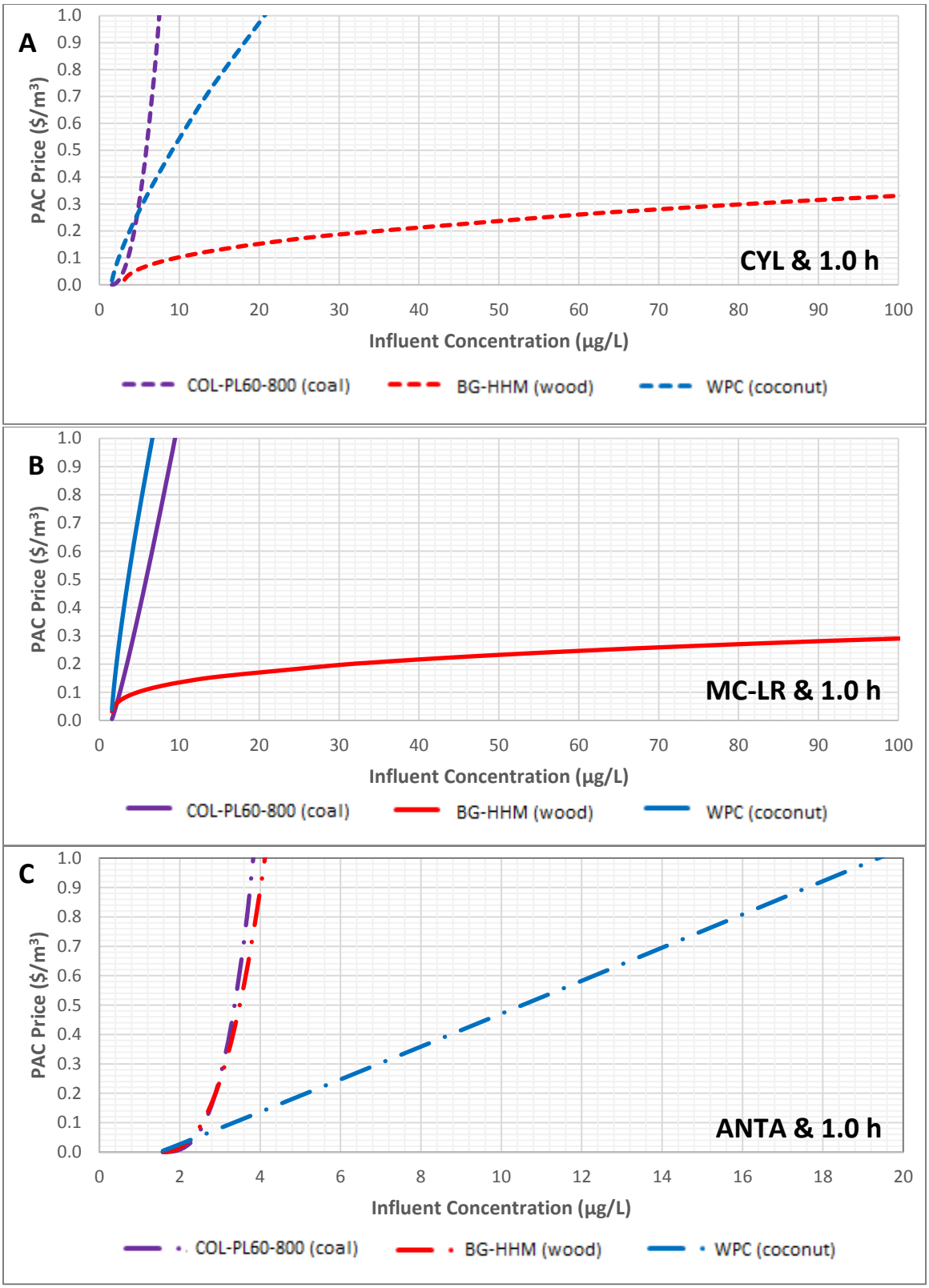

Figure B.74 Estimate of PAC costs for adsorption of cyanotoxins at influent concentrations in Lake Erie water, based on SEBCM under 1 h non-equilibrium conditions, given target cyanotoxin concentration of 1.5 µg/L. A) CYL adsorption, B) MC-LR adsorption, C) ANTA adsorption

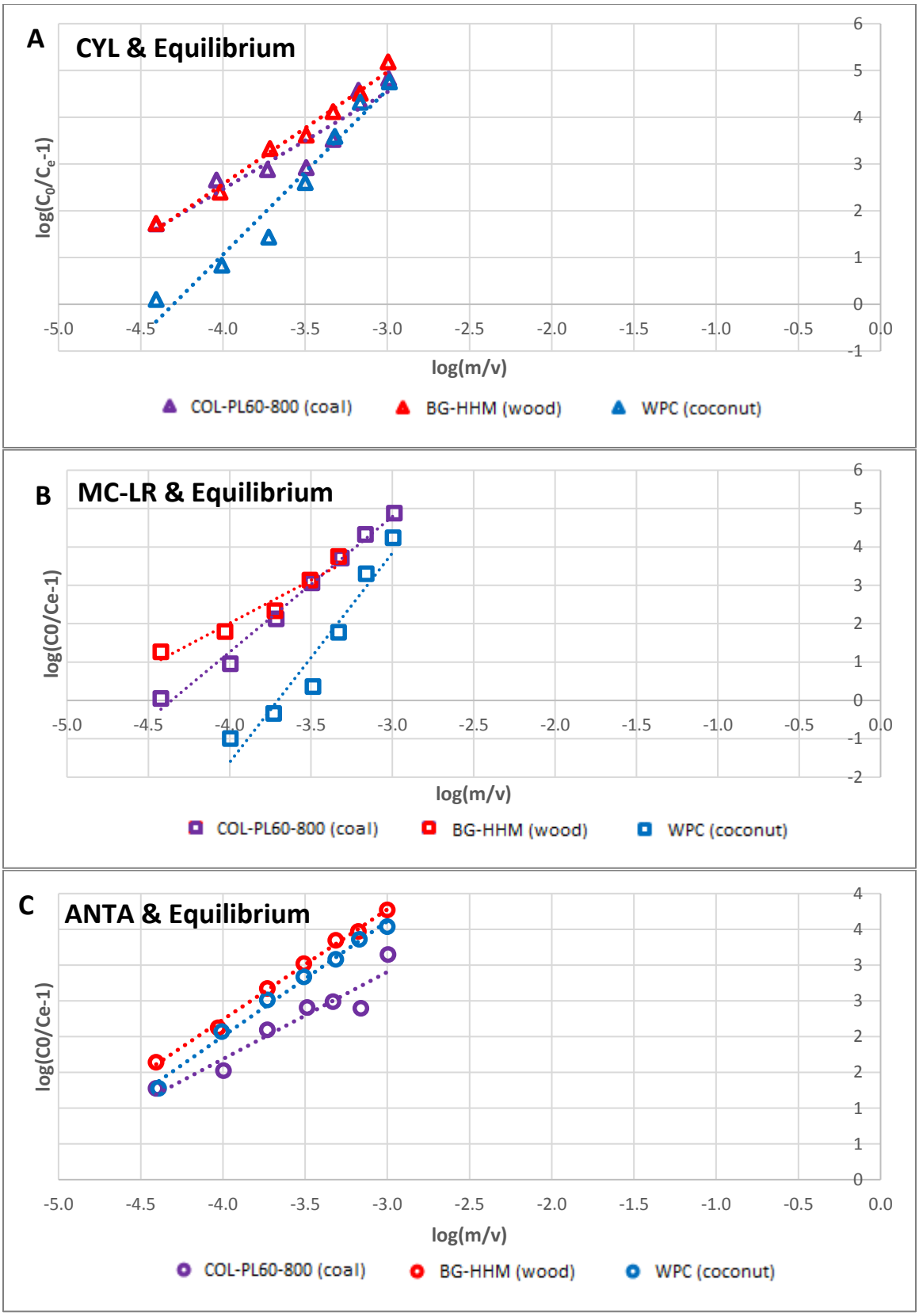

Figure B.75 SEBCM model fitting on the equilibrium carbon loading data for the adsorption of A) CYL, B) MC-LR, and C) ANTA in Lake Erie water

Table B.40 SEBCM fitting parameters using the equilibrium carbon loading data for the adsorption of CYL, MC-LR, and ANTA in Lake Erie Water

Cyanotoxin	PAC	lnA	1/n1	R2
CYL	COL-PL60-800 (coal)	-10.766	0.48	0.890
	BG-HHM (wood)	-12.156	0.42	0.987
	WPC (coconut)	-15.164	0.28	0.958
MC-LR	COL-PL60-800 (coal)	-15.388	0.28	0.988
	BG-HHM (wood)	-10.981	0.45	0.949
	WPC (coconut)	-20.204	0.18	0.935
ANTA	COL-PL60-800 (coal)	-6.556	0.82	0.914
	BG-HHM (wood)	-8.401	0.65	0.997
	WPC (coconut)	-8.437	0.62	0.992

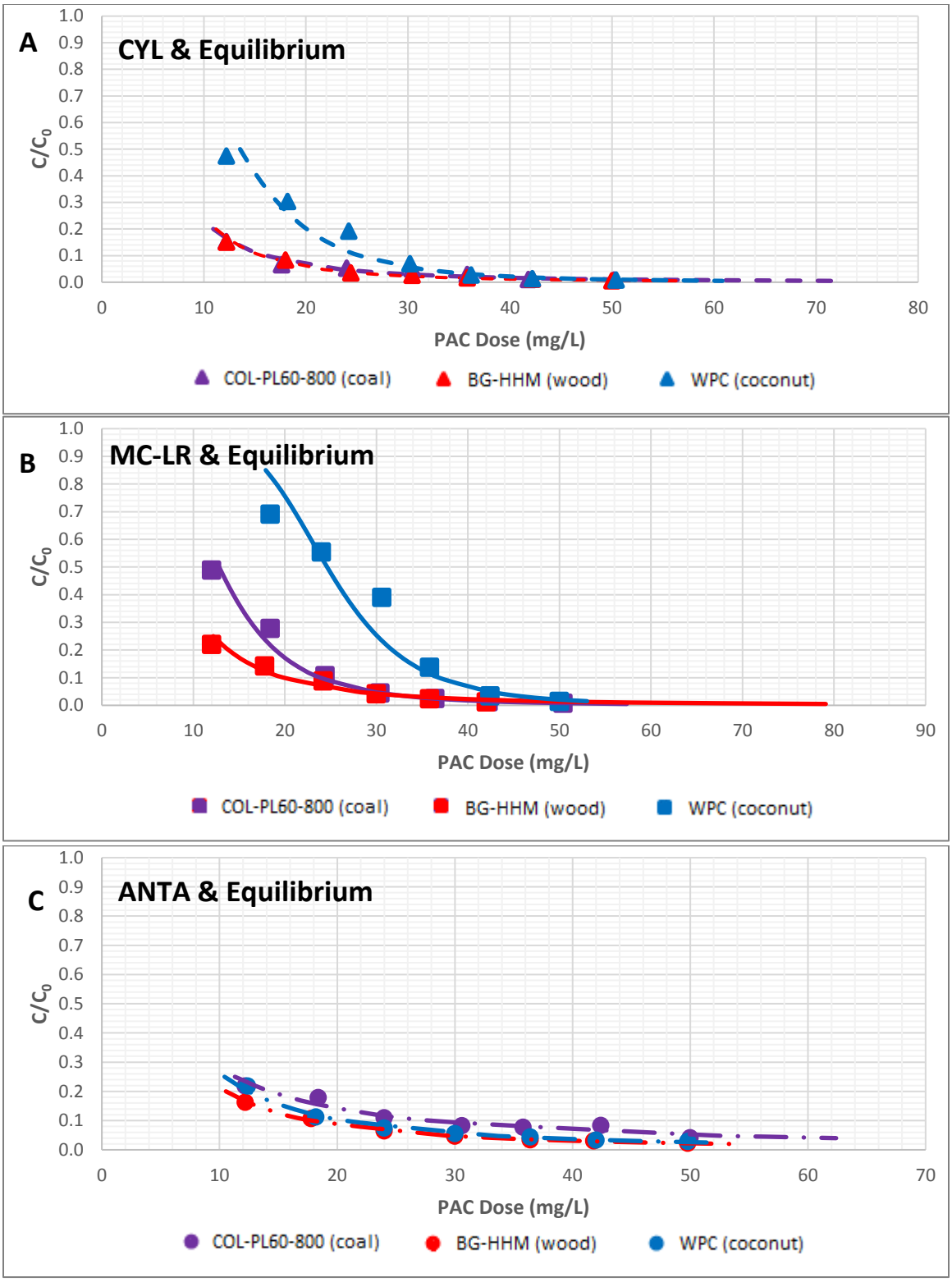

Figure B.76 Cyanotoxin adsorption in the presence of NOM in Lake Erie water using coal-, wood-, and coconut-based PACs, based on the equilibrium data. A) CYL adsorption, B) MC-LR adsorption, C) ANTA adsorption

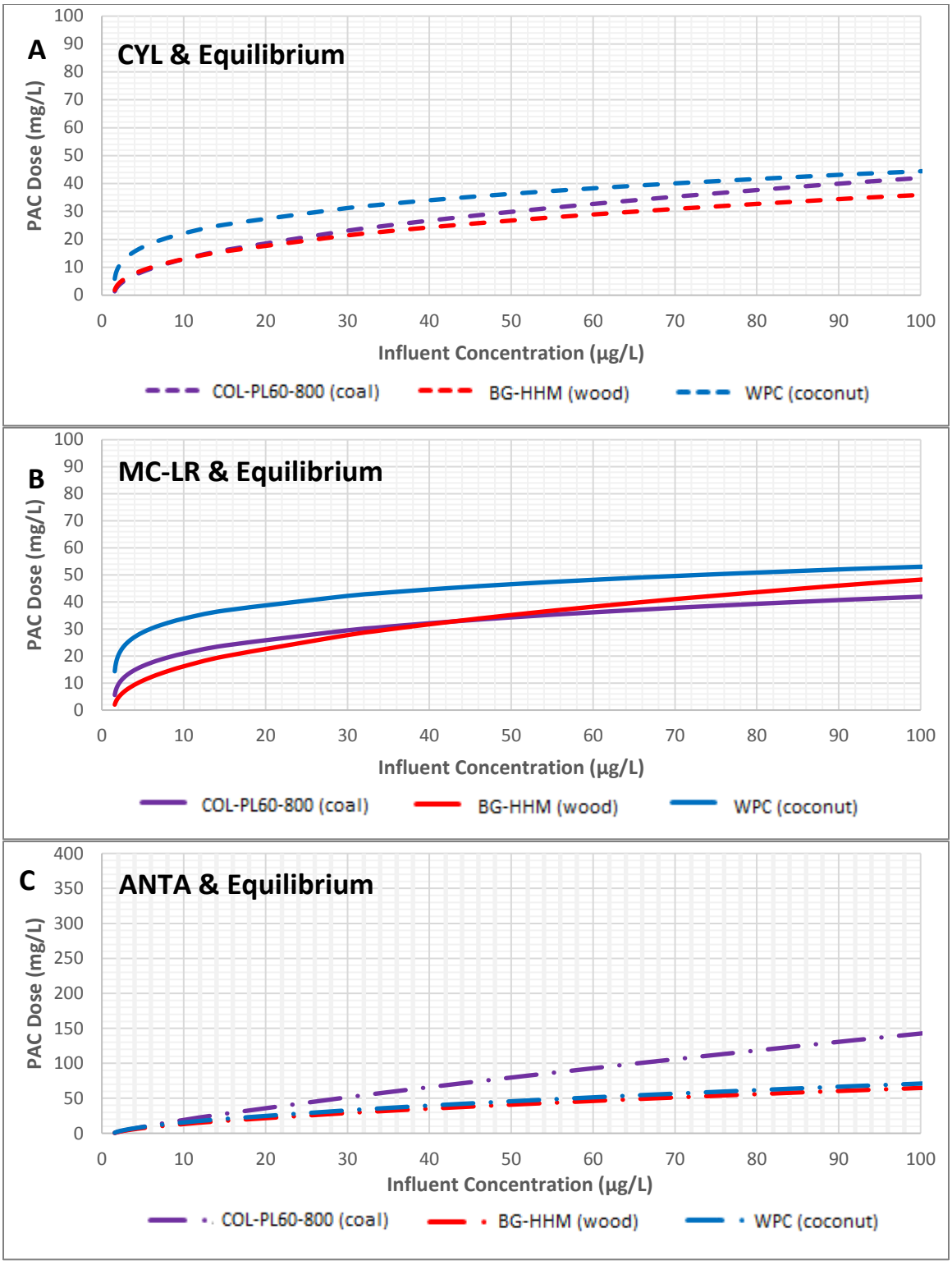

Figure B.77 Estimates of PAC dose for coal-, wood-, and coconut-based PACs for adsorption of A) CYL, B) MC-LR, and C) ANTA adsorption in Lake Erie water, based on SEBCM under equilibrium condition, given target concentration of 1.5 µg/L

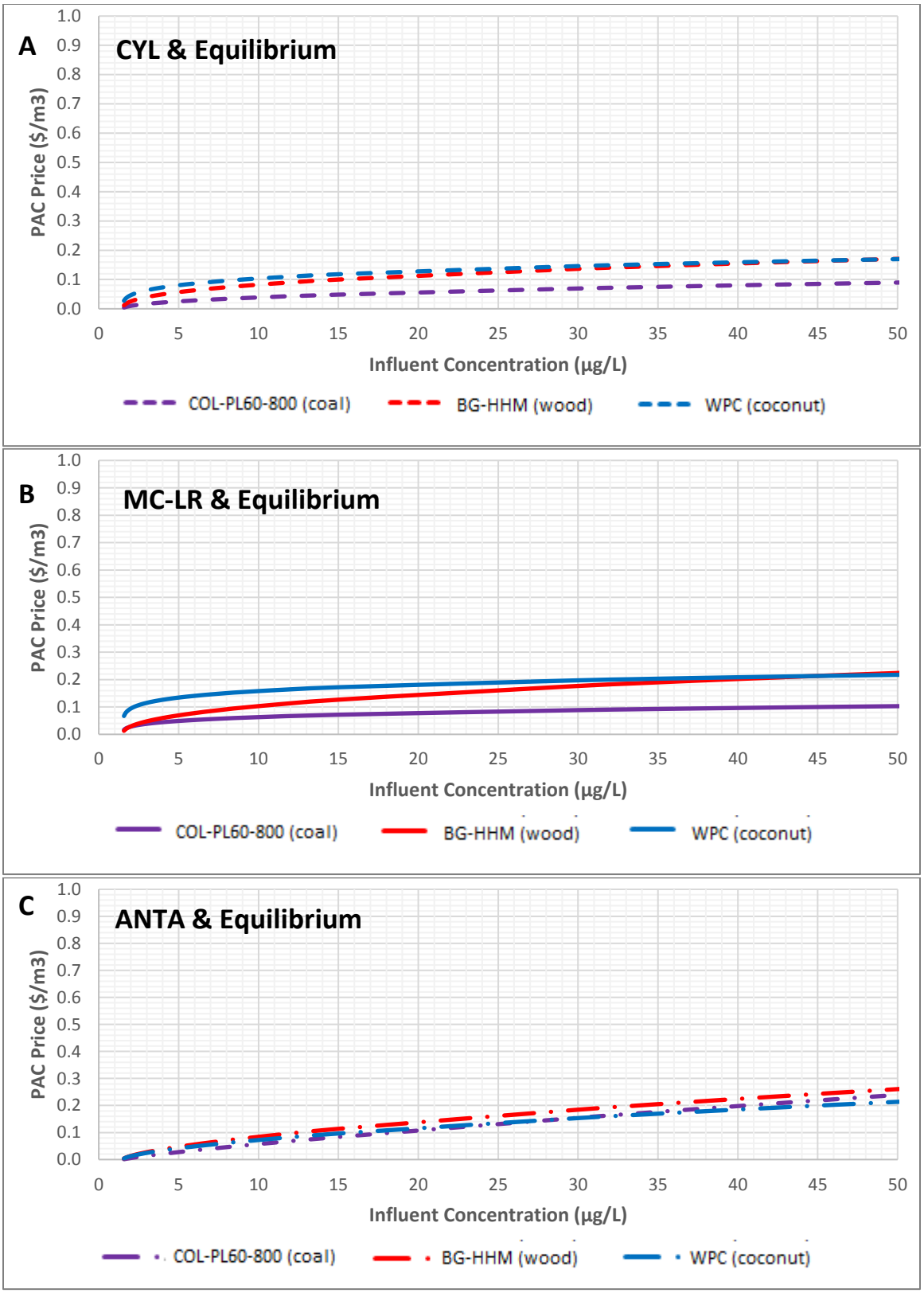

Figure B.78 Estimate of PAC costs for adsorption of cyanotoxins at influent concentrations in Lake Erie water, based on SEBCM under equilibrium conditions, given target cyanotoxin concentration of 1.5 µg/L. A) CYL adsorption, B) MC-LR adsorption, C) ANTA adsorption

Appendix B.4 Surface Water Properties (Lake Erie)

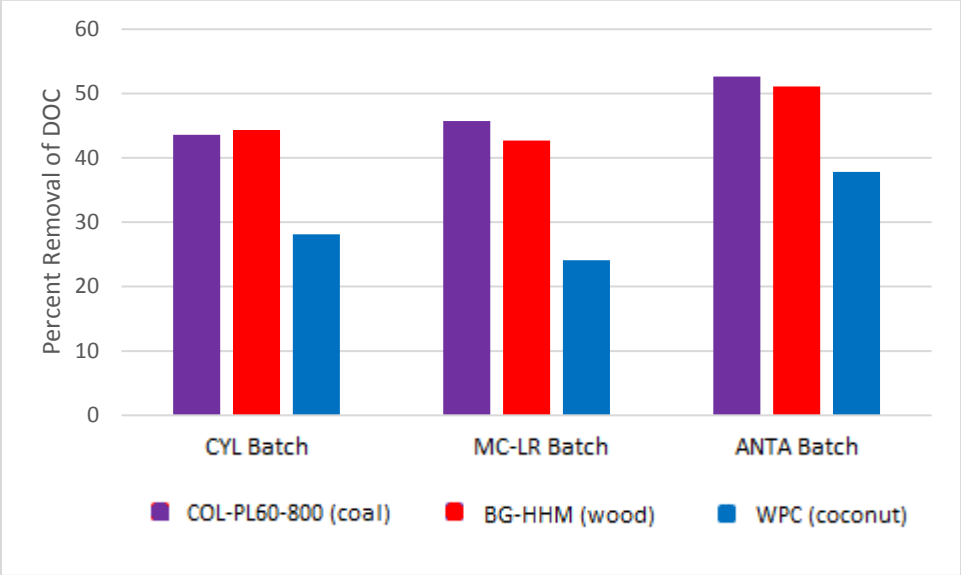

Figure B.79 Percent Removal of DOC after adsorption experiment

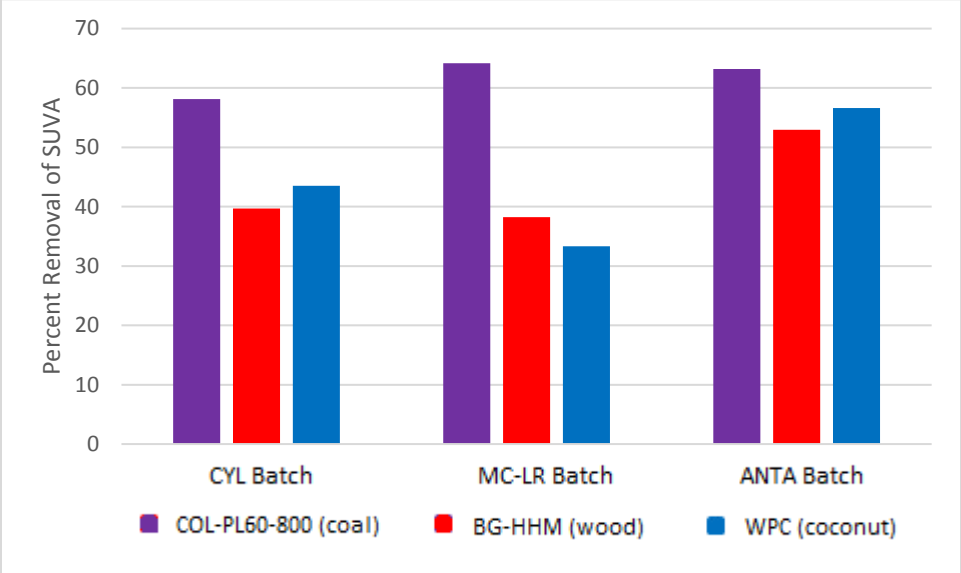

Figure B.80 Percent Reduction of SUVA after adsorption experiment

Appendix C

Additional Information for Chapter 5

Appendix C.1 Rate of CYL Adsorption by GAC in Ultrapure Water

Table C.1 CYL kinetic data determined with virgin coal-based GAC in ultrapure water

Time (d)	IS-Area Count	CYL-Area Count	Response Ratio	Concentration (µg/L)
0.00	461971	275889	0.60	132.3
0.04	465166	271563	0.58	129.3
0.08	446005	259497	0.58	128.8
0.17	453454	263928	0.58	128.9
0.25	441026	257243	0.58	129.2
0.38	458554	248086	0.54	119.8
0.50	456446	247971	0.54	120.3
1	472810	212260	0.45	99.3
2	460827	154340	0.33	74.0
3	503535	119452	0.24	52.3
4	493535	98520	0.20	43.9
5	619901	76840	0.12	27.1
6	561161	52889	0.09	20.5
7	653308	37227	0.06	12.2
8	664745	27532	0.04	8.8
9	683919	21184	0.03	6.4
10	574432	14125	0.02	5.0
11	633134	10291	0.02	3.2
12	630488	7576	0.01	2.2
13	610195	5666	0.01	1.6

Table C.2 CYL kinetic data determined with virgin wood-based GAC in ultrapure water

Time (d)	IS-Area Count	CYL-Area Count	Response Ratio	Concentration (µg/L)
0.00	435452	211511	0.49	107.5
0.02	429077	206259	0.48	106.4
0.04	438440	209630	0.48	105.8
0.08	404560	189954	0.47	103.9
0.25	348797	144446	0.41	91.6
1.00	384320	115572	0.30	66.4
2.00	319658	76320	0.24	52.6
3	296376	60704	0.20	45.1
4	390880	67667	0.17	38.0
5	439911	58512	0.13	29.1
6	431352	53123	0.12	26.9
8	493932	47181	0.10	20.8
9	437591	40677	0.09	20.2

Table C.3 CYL kinetic data determined with virgin coconut-based GAC in ultrapure water

Time (d)	IS-Area Count	CYL-Area Count	Response Ratio	Concentration (µg/L)
0.00	467359	215343	0.46	101.9
0.02	488883	223438	0.46	101.1
0.04	479117	215786	0.45	99.6
0.08	434415	193788	0.45	98.7
0.25	442976	194233	0.44	97.0
1.00	389930	147467	0.38	83.6
2.00	377452	90104	0.24	52.6
3	408709	64199	0.16	34.5
4	458115	49355	0.11	23.5
5	411638	28325	0.07	14.8
6	492118	23317	0.05	10.1
8	522626	12757	0.02	5.0
9	527768	10154	0.02	3.8
10	522545	7279	0.01	2.7
11	454464	5655	0.01	2.3
12	340090	4039	0.01	2.2

Table C.4 CYL kinetic data determined with pre-loaded coal-based GAC in ultrapure water

Time (d)	IS-Area Count	CYL-Area Count	Response Ratio	Concentration (µg/L)
0.00	454672	214641	0.47	104.5
0.02	488686	229394	0.47	103.9
0.04	467559	217887	0.47	103.1
0.08	465035	214716	0.46	102.2
0.25	336014	154436	0.46	101.7
1.00	409240	184538	0.45	99.8
2.00	462990	191635	0.41	91.5
3	427174	172859	0.40	89.5
4	524012	198370	0.38	83.7
5	484154	177052	0.37	80.8
6	450551	161307	0.36	79.1
8	423061	139457	0.33	72.8
9	501229	159200	0.32	70.1
10	502306	153219	0.31	67.3
11	482657	138700	0.29	63.4
12	575440	151327	0.26	58.0
13	499898	115708	0.23	51.0
16	498895	94050	0.19	41.4
17	572556	99882	0.17	38.3
19	511277	86161	0.17	37.0
20	483333	79951	0.17	36.3
21	549752	89519	0.16	35.7
23	534649	85732	0.16	35.2

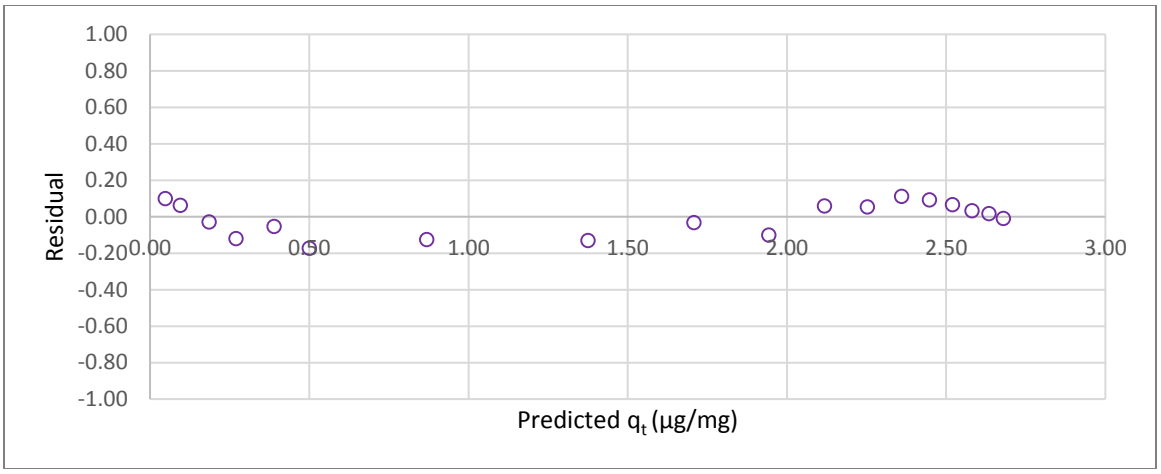

Figure C.1 Residual plot for pseudo-second order fit of CYL adsorption by the virgin F-300 (coal)

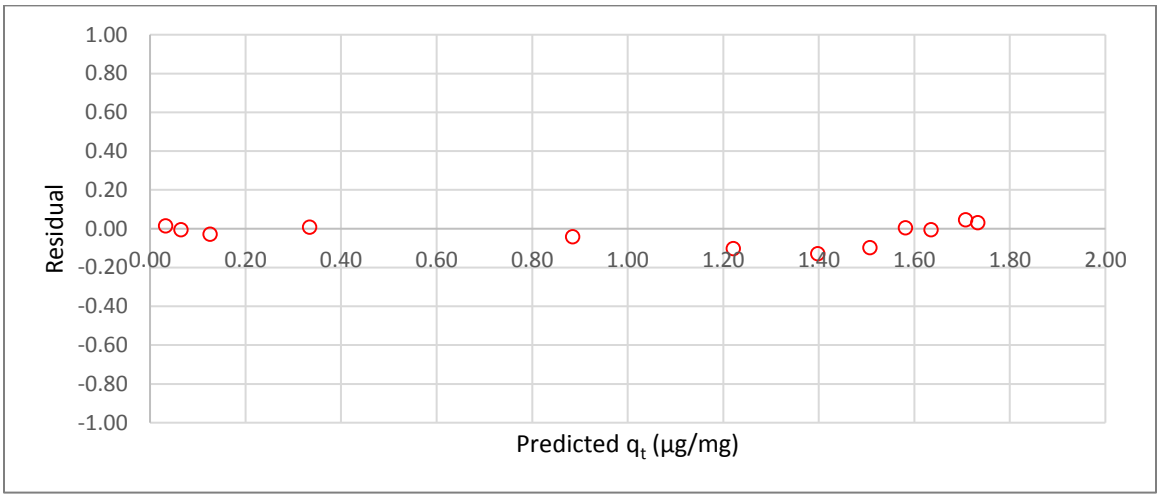

Figure C.2 Residual plot for pseudo-second order fit of CYL adsorption by the virgin C Gran (wood)

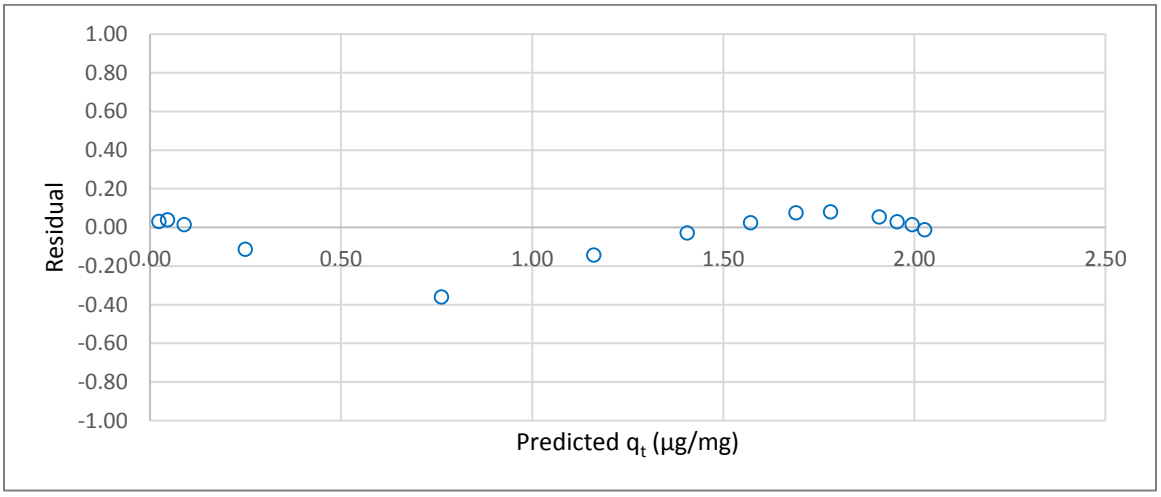

Figure C.3 Residual plot for pseudo-second order fit of CYL adsorption by the virgin Aqua Carb (coconut)

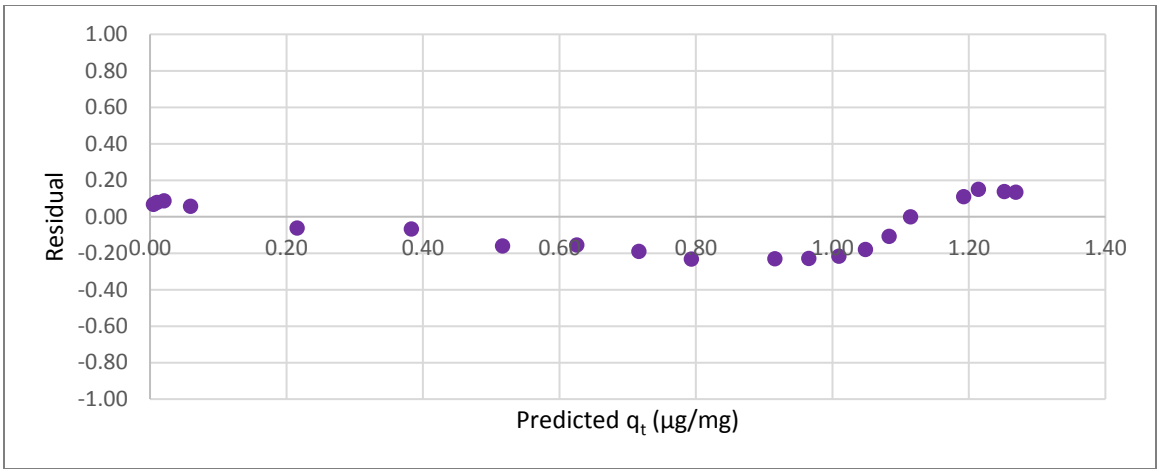

Figure C.4 Residual plot for pseudo-second order fit of CYL adsorption by the pre-loaded F-300 (coal)

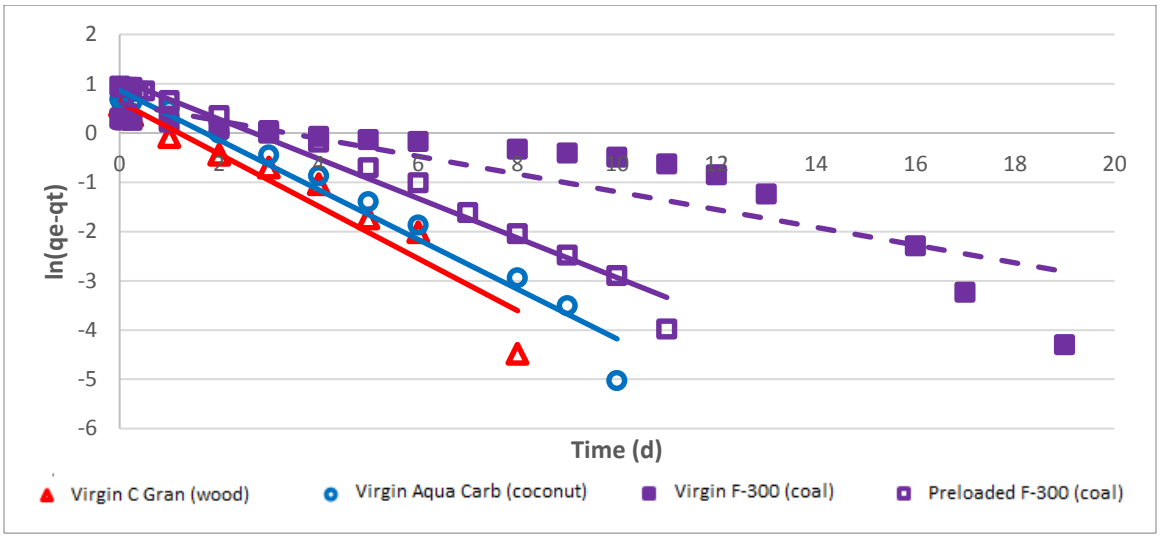

Figure C.5 Pseudo-first order kinetic model fits using virgin and pre-loaded GACs in ultrapure water

Table C.5 Pseudo-first and second order kinetic model parameters for virgin and pre-loaded GACs in ultrapure water

Model	GAC	Equilibrium Carbon Capacity, q_e experimental (µg/mg)	Equilibrium Carbon Capacity, q_e predicted (µg/mg)	k_1 (day^{-1}) or k_2 (mg/µg/day)	R^2
Pseudo-First Order	Virgin F-300 (coal)	2.67	2.96	0.40	0.80
	Virgin C Gran (wood)	1.76	1.88	0.53	0.94
	Virgin Aqua Carb (coconut)	2.02	2.38	0.50	0.97
	Preloaded F-300 (coal)	1.40	1.83	0.18	0.80
Pseudo-Second Order	Virgin F-300 (coal)	2.67	3.31	0.11	0.95
	Virgin C Gran (wood)	1.76	1.97	0.41	0.99
	Virgin Aqua Carb (coconut)	2.02	2.43	0.19	0.94
	Preloaded F-300 (coal)	1.40	1.71	0.08	0.77

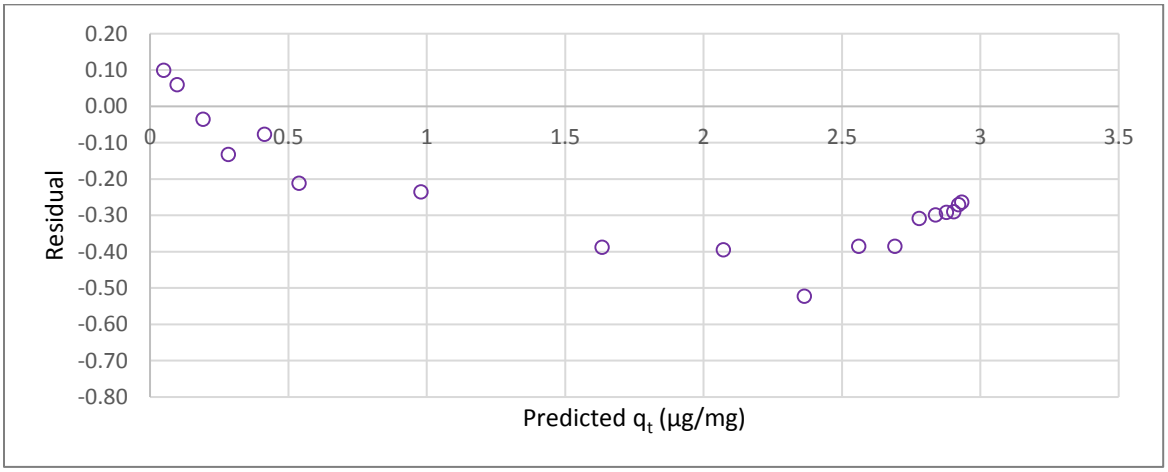

Figure C.6 Residual plot for pseudo-first order fit of CYL adsorption by the virgin F-300 (coal)

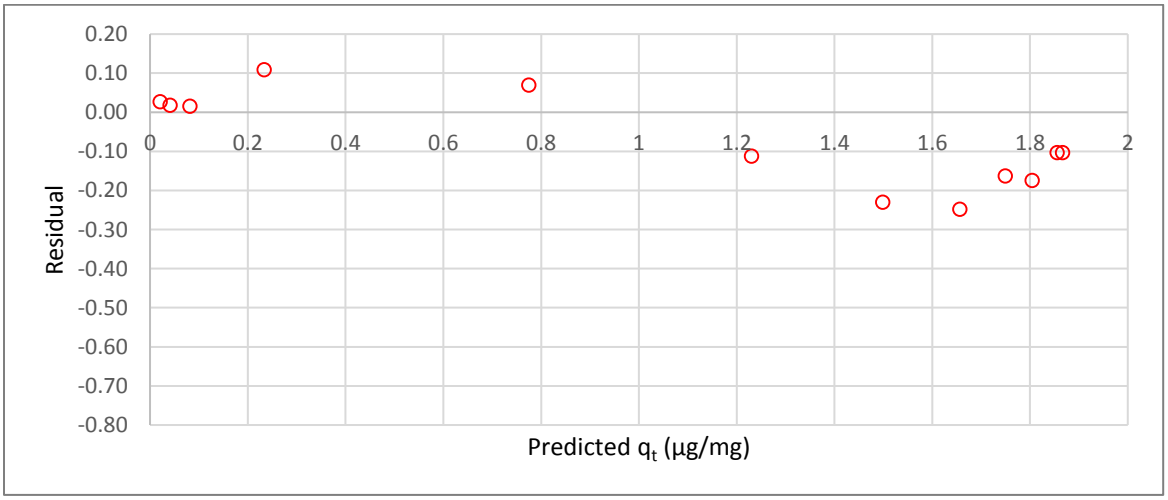

Figure C.7 Residual plot for pseudo-first order fit of CYL adsorption by the virgin C Gran (wood)

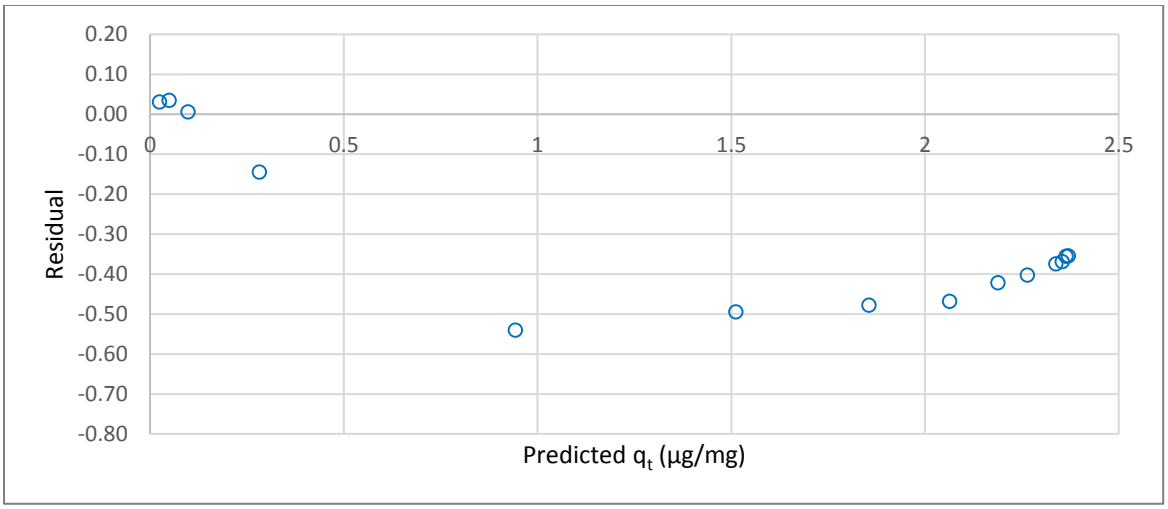

Figure C.8 Residual plot for pseudo-first order fit of CYL adsorption by the virgin Aqua Carb (coconut)

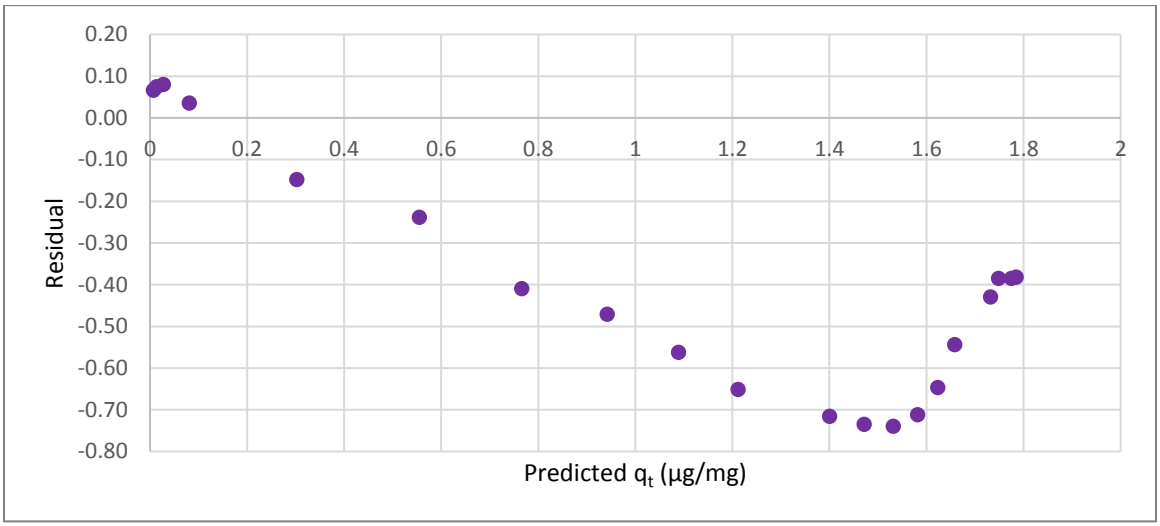

Figure C.9 Residual plot for pseudo-first order fit of CYL adsorption by the pre-loaded F-300 (coal)

Appendix C.2 Isotherms of CYL Adsorption by GAC in Ultrapure Water

Table C.6 Equilibrium data for virgin coal-based F-300 GAC in ultrapure water

Sample	Carbon dose (mg/L)	Equilibrium toxin CYL concentration (µg/L)	Equilibrium Capacity, q_e (µg/mg)
CYL-F300-1	7.8	75.2	7.3
CYL-F300-2	11.6	56.5	6.5
CYL-F300-3	17.2	33.7	5.7
CYL-F300-4	24.4	20.0	4.6
CYL-F300-5	30.4	16.4	3.8
CYL-F300-6	35.8	8.0	3.5
CYL-F300-7	42.4	4.9	3.0
CYL-F300-8	50.4	2.2	2.6

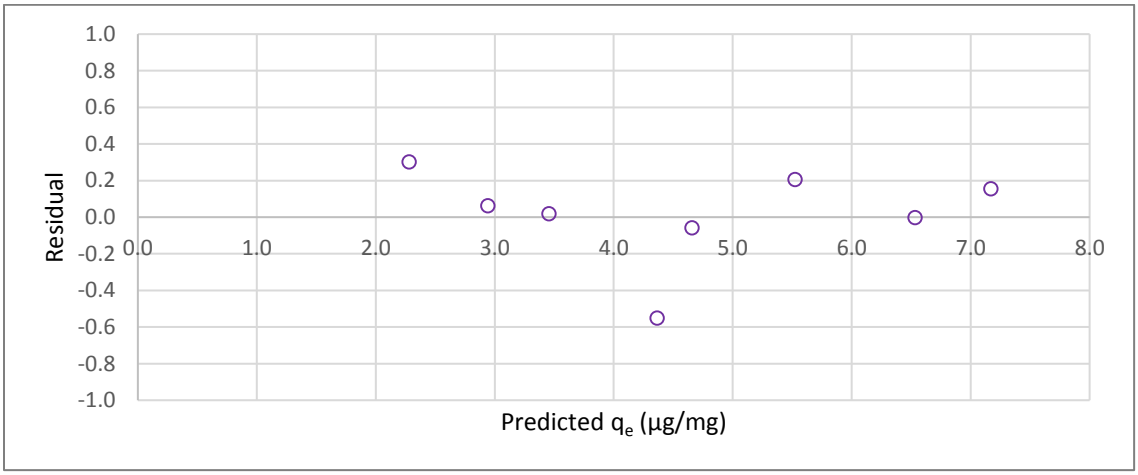

Figure C.10 Residual plot for Freundlich isotherm fitting of CYL adsorption by the virgin F-300 (coal)

Table C.7 Equilibrium data for virgin wood-based C Gran GAC in ultrapure water

Sample	Carbon dose (mg/L)	Equilibrium toxin CYL concentration (µg/L)	Equilibrium Capacity, q_e (µg/mg)
CYL-C Gran-1	8.4	72.9	4.3
CYL-C Gran-2	12.8	64.2	3.5
CYL-C Gran-3	18.2	53.3	3.0
CYL-C Gran-4	23.2	44.5	2.8
CYL-C Gran-5	30.8	33.6	2.4
CYL-C Gran-6	37.0	27.6	2.2
CYL-C Gran-7	42.4	26.8	1.9
CYL-C Gran-8	50.2	20.2	1.8

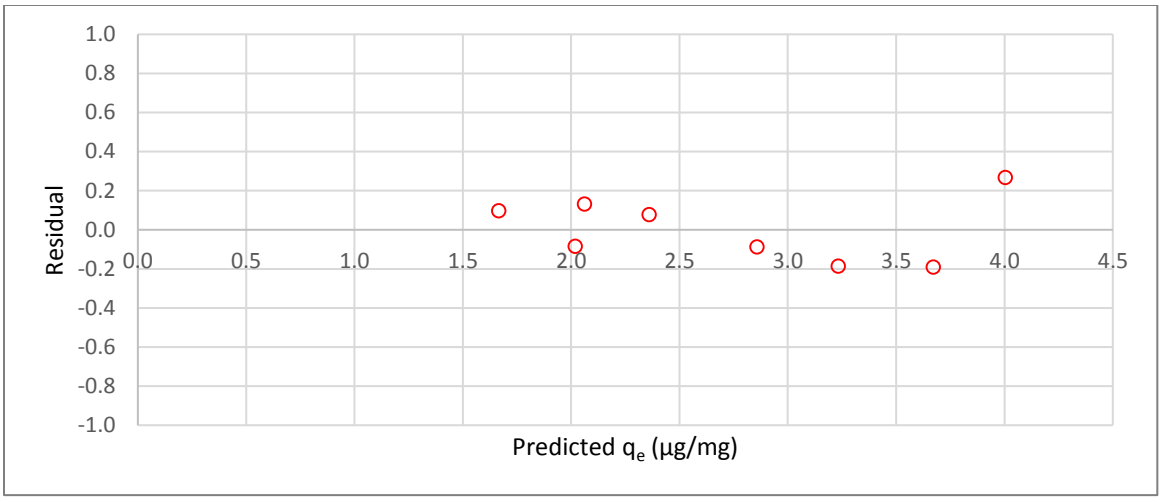

Figure C.11 Residual plot for Freundlich isotherm fitting of CYL adsorption by the virgin C Gran (wood)

Table C.8 Equilibrium data for virgin coconut-based Aqua Carb GAC in ultrapure water

Sample	Carbon dose (mg/L)	Equilibrium toxin CYL concentration (µg/L)	Equilibrium Capacity, qe (µg/mg)
CYL-AquaCarb-1	7.8	49.3	7.01
CYL-AquaCarb-2	12.2	39.4	5.29
CYL-AquaCarb-3	18.4	24.6	4.31
CYL-AquaCarb-4	24.2	17.5	3.57
CYL-AquaCarb-5	30.2	10.0	3.11
CYL-AquaCarb-6	35.4	4.9	2.80
CYL-AquaCarb-7	42.0	2.7	2.41
CYL-AquaCarb-8	50.4	2.3	2.02

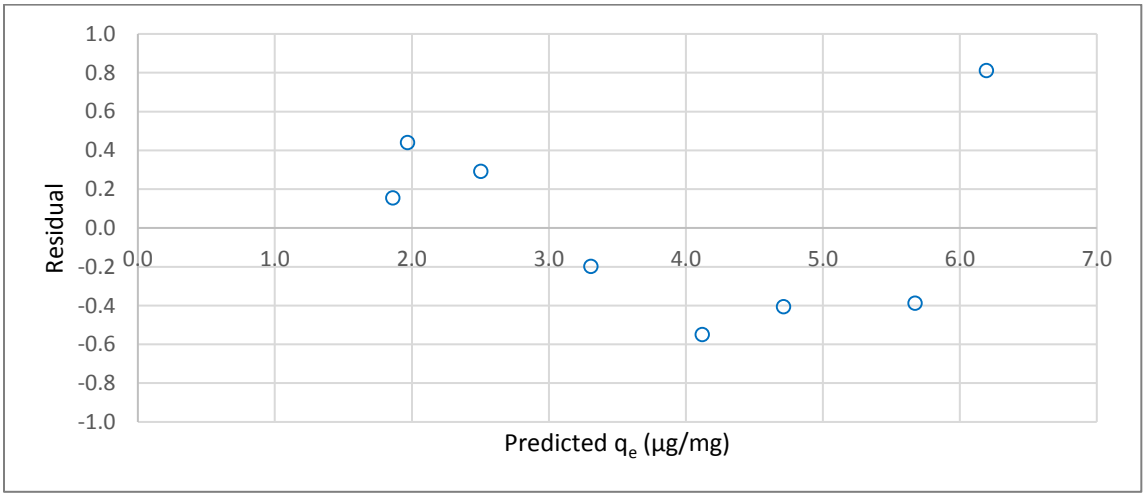

Figure C.12 Residual plot for Freundlich isotherm fitting of CYL adsorption by the virgin Aqua Carb (coconut)

Table C.9 Equilibrium data for preloaded coal-based F-300 GAC in ultrapure water

Sample	Carbon dose (mg/L)	Equilibrium toxin CYL concentration (µg/L)	Equilibrium Capacity, qe (µg/mg)
CYL-Preloaded-1	10.0	82.5	2.5
CYL-Preloaded-2	12.4	76.3	2.5
CYL-Preloaded-3	18.8	67.7	2.1
CYL-Preloaded-4	24.2	58.9	2.0
CYL-Preloaded-5	30.2	51.4	1.9
CYL-Preloaded -6	36.2	47.5	1.7
CYL-Preloaded-7	41.8	40.8	1.6
CYL-Preloaded-8	50.8	36.3	1.4

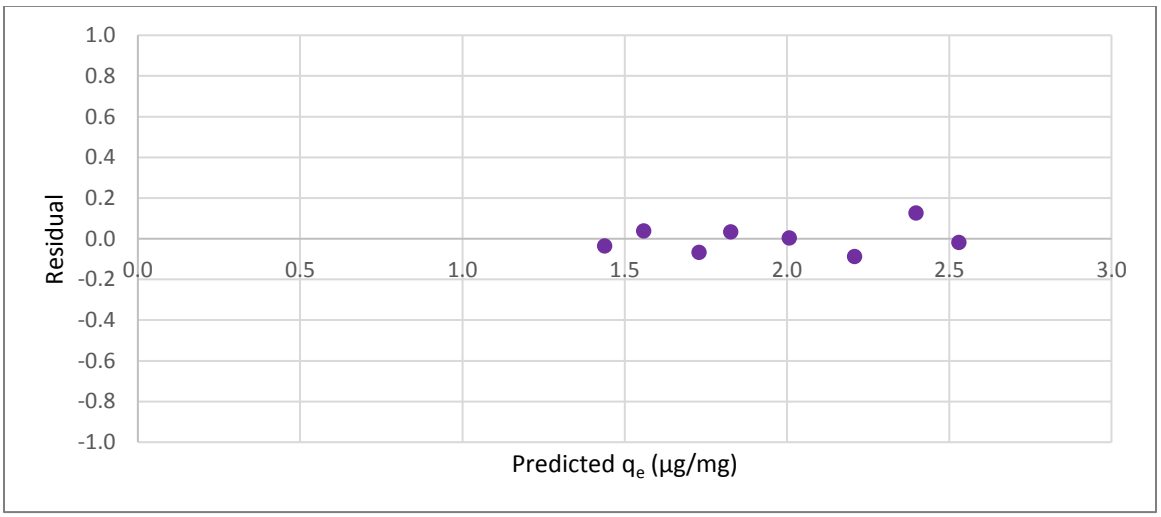

Figure C.13 Residual plot for Freundlich isotherm fitting of CYL adsorption by the pre-loaded F-300 (coal)